Deep Learning in CT

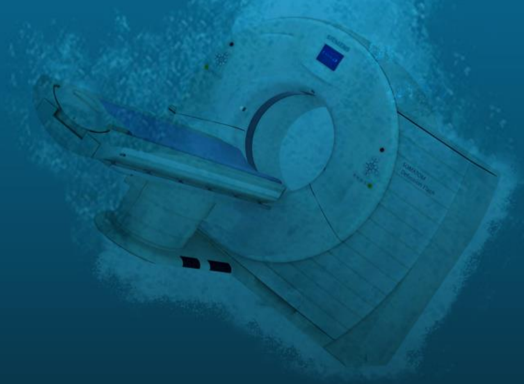

Marc Kachelrieß

German Cancer Research Center (DKFZ)

Heidelberg, Germany

www.dkfz.de/ct

DEUTSCHES KREBSFORSCHUNGSZENTRUM
IN DER HELMHOLTZ-GEMEINSCHAFT

Fully Connected Neural Network

- Each layer fully connects to previous layer
- Difficult to train (many parameters in *W* and *b*)
- Spatial relations not necessarily preserved

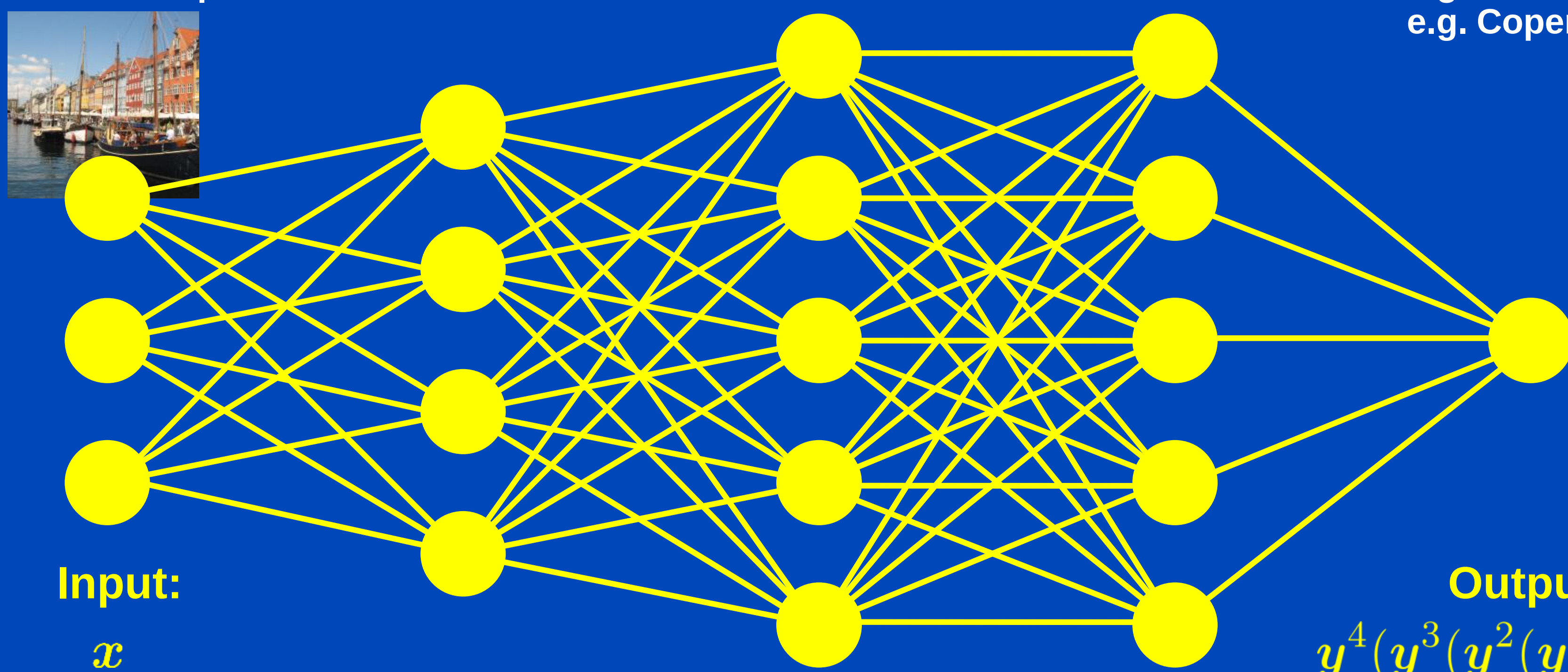

$\boldsymbol{y}(\boldsymbol{x}) = \boldsymbol{f}(\boldsymbol{W}\cdot\boldsymbol{x}+\boldsymbol{b})$ with $\boldsymbol{f}(\boldsymbol{x}) = \big(f(x_1), f(x_2), \dots\big)$ point-wise scalar, e.g. $f(x) = x \vee 0 = \mathrm{ReLU}$

Convolutional Neural Network (CNN)

- **Replace dense *W* in $y(x) = f(W \cdot x + b)$ by a sparse matrix *W* with sparsity being of convolutional type.**
- **CNNs consist (mainly) of convolutional layers.**
- **Convolutional layers are not fully connected.**
- **Convolutional layers are connected by small, say 3×3, convolution kernels whose entries need to be found by training.**
- **CNNs preserve spatial relations to some extent.**

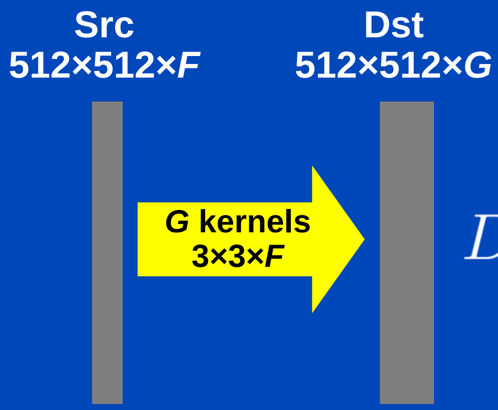

$$D_{i,j,g} = \sum_f S_{i,j,f} * K^g_{i,j,f} = \sum_{a,b,f} S_{i-a,j-b,f} K^g_{a,b,f}$$

Attention: No convolution in depth direction!

Here, a 2D example is shown. Conv layers also exist in 3D and higher dimensions.

U-Net[1]

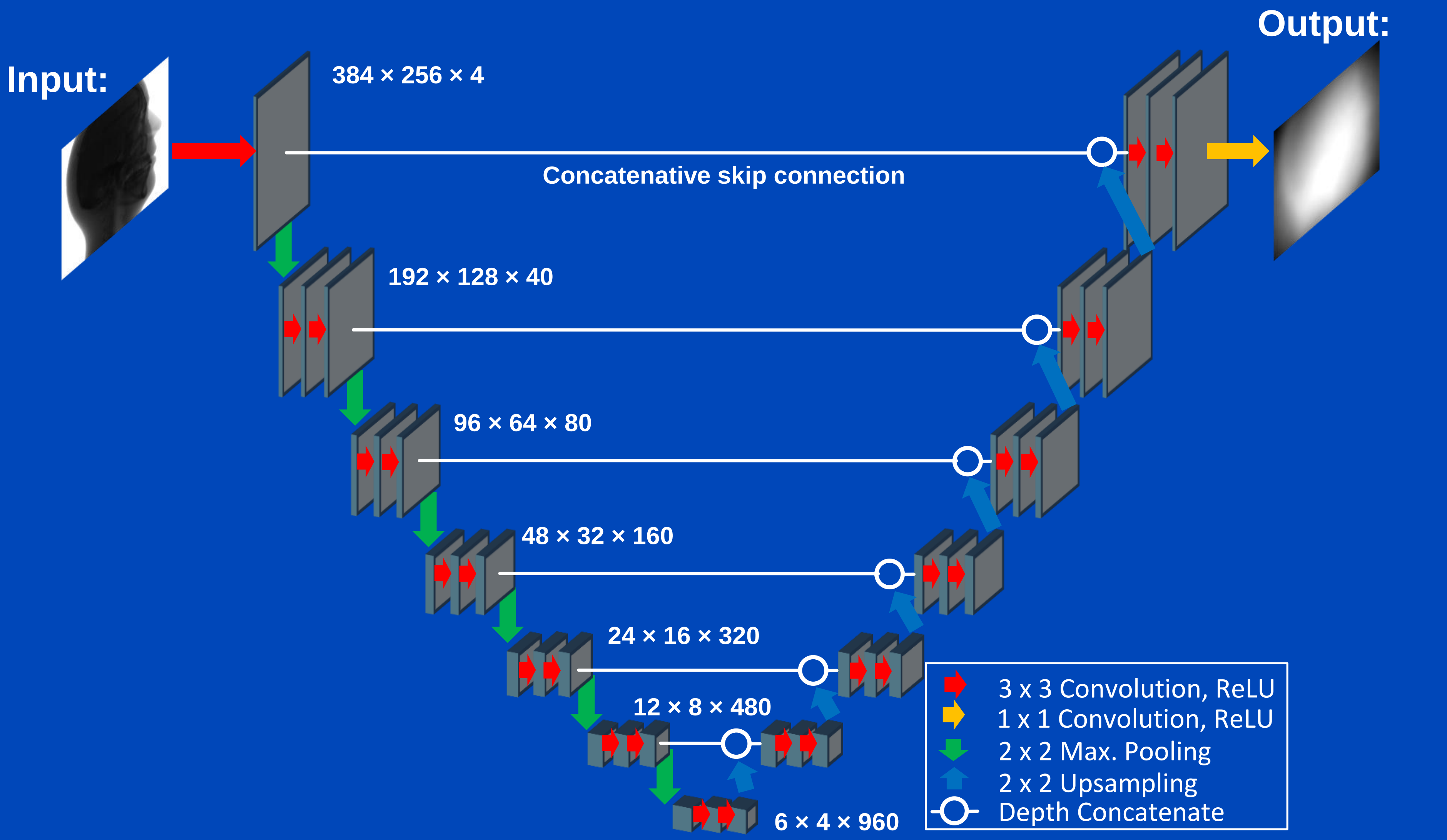

[1]O. Ronneberger, P. Fischer, and T. Brox. U-net: Convolutional networks for biomedical image segmentation. Proc. MICCAI:234-241, 2015.

Activation Functions

Function	Equation	Plot
Identity	$f(x) = x$	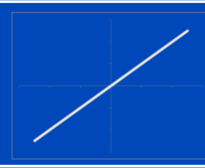
Sigmoid	$f(x) = \dfrac{1}{1+e^{-x}}$	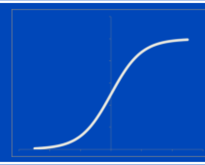
Hard sigmoid	$f(x) = \begin{cases} 0 & \text{for } x < -\alpha \\ \frac{\alpha+x}{2\alpha} & \text{for } -\alpha \leq x < \alpha \\ 1 & \text{for } x \geq \alpha \end{cases}$	
Tanh	$f(x) = \dfrac{2}{1+e^{-2x}} - 1$	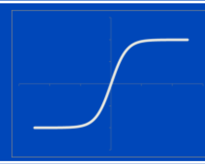
Softsign	$f(x) = \dfrac{x}{1+\lvert x\rvert}$	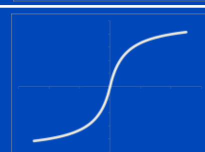
Softplus	$f(x) = \log(1 + \exp x)$	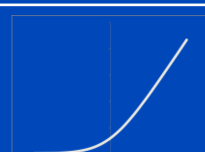

Function	Equation	Plot
ReLU	$f(x) = \begin{cases} 0 & \text{for } x < 0 \\ x & \text{for } x \geq 0 \end{cases}$	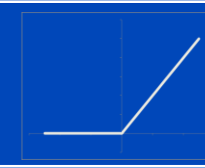
Leaky ReLU	$f(x) = \begin{cases} \alpha x & \text{for } x < 0 \\ x & \text{for } x \geq 0 \end{cases}$	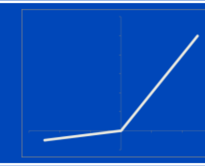
ELU	$f(x) = \begin{cases} \alpha(e^x - 1) & \text{for } x < 0 \\ x & \text{for } x \geq 0 \end{cases}$	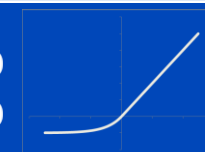
Inverse square root LU	$f(x) = \begin{cases} \frac{x}{\sqrt{1+\alpha x^2}} & \text{for } x < 0 \\ x & \text{for } x \geq 0 \end{cases}$	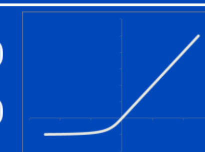
…	…	…

Loss Function

- The neural network parameters (weights and biases) *w* are chosen by minimizing a loss function (cost function)

$$\boldsymbol{w} = \arg\min_{\boldsymbol{w}} \sum_{n=1}^{N} L(\boldsymbol{x}_n, \boldsymbol{y}_n, \boldsymbol{w})$$

  with x_n being the training data input, $y(x_n, w)$ being the network output, and y_n being the so-called labels, i.e. the training target, and *N* being the number of training samples.

- An example for such a loss function is the MSE loss

$$L(\boldsymbol{x}_n, \boldsymbol{y}_n, \boldsymbol{w}) = \big(\boldsymbol{y}(\boldsymbol{x}_n, \boldsymbol{w}) - \boldsymbol{y}_n\big)^2$$

Gradient Descent

- Walk along the direction of the negative gradient
- Steepest descent
- Learning rate η

$$\boldsymbol{w}^{\text{new}} = \boldsymbol{w}^{\text{old}} - \eta\, \nabla_{\boldsymbol{w}}\, L(\boldsymbol{x}_n, \boldsymbol{y}_n, \boldsymbol{w})$$

- Easy to understand, but not optimal
- Methods in use
  - Batch gradient descent
  - Sochastic gradient descent
  - Mini-batch gradient descent
  - Conjugate gradient descent
  - Quasi Newton methods
  - Momentum methods
  - …

What is an Autoencoder?

- In and output domain are the same, here *x*.
- Bottleneck *z* enforces the encoder and decoder to do a good job.

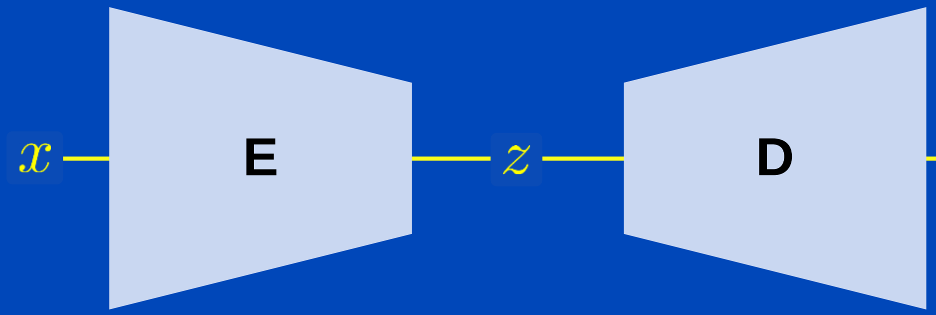

$$x' = D(z) = \\ = D(E(x))$$

- Examples:
  - Principal component analysis (linear autoencoder), lossless
  - PCA with dimensionality reduction (nonlinear due to clipping), lossy
  - Image compression and decoding, e.g. jpeg, lossy
- Latent space typically not interpretable.

What is a Variational Autoencoder?

- Make latent space regular.
- Allow to sample in latent space from a given distribution, here: normal distribution.

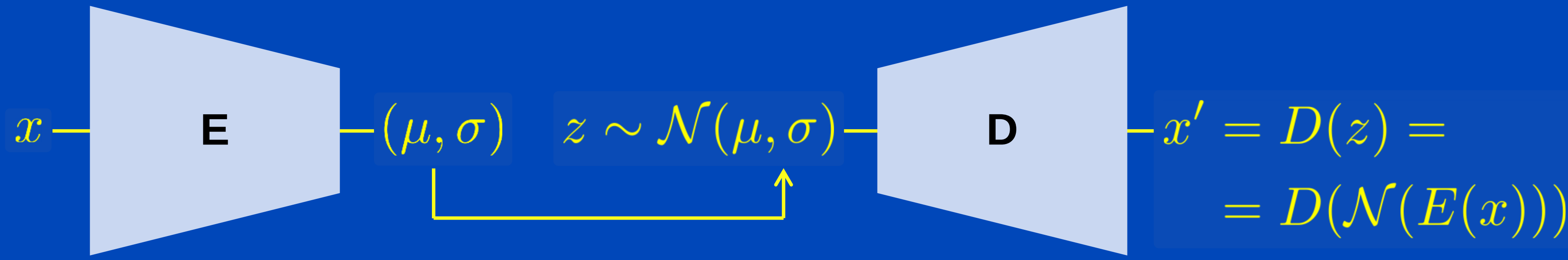

- The VAE is a generative model.
- It allows to generate new data by sampling new values from the normal distribution.

Generative Adversarial Network[1] (GAN)

- Useful, if no direct ground truth (GT) is available, the training data are unpaired, unsupervised learning

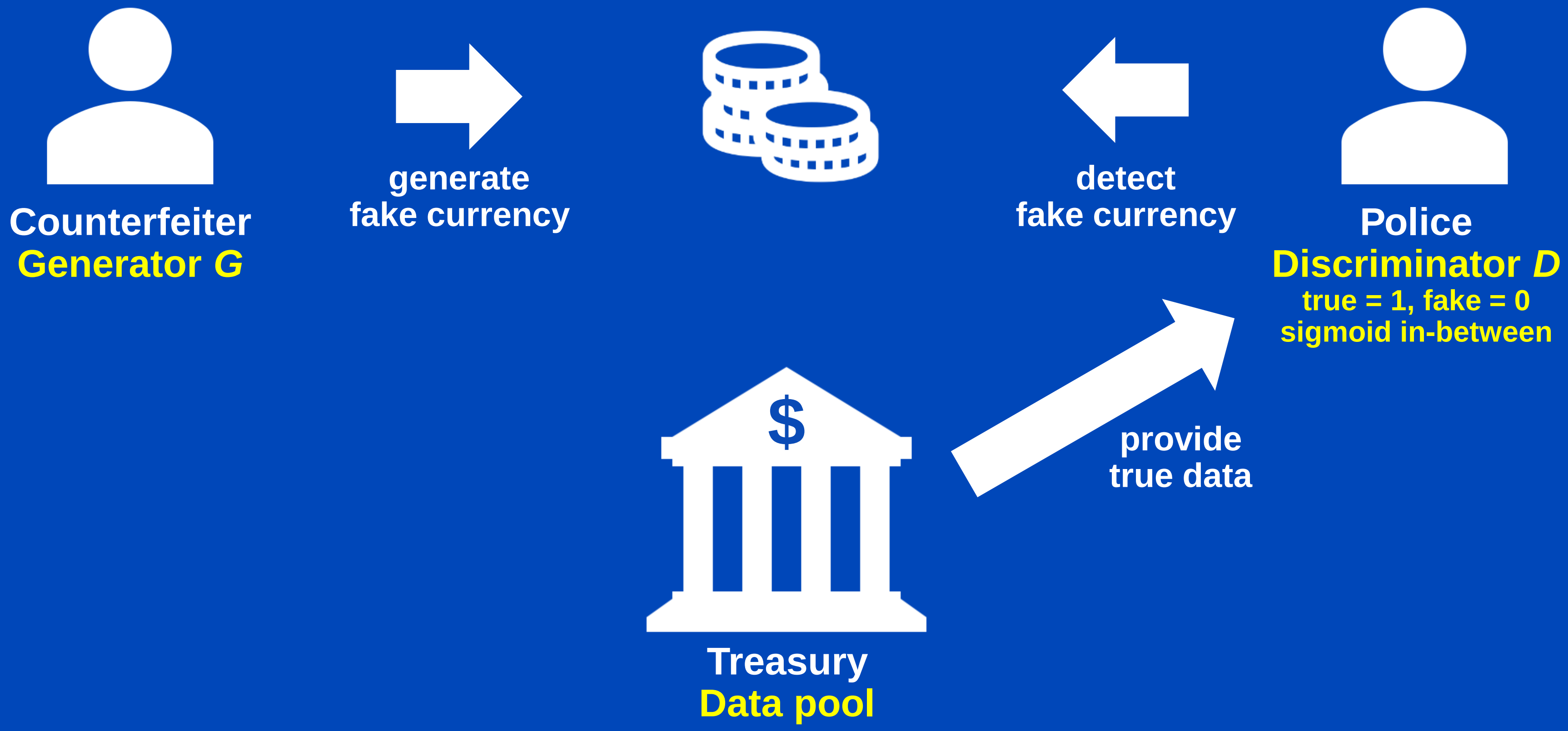

[1] I. Goodfellow et al. Generative Adversarial Nets, arXiv 2014

Generative Adversarial Network (GAN)

- **Typical loss function and minimax game:**

$$\min_G \max_D L(D,G) := \mathrm{E}_x \ln\big(1 - D(G(x))\big) + \mathrm{E}_y \ln D(y)$$

- **Conditional GAN**[1]
  - Conditional GANs sample the generator input *x* not from a uniform distribution but from a conditional distribution, e.g. noisy CT images.
  - Need some measure to ensure similarity to input distribution (e.g. pixelwise loss added to the minimax loss function)
- **Cycle GAN**[2]
  - Two GANs ($X \rightarrow Y$ and $Y \rightarrow X$)
  - Demand cyclic consistency, i.e. $x = G_X(G_Y(x))$ and $y = G_Y(G_X(x))$

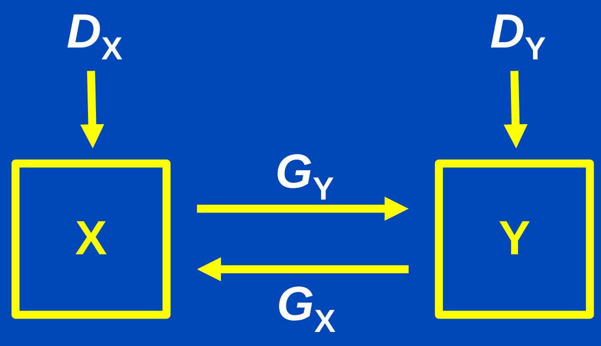

Fitting

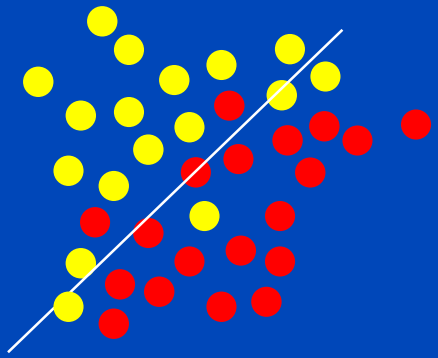

Fitting

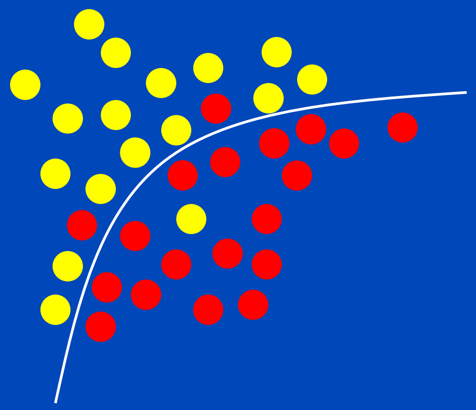

Fitting

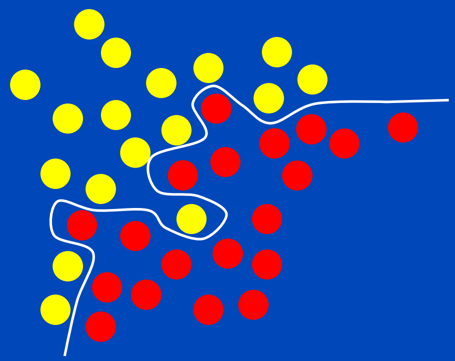

Fitting

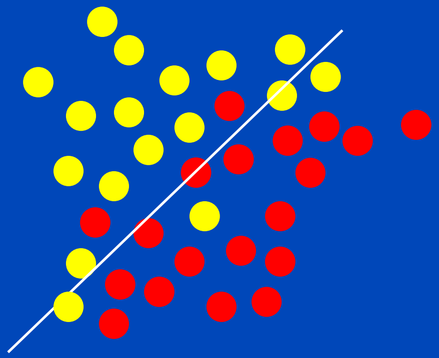

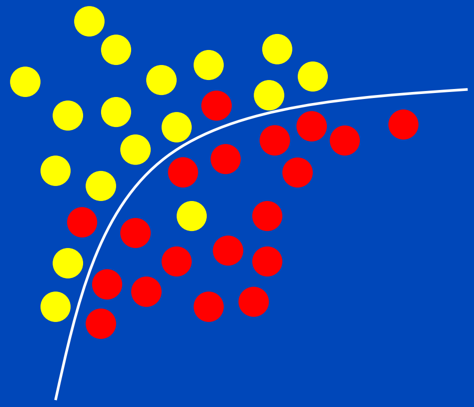

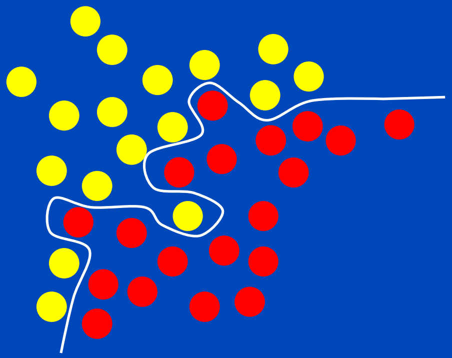

underfit **reasonable** **overfit**

Learning Curve

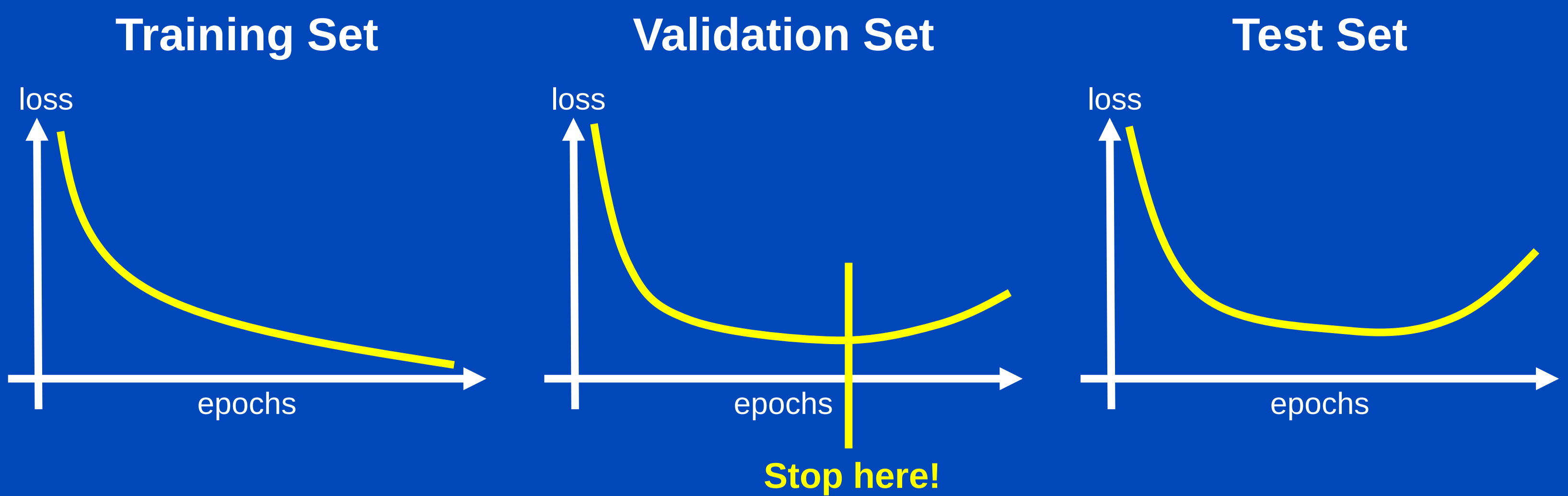

- **Training and validation set are part of the training**
- **Do not use test set for training**
- **Early stopping (at minimum validation loss)**
- **Training : Validation : Test ≈ 70 : 20 : 10**

Part 1:

Making up Data

Limited Angle Example

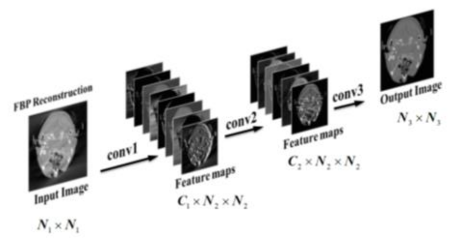

GT FBP (150°) CNN

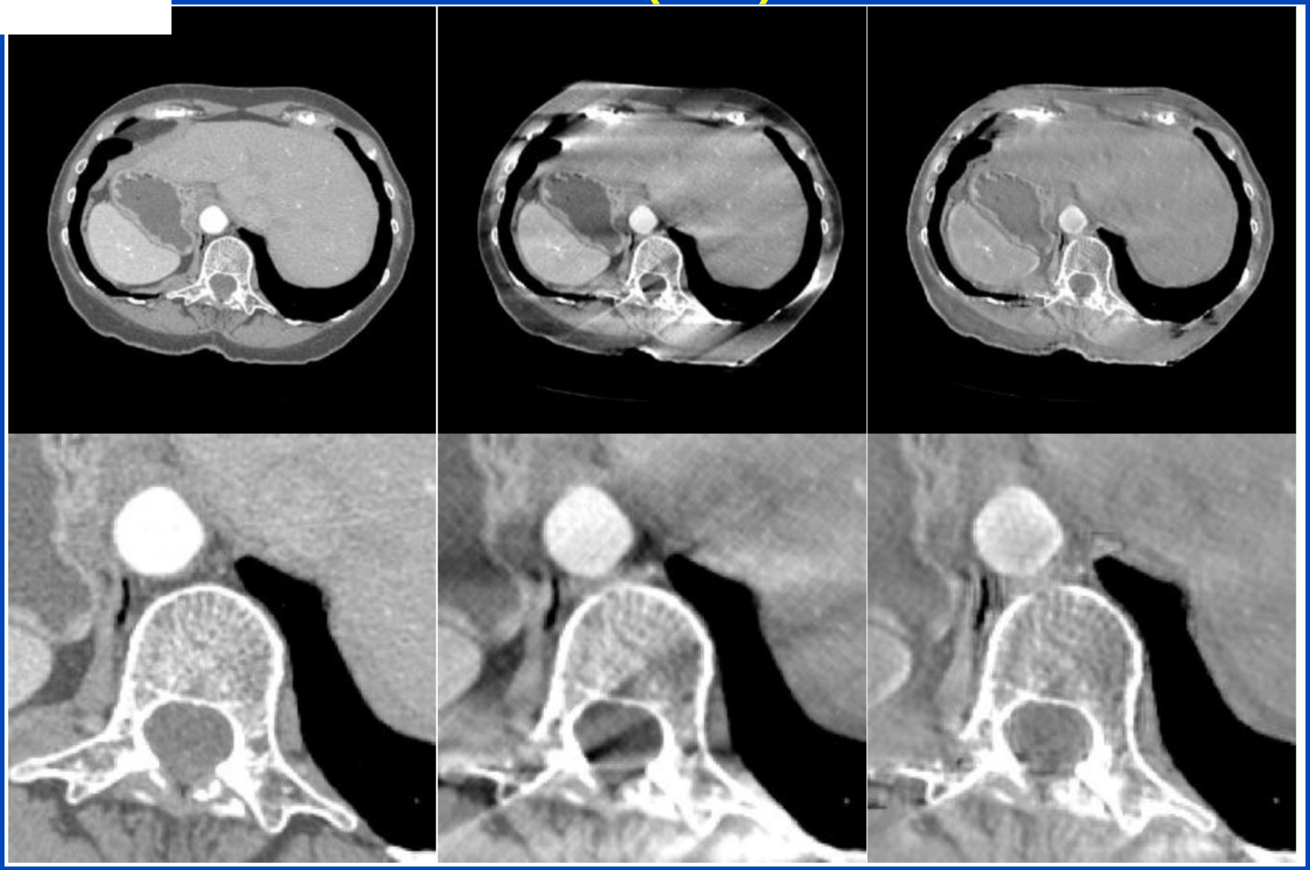

Image Prediction for Limited-Angle Tomography via Deep Learning with Convolutional Neural Network.
Hanming Zhang, Liang Li, Kai Qiao, Linyuan Wang, Bin Yan, Lei Li, Guoen Hu. arXiv 2016.

Deep MAR Examples

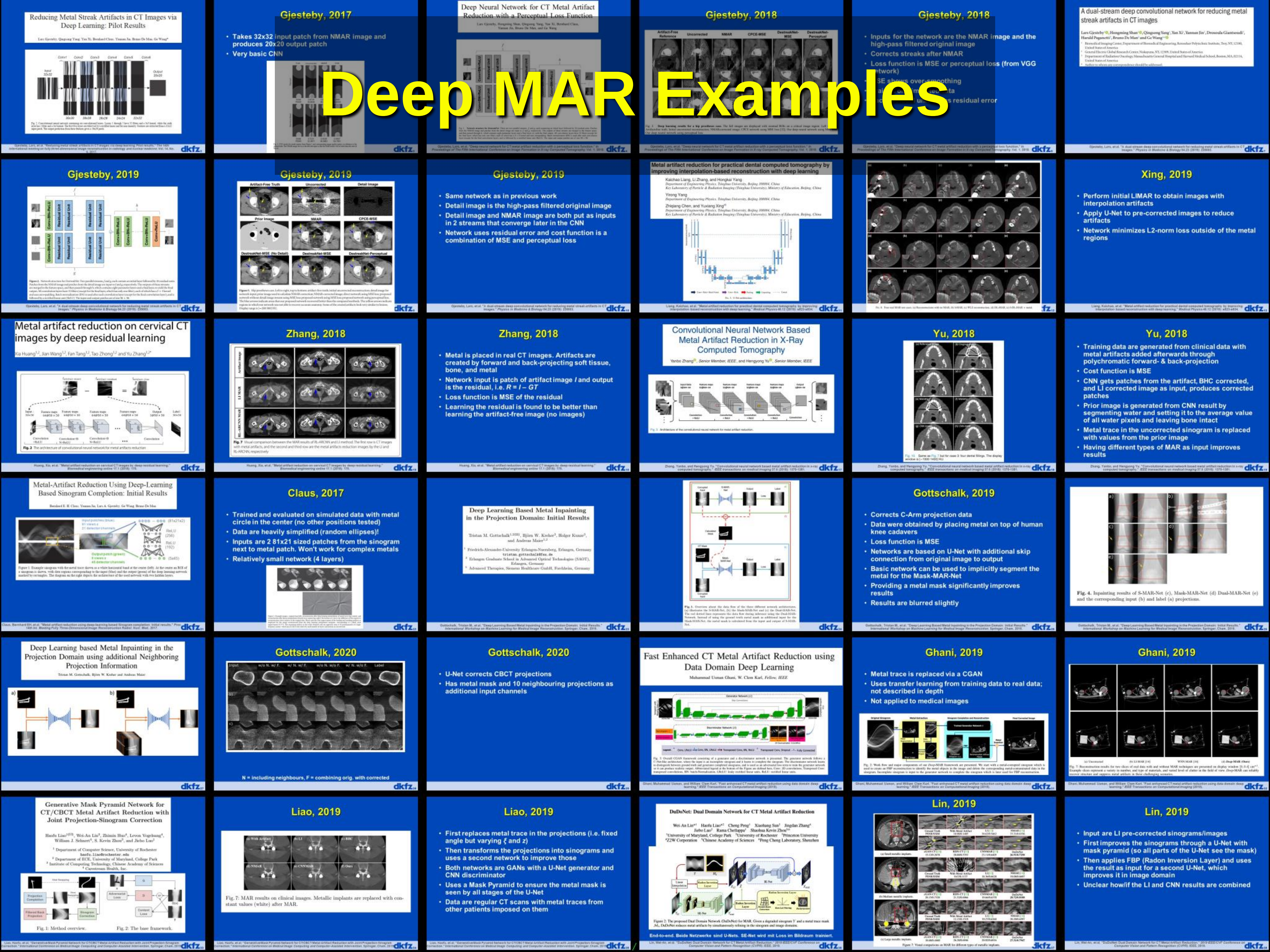

MAR Example

- Deep CNN-driven patch-based combination of the advantages of several MAR methods trained on simulated artifacts

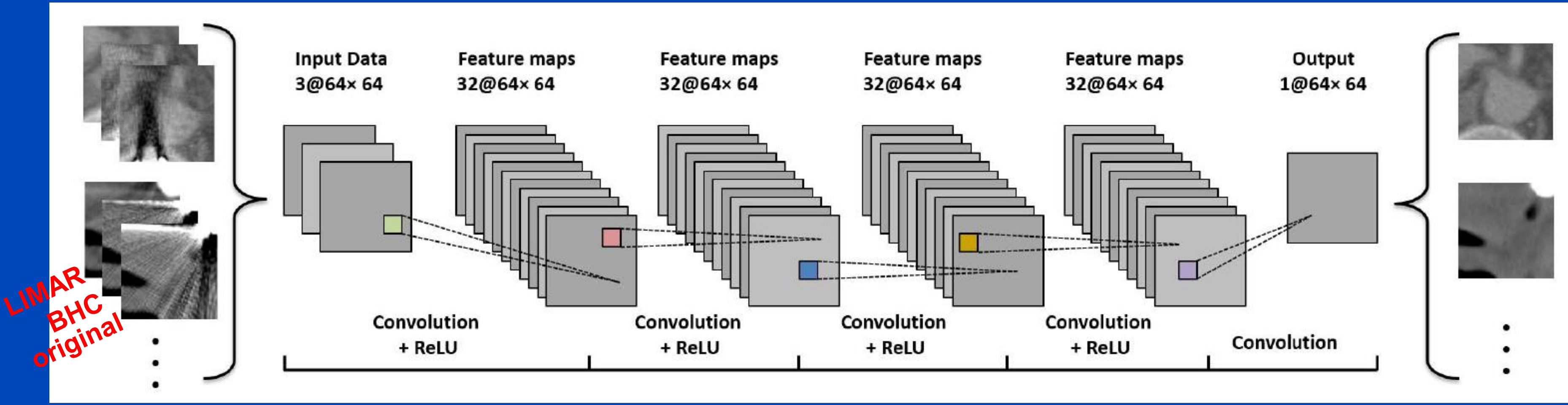

- followed by segmentation into tissue classes
- followed by forward projection of the CNN prior and replacement of metal areas of the original sinogram
- followed by reconstruction

Yanbo Zhang and Hengyong Yu. Convolutional Neural Network Based Metal Artifact Reduction in X-Ray Computed Tomography. TMI 37(6):1370-1381, June 2018.

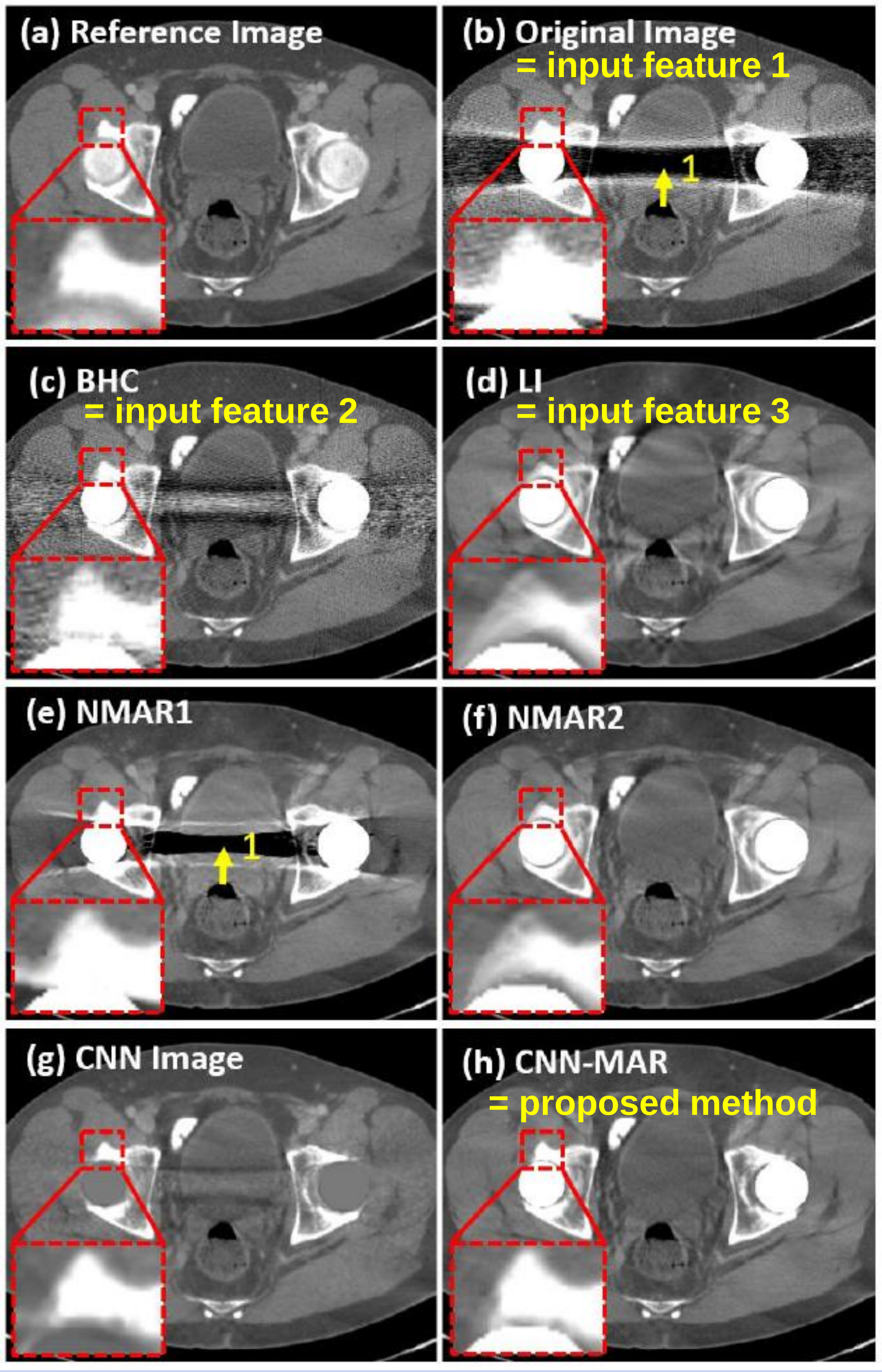
(a) Reference Image
(b) Original Image
= input feature 1
1
(c) BHC
= input feature 2
(d) LI
= input feature 3
(e) NMAR1
1
(f) NMAR2
(g) CNN Image
(h) CNN-MAR
= proposed method

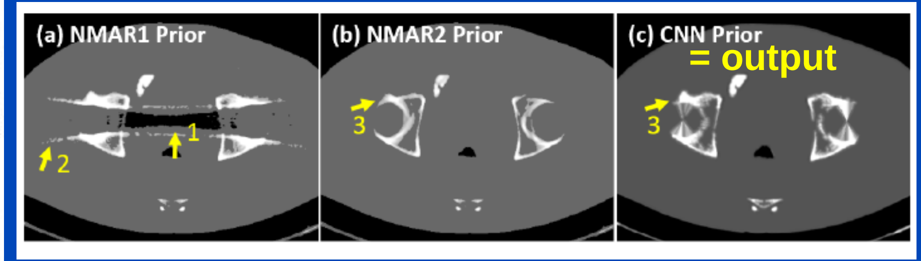
(a) NMAR1 Prior
1
2
(b) NMAR2 Prior
3
(c) CNN Prior
= output
3

MAR without Machine Learning is a Good Alternative: Frequency Split Normalized MAR[1,2]

Uncorrected

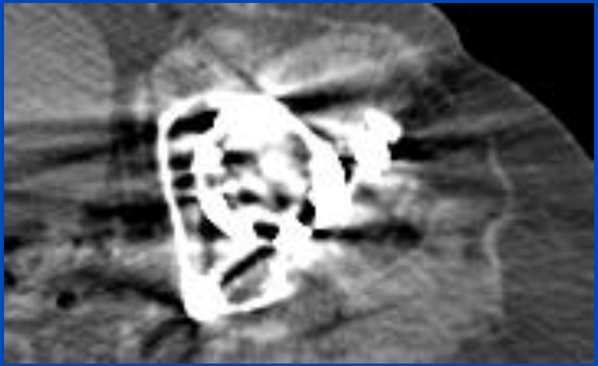

FSLIMAR

FSNMAR

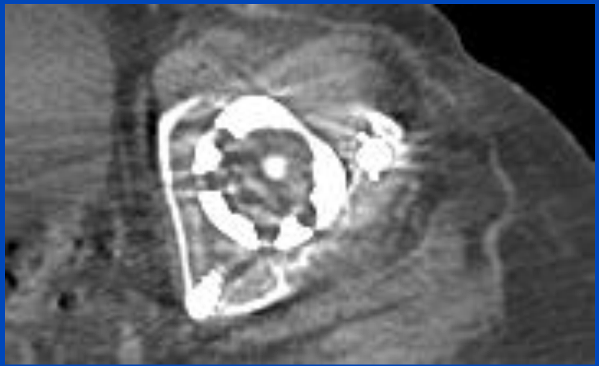

Patient with bilateral hip prosthesis, Somatom Definition Flash, (C=40/W=500).

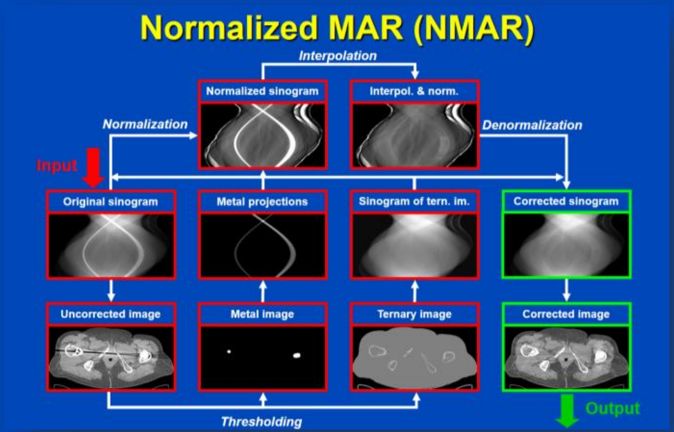

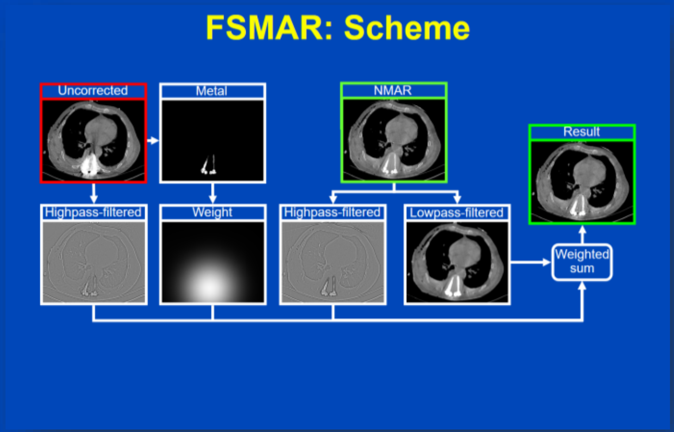

[1]E. Meyer, M. Kachelrieß. Normalized metal artifact reduction (NMAR) in computed tomography. Med. Phys. 37(10):5482-5493, Oct. 2010.
[2]E. Meyer, M. Kachelrieß. Frequency split metal artifact reduction (FSMAR) in CT. Med. Phys. 39(4):1904-1916, April 2012.

Summary on Deep MAR

- **Most common uses for networks:**
  - Improve image quality in image domain after MAR
  - Use network for the sinogram inpainting
  - Produce a prior image, e.g. for NMAR
- **Additional observations:**
  - Training data are often produced by segmenting an artifact-free CT image, adding metal and applying a polychromatic forward projection to different types of tissue separately.
  - As of today, it seems hard to outperform NMAR, or hard to give convincing clinical examples.

Resolution Improvement Example

- 2D U-net to converts 5 mm thick images into 1 mm ones.
- E.g. to “replace a scanning protocol for a 1 mm slice with a 5 mm protocol”

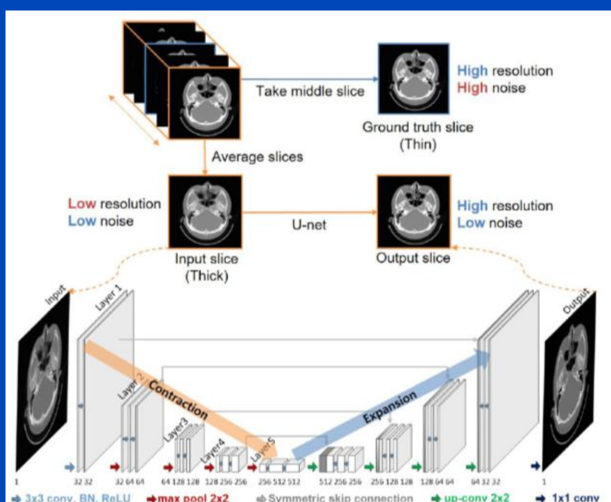

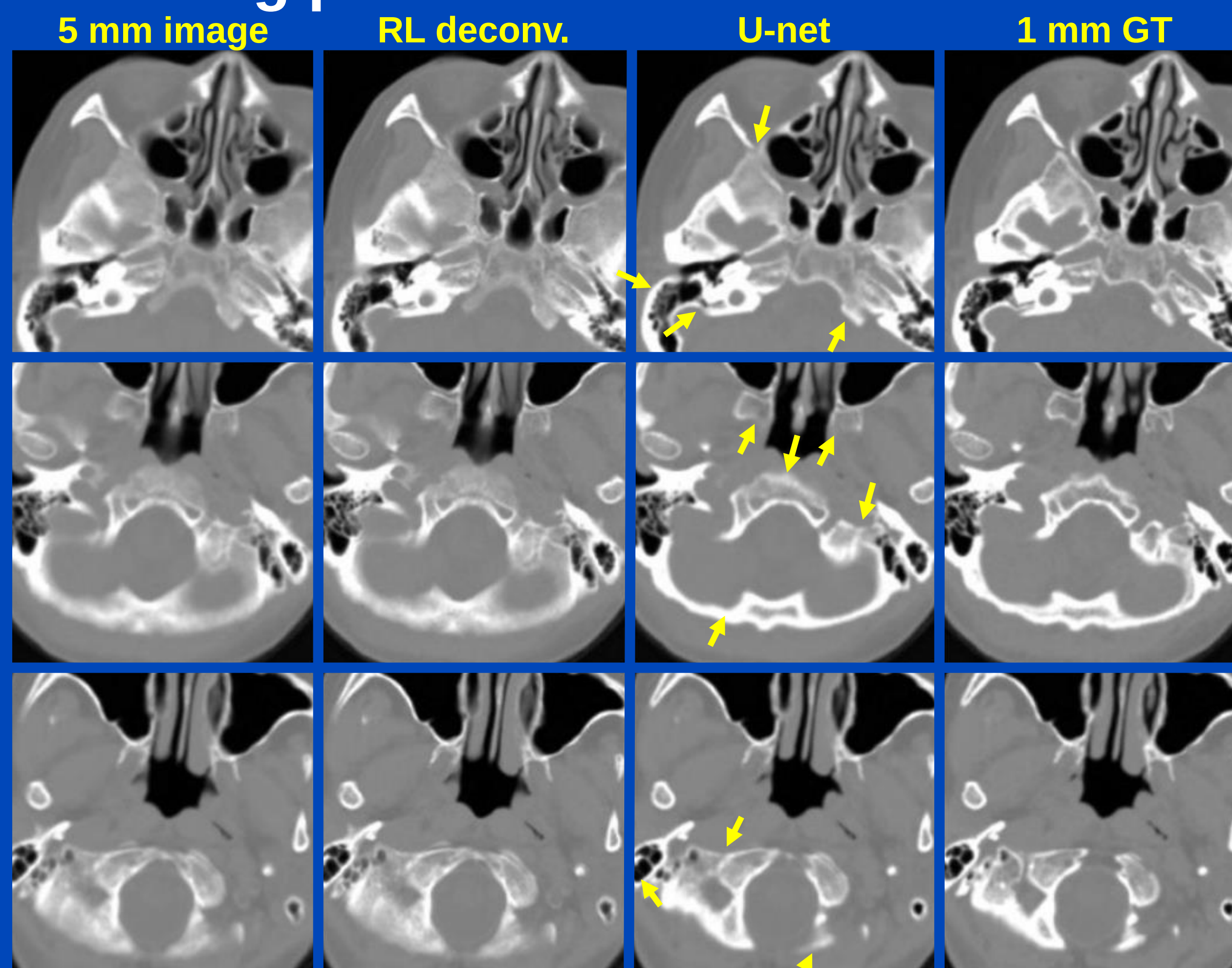

Junyoung Park, Donghwi Hwang, Kyeong Yun Kim, Seung Kwan Kang, Yu Kyeong Kim and Jae Sung Lee. Computed tomography super-resolution using deep convolutional neural network. Phys. Med. Biol. 63: 145011, 2018

dkfz.

Canon's PIQE

- PIQE (precise IQ engine) is trained to convert low resolution images into high resolution images
- Training data are taken from Canon's Precision CT that has small detector pixels (0.25 mm at iso).
- Claims:
  - Improved visualization of plaque
  - Reduction in blooming artifacts

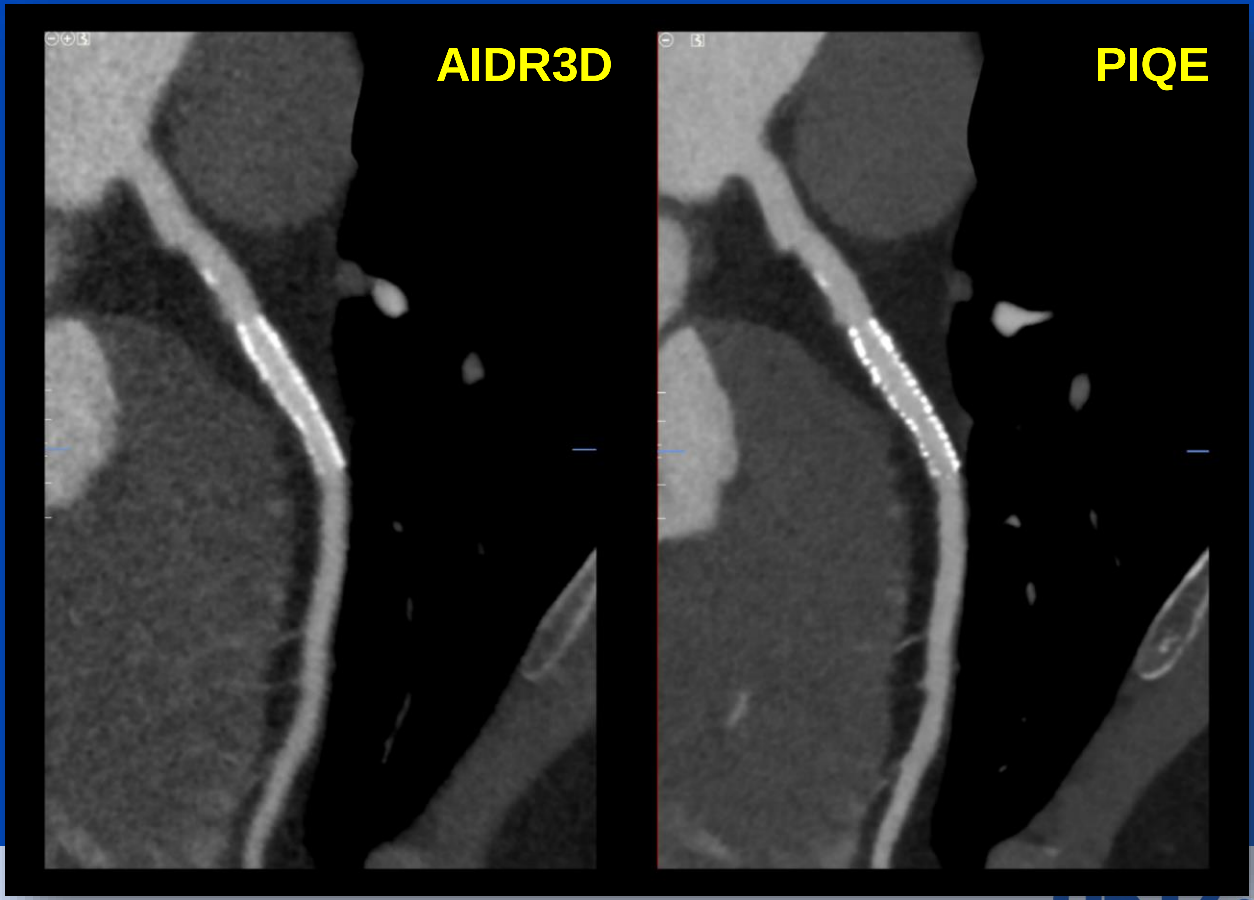

Image taken from at.medical.canon

Sparse View Restoration Example

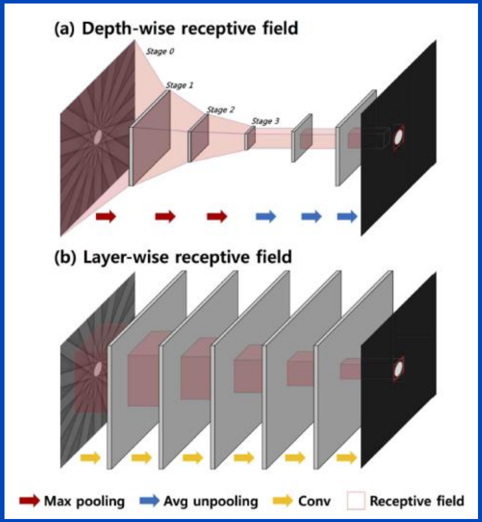

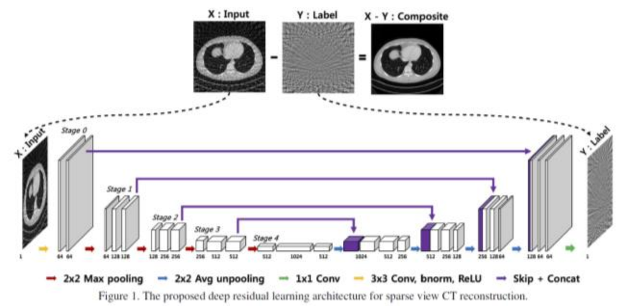

Figure 1. The proposed deep residual learning architecture for sparse view CT reconstruction.

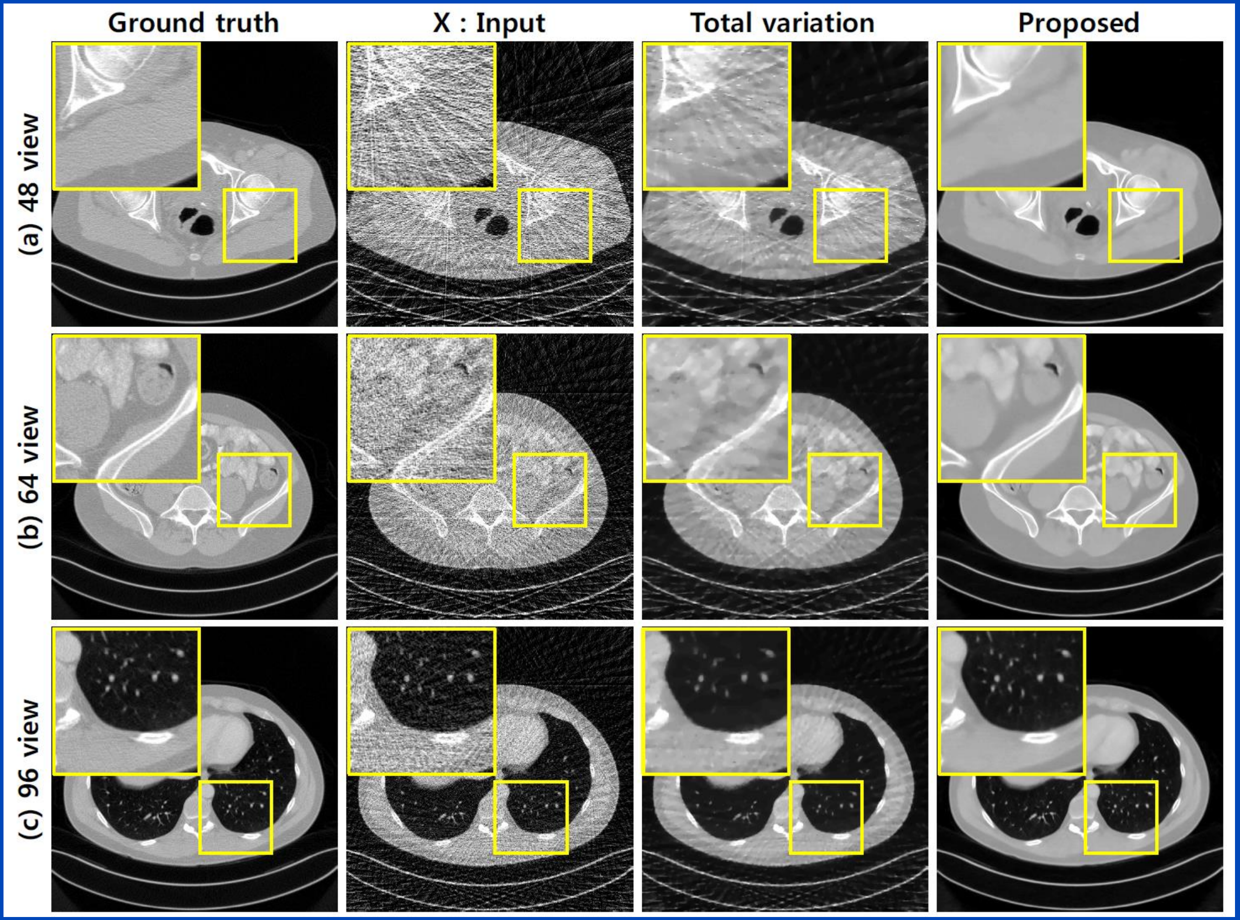

Yo Seob Han, Jaejun Yoo and Jong Chul Ye. Deep Residual Learning for Compressed Sensing CT Reconstruction via Persistent Homology Analysis. ArXiv 2016.

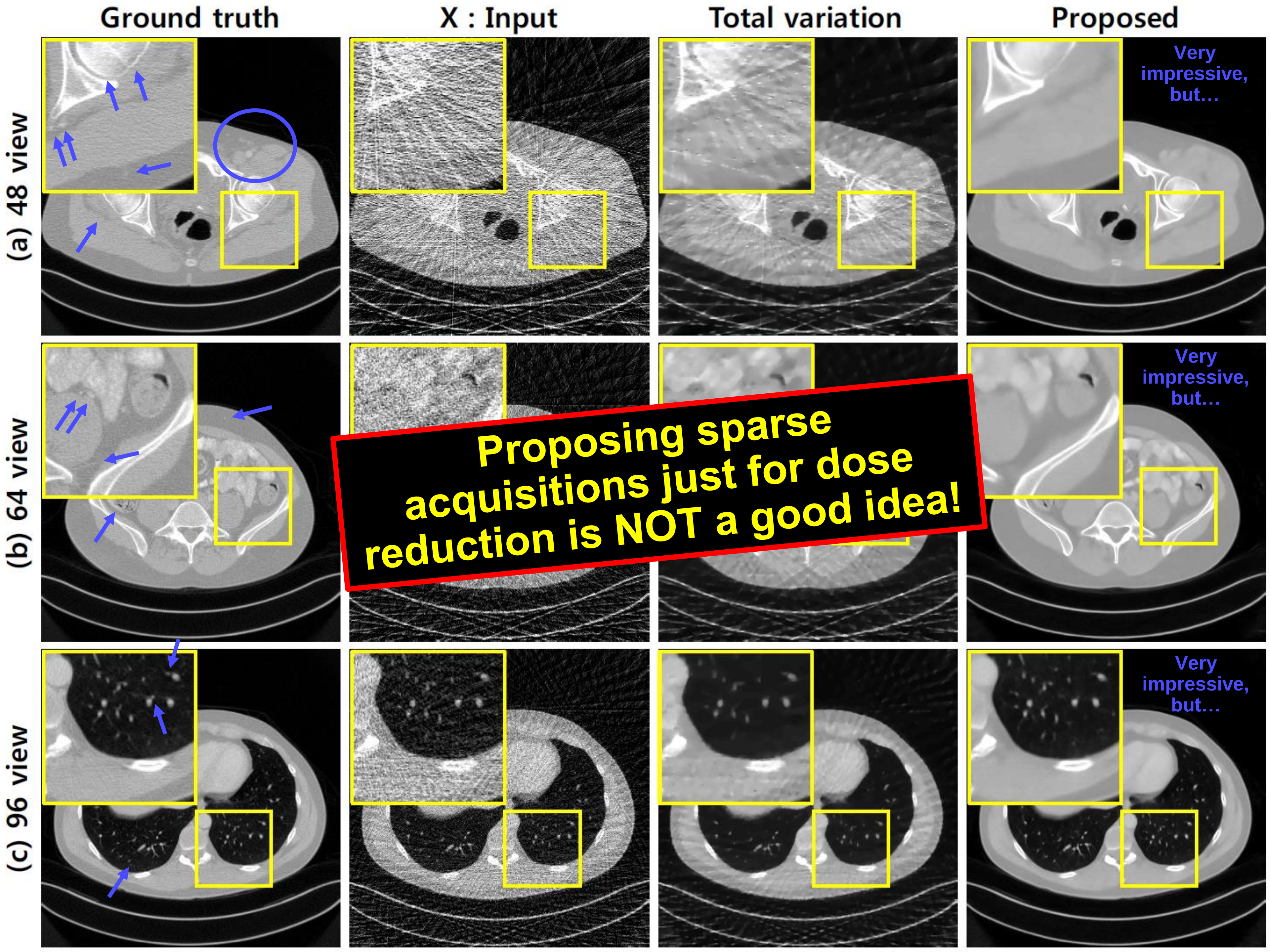
Ground truth
X : Input
Total variation
Proposed
(a) 48 view
(b) 64 view
(c) 96 view
Very impressive, but…
Very impressive, but…
Very impressive, but…
Proposing sparse acquisitions just for dose reduction is NOT a good idea!

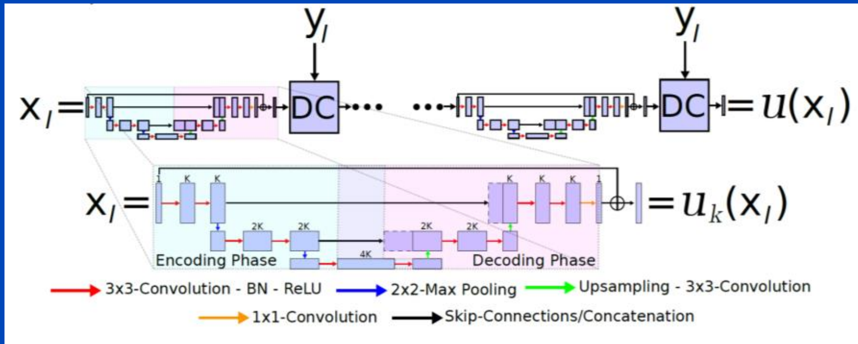

Sparse CT Recon with Data Consistency Layers (DCLs)

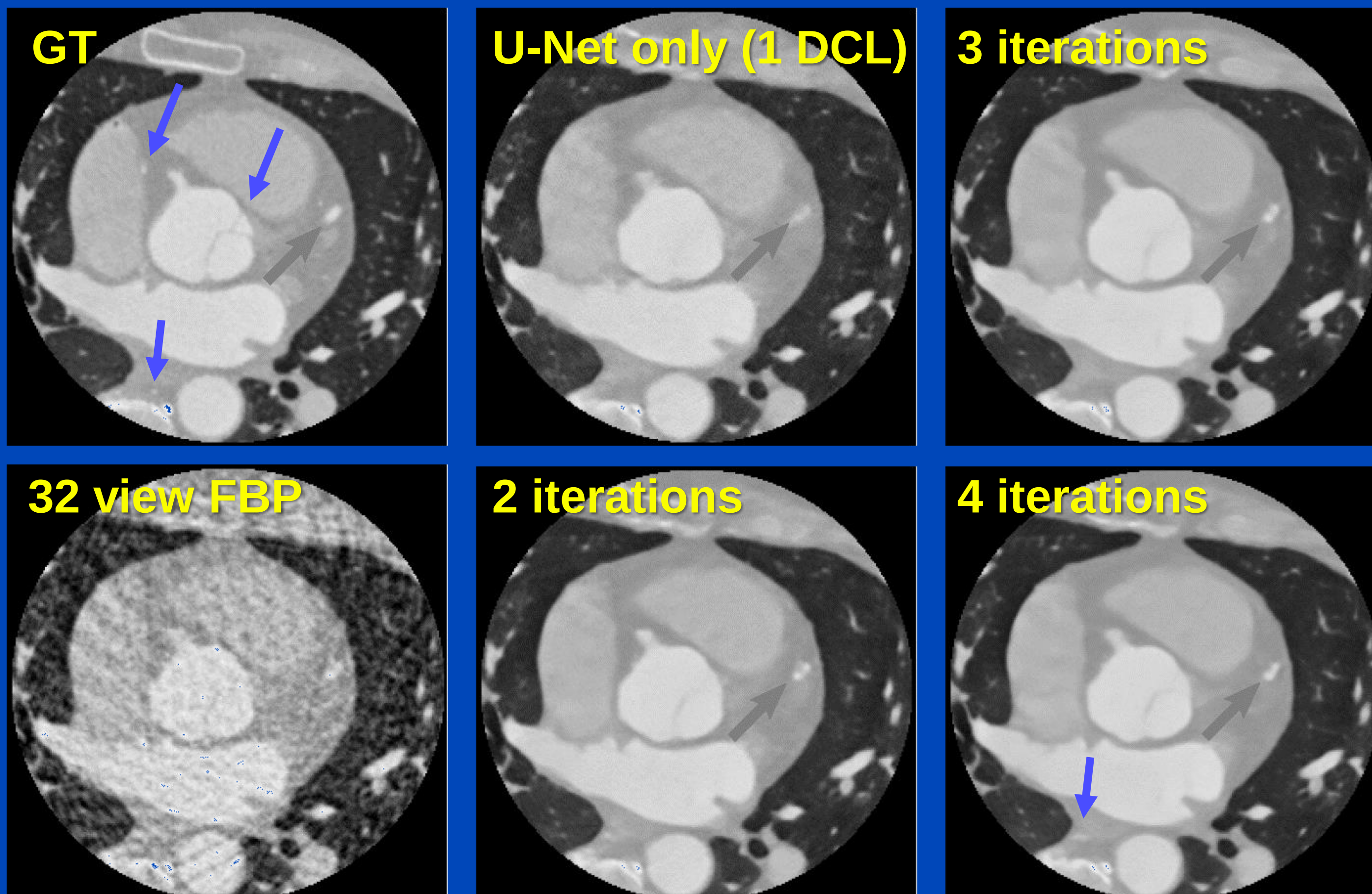

A. Kofler, M. Haltmeier, C. Kolbitsch, M. Kachelrieß, and M. Dewey. A U-Nets Cascade for Sparse View Computed Tomography, MICCAI 2018

Part 2:

Noise Reduction

Noise Removal Example 2

- **Task: Reduce noise from low dose CT images.**
- **A conditional generative adversarial networks (GAN) is used**
- **Generator *G*:**
  - **3D CNN that operates on small cardiac CT sub volumes**
  - **Seven 3×3×3 convolutional layers yielding a receptive field of 15×15×15 voxels for each destination voxel**
  - **Depths (features) from 32 to 128**
  - **Batch norm only in the hidden layers**
  - **Subtracting skip connection**
- **Discriminator *D*:**
  - **Sees either routine dose image or a generator-denoised low dose image**
  - **Two 3×3×3 layers followed by several 3×3 layers with varying strides**
  - **Feedback from *D* prevents smoothing.**
- **Training:**
  - **Unenhanced (why?) patient data acquired with Philips Briliance iCT 256 at 120 kV.**
  - **Two scans (why?) per patient, one with 0.2 mSv and one with 0.9 mSv effective dose.**

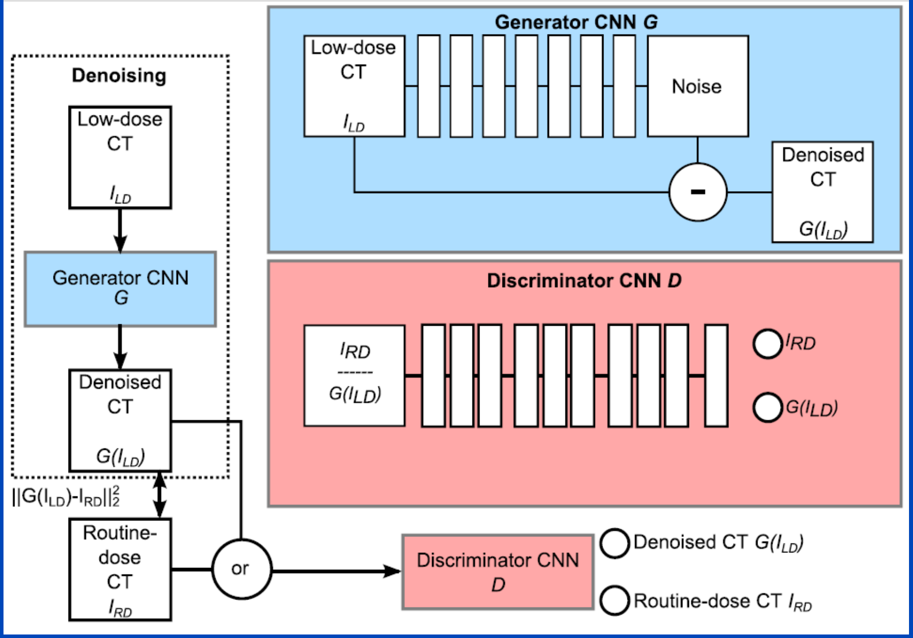

J. Wolterink, T. Leiner, M. Viergever, and I. Išgum. Generative Adversarial Networks for Noise Reduction in Low-Dose CT. IEEE TMI 36(12):2536-2544, Dec. 2017.

Noise Removal Example 2

- G_1 and G_2 include supervised learning and thus perform only with phantom measurements.
- G_3 is unsupervised.
- G_3 is said to generate images with a more similar appearance to the routine-dose CT. Feedback from the discriminator *D* prevents smoothing the image.

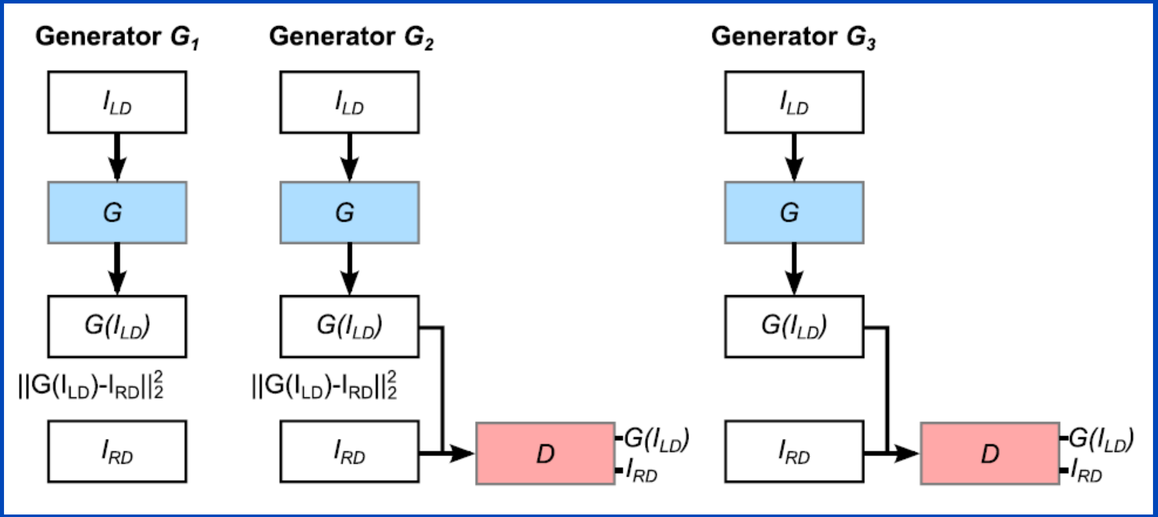

J. Wolterink, T. Leiner, M. Viergever, and I. Išgum. Generative Adversarial Networks for Noise Reduction in Low-Dose CT. IEEE TMI 36(12):2536-2544, Dec. 2017.

Noise Removal Example 2

Low dose image (0.2 mSv)

J. Wolterink, T. Leiner, M. Viergever, and I. Išgum. Generative Adversarial Networks for Noise Reduction in Low-Dose CT. IEEE TMI 36(12):2536-2544, Dec. 2017.

Noise Removal Example 2

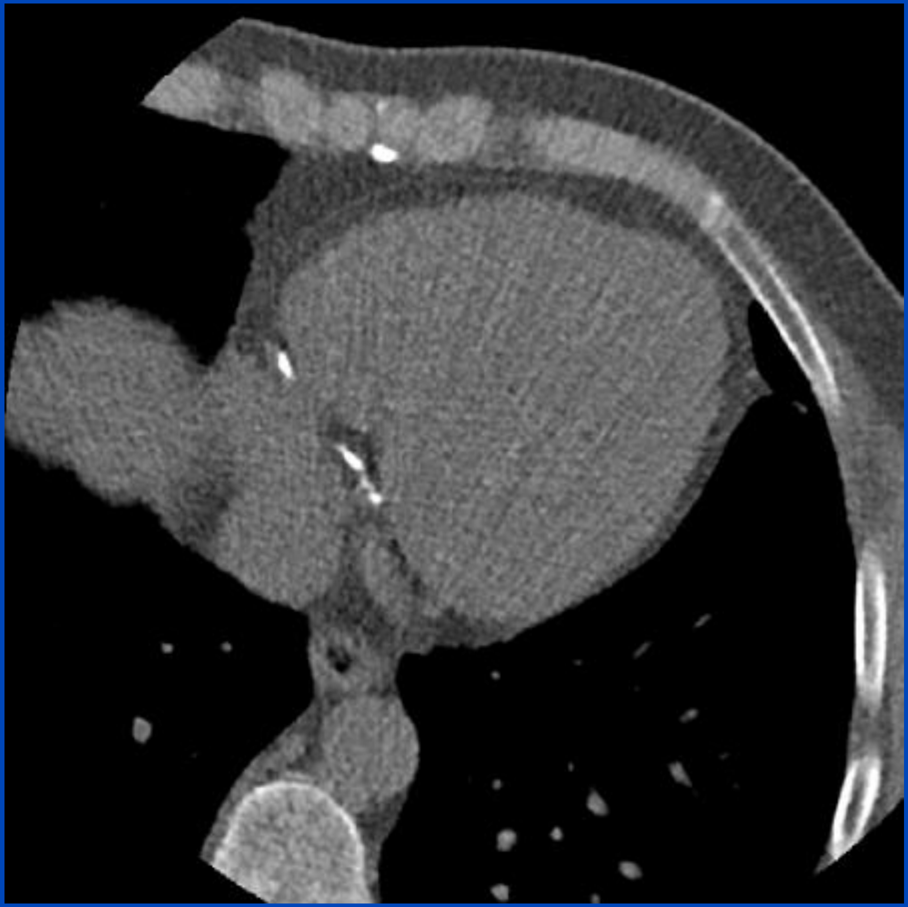

iDose level 3 reconstruction (0.2 mSv)

J. Wolterink, T. Leiner, M. Viergever, and I. Išgum. Generative Adversarial Networks for Noise Reduction in Low-Dose CT. IEEE TMI 36(12):2536-2544, Dec. 2017.

Noise Removal Example 2

Denoised low dose image (0.2 mSv)

J. Wolterink, T. Leiner, M. Viergever, and I. Išgum. Generative Adversarial Networks for Noise Reduction in Low-Dose CT. IEEE TMI 36(12):2536-2544, Dec. 2017.

Noise Removal Example 2

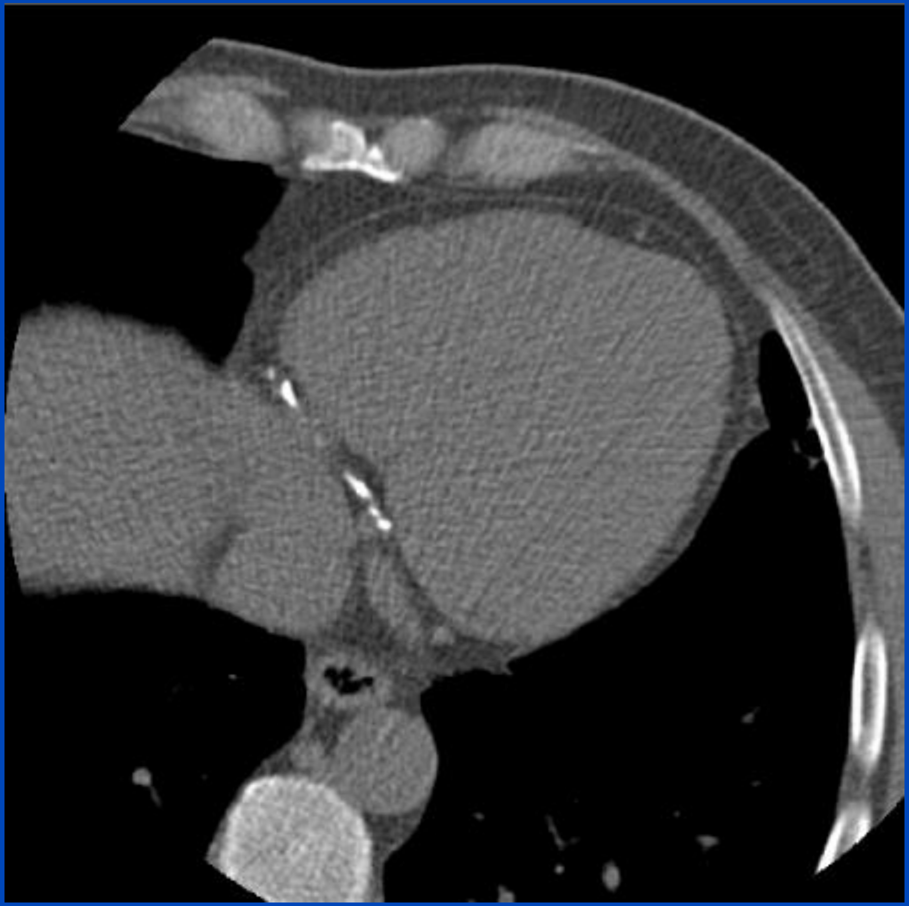

Normal dose image (0.9 mSv)

J. Wolterink, T. Leiner, M. Viergever, and I. Išgum. Generative Adversarial Networks for Noise Reduction in Low-Dose CT. IEEE TMI 36(12):2536-2544, Dec. 2017.

Noise Removal Example 3

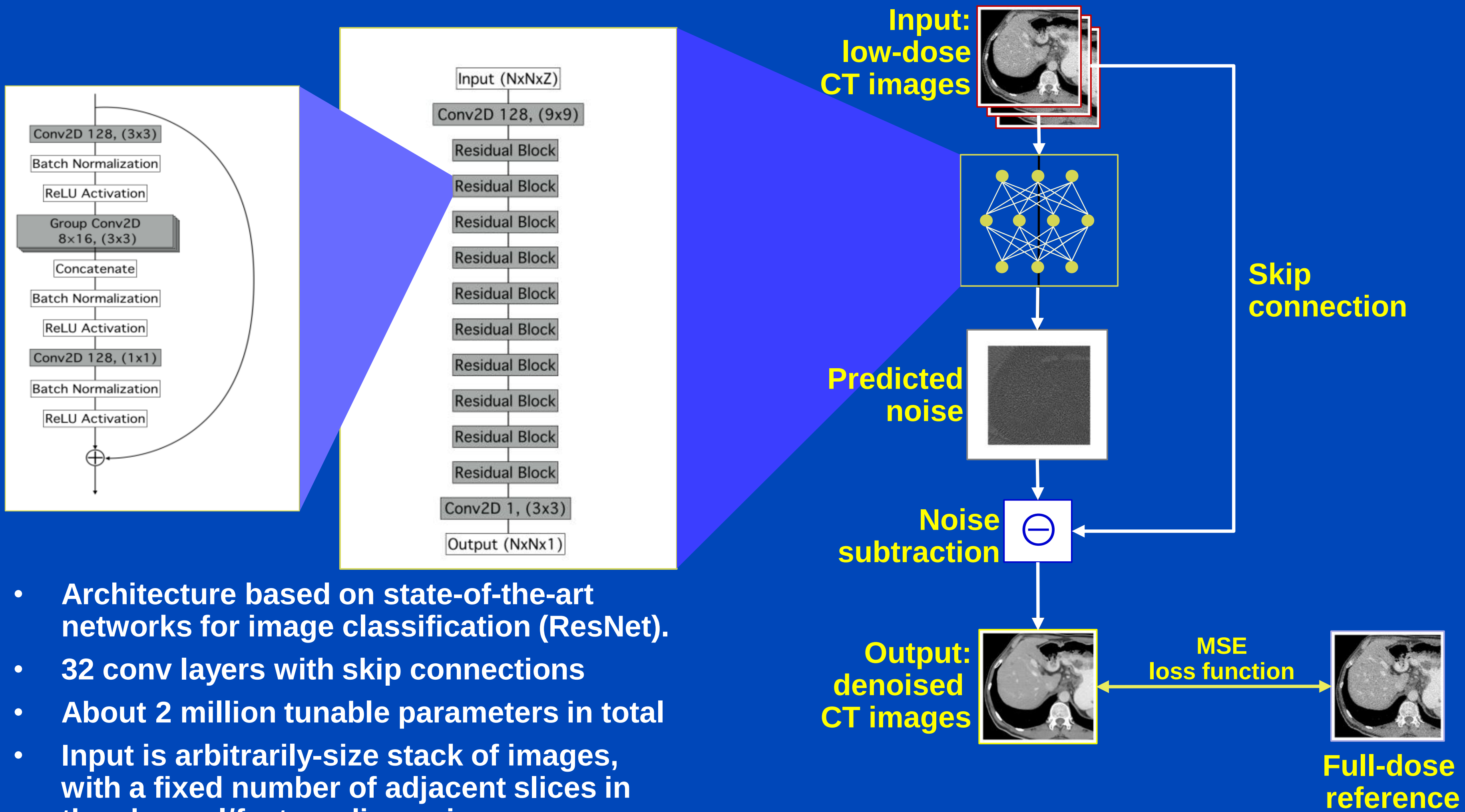

- Architecture based on state-of-the-art networks for image classification (ResNet).
- 32 conv layers with skip connections
- About 2 million tunable parameters in total
- Input is arbitrarily-size stack of images, with a fixed number of adjacent slices in the channel/feature dimension.

Andrew D. Missert, Shuai Leng, Lifeng Yu, and Cynthia H. McCollough. Noise Subtraction for Low-Dose CT Images Using a Deep Convolutional Neural Network. Proceedings of the 5th CT-Meeting: 399-402, 2018.

Noise Removal Example 3

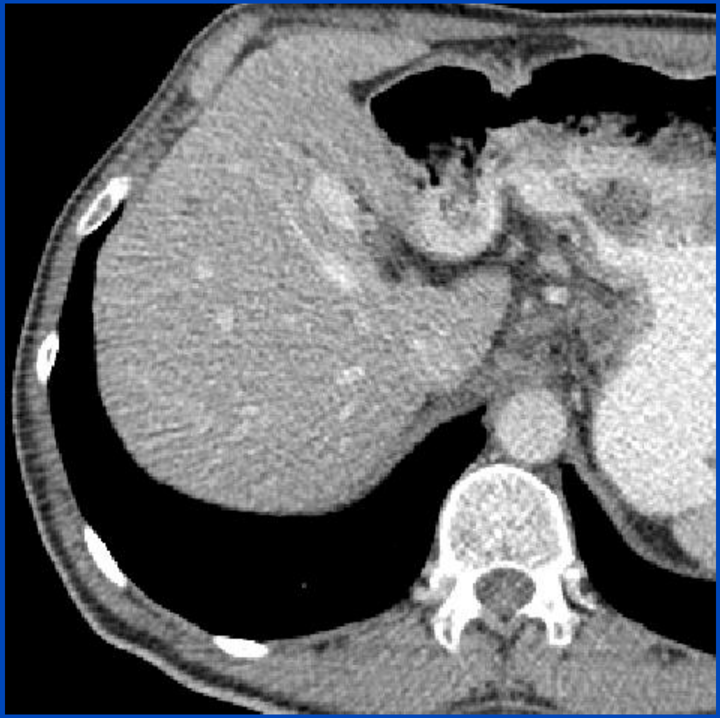

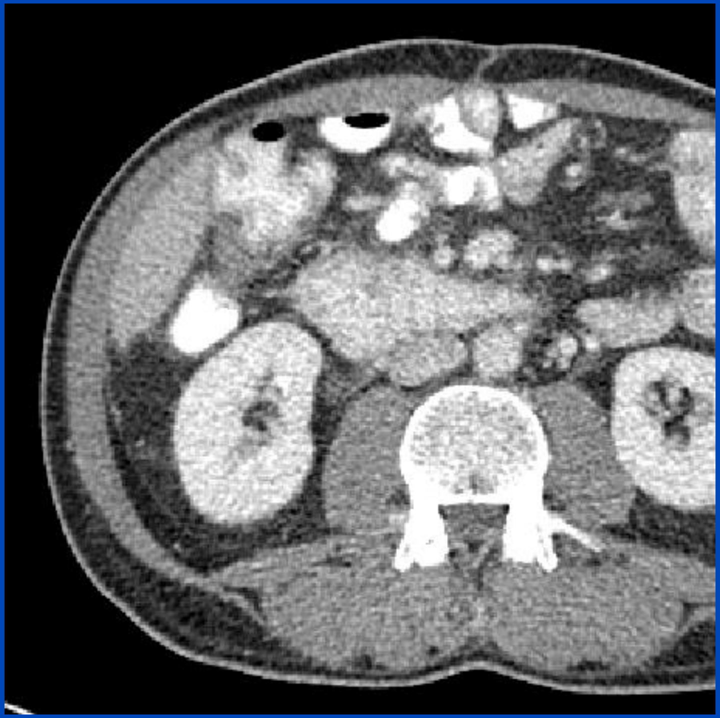

Low dose images (1/4 of full dose)

Andrew D. Missert, Shuai Leng, Lifeng Yu, and Cynthia H. McCollough. Noise Subtraction for Low-Dose CT Images Using a Deep Convolutional Neural Network. Proceedings of the 5th CT-Meeting: 399-402, 2018.

Noise Removal Example 3

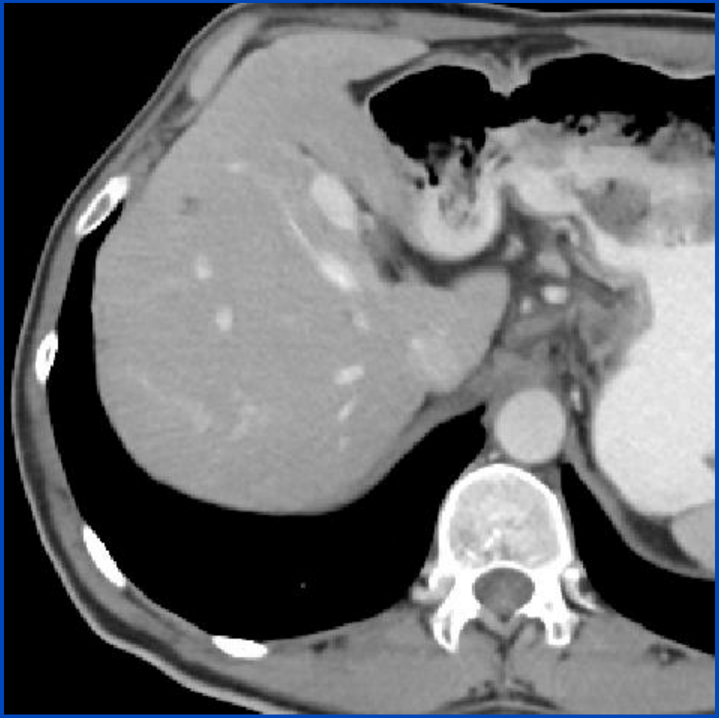

Denoised low dose

Andrew D. Missert, Shuai Leng, Lifeng Yu, and Cynthia H. McCollough. Noise Subtraction for Low-Dose CT Images Using a Deep Convolutional Neural Network. Proceedings of the 5th CT-Meeting: 399-402, 2018.

Noise Removal Example 3

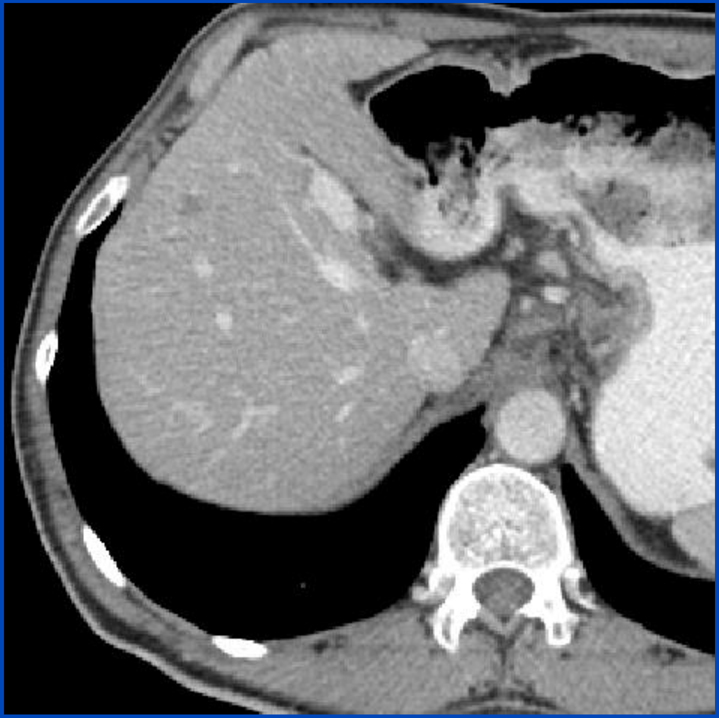

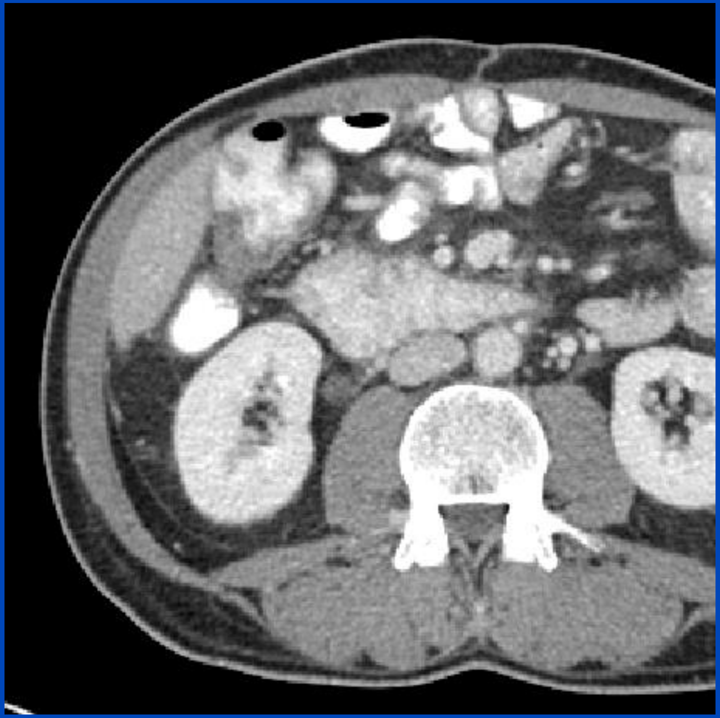

Full dose

Noise Removal Example 3

Denoised full dose

Noise Removal Example 3

Denoised low dose

Noise Removal: Canon's AiCE

- Advanced intelligent Clear-IQ Engine (AiCE)
- Trained to restore low-dose CT data to match the properties of FIRST, the model-based IR of Canon.
- FIRST is applied to high-dose CT images to obtain a high fidelity training target

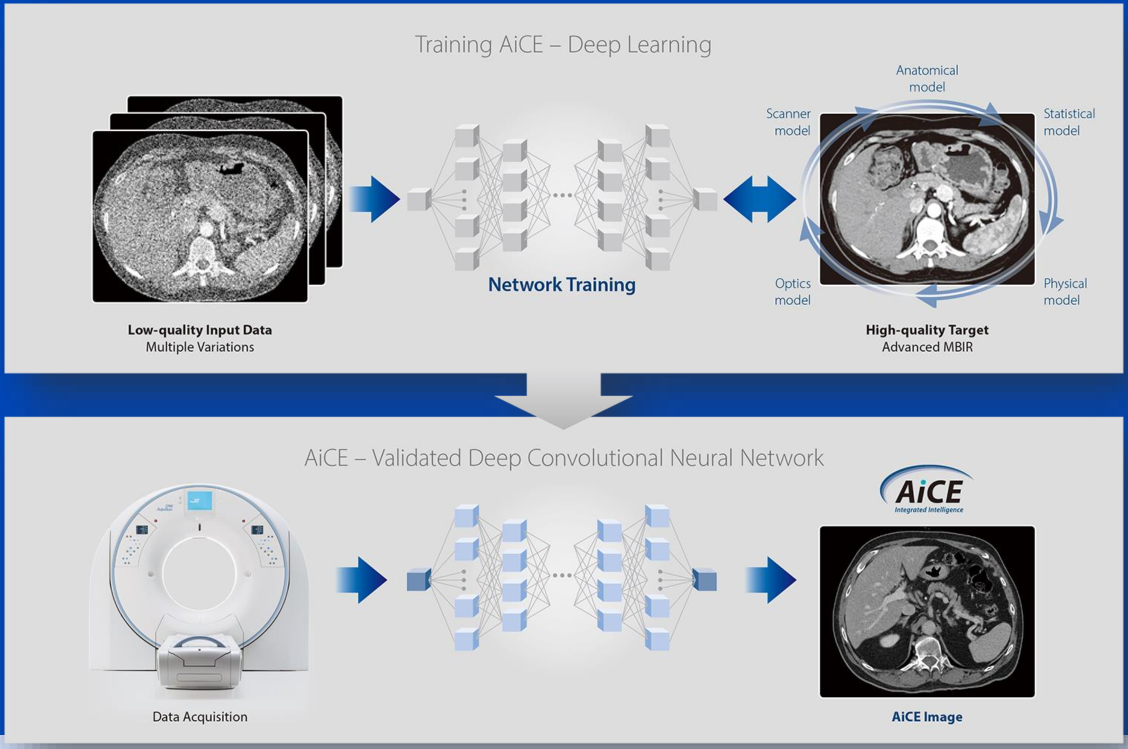

K. Boedeker. AiCE Deep Learning Reconstruction: Bringing the Power of Ultra High Resolution CT to Routine Imaging. Whitepaper, Canon, 2019.

U = 100 kV
CTDI = 0.6 mGy
DLP = 24.7 mGy·cm
D_{eff} = 0.35 mSv

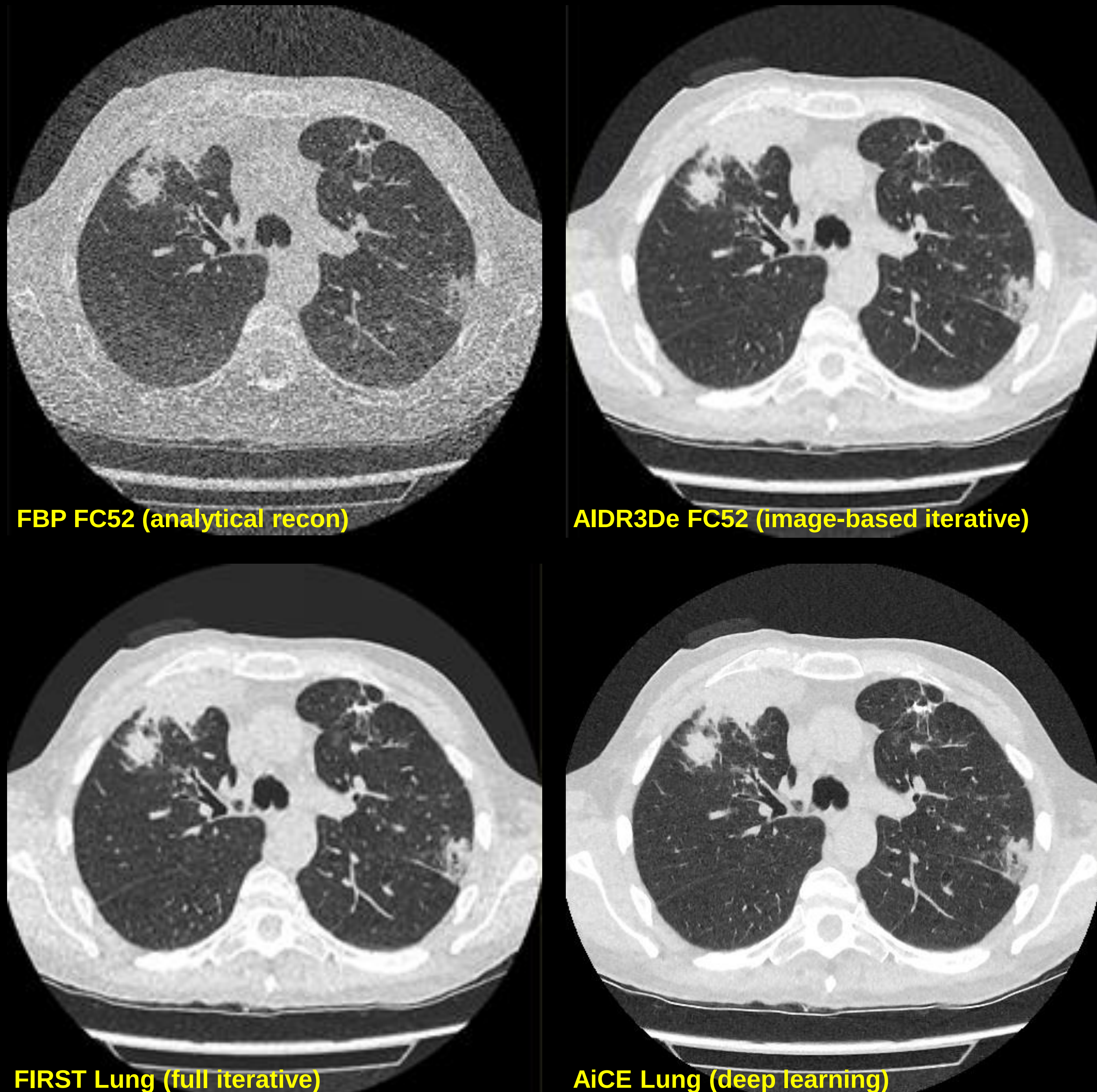

Courtesy of
Radboudumc,
the Netherlands

Noise Reduction: GE's True Fidelity

- Based on a deep CNN
- Trained to restore low-dose CT data to match the properties of high quality FBP datasets.
- Said to preserve noise texture and NPS

The 20 cm water phantom (GE Healthcare, WI, US) was scanned on Revolution CT with two CTDIvol levels: 4.9mGy and 15.1mGy, and 2.5 mm thick images were reconstructed using FBP, ASiR-V 100% and DLIR-H (Fig. 11a). ASiR-V 100% and DLIR-H were selected for the highest potential visible change in image texture relative to the FBP reference at higher dose, for a challenging setup to compare the impact of the iterative reconstruction and deep-learning technologies on image appearance. The normalized NPS curves (Fig. 11b) show that images of low-dose DLIR have the same NPS characteristics as the images of high-dose FBP, whereas iterative reconstruction produces results that are clearly different.

FBP, 15.1 mGy | ASiR-V 100%, 4.9 mGy | DLIR-H, 4.9 mGy

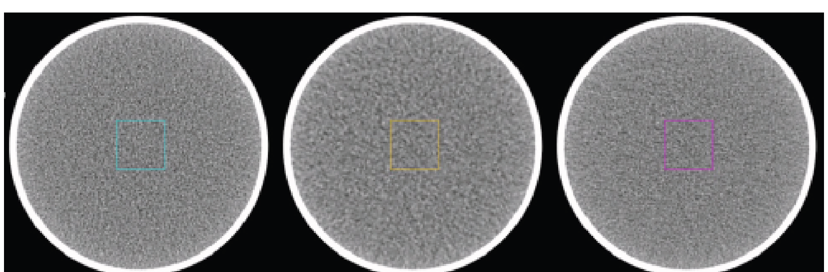

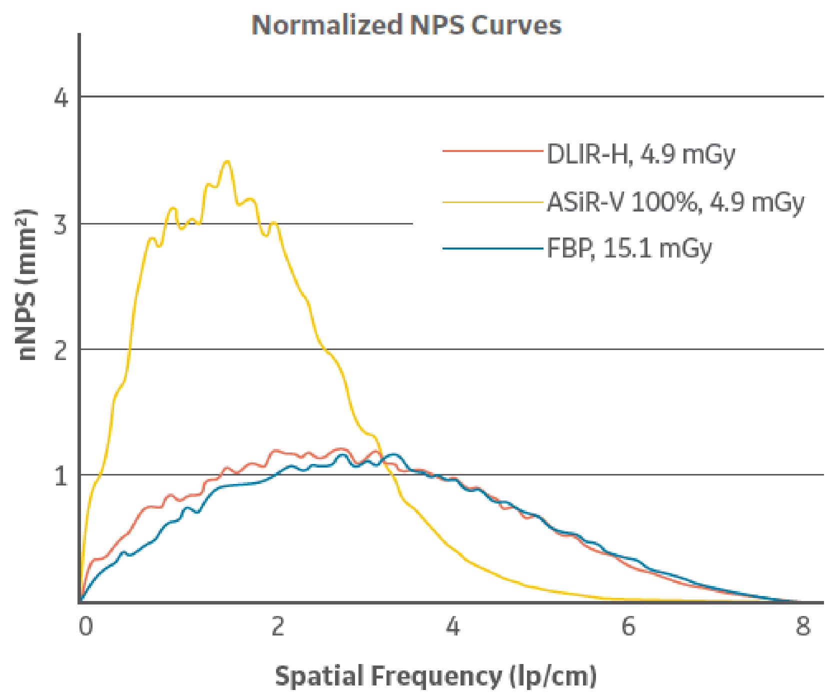

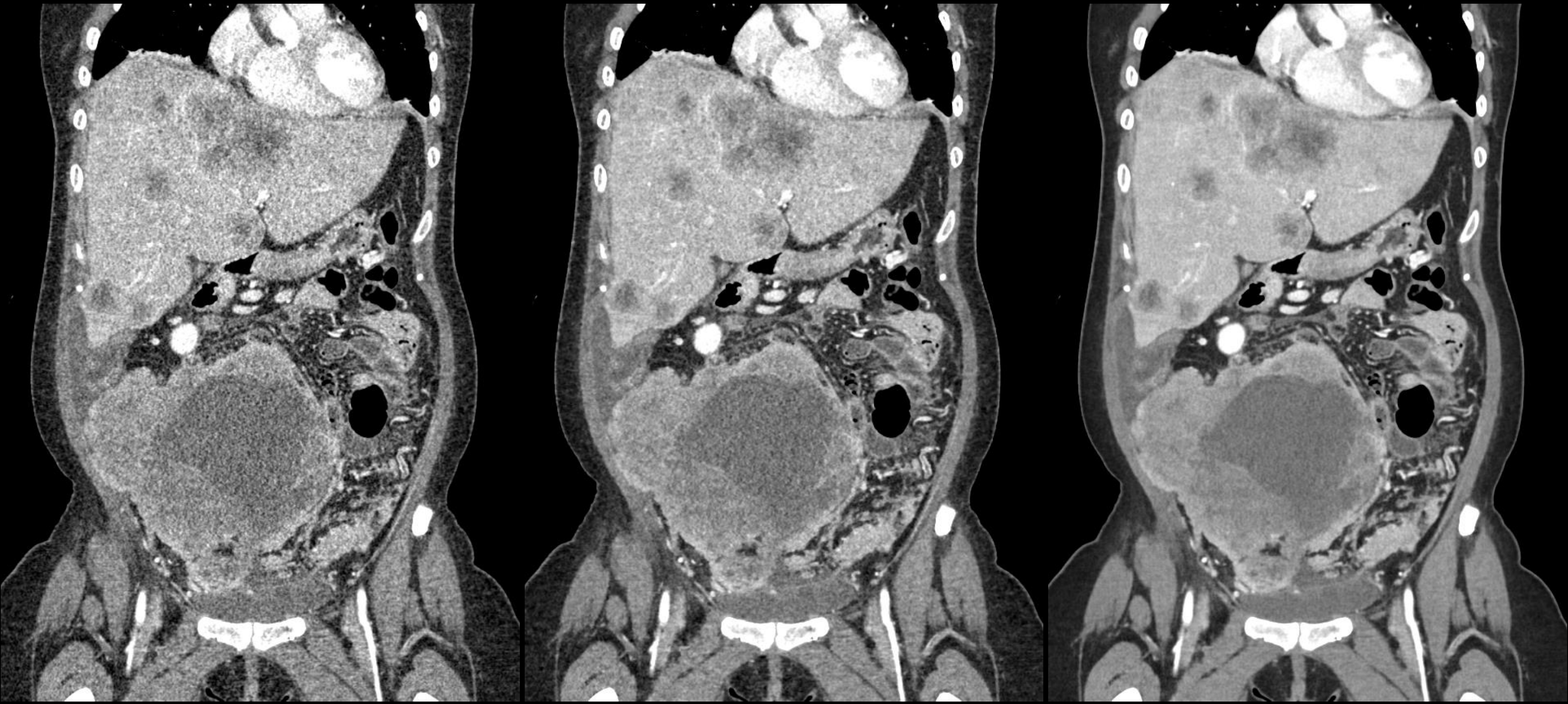

FBP

ASIR V 50%

True Fidelity

Courtesy of GE Healthcare

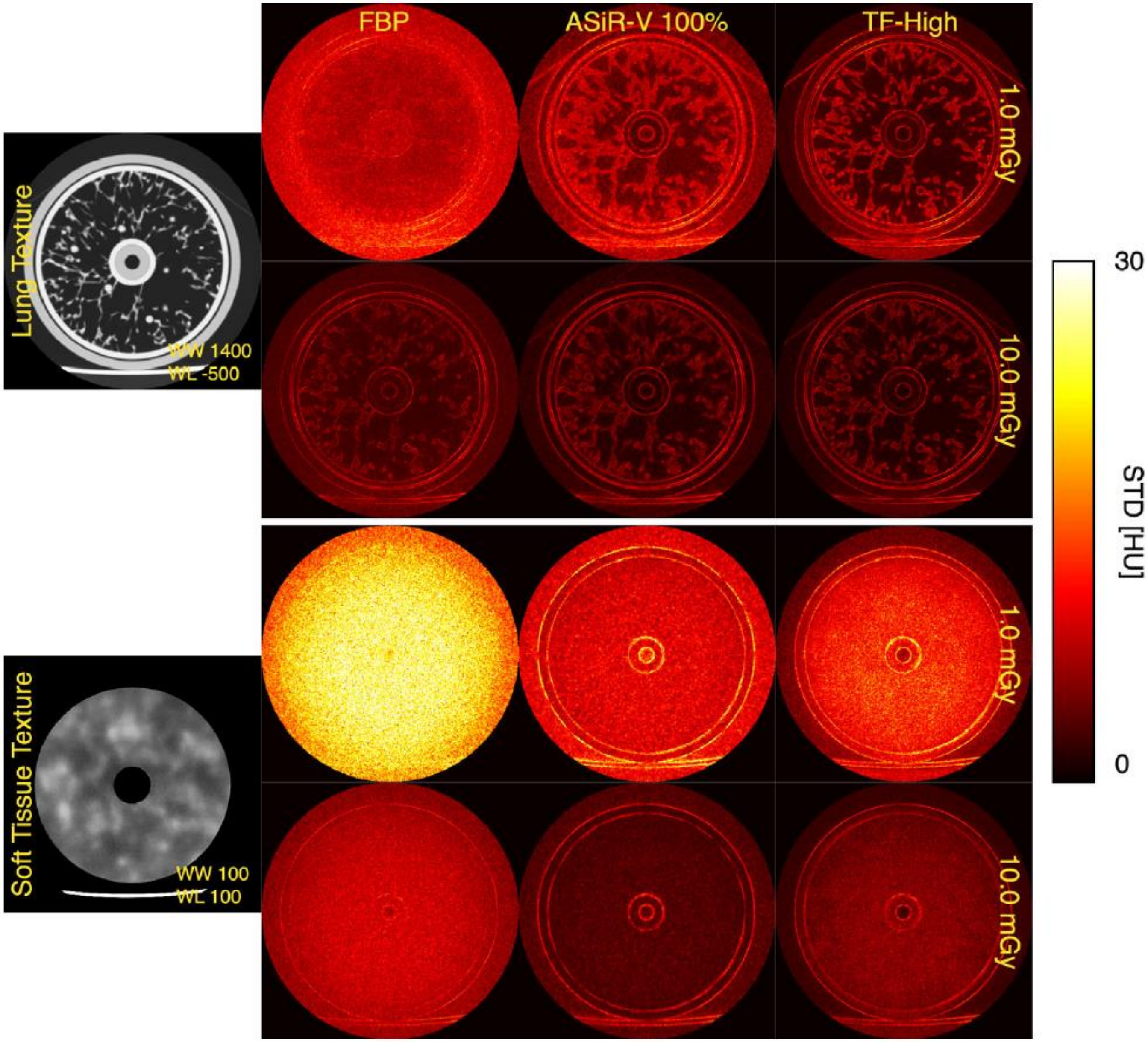

Solomon et al. Noise and spatial resolution properties of a commercially available deep learning-based CT reconstruction algorithm. Med. Phys. 47(9):3961-3971, Sept. 2020

Noise Removal: Philips' Precise Image

- Noise-injected data serve as low dose examples while their original reconstructions are the labels. A CNN learns how to denoise the low dose images.

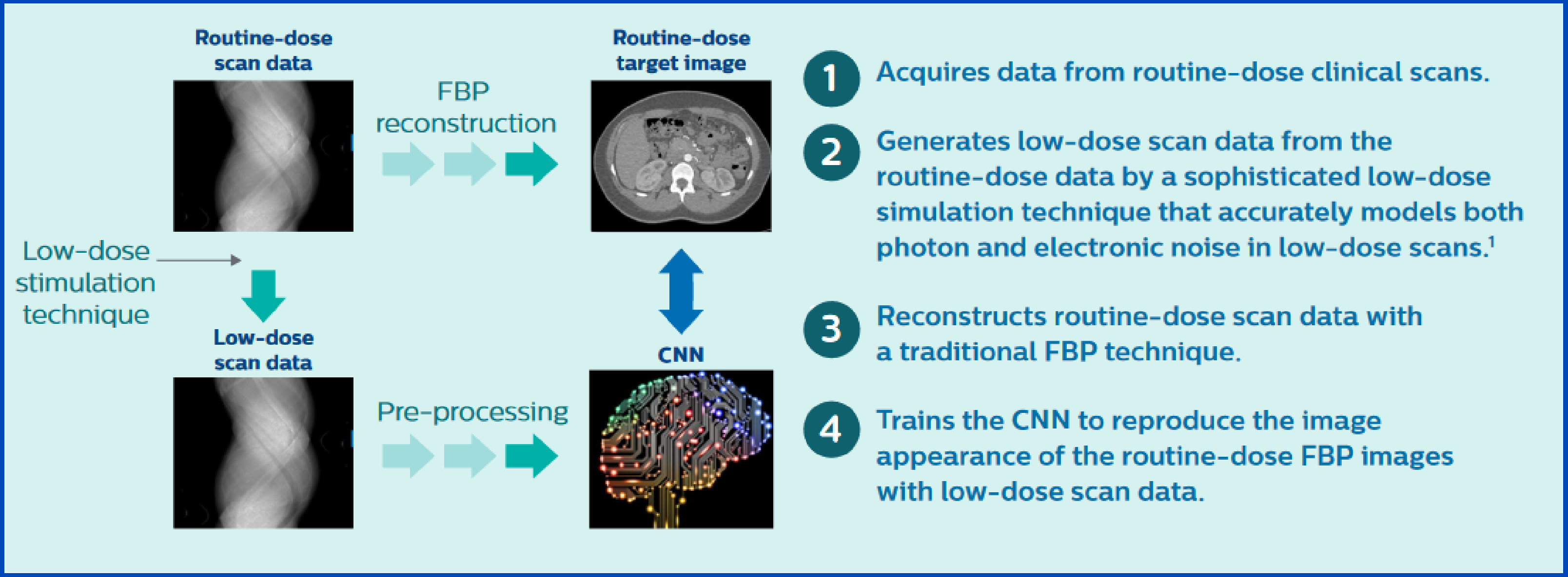

Taken from https://www.philips.com/c-dam/b2bhc/master/resource-catalog/landing/precise-suite/incisive_precise_image.pdf

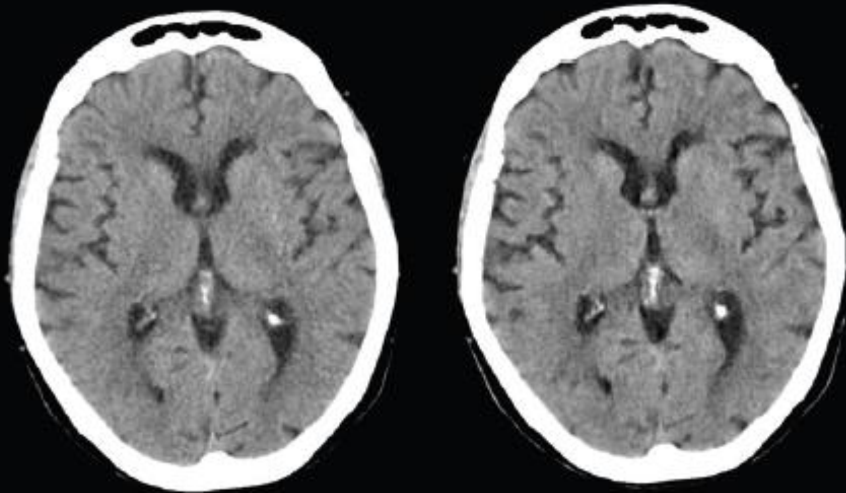

iDose⁴ 1.4 mSv

Precise Image 0.7 mSv

iDose⁴ 5.1 mSv

Precise Image 2.6 mSv

iDose⁴ 1.5 mSv

Precise Image 0.75 mSv

iDose⁴ 5.4 mSv

Precise Image 2.6 mSv

Study	Topic	Dose Reduction	Assessment	Reconstruction
Beregi et al., 2022	low-dose abdomen phantom	79%	objective	AiCE
Hirai et al., 2022a	low-dose multiphase hepatic	52%	objective, subjective	AiCE
Hirai et al., 2022b	low-dose pediatric 80 kV	54%	objective, subjective	AiCE
Jin et al., 2022	low-dose interstitial lung disease	62%	objective, subjective	AiCE
Loffroy et al., 2022	low-dose head & neck	43%	objective, subjective	AiCE
Sun et al., 2022	ultra-low-dose urolithiasis	75%	objective, subjective	AiCE
Yoshioka et al., 2022	low-dose contrast abdomen	40%	objective, subjective	AiCE
Awai et al., 2021	low-dose abdominal UHR	30%	objective, subjective	AiCE
Dillman et al., 2021	pediatric detectability	52%	objective, subjective	AiCE
Loffroy et al., 2021	cardiac CTA stroke	40%	objective, subjective	AiCE
Kalra et al., 2020	low-dose lesion detection	83%	subjective	AiCE
Willemink et al., 2023	principles & prospects	71%	mixed	meta
Strigari et al., 2023	image quality phantom	96%	objective	Precise Image
Deng et al., 2022	ultra-low-dose pulmonary nodules phantom	72%	objective, subjective	TrueFidelity
Lee et al., 2021	pediatric chest & abdomen	63%	objective, subjective	TrueFidelity

- Awai, Kazuo, et al. "Deep learning reconstruction of equilibrium phase CT images in obese patients." *European Journal of Radiology* 133 (2020): 109349.
- Awai, Kazuo, et al. "Diagnostic value of deep learning reconstruction for radiation dose reduction at abdominal ultra-high-resolution CT." *European radiology* 31 (2021): 4700-4709.
- Beregi, Jean-Paul, et al. "Comparison of two deep learning image reconstruction algorithms in chest CT images: a task-based image quality assessment on phantom data." *Diagnostic and Interventional Imaging* 103.1 (2022): 21-30.
- Beregi, Jean-Paul, et al. "Comparison of two versions of a deep learning image reconstruction algorithm on CT image quality and dose reduction: A phantom study." *Medical Physics* 48.10 (2021): 5743-5755.
- Beregi, Jean-Paul, et al. "Effect of a new deep learning image reconstruction algorithm for abdominal computed tomography imaging on image quality and dose reduction compared with two iterative reconstruction algorithms: a phantom study." *Quantitative Imaging in Medicine and Surgery* 12.1 (2022): 229.
- Boone, John M., et al. "Performance of high-resolution CT for detection and discrimination tasks related to stenotic lesions-a phantom study using model observers." *Medical Physics* (2022).
- Dabli, Djamel, et al. "Improved image quality and dose reduction in abdominal CT with deep-learning reconstruction algorithm: a phantom study." *European Radiology* 33.1 (2023): 699-710.
- Deng, Lei, et al. "The influence of a deep learning image reconstruction algorithm on the image quality and auto-analysis of pulmonary nodules at ultra-low dose chest CT: a phantom study." *Quantitative Imaging in Medicine and Surgery* 12.5 (2022): 2777.
- Dillman, Jonathan R., et al. "Improving image quality and reducing radiation dose for pediatric CT by using deep learning reconstruction." *Radiology* 298.1 (2021): 180-188.
- Frandon, Julien, et al. "Image quality and dose reduction opportunity of deep learning image reconstruction algorithm for CT: a phantom study." *European radiology* 30 (2020): 3951-3959.
- Hawkins, R.M., et al. "The future of CT: deep learning reconstruction." *Clinical radiology* 76.6 (2021): 407-415.
- Hirai, Toshinori, et al. "Radiation dose optimization potential of deep learning-based reconstruction for multiphase hepatic CT: A clinical and phantom study." *European Journal of Radiology* 151 (2022): 110280.
- Hirai, Toshinori, et al. "Radiation dose reduction for 80-kVp pediatric CT using deep learning–based reconstruction: a clinical and phantom study." *American Journal of Roentgenology* 219.2 (2022): 315-324.
- Hwang, Dae Hyun, et al. "Improvement in Image Quality and Visibility of Coronary Arteries, Stents, and Valve Structures on CT Angiography by Deep Learning Reconstruction." *Korean Journal of Radiology* 23.11 (2022): 1044-1054.
- Ishigami, Kousei, et al. "Impact of a new deep-learning-based reconstruction algorithm on image quality in ultra-high-resolution CT: clinical observational and phantom studies." *The British Journal of Radiology* 96.1141 (2023): 20220731.
- Ito, Katsuyoshi, et al. "Assessment of gastric wall structure using ultra-high-resolution computed tomography." *European Journal of Radiology* 146 (2022): 110067.
- Jahnke, Paul, et al. "Deep learning reconstruction improves radiomics feature stability and discriminative power in abdominal CT imaging: A phantom study." *European radiology* 32.7 (2022): 4587-4595.
- Jang, Joo Yeon, et al. "Comparison of a Deep Learning-Based Reconstruction Algorithm with Filtered Back Projection and Iterative Reconstruction Algorithms for Pediatric Abdominopelvic CT." *Korean Journal of Radiology* 23.7 (2022): 752.
- Jin, Zhengyu, et al. "Can deep learning improve image quality of low-dose CT: a prospective study in interstitial lung disease." *European Radiology* (2022): 1-12.
- Jin, Zhengyu, et al. "Image quality comparison of lower extremity CTA between CT routine reconstruction algorithms and deep learning reconstruction." *BMC Medical Imaging* 23.1 (2023): 33.
- Johnsson, Åse A., et al. "Evaluation of deep-learning image reconstruction for chest CT examinations at two different dose levels." *Journal of Applied Clinical Medical Physics* (2022): e13871.
- Kalra, Mannudeep, et al. "Image quality and lesion detection on deep learning reconstruction and iterative reconstruction of submillisievert chest and abdominal CT." *American Journal of Roentgenology* 214.3 (2020): 566-573.
- Kato, Toyoyuki, et al. "Deep-learning reconstruction for ultra-low-dose lung CT: Volumetric measurement accuracy and reproducibility of artificial ground-glass nodules in a phantom study." *The British Journal of Radiology* 95.1130 (2022): 20210915.
- Kim, Young Hoon, et al. "Dose reduction potential of vendor-agnostic deep learning model in comparison with deep learning–based image reconstruction algorithm on CT: A phantom study." *European radiology* 32.2 (2022): 1247-1255.
- Lee, Mi-Jung, et al. "Image quality assessment of pediatric chest and abdomen CT by deep learning reconstruction." *BMC Medical Imaging* 21.1 (2021): 1-11.
- Li, Meng, et al. "The Value of Deep Learning Image Reconstruction in Improving the Quality of Low-Dose Chest CT Images." *Diagnostics* 12.10 (2022): 2560.
- Loffroy, Romaric, et al. "Deep learning reconstruction versus iterative reconstruction for cardiac CT angiography in a stroke imaging protocol: reduced radiation dose and improved image quality." *Quantitative Imaging in Medicine and Surgery* 11.1 (2021): 392.
- Loffroy, Romaric, et al. "Deep Learning-Based Reconstruction vs. Iterative Reconstruction for Quality of Low-Dose Head-and-Neck CT Angiography with Different Tube-Voltage Protocols in Emergency-Department Patients." *Diagnostics* 12.5 (2022): 1287.
- Marin, Daniele, et al. "Effect of deep learning image reconstruction in the prediction of resectability of pancreatic cancer: Diagnostic performance and reader confidence." *European journal of radiology* 141 (2021): 109825.
- Nakamoto, Yuji, et al. "Evaluation of moyamoya disease in CT angiography using ultra-high-resolution computed tomography: Application of deep learning reconstruction." *European Journal of Radiology* 151 (2022): 110294.
- Prokop, Mathias, et al. "Abdominopelvic CT image quality: evaluation of thin (0.5-mm) slices using deep learning reconstruction." *American Journal of Roentgenology* 220.3 (2023): 381-388.
- Sakuma, Hajime, et al. "Deep learning image reconstruction for improving image quality of contrast-enhanced dual-energy CT in abdomen." *European Radiology* 32.8 (2022): 5499-5507.
- Sechopoulos, Ioannis, et al. "Deep learning–based reconstruction may improve non-contrast cerebral CT imaging compared to other current reconstruction algorithms." *European radiology* 31 (2021): 5498-5506.
- Strigari, Lidia, et al. "Image quality evaluation of the Precise image CT deep learning reconstruction algorithm compared to Filtered Back-projection and iDose4: a phantom study at different dose levels." *Physica Medica* 106 (2023): 102517.
- Sun, Hao, et al. "Value of deep learning reconstruction at ultra-low-dose CT for evaluation of urolithiasis." *European radiology* 32.9 (2022): 5954-5963.
- Teixeira, Pedro, et al. "Clinical acceptance of deep learning reconstruction for abdominal CT imaging: objective and subjective image quality and low-contrast detectability assessment." *European Radiology* 32.5 (2022): 3161-3172.
- van der Molen, Aart J., et al. "The effect of deep learning reconstruction on abdominal CT densitometry and image quality: a systematic review and meta-analysis." *European Radiology* 32.5 (2022): 2921-2929.
- Wang, Yi-Ning, et al. "The impact of deep learning reconstruction on image quality and coronary CT angiography-derived fractional flow reserve values." *European Radiology* 32.11 (2022): 7918-7926.
- Willemink, Martin J., et al. "Deep Learning Image Reconstruction for CT: Technical Principles and Clinical Prospects." *Radiology* 306.3 (2023): e221257.
- Yang, Woo Jung, et al. "Cardiac CTA image quality of adaptive statistical iterative reconstruction-V versus deep learning reconstruction “TrueFidelity” in children with congenital heart disease." *Medicine* 101.42 (2022): e31169.
- Yokoyama, Kenichi, et al. "Image quality and radiologists’ subjective acceptance using model-based iterative and deep learning reconstructions as adjuncts to ultrahigh-resolution CT in low-dose contrast-enhanced abdominopelvic CT: phantom and clinical pilot studies." *Abdominal Radiology* (2022): 1-12.
- Yoshioka, Kunihiro, et al. "Deep learning reconstruction allows low-dose imaging while maintaining image quality: comparison of deep learning reconstruction and hybrid iterative reconstruction in contrast-enhanced abdominal CT." *Quantitative Imaging in Medicine and Surgery* 12.5 (2022): 2977.
- Yun, Sook Mi, et al. "CT iterative vs deep learning reconstruction: comparison of noise and sharpness." *European radiology* 31 (2021): 3156-3164.

True and Fake DECT

Existing true DECT approaches (for more than one decade):

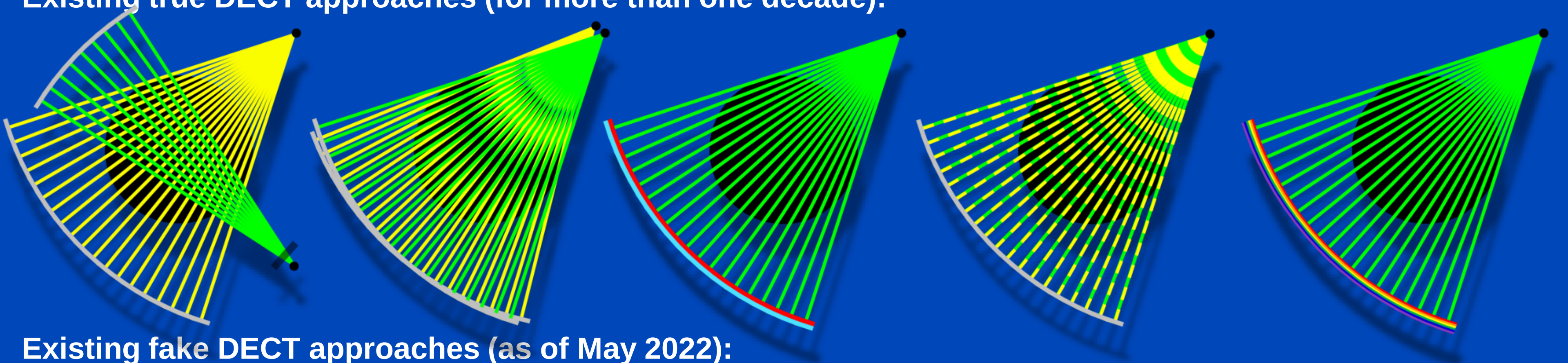

Existing fake DECT approaches (as of May 2022):

[1] J. Ma, Y. Liao, Y. Wang, S. Li, J. He, D. Zeng, Z. Bian, "Pseudo dual energy CT imaging using deep learning-based framework: basic material estimation", *SPIE Medical Imaging 2018*.

[2] W. Zhao, T. Lv, P. Gao, L. Shen, X. Dai, K. Cheng, M. Jia, Y. Chen, L. Xing, "A deep learning approach for dual-energy CT imaging using a single-energy CT data", *Fully3D 2019.*

[3] D. Lee, H. Kim, B. Choi, H. J. Kim, "Development of a deep neural network for generating synthetic dual-energy chest x-ray images with single x-ray exposure", PMB 64(11), 2019.

[4] L. Yao, S. Li, D. Li, M. Zhu, Q. Gao, S. Zhang, Z. Bian, J. Huang, D. Zeng, J. Ma, "Leveraging deep generative model for direct energy-resolving CT imaging via existing energy-integrating CT images", *SPIE Medical Imaging 2020*.

[5] D. P. Clark, F. R. Schwartz, D. Marin, J. C. Ramirez-Giraldo, C. T. Badea, "Deep learning based spectral extrapolation for dual-source, dual-energy x-ray CT", Med. Phys. 47 (9): 4150–4163, 2020.

[6] C. K. Liu, C. C. Liu, C. H. Yang, H. M. Huang, "Generation of brain dual-energy CT from single-energy CT using deep learning", Journal of Digital Imaging 34(1):149–161, 2021.

[7] T. Lyu, W. Zhao, Y. Zhu, Z. Wu, Y. Zhang, Y. Chen, L. Luo, S. Li, L. Xing, "Estimating dual-energy CT imaging from single-energy CT data with material decomposition convolutional neural network", Medical Image Analysis 70:1–10, 2021.

[8] F. R. Schwartz, D. P. Clark, Y. Ding, J. C. Ramirez-Giraldo, C. T. Badea, D. Marin, "Evaluating renal lesions using deep-learning based extension of dual-energy FoV in dual-source CT—A retrospective pilot study", European Journal of Radiology 139:109734, 2021.

[9] Y. Li, X. Tie, K. Li, J. W. Garrett, G.-H. Chen, "Deep-En-Chroma: mining the spectral fingerprints in single-kV CT acquisitions using energy integration detectors", *SPIE Medical Imaging 2022*.

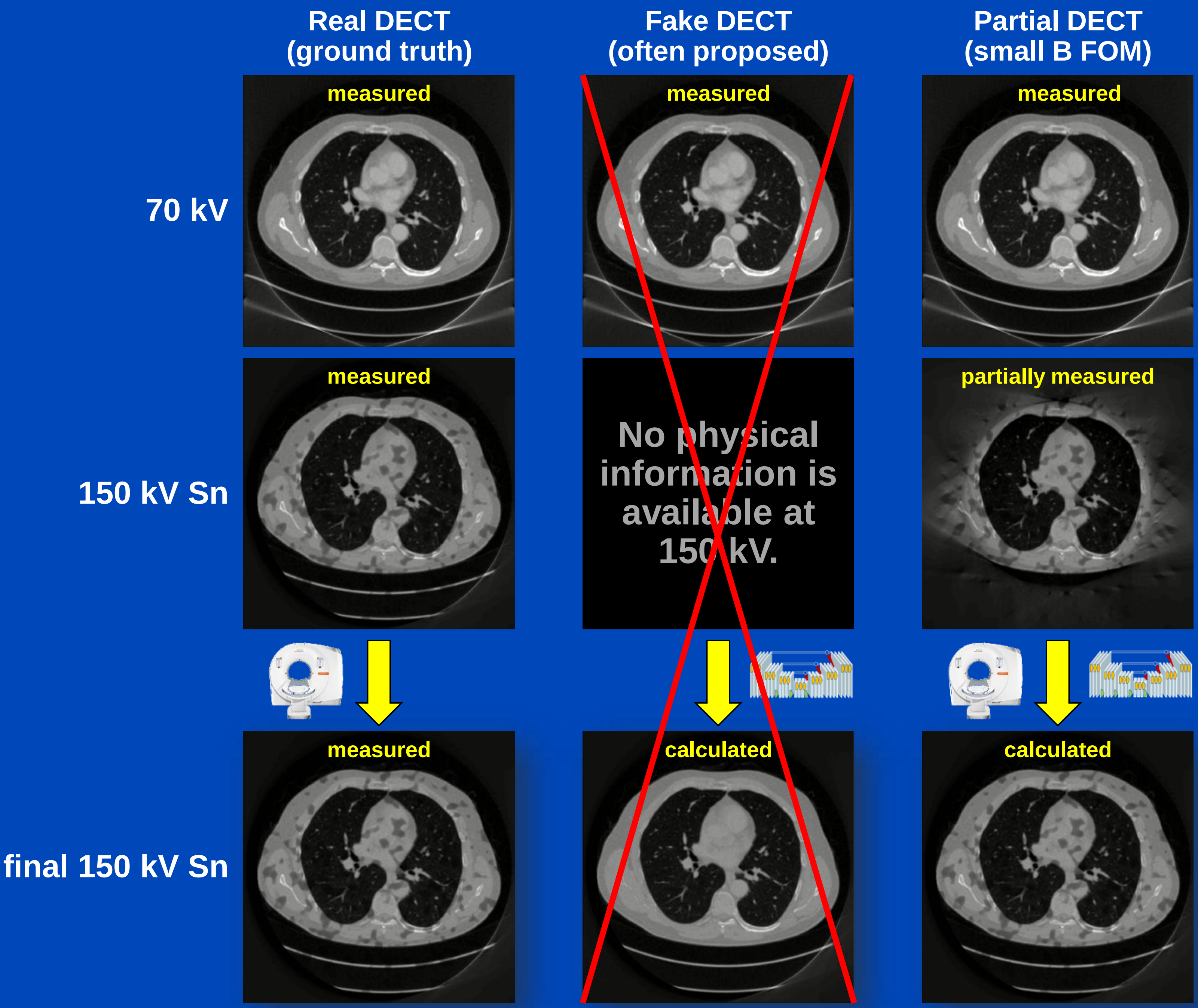
Real DECT
(ground truth)
Fake DECT
(often proposed)
Partial DECT
(small B FOM)
70 kV
150 kV Sn
final 150 kV Sn
measured
measured
measured
measured
No physical information is available at 150 kV.
partially measured
measured
calculated
calculated

Algorithm for Partial DECT

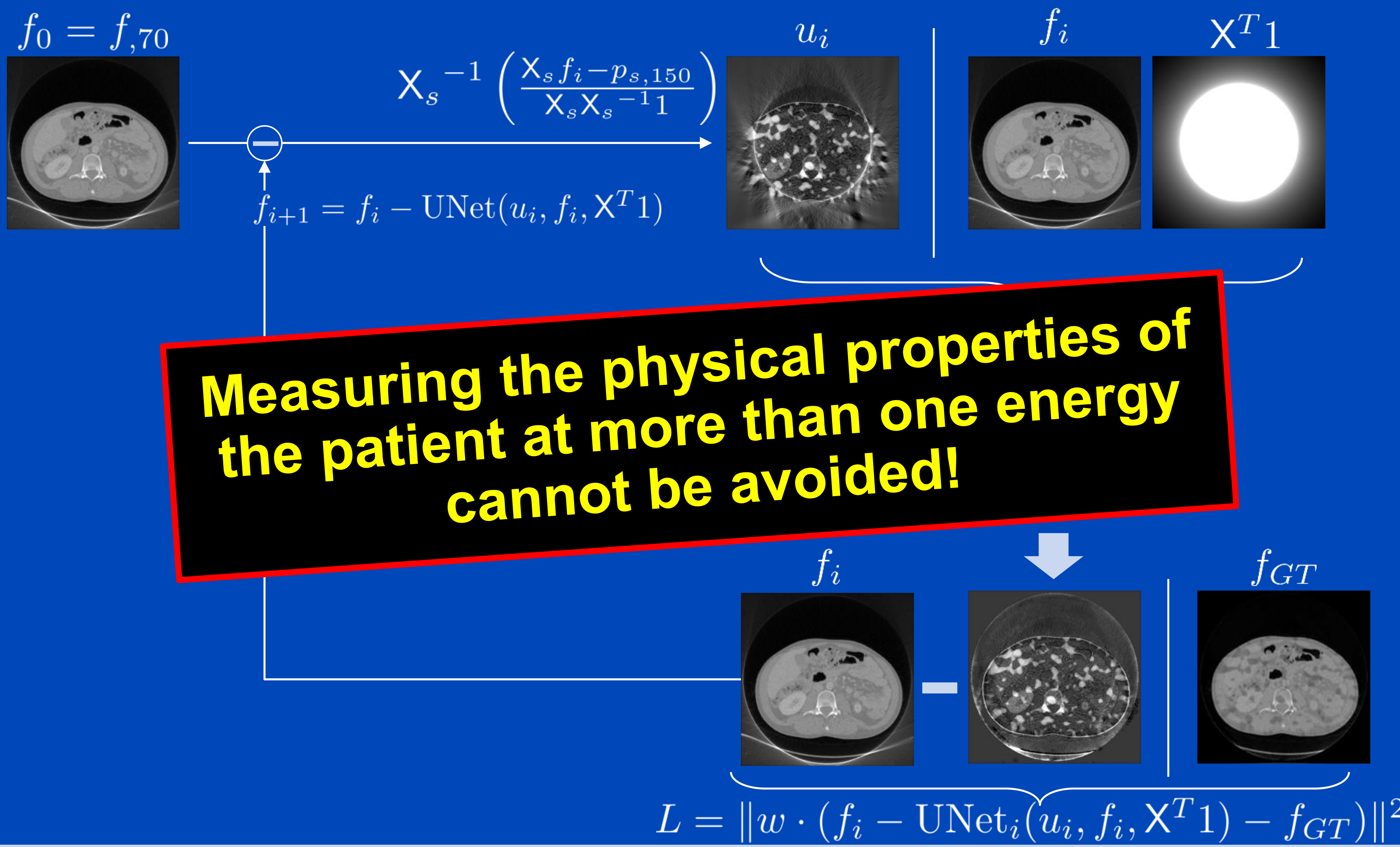

Measuring the physical properties of the patient at more than one energy cannot be avoided!

Part 3:

Replacement of Lengthy Computations
Fast Physics

Deep Scatter Estimation

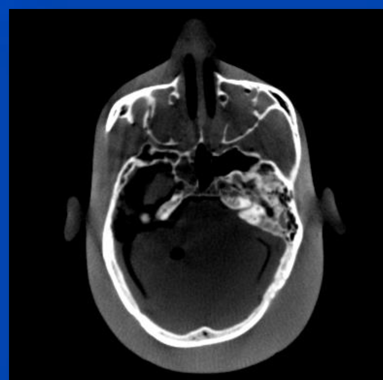

???

In real time?

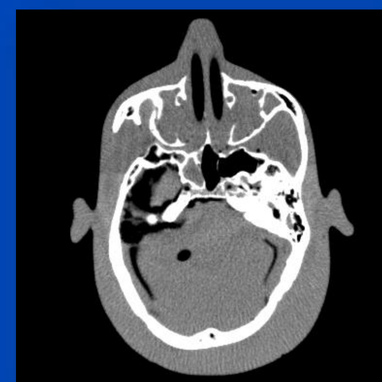

Deep Scatter Estimation (DSE)

TOP DOWNLOADED PAPER 2018-2019

CONGRATULATIONS TO

Marc Kachelriess

whose paper has been r…

WILEY

MEDICAL PHYSICS

The International Journal of Medical Physics Research and Practice

Congratulations — your work was one of the top downloaded in recent publication history!

Dear MARC

… research, published in *Medical Physics*, is …aded papers!

…ion for medical CT using the deep …d and robustness analysis with …nies, dose levels, tube voltages, and

This work received the
Behnken-Berger Award
at the DGMP annual meeting 2021

BEHNKEN-BERGER STIFTUNG

…APER 2018-2019

…ATIONS TO

Joscha Maier

whose paper has been recognized as one of the most read in

Medical Physics

Motivation

- X-ray scatter is a major cause of image quality degradation in CT and CBCT.
- Appropriate scatter correction is crucial to maintain the diagnostic value of the CT examination.

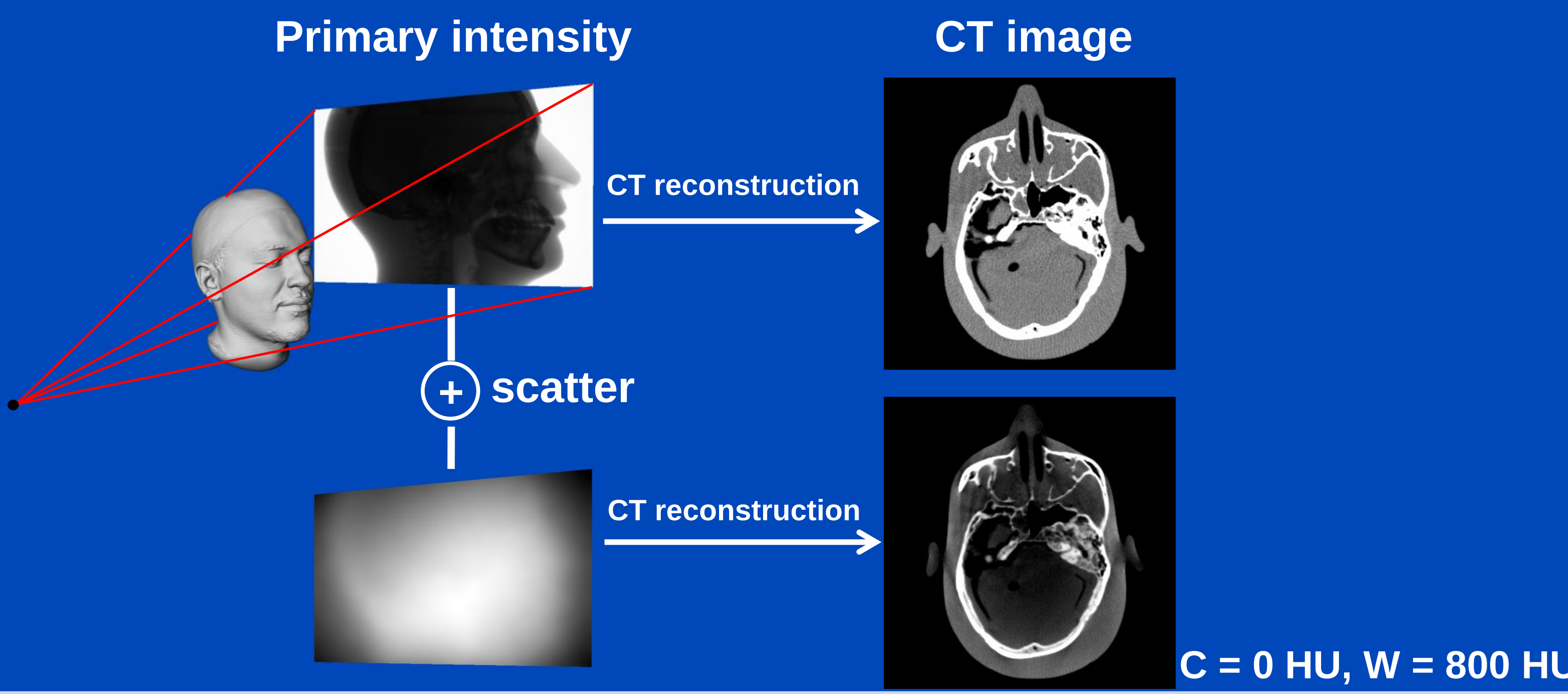

Scatter Correction

Scatter suppression

- Anti-scatter grids
- Collimators
- …

Scatter estimation

- Monte Carlo simulation
- Kernel-based approaches
- Boltzmann transport
- Primary modulation
- Beam blockers
- …

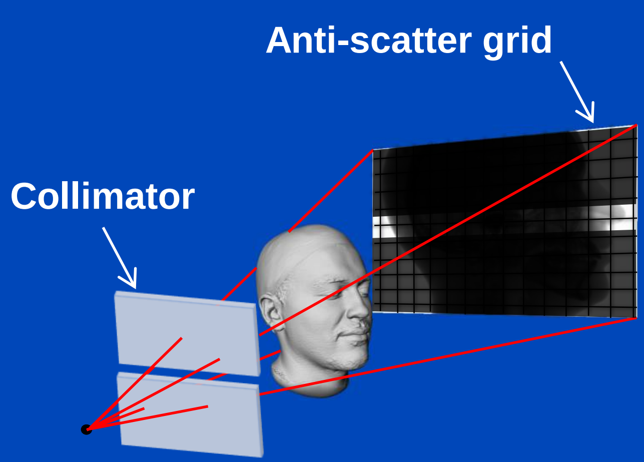

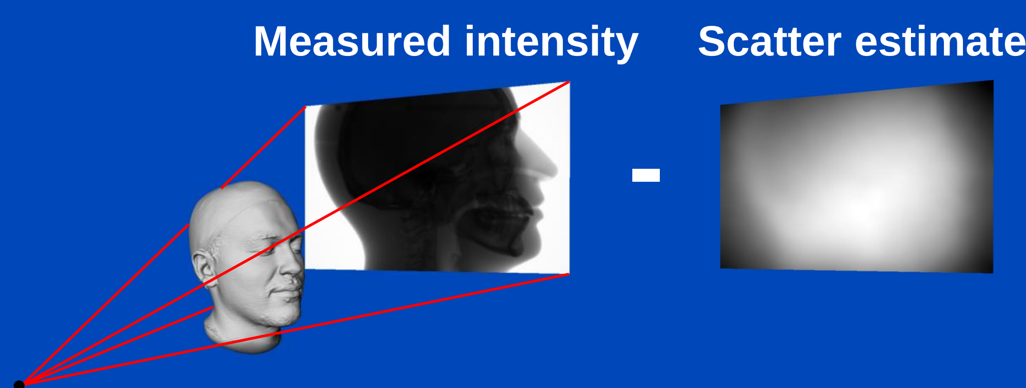

Monte Carlo Scatter Estimation

- Simulation of photon trajectories according to physical interaction probabilities.
- Simulating a large numb ... ries well approxima ...

1 to 10 hours per tomographic data set

Deep Scatter Estimation

Network architecture & scatter estimation framework

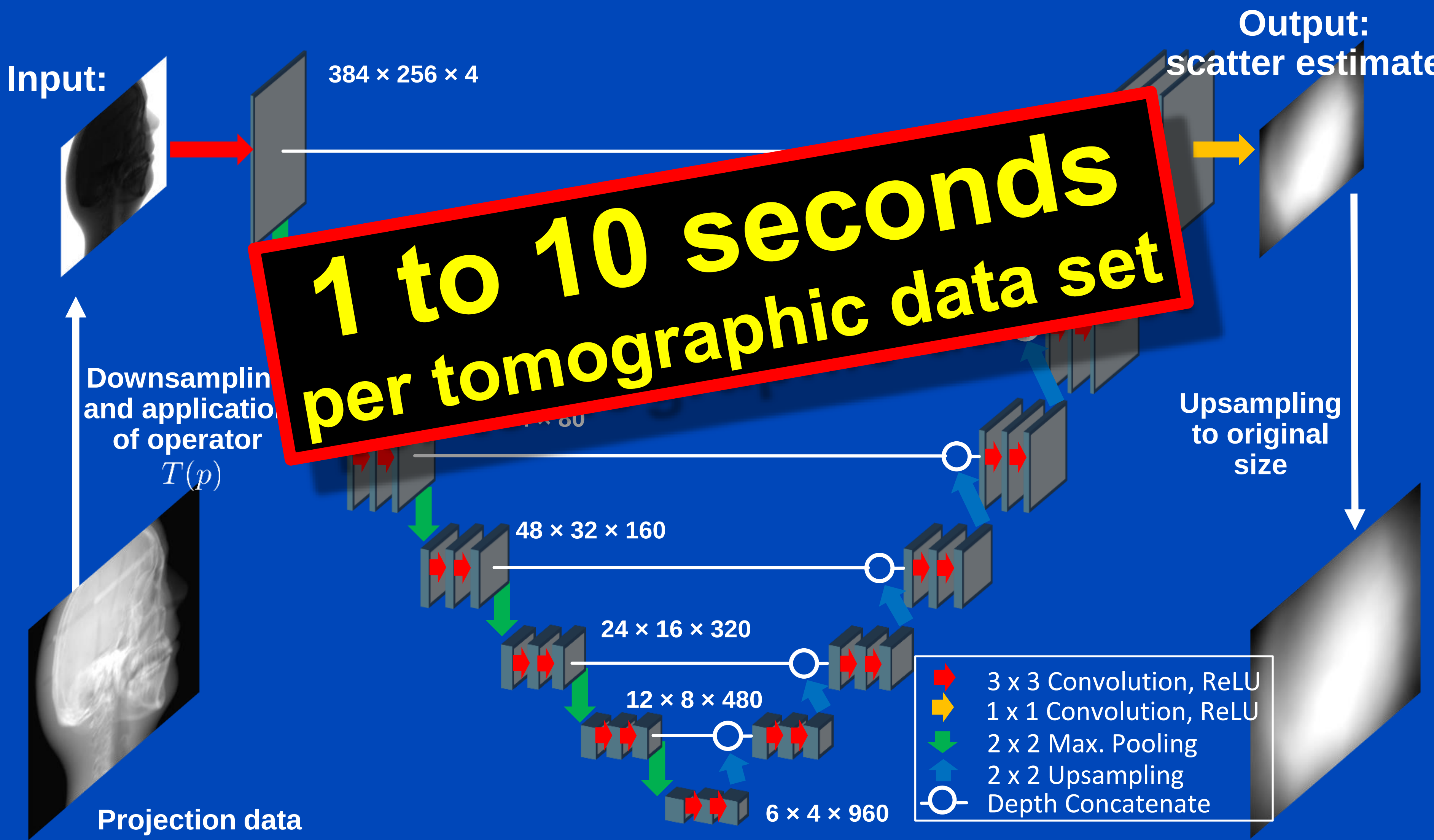

J. Maier, M. Kachelrieß et al. Deep scatter estimation (DSE). SPIE 2017 and Journal of Nondestructive Evaluation 37:57, July 2018.
J. Maier, M. Kachelrieß et al. Robustness of DSE. Med. Phys. 46(1):238-249, January 2019.

Training the DSE Network

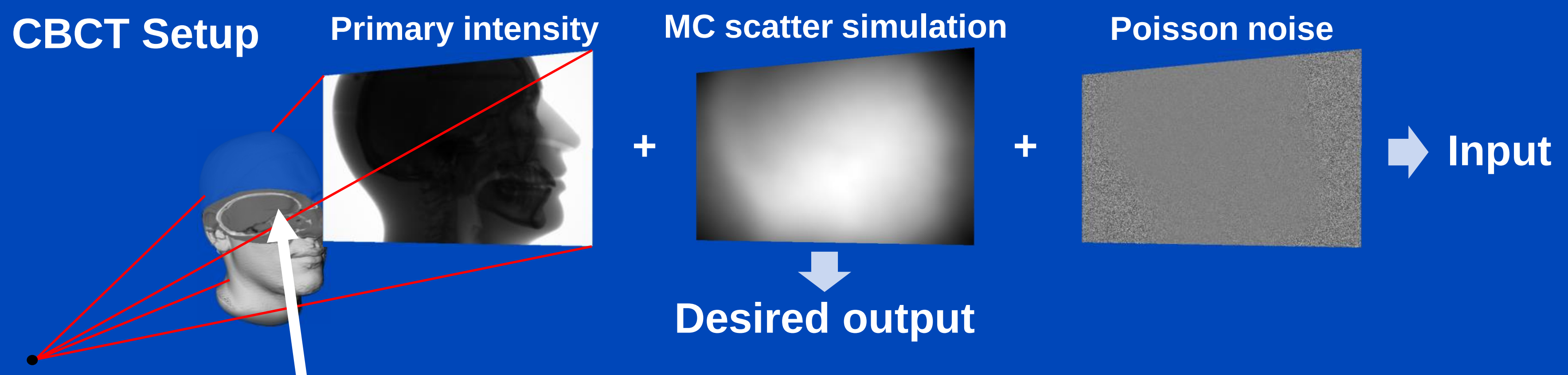

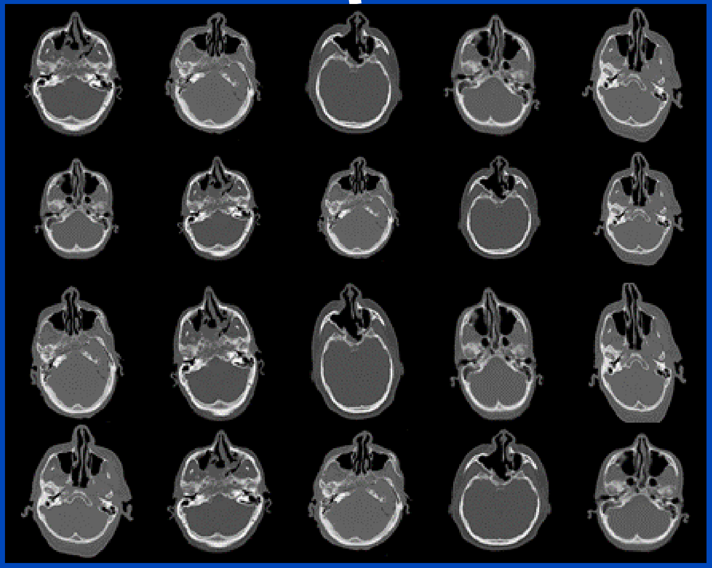

- Simulation of 6000 projections using different heads and acquisition parameters (80 kV, …, 140 kV in steps of 20 kV).
- Splitting into 80% training and 20% validation data.
- Mean *S/P* = 0.9
- 90th percentile *S/P* = 1.32
- Training minimizes MSE pixel-wise loss on a GeForce GTX 1080 for 80 epochs.

J. Maier, M. Kachelrieß et al. Deep scatter estimation (DSE). SPIE 2017 and Journal of Nondestructive Evaluation 37:57, July 2018.
J. Maier, M. Kachelrieß et al. Robustness of DSE. Med. Phys. 46(1):238-249, January 2019.

PEP

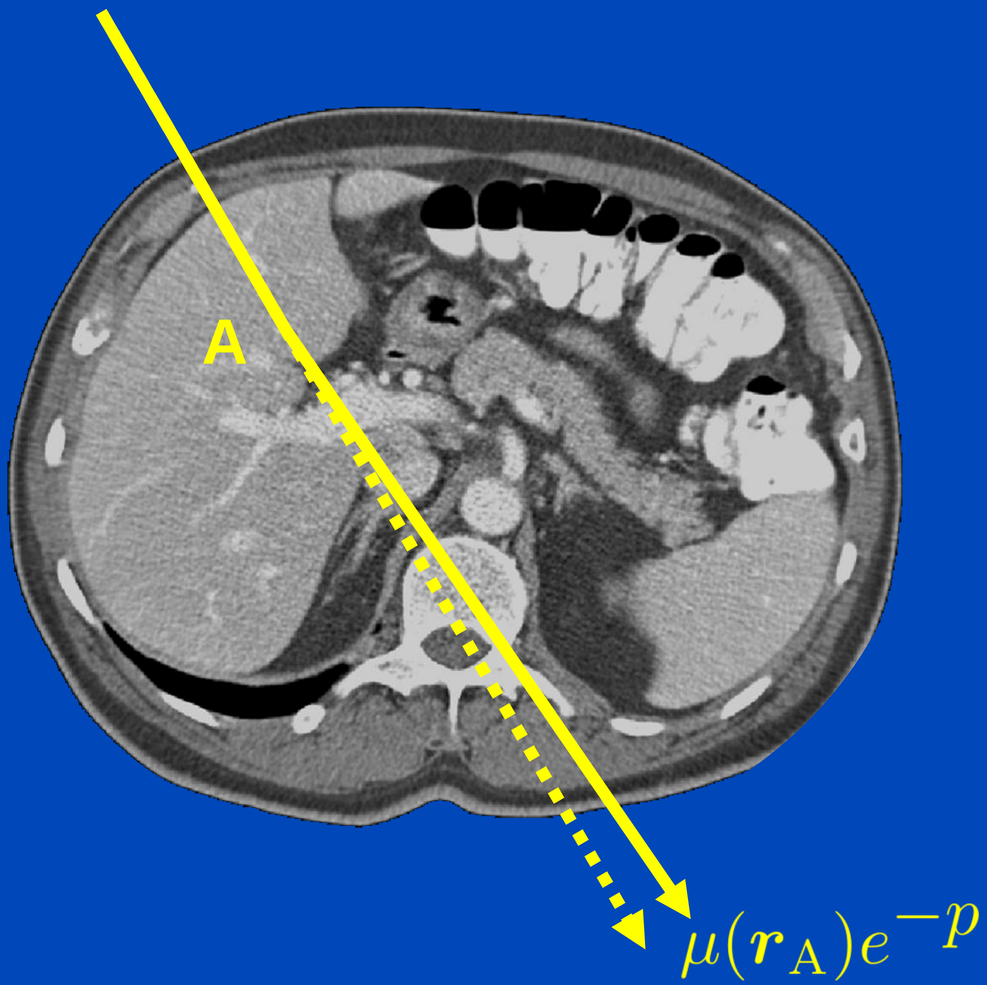

PEP

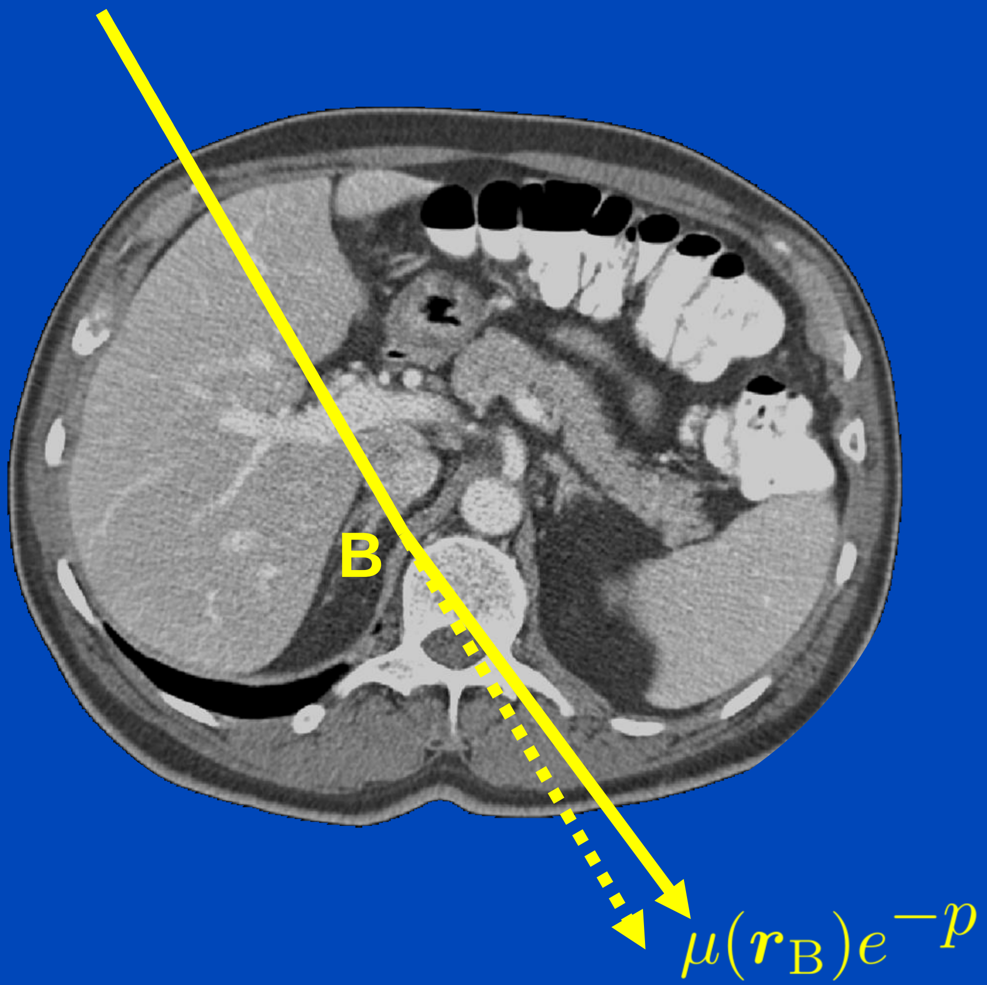

PEP

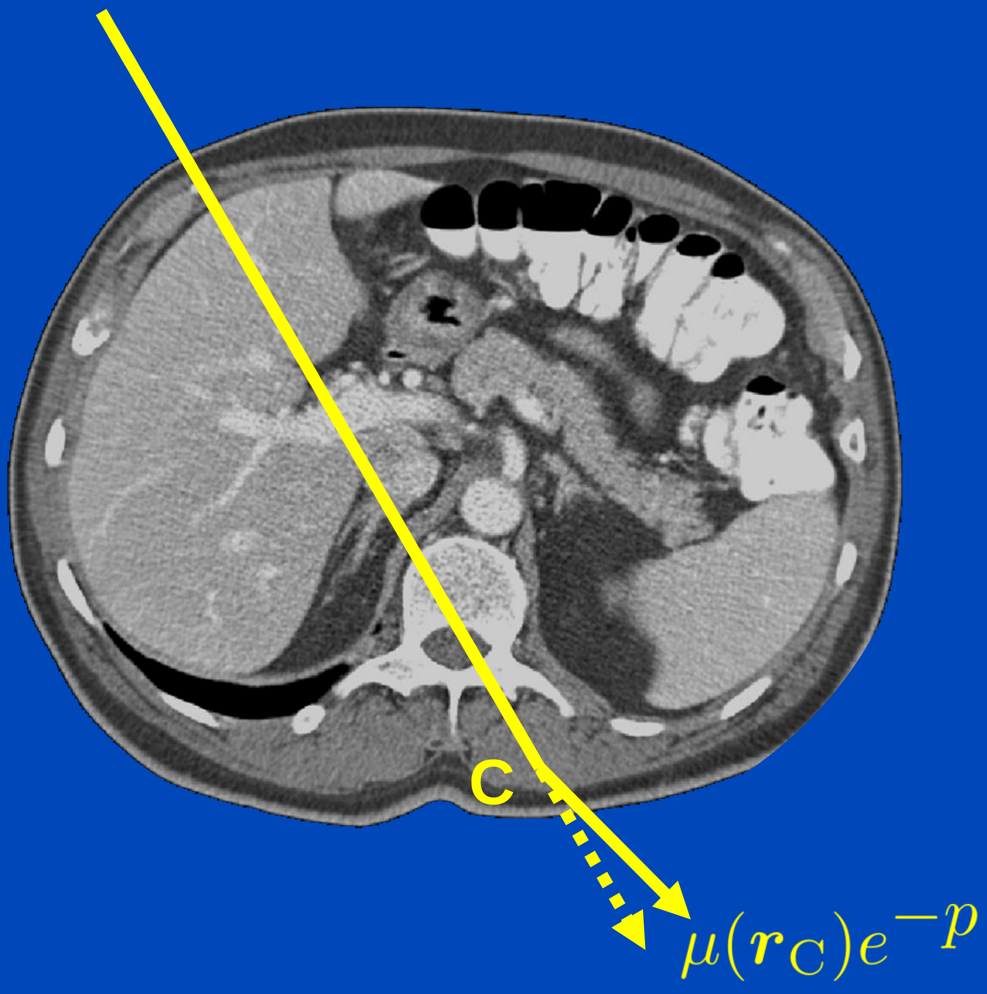

PEP

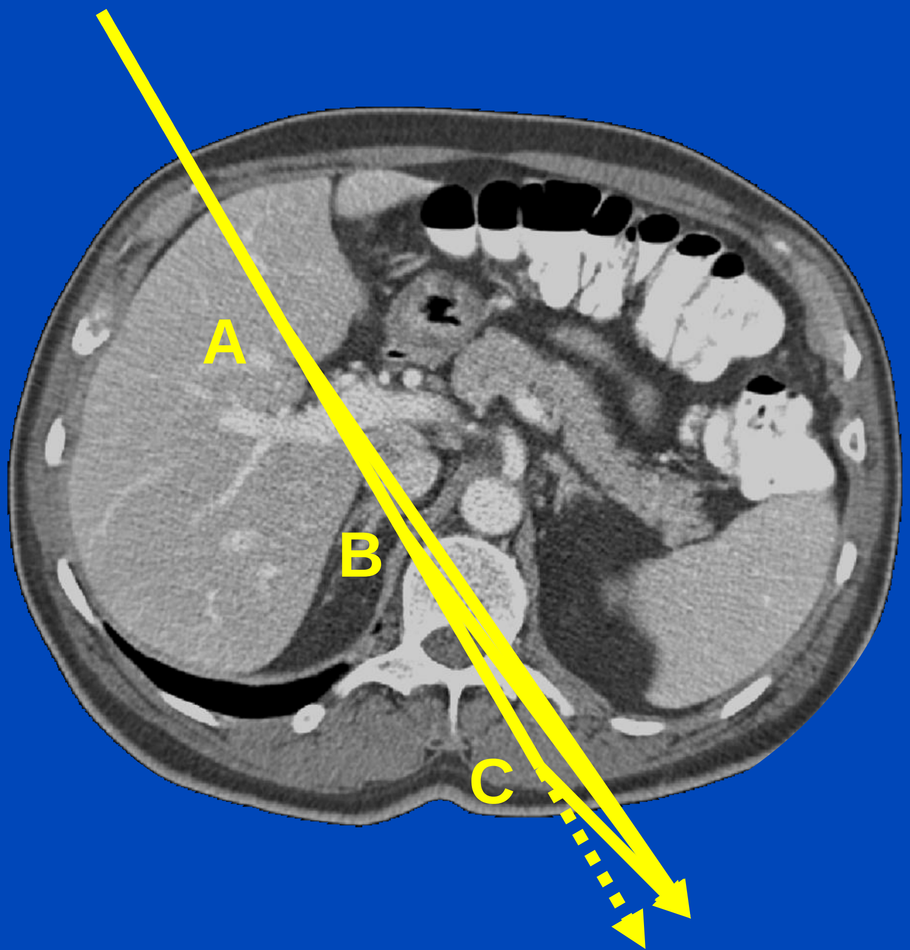

$$\big(\mu(\boldsymbol{r}_\mathrm{A})+\mu(\boldsymbol{r}_\mathrm{B})+\mu(\boldsymbol{r}_\mathrm{C})\big)e^{-p} = p\,e^{-p}$$

PEP for CT

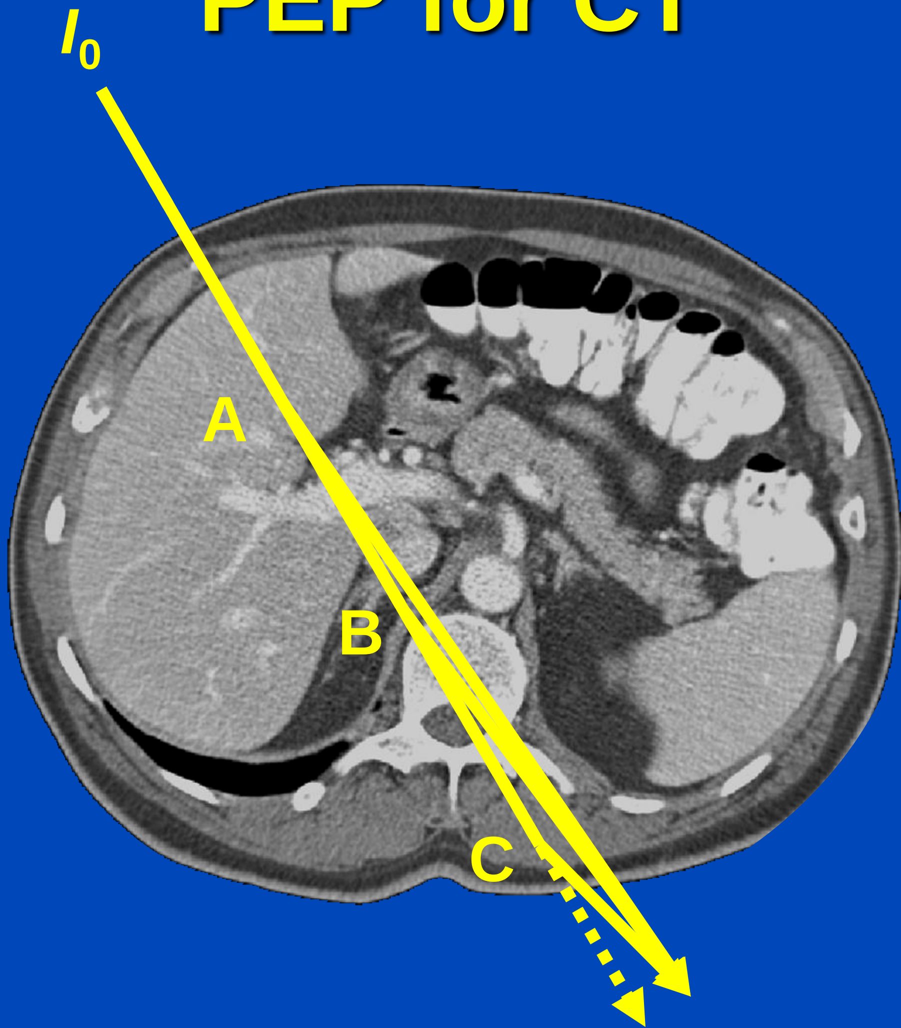

$$I_0\big(\mu(\boldsymbol{r}_\mathrm{A})+\mu(\boldsymbol{r}_\mathrm{B})+\mu(\boldsymbol{r}_\mathrm{C})\big)e^{-p}=I_0\,p\,e^{-p}$$

Results on Simulated Projection Data

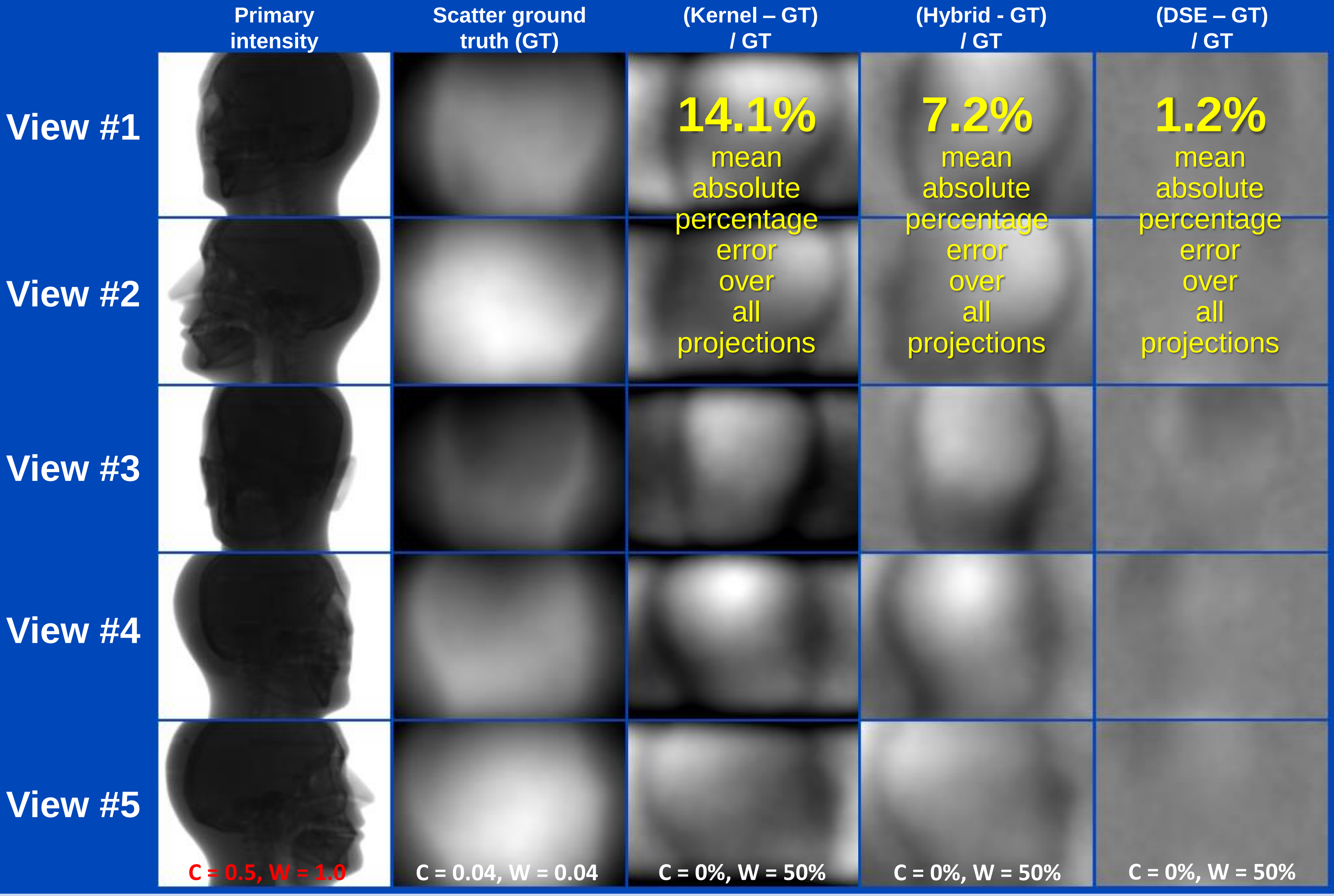

DSE trained to estimate scatter from **primary plus scatter**: High accuracy

Results on Simulated Projection Data

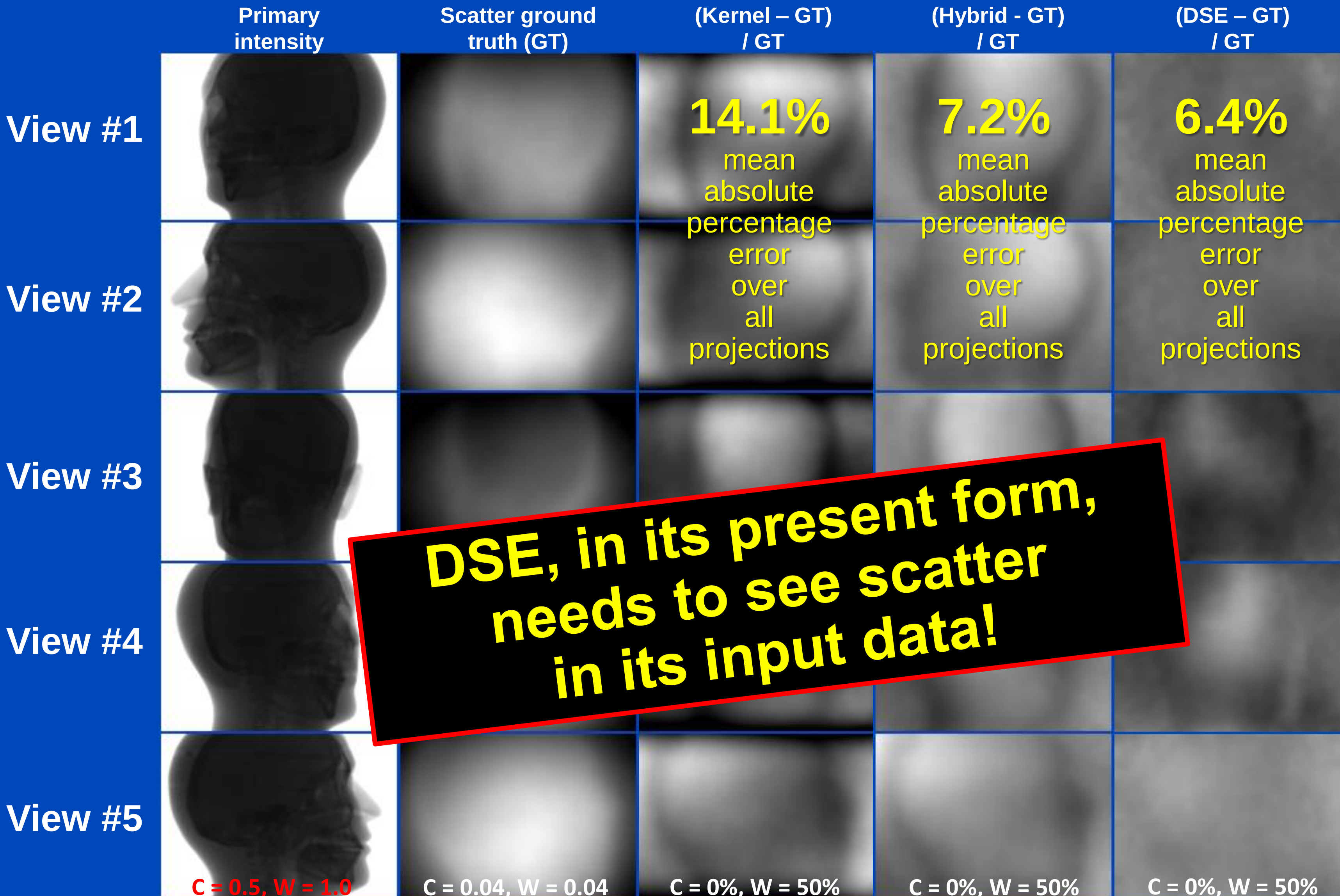

DSE trained to estimate scatter from **primary only**: Low accuracy

Results on Simulated Projection Data

	Primary intensity	Scatter ground truth (GT)	(Kernel – GT) / GT	(Hybrid - GT) / GT	(DSE – GT) / GT

View #1

View #2

View #3

View #4

View #5

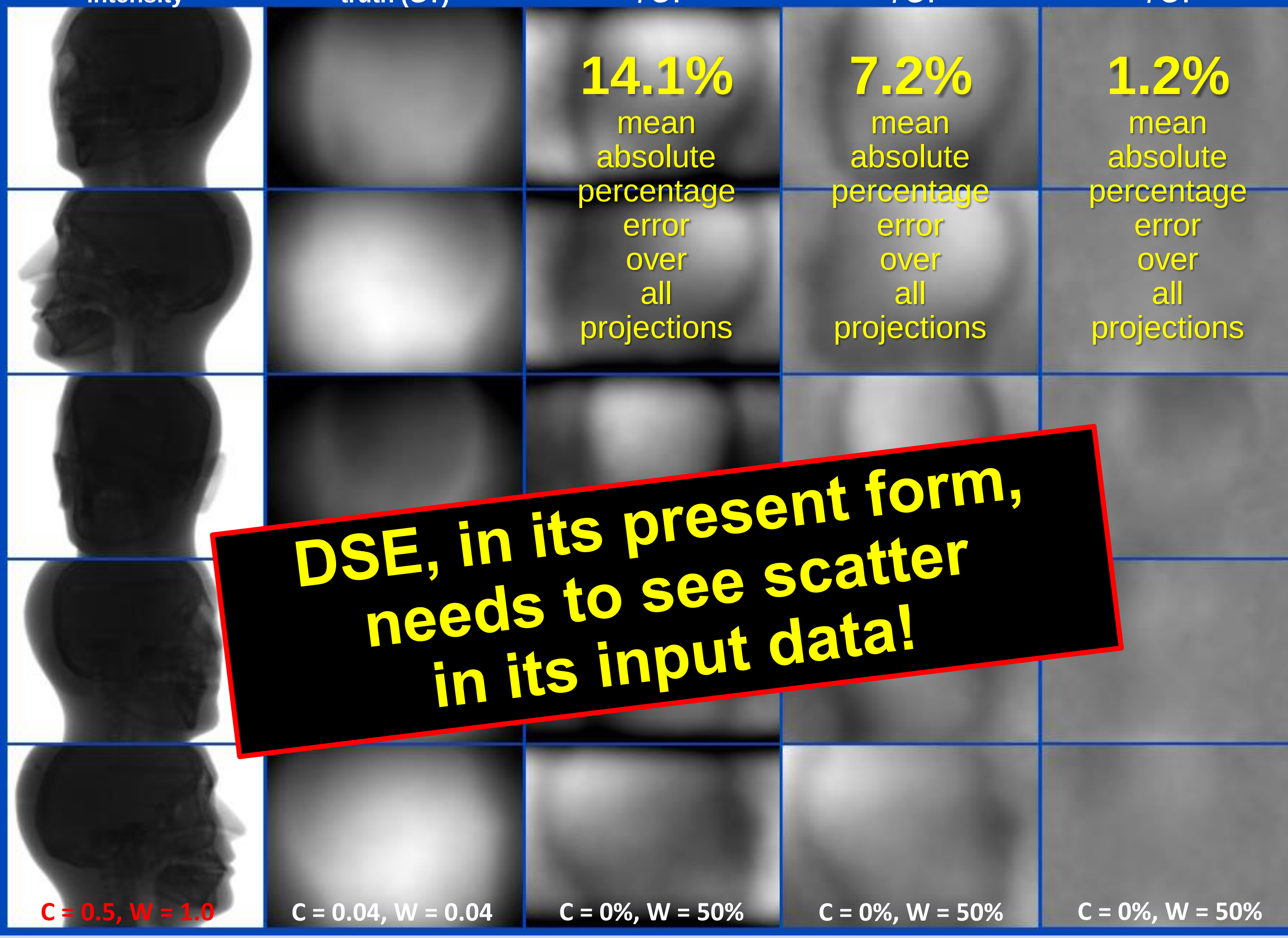

DSE trained to estimate scatter from **primary plus scatter**: High accuracy

Reconstructions of Simulated Data

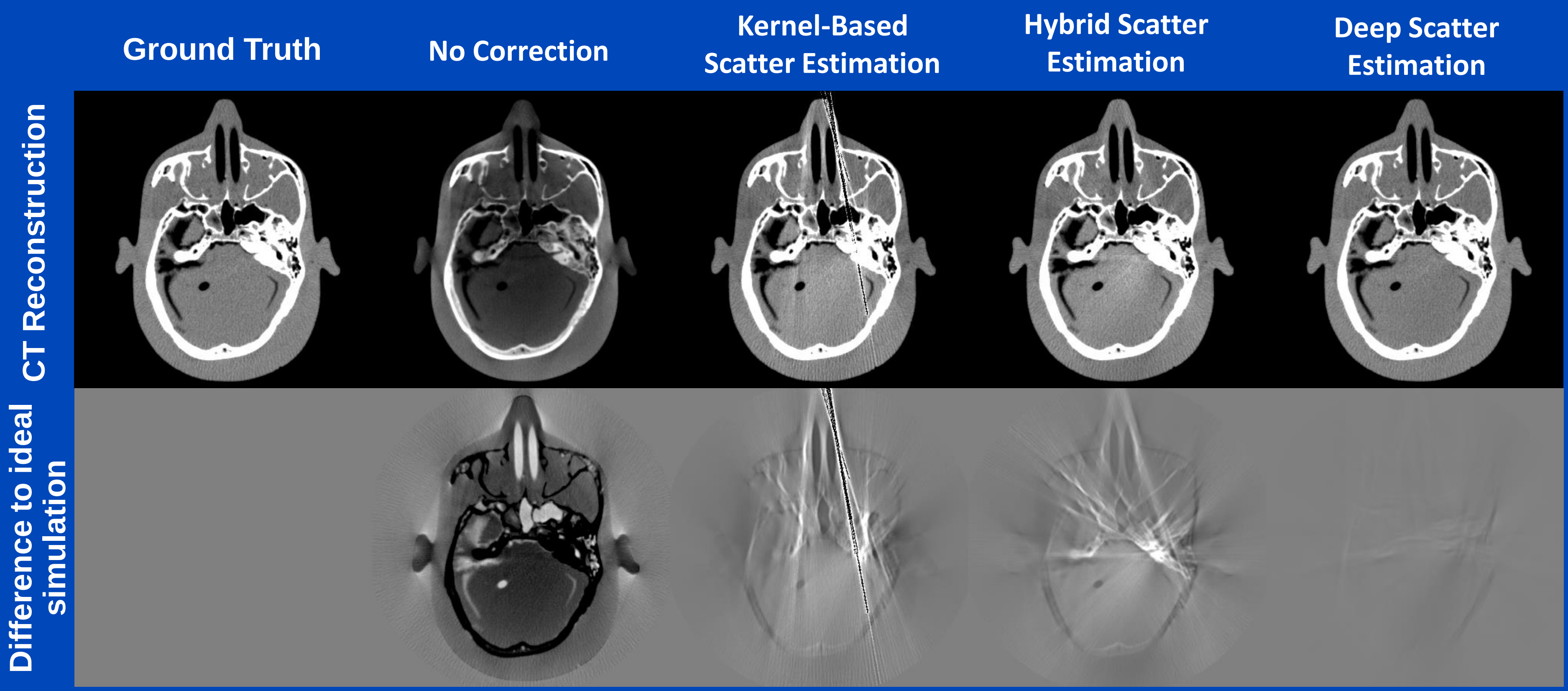

C = 0 HU, *W* = 1000 HU

J. Maier, M. Kachelrieß et al. Deep scatter estimation (DSE). SPIE 2017 and Journal of Nondestructive Evaluation 37:57, July 2018.
J. Maier, M. Kachelrieß et al. Robustness of DSE. Med. Phys. 46(1):238-249, January 2019.

Testing of the DSE Network for Measured Data (120 kV)

DKFZ table-top CT

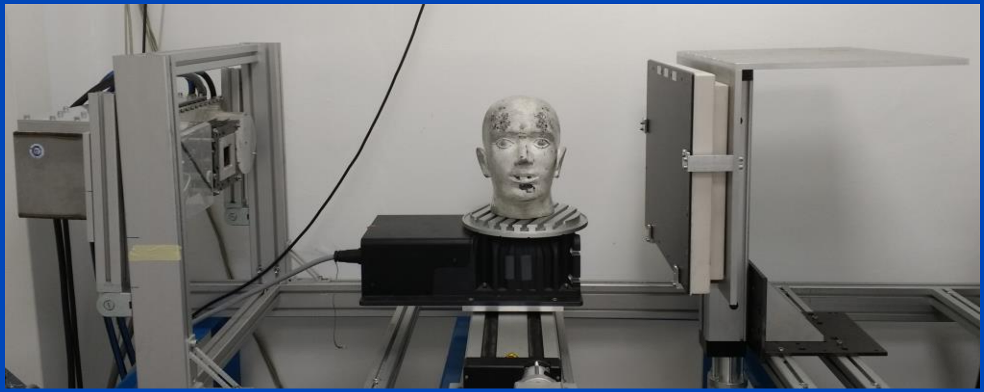

- Measurement of a head phantom at our in-house table-top CT.
- Slit scan measurement serves as ground truth.

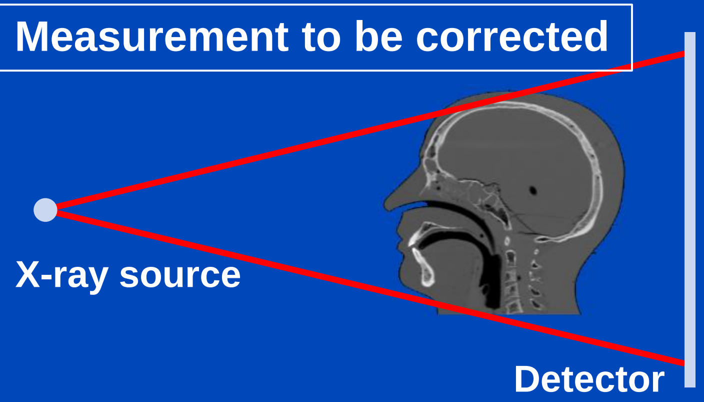

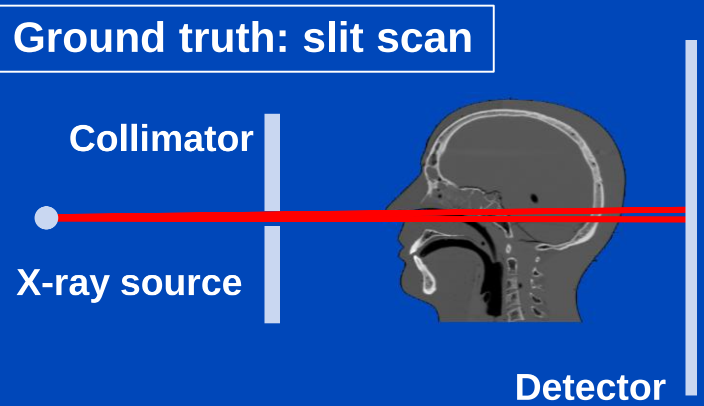

Reconstructions of Measured Data

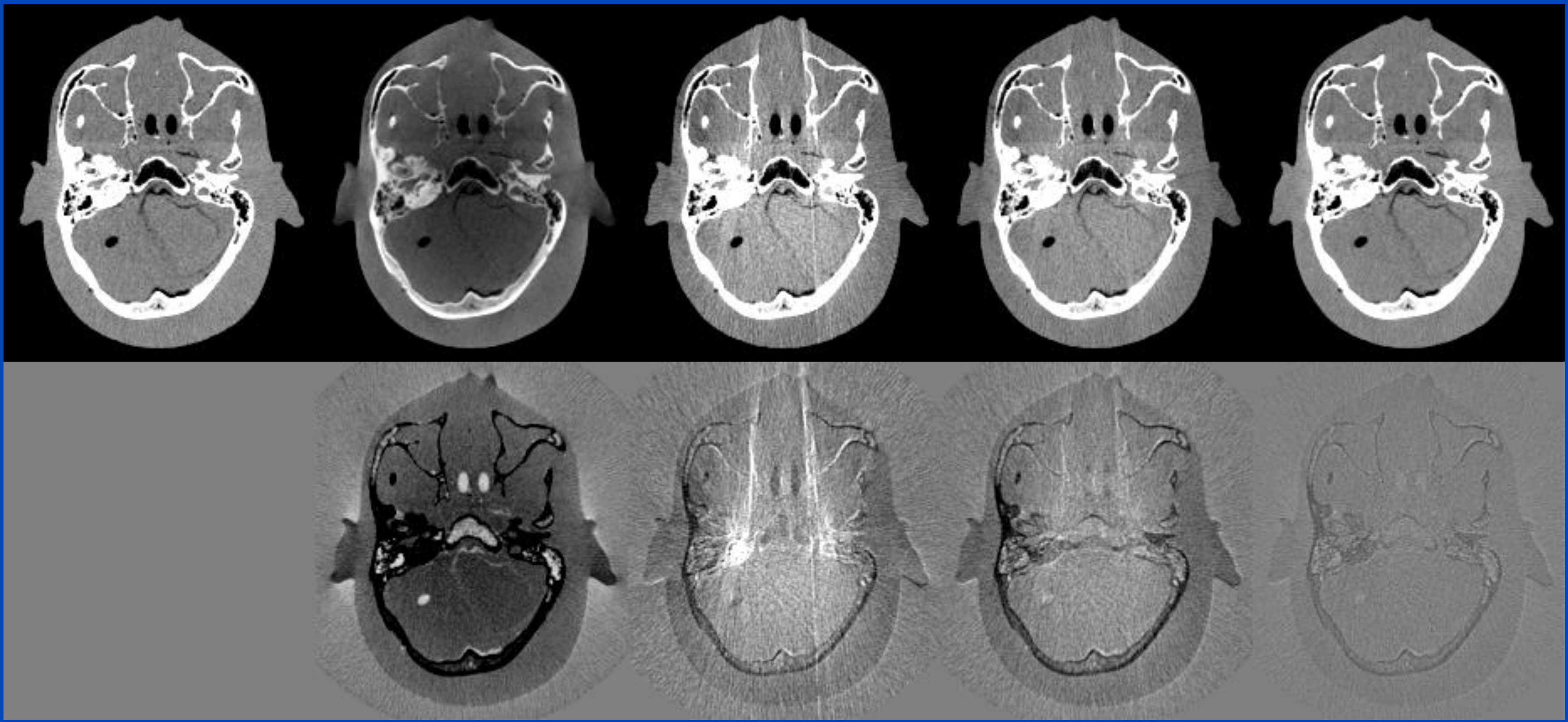

C = 0 HU, W = 1000 HU

J. Maier, M. Kachelrieß et al. Deep scatter estimation (DSE). SPIE 2017 and Journal of Nondestructive Evaluation 37:57, July 2018.
J. Maier, M. Kachelrieß et al. Robustness of DSE. Med. Phys. 46(1):238-249, January 2019.

A simple detruncation was applied to the rawdata before reconstruction. Images were clipped to the FOM before display. C = -200 HU, W = 1000 HU.

Truncated DSE

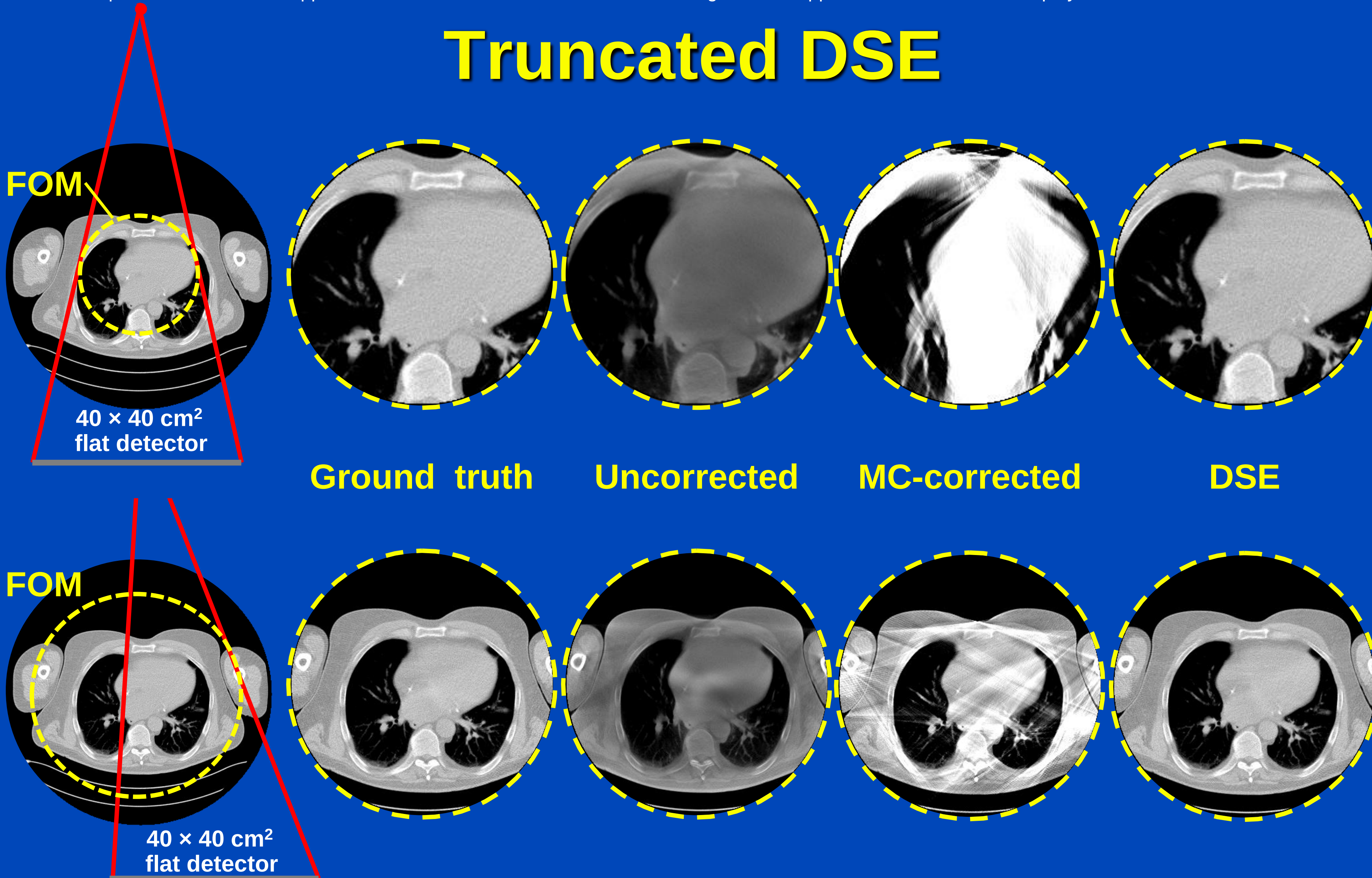

To learn why MC fails at truncated data and what significant efforts are necessary to cope with that situation see [Kachelrieß et al. Effect of detruncation on the accuracy of MC-based scatter estimation in truncated CBCT. Med. Phys. 45(8):3574-3590, August 2018].

Does DSE Generalize to Different Anatomical Regions?

- Simulation parameters:
  - 7 head and 14 thorax/abdomen clinical CT data sets
  - Apply affine transforms to obtain 28 volumes for each region
  - Regions: head, thorax and abdomen
  - Tube Voltage: 120 kV, 140 kV.
  - Prior volumes: 28 head phantoms
  - Simulate 45 projections over 360° for each volume and voltage
  - Number of z-Positions: 1 for head, 4 for thorax and abdomen
  - Data augmentation for head: vertical & horizontal flipping
  - Total number of projections: $2 \times 28 \times 45 \times 2 \times 2 = 10080$

Results

KSE	Head	Thorax	Abdomen
Head	14.5	26.8	32.5
Thorax	16.2	18.5	19.4
Abdomen	16.8	22.1	17.8
All data	14.9	20.5	19.3

DSE	Head	Thorax	Abdomen
Head	1.2	21.1	32.7
Thorax	8.8	1.5	9.1
Abdomen	11.9	10.9	1.3
All data	1.8	1.4	1.4

Values shown are the mean absolute percentage errors (MAPEs) of the testing data.
Note that thorax and head suffer from truncation due to the small size of the 40×30 cm flat detector.

Scatter in Dual Source CT (DSCT)

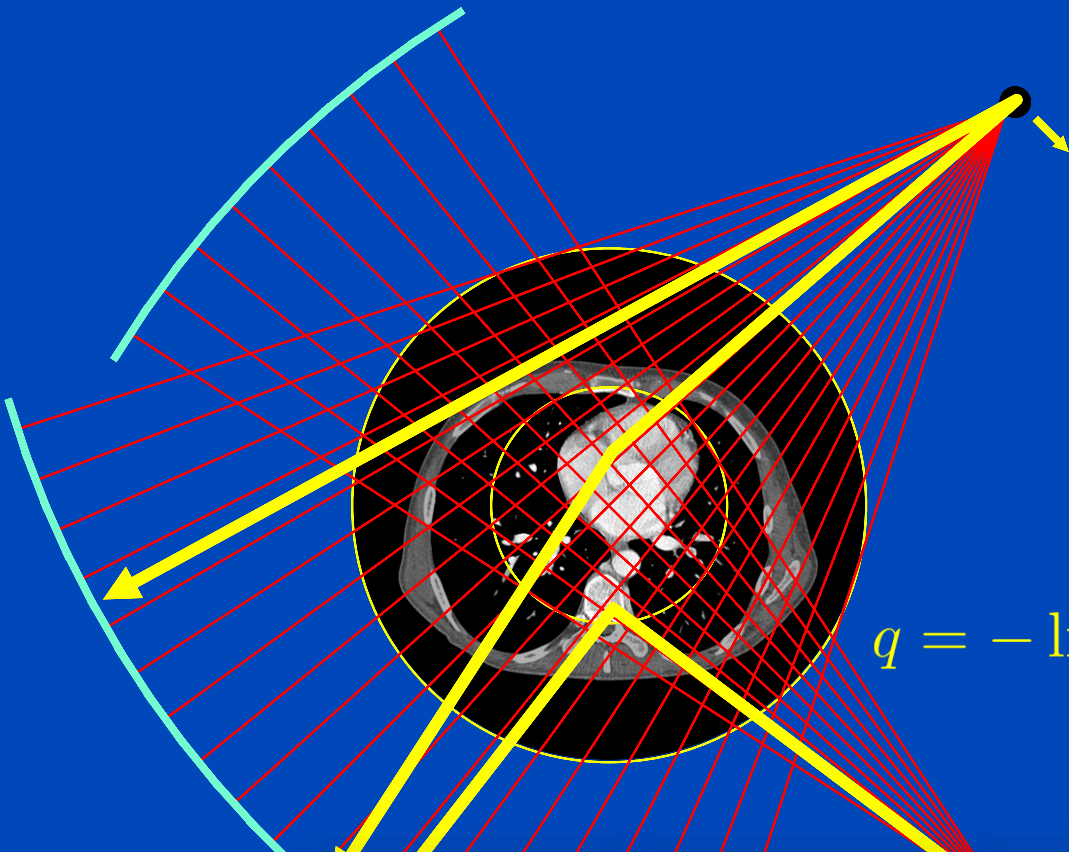

Siemens SOMATOM Force
dual source cone-beam spiral CT

$$q = -\ln \frac{I_{\text{primary}} + S_{\text{forward}} + \rho\, S_{\text{cross}}}{I_0}$$

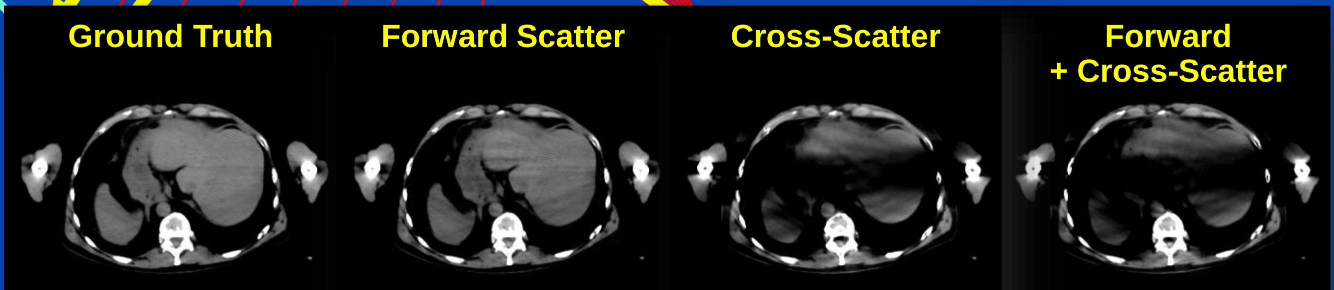

C = 40 HU, *W* = 300 HU, with 2D anti-scatter grid

J. Erath, T. Vöth, J. Maier, E. Fournié, M. Petersilka, K. Stierstorfer, and M. Kachelrieß. Deep learning-based forward and cross-scatter correction in dual source CT. Med. Phys. 48:4824–4842, July 2021.

dkfz.

Measurement-Based Scatter Estimation

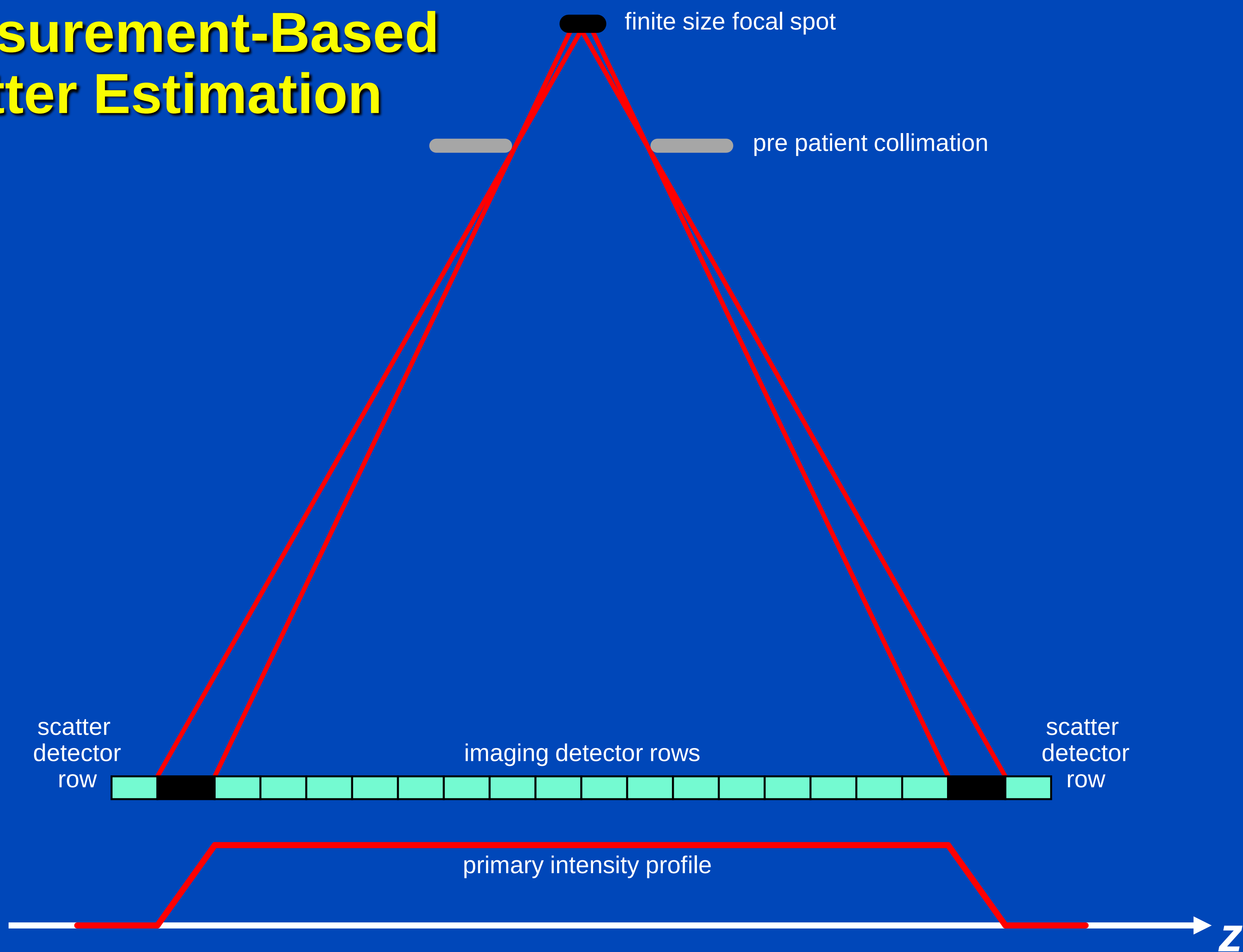

J. Erath, T. Vöth, J. Maier, E. Fournié, M. Petersilka, K. Stierstorfer, and M. Kachelrieß. Deep learning-based forward and cross-scatter correction in dual source CT. Med. Phys. 48:4824–4842, July 2021.

Cross-DSE

Ground Truth | Uncorrected | xDSE (2D, xSSE) | Measurement-based

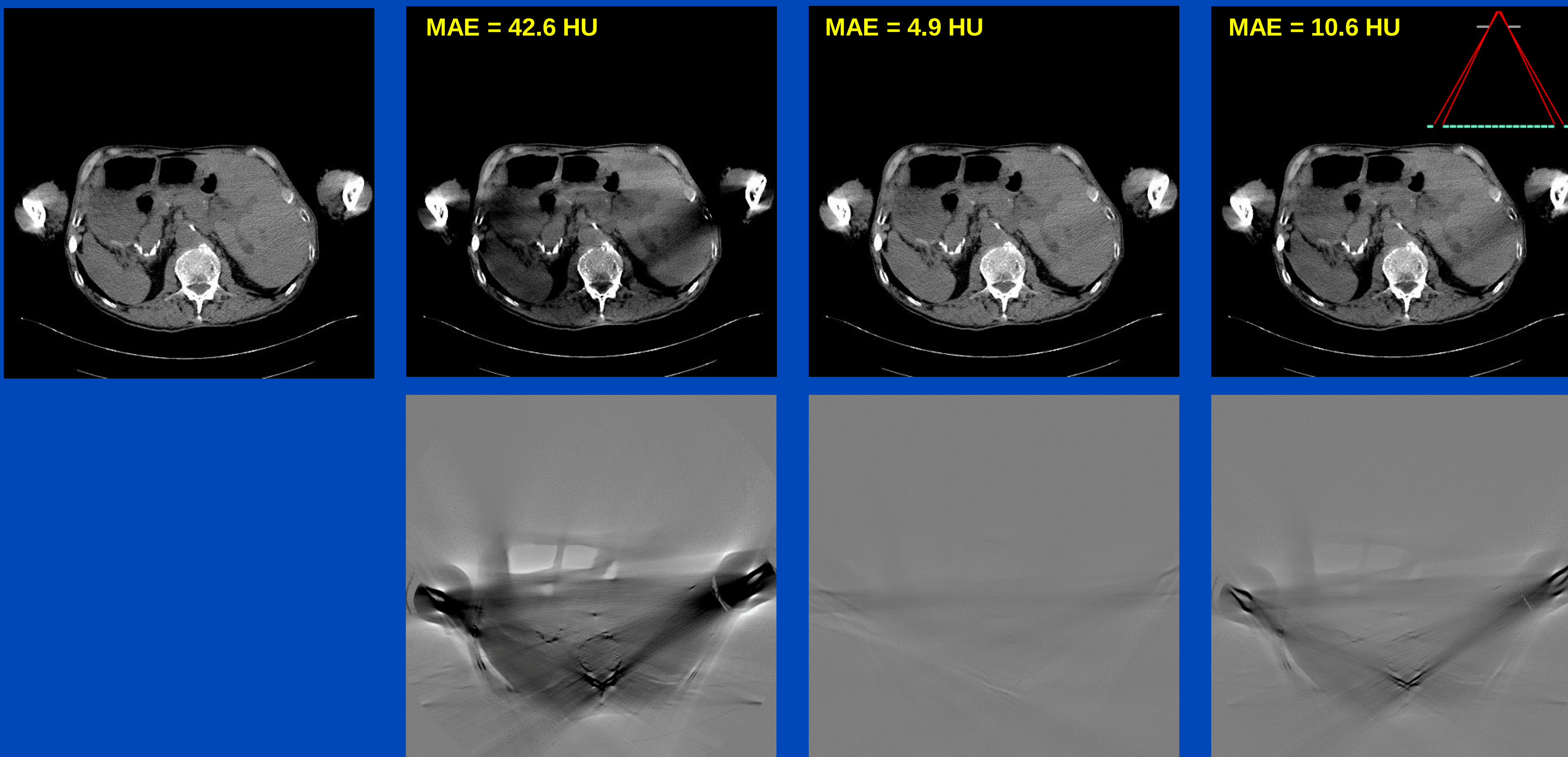

xDSE (2D, xSSE) maps
primary + forward scatter + cross-scatter + cross-scatter approximation → cross-scatter

Images C = 40 HU, W = 300 HU, difference images C = 0 HU, W = 300 HU

J. Erath, T. Vöth, J. Maier, E. Fournié, M. Petersilka, K. Stierstorfer, and M. Kachelrieß. Deep learning-based forward and cross-scatter correction in dual source CT. Med. Phys. 48:4824–4842, July 2021.

Conclusions on DSE

- DSE needs about 3 ms per CT and 10 ms per CBCT projection (as of 2020).
- DSE is a fast and accurate alternative to MC simulations.
- DSE outperforms kernel-based approaches in terms of accuracy and speed.
- Facts:
  - DSE can estimate scatter from a single (!) x-ray image.
  - DSE can accurately estimate scatter from a primary+scatter image.
  - DSE generalizes to all anatomical regions.
  - DSE works for geometries and beam qualities differing from training.
  - DSE may outperform MC even though DSE is trained with MC.
- DSE is not restricted to reproducing MC scatter estimates.
- DSE can rather be trained with any other scatter estimate, including those based on measurements.

J. Maier, M. Kachelrieß et al. Deep scatter estimation (DSE). SPIE 2017 and Journal of Nondestructive Evaluation 37:57, July 2018.
J. Maier, M. Kachelrieß et al. Robustness of DSE. Med. Phys. 46(1):238-249, January 2019.

Scatter Artifacts of Coarse ASG

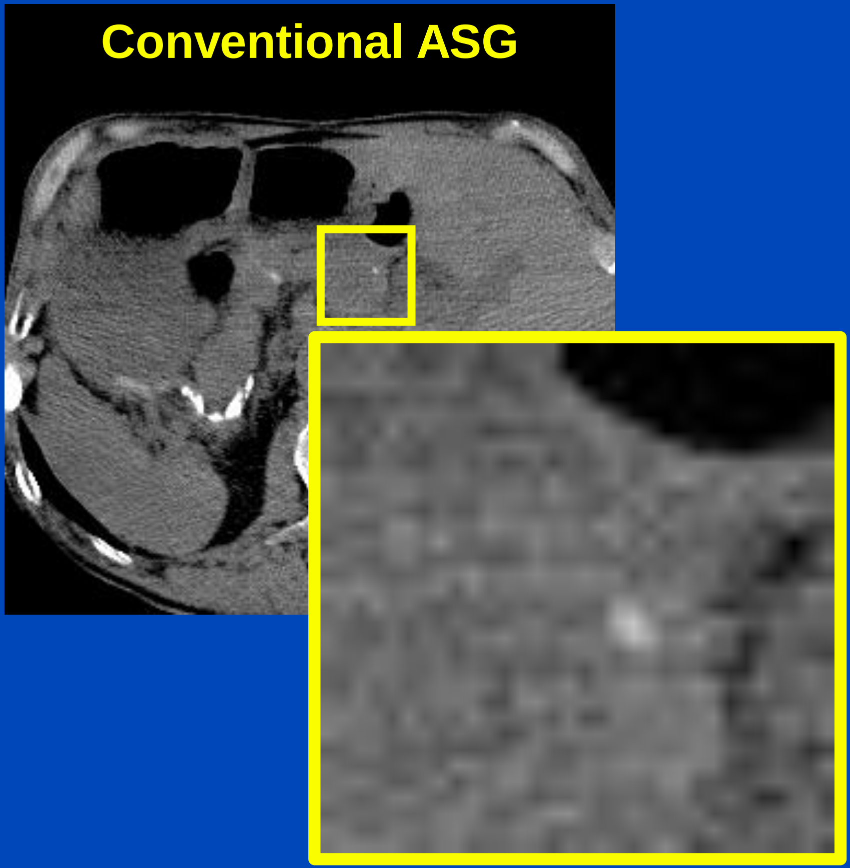

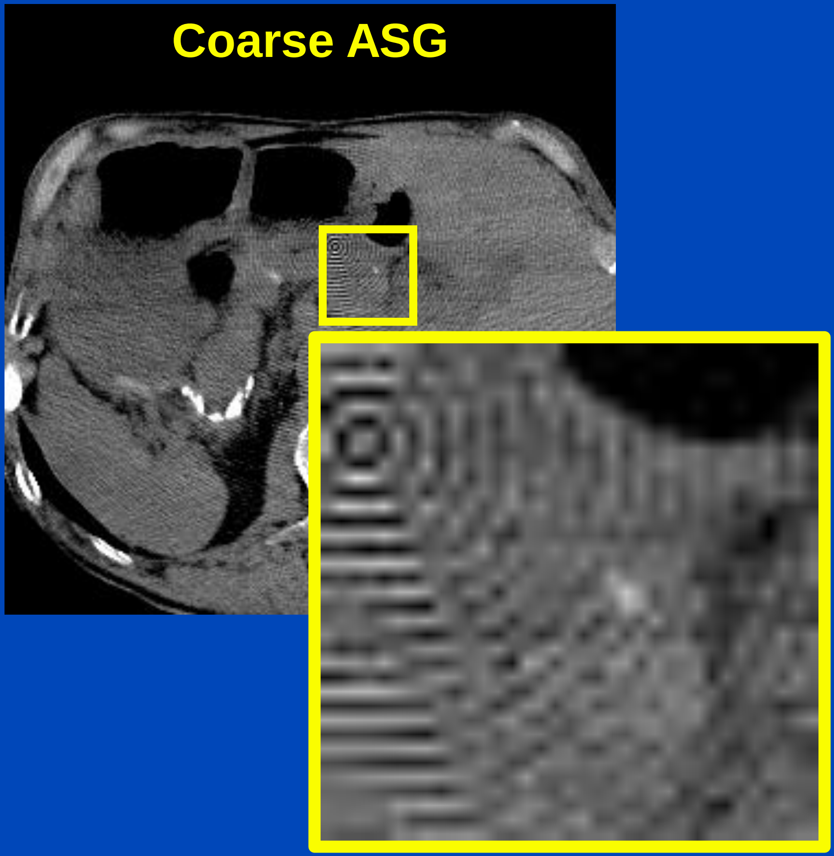

Coarse ASG can lead to scatter-induced moiré artifacts.

Scatter of Coarse ASG

Conventional ASG
Somatom Force
920 × 96 detector pixels
pixel size 0.52 × 0.56 mm at iso

Coarse ASG
Naeotom Alpha
1376 × 144 macro pixels
pixel size 0.3 × 0.352 mm at iso

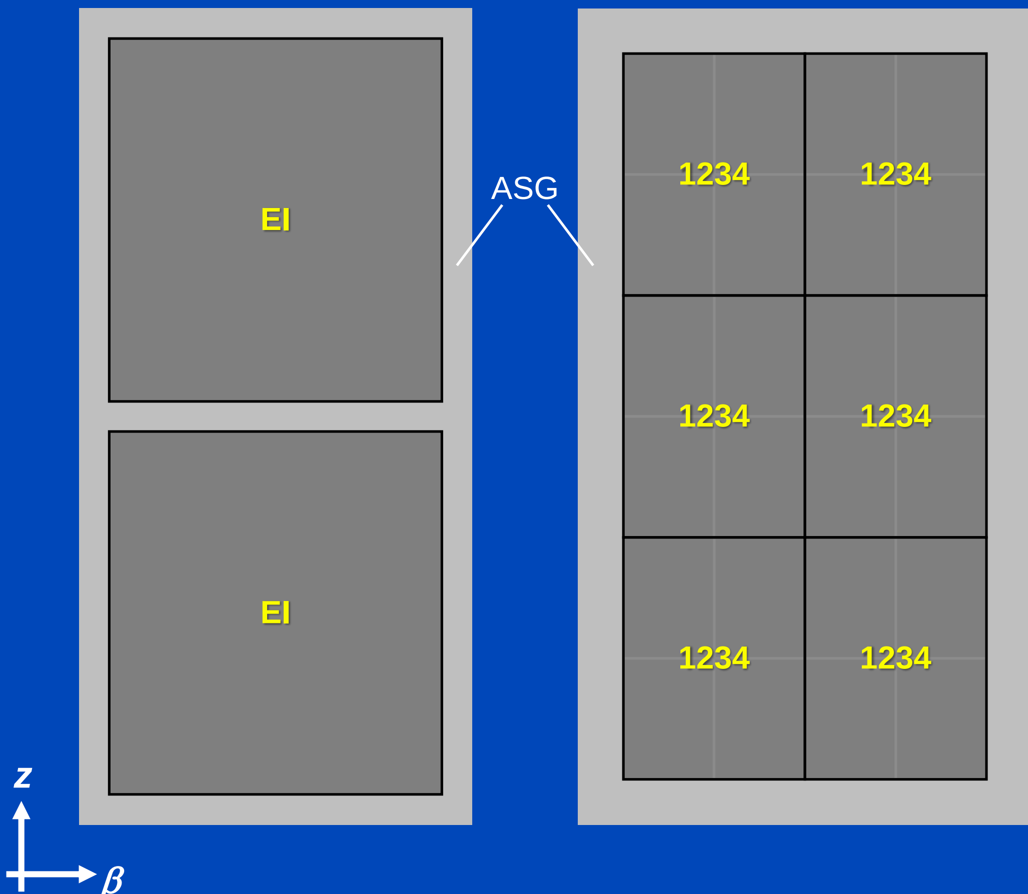

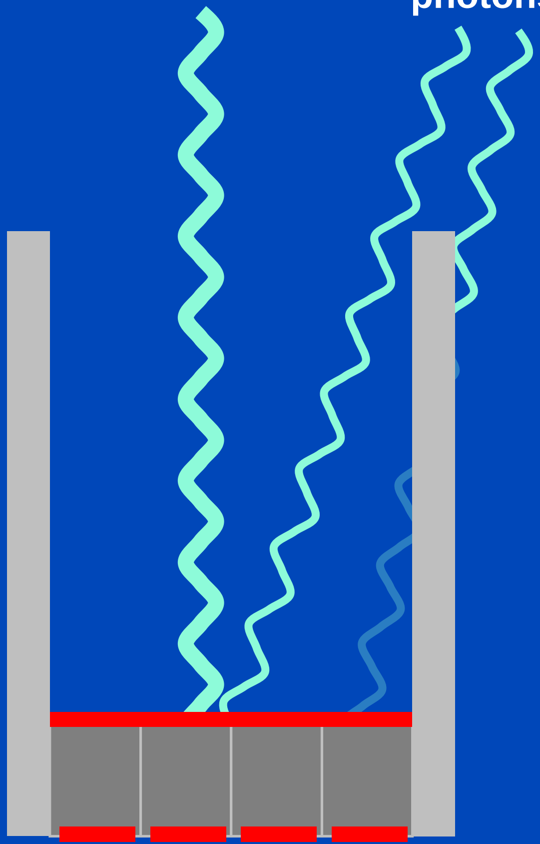

Coarse ASGs lead to changing scatter intensity between neighboring pixels.

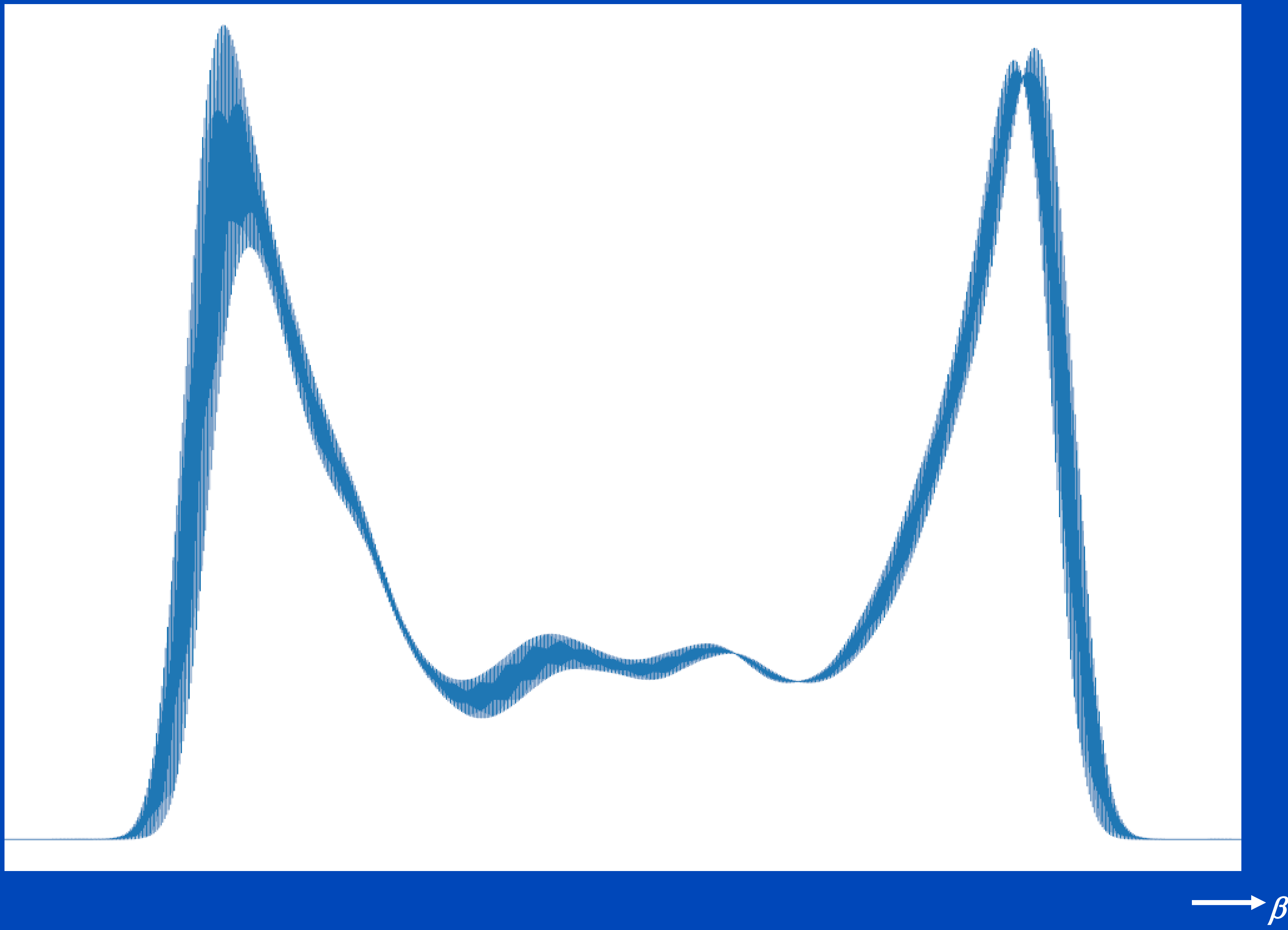

Scatter distribution averaged over all detector rows

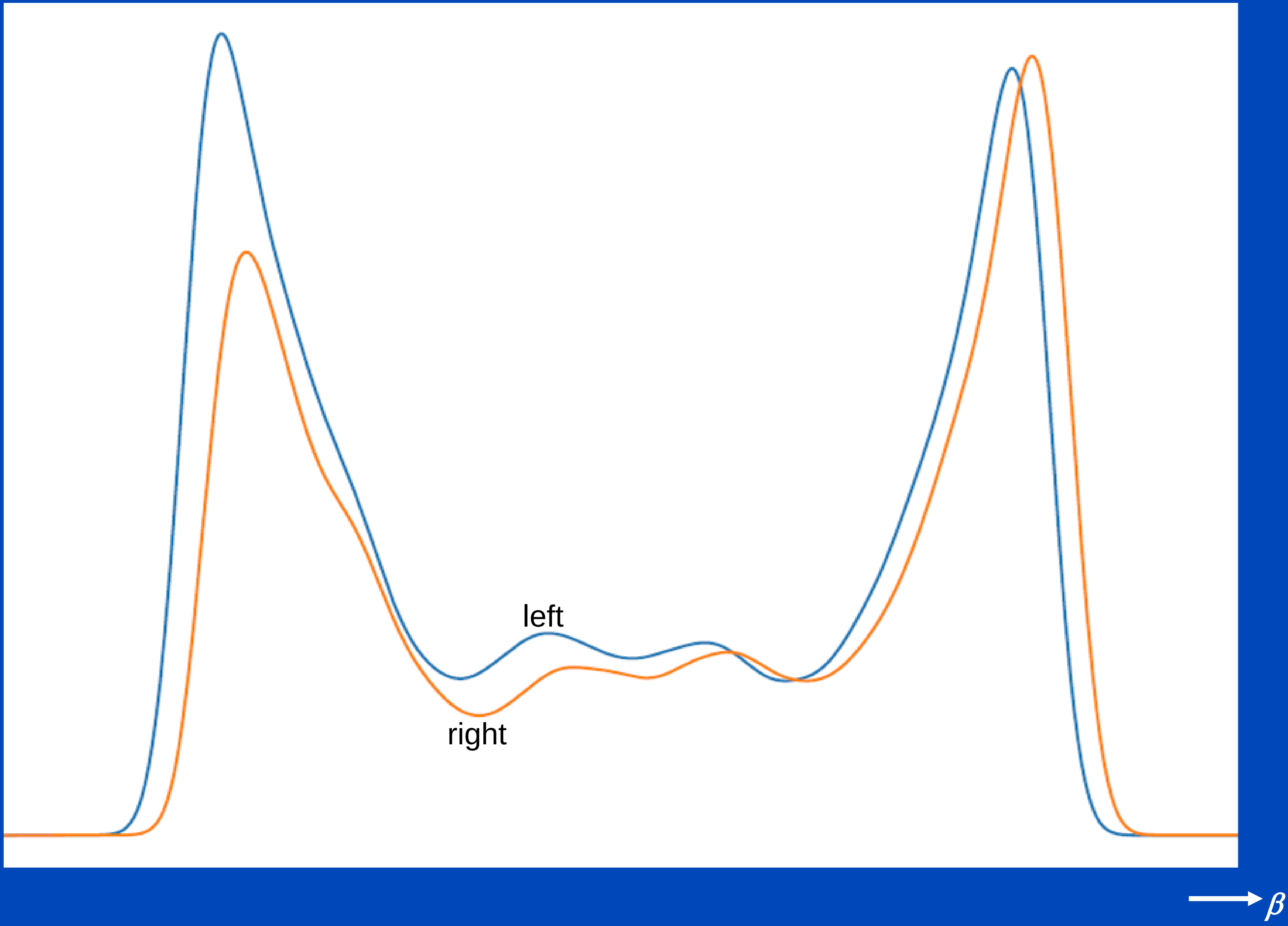

Scatter distribution averaged over all detector rows

Training and Validation Data

- Monte Carlo simulation with the geometry of the photon counting CT scanner NAEOTOM Alpha (Siemens Healthineers)
- 12 patients for training and 4 for validation
- 14 z-positions with 36 projections each simulated for each patient
- 8064 paired scatter and primary data pairs
- Simulation of coarse ASG with macro pixel with detector dimension of 1376 × 144 pixels
- 6 different macro pixels locations
- Smooth only across same macro-pixel locations

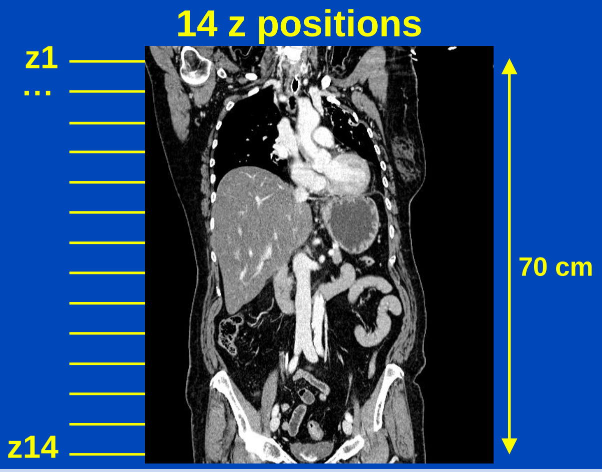

Training and validation patients with high variety and different clinical situations, important to consider scatter-to-primary ratio

Example of validation data set:

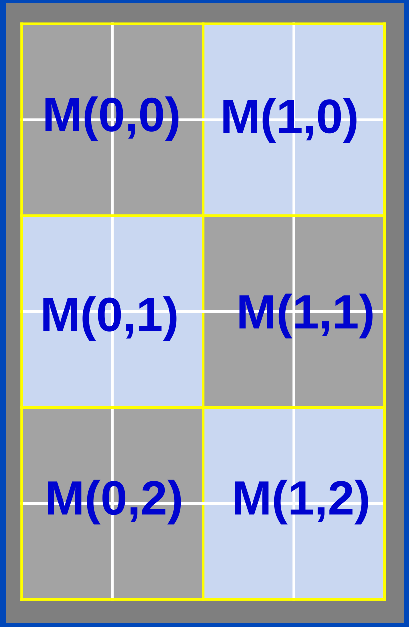

DSE for coarse ASG

Detector dimension
1376×144
Input mapping

$$p = -\ln\left(\frac{I_{\text{primary}}}{I_0} + \frac{I_{\text{scatter}}}{I_0}\right)$$

Each channel corresponds to a different pixel position between the lamallea of the ASG

Merging 6 different channels to obtain total scatter correction term

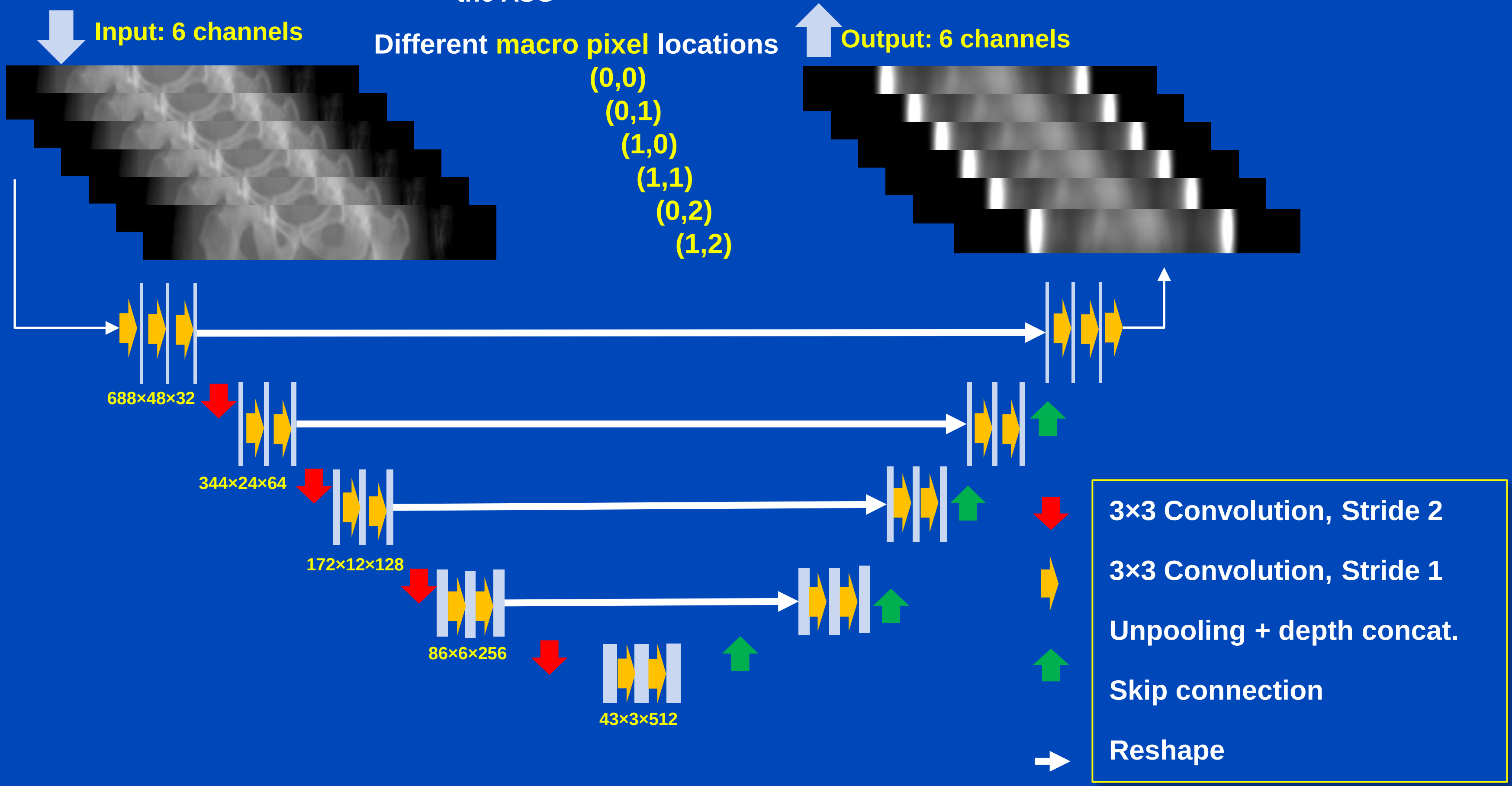

This paper received the "Highest Impact Paper Award" for the highest impact score at the 7th International Conference on Image Formation in X-Ray Computed Tomography in June 2022

Results in Reconstructed Images

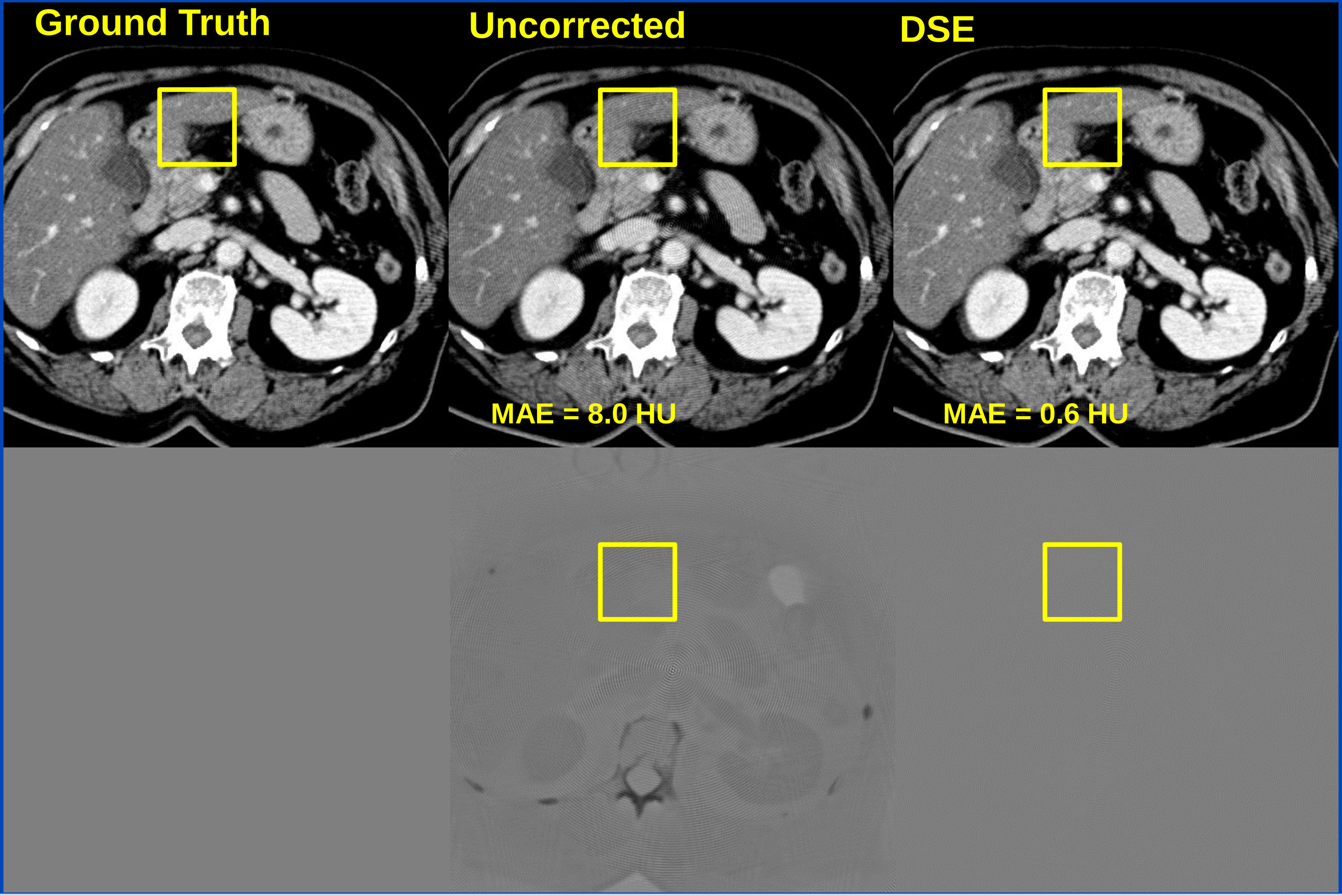

Simulated Reconstruction *C* = 0 HU, *W* = 400 HU,
Difference to GT *C* = 0 HU, *W* = 50 HU

Results in Reconstructed Images

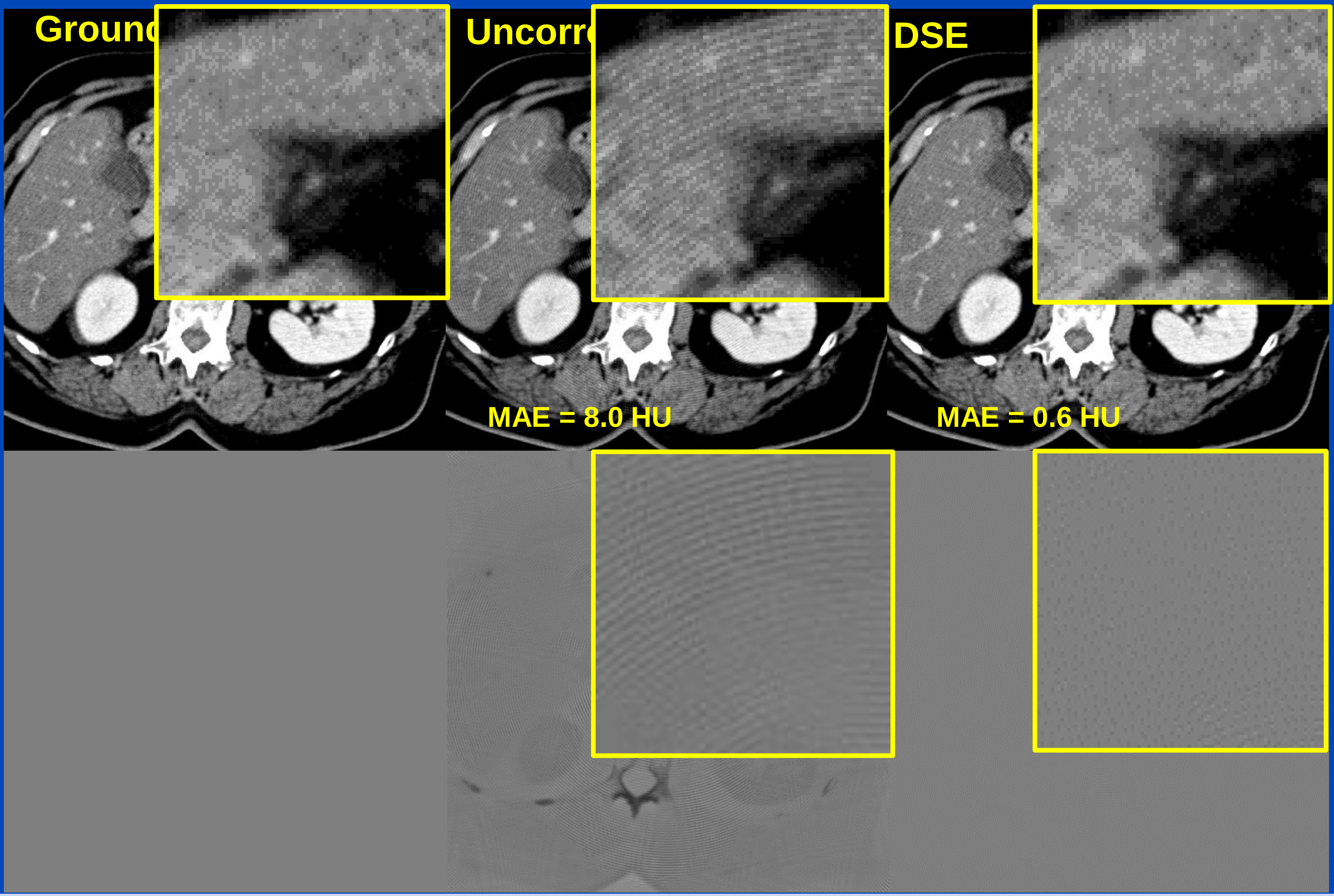

Simulated Reconstruction *C* = 0 HU, *W* = 400 HU,
Difference to GT *C* = 0 HU, *W* = 50 HU

Conclusions

- Coarse anti-scatter grid can lead to moiré artifacts due to scattered radiation.
- DSE reduces the mean absolute error (MAE) from about 9 HU to under 1 HU.
- The moiré pattern‘s amplitude can be reduced from 30 HU to less than 5 HU.

Deep Dose Estimation

???

In real time?

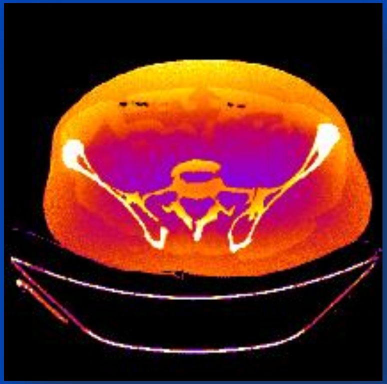

Estimation of Dose Distributions

- **Useful to study dose reduction techniques**
  - **Tube current modulation**
  - **Prefiltration and shaped filtration**
  - **Tube voltage settings**
  - **…**
- **Useful to estimate patient dose**
  - **Risk assessment requires segmentation of the organs (difficult)**
  - **Often semiantropomorphic patient models take over**
  - **The infamous k-factors that convert DLP into D_{eff} are derived this way, e.g. k_{chest} = 0.014 mSv/mGy/cm**
  - **…**
- **Could be useful for patient-specific CT scan protocol optimization**
- **However: Dose estimation does not work in real time!**

J. Maier, L. Klein, E. Eulig, S. Sawall, and M. Kachelrieß. Real-time estimation of patient-specific dose distributions for medical CT using the deep dose estimation. Med. Phys. 49(4):2259-2269, April 2022. *Best Paper within Machine Learning at ECR 2019!*

Motivation

- The potential risk of ionizing radiation makes dose assessment an important issue in CT imaging.
- Limitation of common metrics (e.g. $CTDI_w$, $CTDI_{vol}$, DLP, k-factor, SSDE, …) to provide information on organ or patient dose.

CTDI phantom | **Small patient** | **Medium patient** | **Large patient**

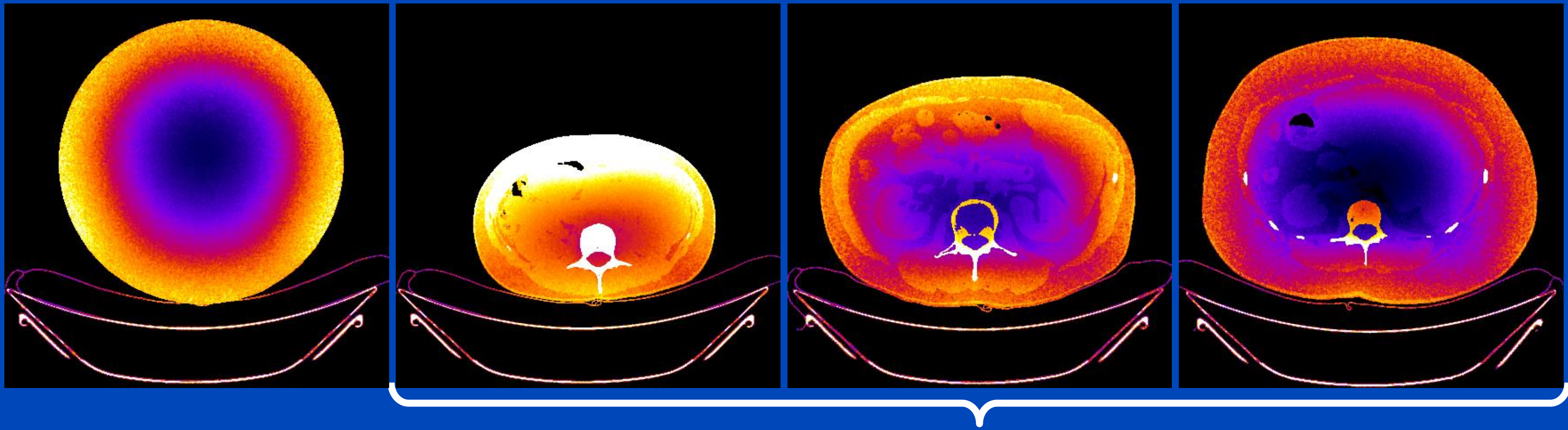

Same CTDI, but different dose distribution

Dose values in air voxels are set to zero (black) in this presentation.

MC Dose Simulation for a 360° Scan

Patient

Dose

ative Dose

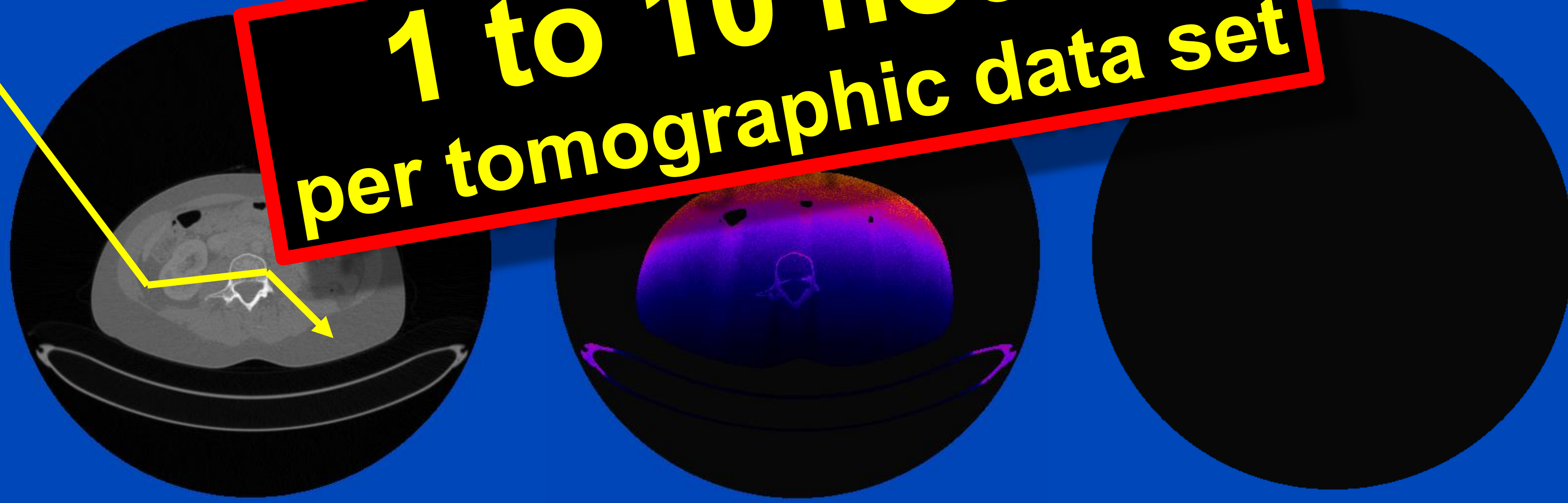

1 to 10 hours per tomographic data set

J. Maier, L. Klein, E. Eulig, S. Sawall, and M. Kachelrieß. Real-time estimation of patient-specific dose distributions for medical CT using the deep dose estimation. Med. Phys. 49(4):2259-2269, April 2022. *Best Paper within Machine Learning at ECR 2019!*

Influence of Bowtie Filter

- Commercial CT-scanners are usually equipped with a bowtie filter in order to optimize the patient dose distribution.
- Monte-Carlo dose calculations or statistical reconstruction algorithms require exact knowledge of the bowtie filter.
- The shape as well as the composition of the bowtie filter is usually not disclosed by the CT vendors.

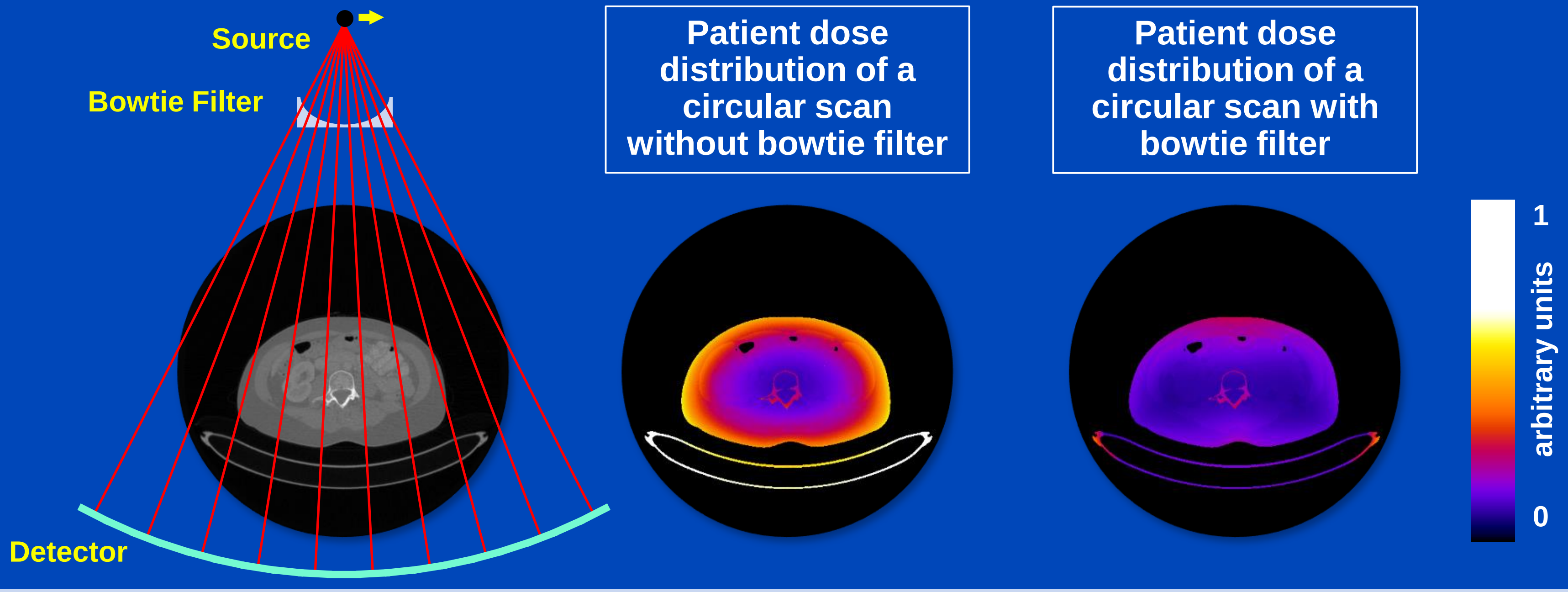

J. Maier, L. Klein, E. Eulig, S. Sawall, and M. Kachelrieß. Real-time estimation of patient-specific dose distributions for medical CT using the deep dose estimation. Med. Phys. 49(4):2259-2269, April 2022. *Best Paper within Machine Learning at ECR 2019!*

dkfz.

Patient-Specific Dose Estimation

- **Accurate solutions:**
  - Monte Carlo (MC) simulation[1], gold standard, stochastic LBTE solver
  - Analytic linear Boltzmann transport equation (LBTE) solver[2]

  → **Accurate but computationally expensive**
- **Fast alternatives:**
  - Application of patient-specific conversion factors to the DLP[3].
  - Application of look-up tables using MC simulations of phantoms[4].
  - Analytic approximation of CT dose deposition[5].

  → **Fast but less accurate**

[1] G. Jarry et al., "A Monte Carlo-based method to estimate radiation dose from spiral CT", Phys. Med. Biol. 48, 2003.
[2] A. Wang et al., "A fast, linear Boltzmann transport equation solver for computed tomography dose calculation (Acuros CTD)". Med. Phys. 46(2), 2019.
[3] B. Moore et al., "Size-specific dose estimate (SSDE) provides a simple method to calculate organ dose for pediatric CT examinations", Med. Phys. 41, 2014.
[4] A. Ding et al., "VirtualDose: a software for reporting organ doses from CT for adult and pediatric patients", Phys. Med. Biol. 60, 2015.
[5] B. De Man, "Dose reconstruction for real-time patient-specific dose estimation in CT", Med. Phys. 42, 2015.

Deep Dose Estimation (DDE)

- Train a UNet to predict patient dose given a CT image and a photo effect dose image
- Training data
  - 15 CT patient data sets segmented into air, fat, soft tissue, and bone
  - Simulate projection data by forward projection (120 kV, 720 projections, circle scans at 20 different z-positions to equally cover pelvis, abdomen, thorax and head).
  - Simulate scans without bowtie, with botwie, with bowtie and TCM
  - In total 15×20×3 = 900 data sets are reconstructed
  - Use Monte Carlo software RayConStruct-MC to calculate the patient dose distribution, thereby accounting for Rayleigh, Compton and photo effect.
  - Calculate photo effect dose distribution by direct backprojection and energy deposition in each voxel
- Training
  - U-Net sees the CT volumes and the corresponding first order (photoeffect) dose volumes and is trained to predict the patient dose distribution.
  - Since bone is underrepresented in all of the data sets, bone voxels received a twenty-fold weight in our MSE-based pixel-wise loss function

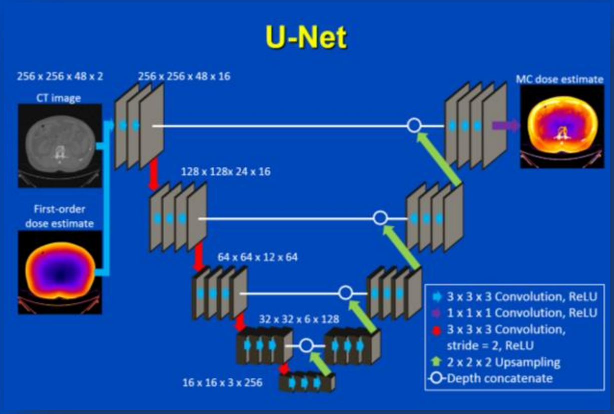

J. Maier, L. Klein, E. Eulig, S. Sawall, and M. Kachelrieß. Real-time estimation of patient-specific dose distributions for medical CT using the deep dose estimation. Med. Phys. 49(4):2259-2269, April 2022. *Best Paper within Machine Learning at ECR 2019!*

Deep Dose Estimation (DDE)

- Combine fast and accurate CT dose estimation using a deep convolutional neural network.
- Train the network to re… …nates given the CT … …mate.

1 to 10 seconds per tomographic data set

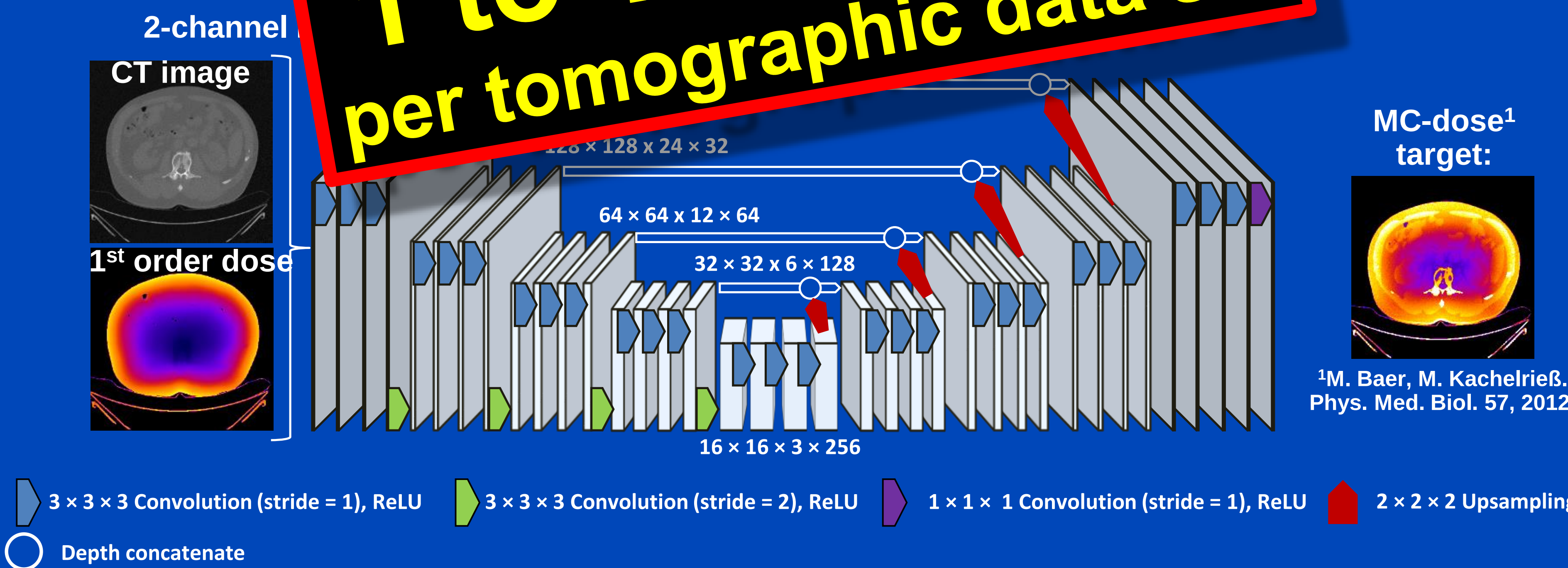

J. Maier, L. Klein, E. Eulig, S. Sawall, and M. Kachelrieß. Real-time estimation of patient-specific dose distributions for medical CT using the deep dose estimation. Med. Phys. 49(4):2259-2269, April 2022. *Best Paper within Machine Learning at ECR 2019!*

dkfz.

First-Order Dose Estimate

- DDE network needs information about the tube current, the tube voltage, shaped filters etc., which is encoded in the first-order dose estimate.
- First order dose-estimate in a voxel with volume V and mass *m* at position *r* :

$$D_{1^{\mathrm{st}}}(\boldsymbol{r}) = \frac{V}{m} \int \frac{d^2N}{d\Omega dE} \sum_{i=\mathrm{PE,\ CS}} P_{\mathrm{int},i}(\boldsymbol{r}, E) E_{\mathrm{dep},i}(E)\, dE$$

Emission characteristic of the x-ray source (including shaped filters)

Interaction probability for photo effect (*i* = PE) and Compton scattering (*i* = CS)

Energy deposition by photo effect (*i* = PE) and Compton scattering (*i* = CS)

$$P_{\mathrm{int,\ PE}}(\boldsymbol{r}, E) = \mu_{\mathrm{PE}}(\boldsymbol{r}, E) \cdot e^{-\int_0^r \mu(r', E) dr'} \qquad E_{\mathrm{dep,\ PE}}(E) = E$$

$$P_{\mathrm{int,\ CS}}(\boldsymbol{r}, E) = \mu_{\mathrm{CS}}(\boldsymbol{r}, E) \cdot e^{-\int_0^r \mu(r', E) dr'} \qquad E_{\mathrm{dep,\ CS}}(E) = \int \frac{d\sigma}{d\Omega}(E) \Delta E_{\mathrm{CS}}(\vartheta) d\Omega$$

Training and Validation

- Simulation of 1440 circular dual-source CT scans (64×0.6 mm, FOM_A = 50 cm, FOM_B = 32 cm) of thorax, abdomen, and pelvis using 12 different patients.

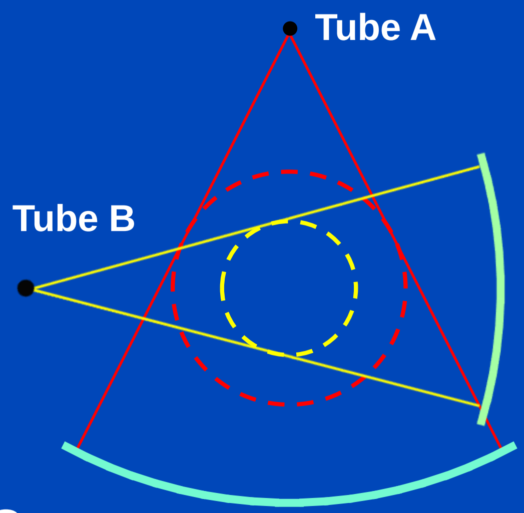

- Simulation with and without bowtie.
- No data augmentation
- Reconstruction on a 512×512×96 grid with 1 mm voxel size, followed by 2×2×2 binning for dose estimation.
- 9 patients were used for training and 3 for testing.
- DDE was trained for 300 epochs on an Nvidia Quadro P6000 GPU using a mean absolute error pixel-wise loss, the Adam optimizer, and a batch size of 4.
- The same weights and biases were used for all cases.

1440 = 12 patients × 20 z-positions × 6 modes (A, A+bowtie, A+bowtie+TCM, B, B+Bowtie, B+bowtie+TCM)

Results

Thorax, tube A, 120 kV, with bowtie

CT image

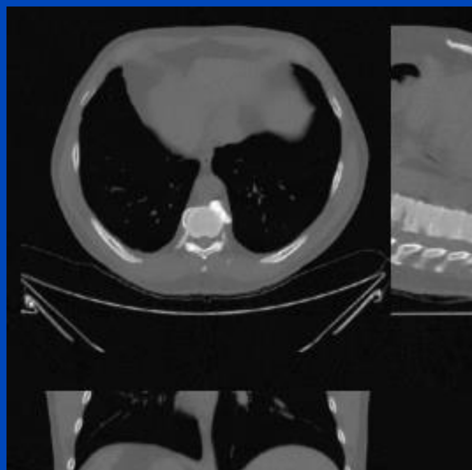

First order dose

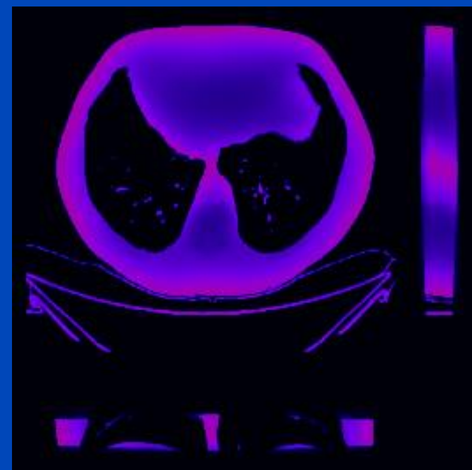

	MC	DDE
48 slices	1 h	0.25 s
whole body	20 h	5 s

MC uses 16 CPU kernels
DDE uses one Nvidia Quadro P600 GPU

DDE training took 74 h for 300 epochs, 1440 samples, 48 slices per sample

MC ground truth

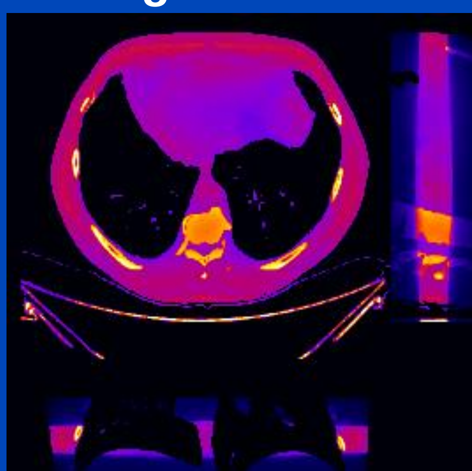

DDE

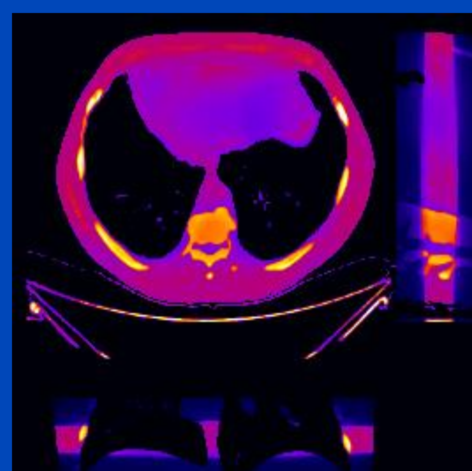

Relative error

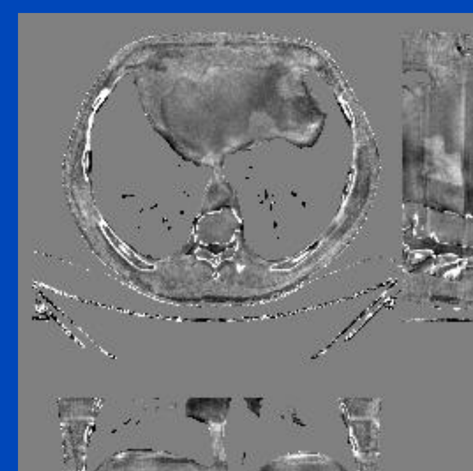

C = 0%
W = 40%

J. Maier, L. Klein, E. Eulig, S. Sawall, and M. Kachelrieß. Real-time estimation of patient-specific dose distributions for medical CT using the deep dose estimation. Med. Phys. 49(4):2259-2269, April 2022. *Best Paper within Machine Learning at ECR 2019!*

Results

Thorax, tube A, 120 kV, no bowtie

CT image

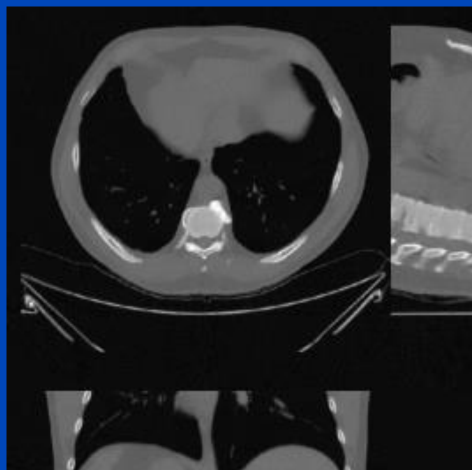

First order dose

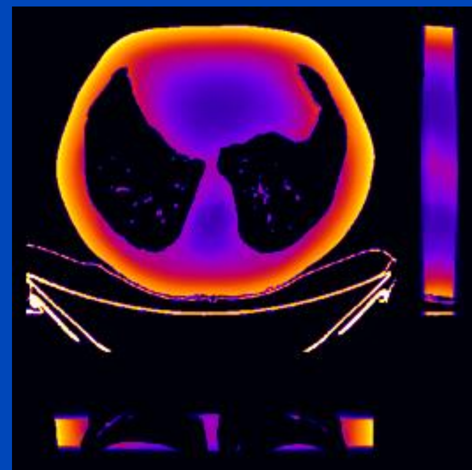

	MC	DDE
48 slices	1 h	0.25 s
whole body	20 h	5 s

MC uses 16 CPU kernels
DDE uses one Nvidia Quadro P600 GPU

DDE training took 74 h for 300 epochs, 1440 samples, 48 slices per sample

MC ground truth

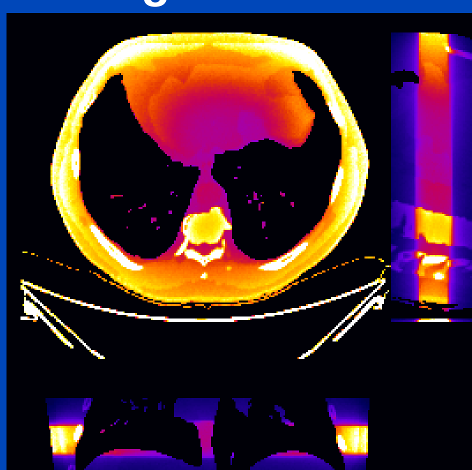

DDE

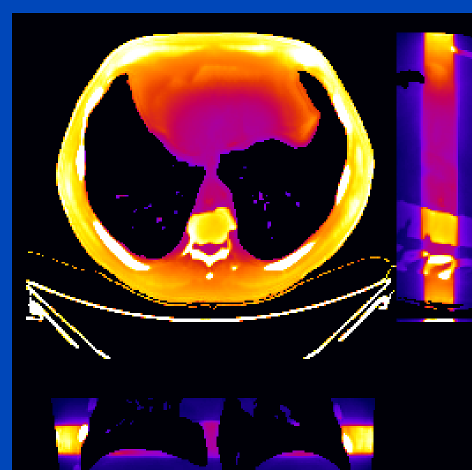

Relative error

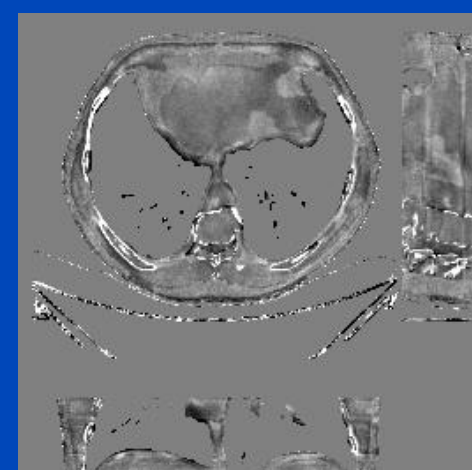

C = 0%
W = 40%

J. Maier, L. Klein, E. Eulig, S. Sawall, and M. Kachelrieß. Real-time estimation of patient-specific dose distributions for medical CT using the deep dose estimation. Med. Phys. 49(4):2259-2269, April 2022. *Best Paper within Machine Learning at ECR 2019!*

Conclusions on DDE

- DDE provides accurate dose predictions
  - for circle scans
  - for sequence scans
  - for partial scans (less than 360°)
  - for limited angle scans (less than 180°)
  - for spiral scans
  - for different tube voltages
  - for scans with and without bowtie filtration
  - for scans with tube current modulation
- In practice it may therefore be not necessary to perform separate training runs for these cases.
- Thus, accurate real-time patient dose estimation may become feasible with DDE.

Part 5:

Other Applications

Patient Risk-Minimizing Tube Current Modulation

1. Coarse reconstruction from two scout views

– E.g. X. Ying, et al. X2CT-GAN: Reconstructing CT from biplanar x-rays with generative adversarial networks.
CVPR 2019.

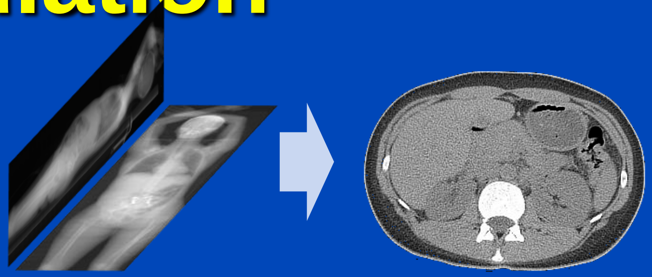

2. Segmentation of radiation-sensitive organs

– E.g. S. Chen, M. Kachelrieß et al., Automatic multi-organ segmentation in dual-energy CT (DECT) with dedicated 3D fully convolutional DECT networks. Med. Phys. 2019.

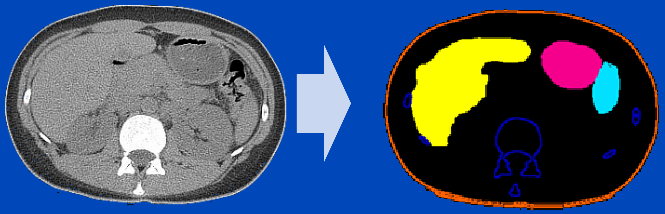

3. Calculation of the effective dose per view using the deep dose estimation (DDE)

– J. Maier, E. Eulig, S. Dorn, S. Sawall and M. Kachelrieß. Real-time patient-specific CT dose estimation using a deep convolutional neural network. IEEE Medical Imaging Conference Record, M-03-178: 3 pages, Nov. 2018.

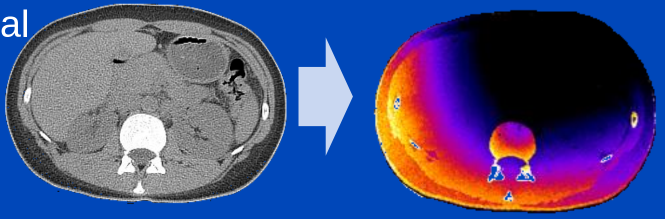

4. Determination of the tube current modulation curve that minimizes the radiation risk

– L. Klein, C. Liu, J. Steidel, L. Enzmann, M. Knaup, S. Sawall, A. Maier, M. Lell, J. Maier, and M. Kachelrieß. Patient-specific radiation risk-based tube current modulation for diagnostic CT. Med. Phys. 49(7):4391-4403, July 2022.

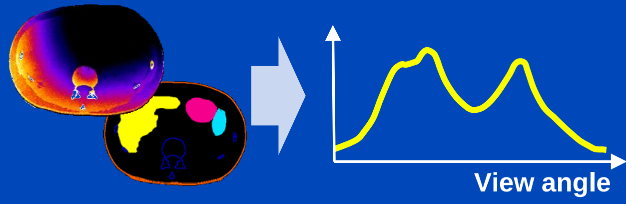

[1]L. Klein, C. Liu, J. Steidel, L. Enzmann, M. Knaup, S. Sawall, A. Maier, M. Lell, J. Maier, and M. Kachelrieß.
Patient-specific radiation risk-based tube current modulation for diagnostic CT. Med. Phys. 49(7):4391-4403, July 2022.

AMERICAN ASSOCIATION of PHYSICISTS IN MEDICINE

Congratulations

This paper received the Sylvia&Moses Greenfield Award for the best scientific paper on imaging in Medical Physics in 2022.

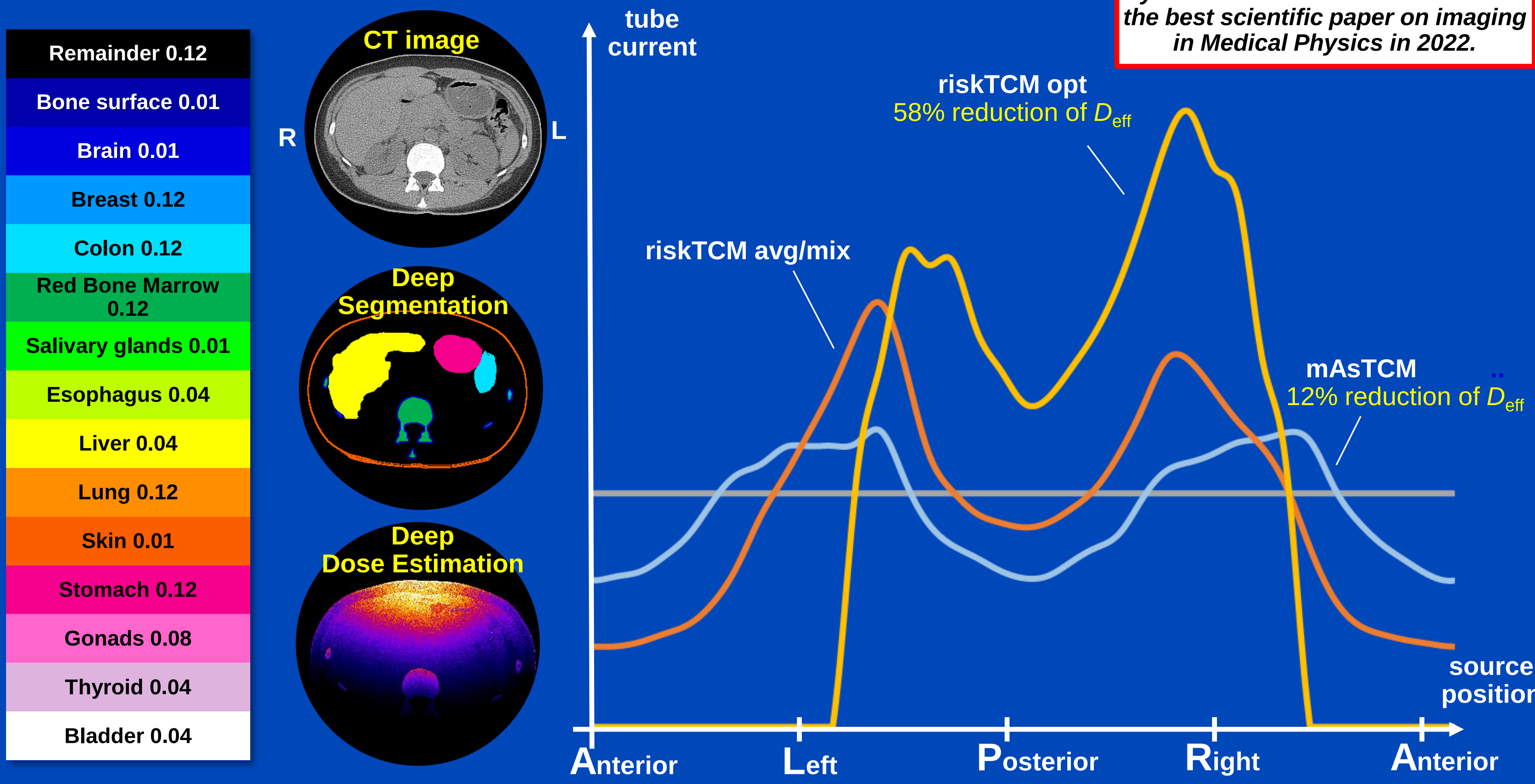

[1]L. Klein, C. Liu, J. Steidel, L. Enzmann, M. Knaup, S. Sawall, A. Maier, M. Lell, J. Maier, and M. Kachelrieß.
Patient-specific radiation risk-based tube current modulation for diagnostic CT. Med. Phys. 49(7):4391-4403, July 2022.
This paper received the Sylvia&Moses Greenfield Award for the best scientific paper on imaging in Medical Physics in 2022.

dkfz.

Patient 03 - Neck

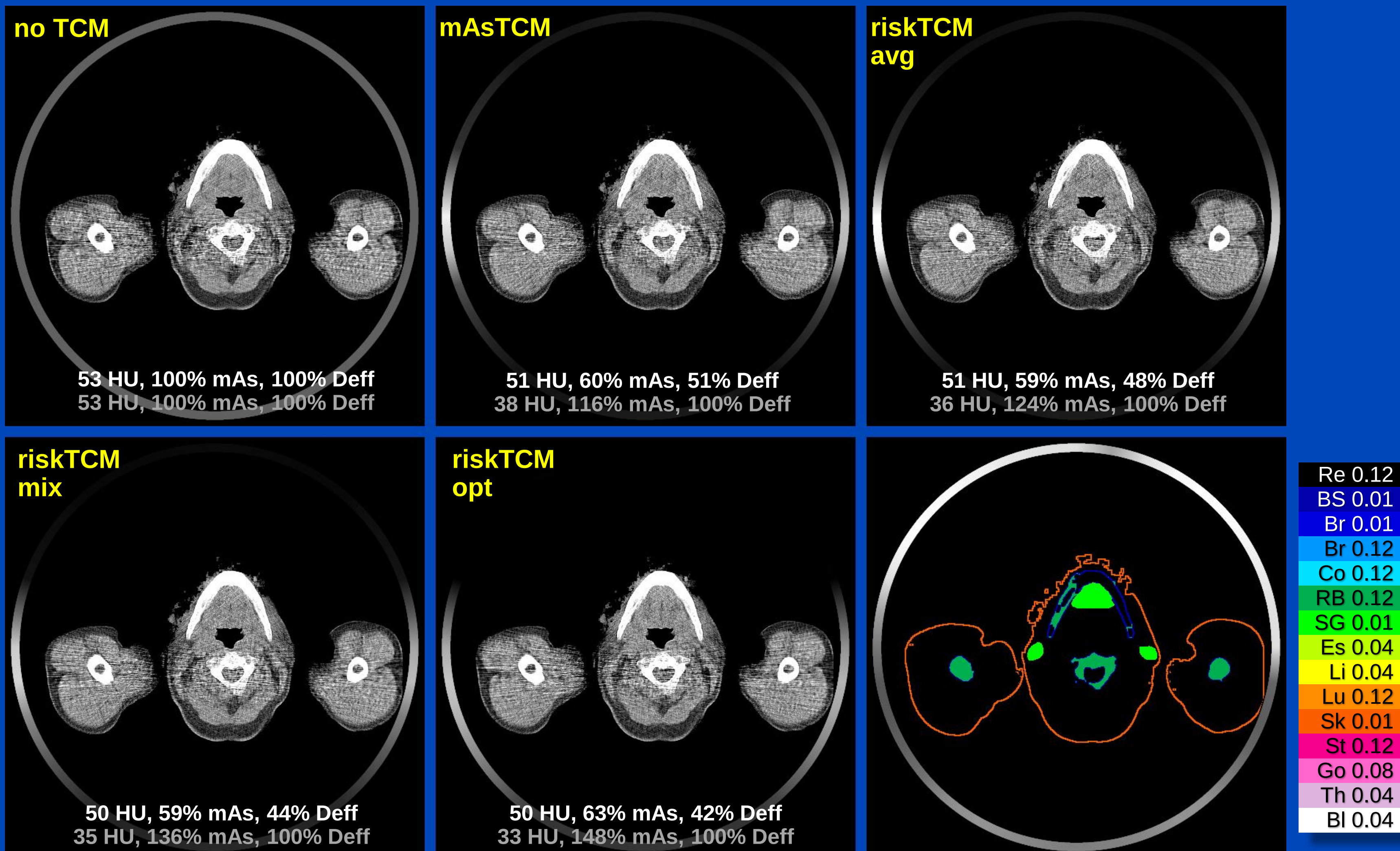

C **= 25 HU,** ***W*** **= 400 HU**

[1]L. Klein, C. Liu, J. Steidel, L. Enzmann, M. Knaup, S. Sawall, A. Maier, M. Lell, J. Maier, and M. Kachelrieß. Patient-specific radiation risk-based tube current modulation for diagnostic CT. Med. Phys. 49(7):4391-4403, July 2022.

This paper received the Sylvia&Moses Greenfield Award for the best scientific paper on imaging in Medical Physics in 2022.

Patient 03 - Pelvis

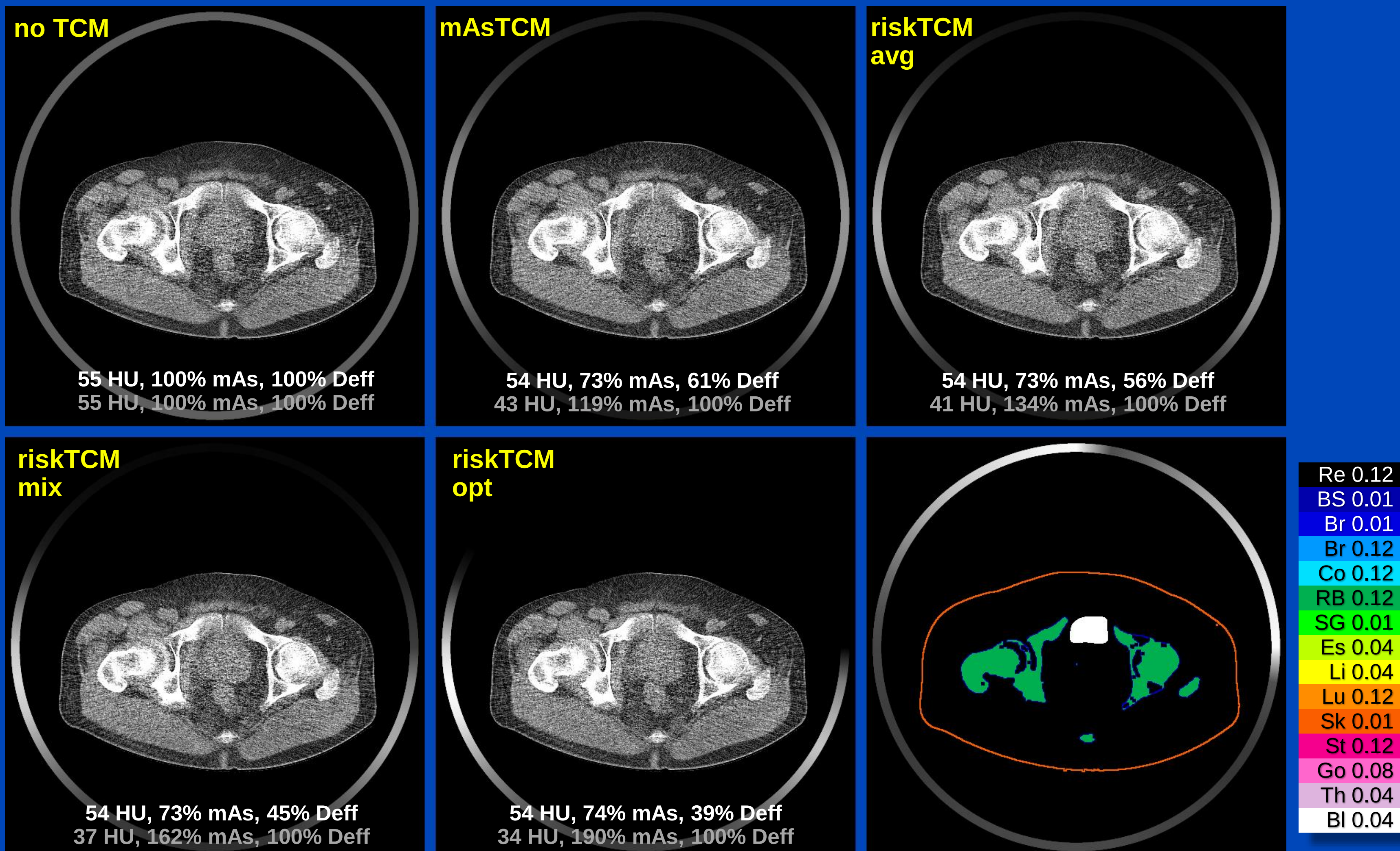

C = 25 HU, *W* = 400 HU

[1]L. Klein, C. Liu, J. Steidel, L. Enzmann, M. Knaup, S. Sawall, A. Maier, M. Lell, J. Maier, and M. Kachelrieß.
Patient-specific radiation risk-based tube current modulation for diagnostic CT. Med. Phys. 49(7):4391-4403, July 2022.
This paper received the Sylvia&Moses Greenfield Award for the best scientific paper on imaging in Medical Physics in 2022.

Patient 04 - Abdomen

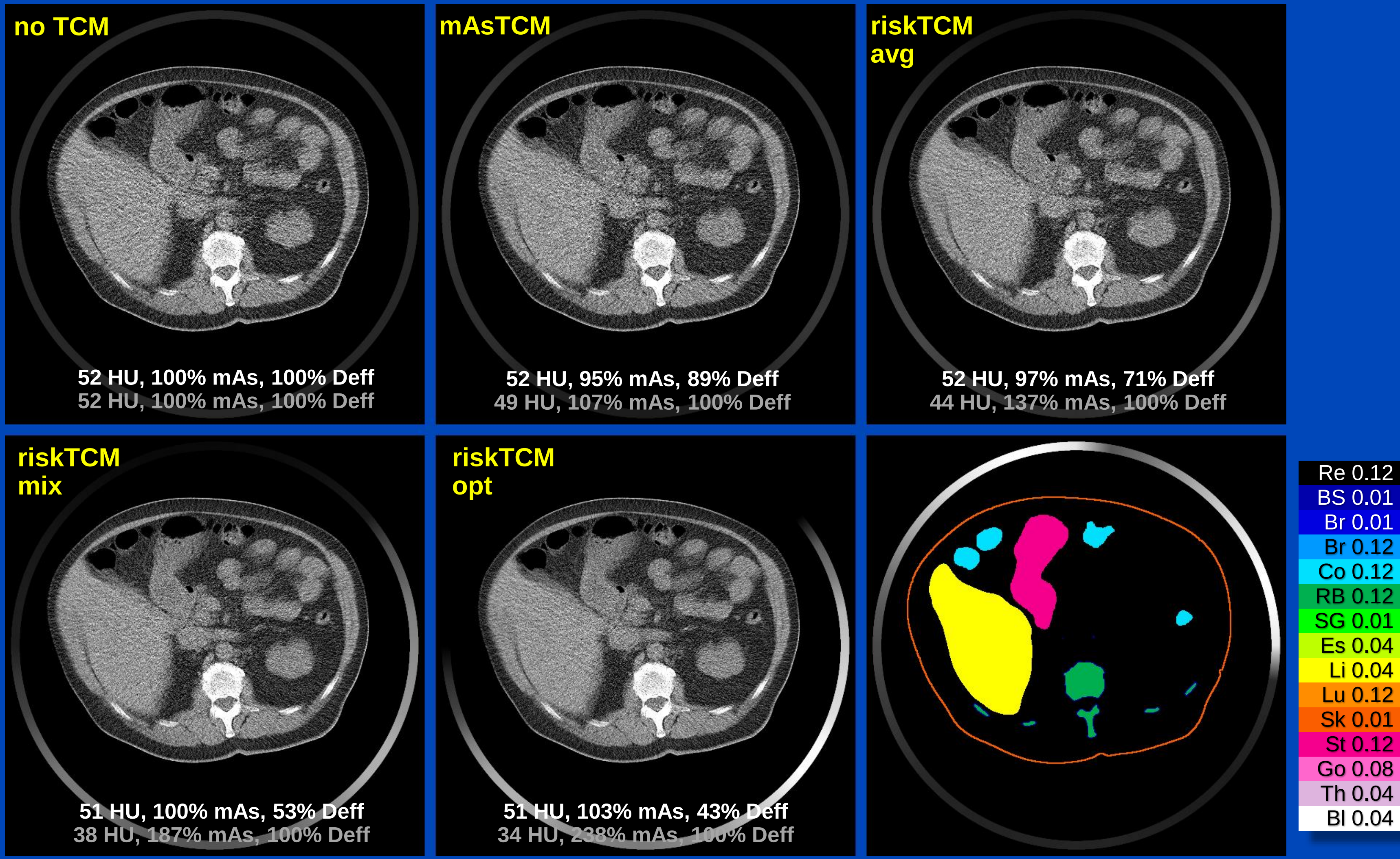

C = 25 HU, *W* = 400 HU

[1]L. Klein, C. Liu, J. Steidel, L. Enzmann, M. Knaup, S. Sawall, A. Maier, M. Lell, J. Maier, and M. Kachelrieß. Patient-specific radiation risk-based tube current modulation for diagnostic CT. Med. Phys. 49(7):4391-4403, July 2022.
This paper received the Sylvia&Moses Greenfield Award for the best scientific paper on imaging in Medical Physics in 2022.

	noTCM	mAsTCM	riskTCM
Head w Arms:			
01	167%	100%	98%
02	156%	100%	85%
03	168%	100%	91%
04	145%	100%	89%
Average	(159±11)%	100%	(91±6)%
Head w/o Arms:			
01	100%	100%	90%
02	121%	100%	88%
03	107%	100%	93%
04	110%	100%	92%
Average	(110±9)%	100%	(91±2)%
Thorax:			
32no	132%	100%	67%
33ko	112%	100%	80%
40mm	116%	100%	81%
42mo	115%	100%	75%
54km	112%	100%	80%
66nm	111%	100%	81%
63mo	115%	100%	76%
Average	(116±7)%	100%	(77±5)%
Abdomen:			
32no	127%	100%	78%
33ko	102%	100%	90%
40mm	108%	100%	84%
42mo	115%	100%	75%
54km	103%	100%	75%
66nm	102%	100%	64%
63mo	110%	100%	69%
Average	(109±9)%	100%	(77±9)%
Pelvis:			
32no	133%	100%	93%
42mo	135%	100%	81%
63mo	139%	100%	89%
Average	(136±2)%	100%	(88±6)%

[1]L. Klein, C. Liu, J. Steidel, L. Enzmann, M. Knaup, S. Sawall, A. Maier, M. Lell, J. Maier, and M. Kachelrieß.
Patient-specific radiation risk-based tube current modulation for diagnostic CT. Med. Phys. 49(7):4391-4403, July 2022.
This paper received the Sylvia&Moses Greenfield Award for the best scientific paper on imaging in Medical Physics in 2022.

Effective Dose at Same Image Noise Relative to mAsTCM

Average over all patients

Head

Tube Voltage	noTCM	mAsTCM	riskTCM
70 kV	**110%** from 100% to 121%	**100%**	**91%** from 80% to 96%
100 kV	**110%** from 100% to 122%	**100%**	**92%** from 83% to 96%
120 kV	**111%** from 101% to 123%	**100%**	**92%** from 84% to 96%
150 kV	**110%** from 101% to 122%	**100%**	**92%** from 86% to 96%

Head+Arms

Tube Voltage	noTCM	mAsTCM	riskTCM
70 kV	**163%** from 145% to 178%	**100%**	**87%** from 84% to 91%
100 kV	**158%** from 139% to 186%	**100%**	**87%** from 83% to 91%
120 kV	**160%** from 142% to 183%	**100%**	**88%** from 84% to 94%
150 kV	**161%** from 144% to 183%	**100%**	**88%** from 82% to 95%

[1]L. Klein, C. Liu, J. Steidel, L. Enzmann, M. Knaup, S. Sawall, A. Maier, M. Lell, J. Maier, and M. Kachelrieß.
Patient-specific radiation risk-based tube current modulation for diagnostic CT. Med. Phys. 49(7):4391-4403, July 2022.
This paper received the Sylvia&Moses Greenfield Award for the best scientific paper on imaging in Medical Physics in 2022.

Effective Dose at Same Image Noise Relative to mAsTCM

Average over all patients

Neck

Tube Voltage	noTCM	mAsTCM	riskTCM
70 kV	**230%** from 175% to 303%	100%	**73%** from 57% to 78%
100 kV	**225%** from 178% to 300%	100%	**76%** from 61% to 80%
120 kV	**221%** from 179% to 299%	100%	**77%** from 62% to 81%
150 kV	**214%** from 175% to 274%	100%	**77%** from 64% to 82%

Thorax

Tube Voltage	noTCM	mAsTCM	riskTCM
70 kV	**113%** from 108% to 118%	100%	**77%** from 67% to 82%
100 kV	**113%** from 107% to 117%	100%	**81%** from 74% to 85%
120 kV	**113%** from 107% to 118%	100%	**82%** from 75% to 86%
150 kV	**113%** from 108% to 118%	100%	**83%** from 76% to 87%

[1]L. Klein, C. Liu, J. Steidel, L. Enzmann, M. Knaup, S. Sawall, A. Maier, M. Lell, J. Maier, and M. Kachelrieß.
Patient-specific radiation risk-based tube current modulation for diagnostic CT. Med. Phys. 49(7):4391-4403, July 2022.
This paper received the Sylvia&Moses Greenfield Award for the best scientific paper on imaging in Medical Physics in 2022.

dkfz.

Effective Dose at Same Image Noise Relative to mAsTCM

Average over all patients

Abdomen

Tube Voltage	noTCM	mAsTCM	riskTCM
70 kV	**113%** from 105% to 135%	**100%**	**69%** from 57% to 76%
100 kV	**113%** from 103% to 137%	**100%**	**71%** from 62% to 79%
120 kV	**114%** from 106% to 135%	**100%**	**72%** from 64% to 79%
150 kV	**115%** from 106% to 136%	**100%**	**73%** from 66% to 80%

Pelvis

Tube Voltage	noTCM	mAsTCM	riskTCM
70 kV	**153%** from 134% to 189%	**100%**	**76%** from 65% to 91%
100 kV	**152%** from 134% to 186%	**100%**	**78%** from 68% to 91%
120 kV	**151%** from 134% to 184%	**100%**	**80%** from 72% to 92%
150 kV	**151%** from 136% to 184%	**100%**	**81%** from 72% to 93%

[1]L. Klein, C. Liu, J. Steidel, L. Enzmann, M. Knaup, S. Sawall, A. Maier, M. Lell, J. Maier, and M. Kachelrieß.
Patient-specific radiation risk-based tube current modulation for diagnostic CT. Med. Phys. 49(7):4391-4403, July 2022.
This paper received the Sylvia&Moses Greenfield Award for the best scientific paper on imaging in Medical Physics in 2022.

Conclusions on RiskTCM

- Risk-specific TCM minimizes the patient risk.
- With D_{eff} as a risk model riskTCM can reduce risk by up to 30%, compared with the gold standard mAsTCM.
- Other risk models, in particular age-, weight- and sex-specific models, can be used with riskTCM as well.
- Note:
  -
  - good for the patient
  - detector flux equalizing TCM = good for the detector

It is up to the vendors to take action!

ECR 2022 – Best Research Presentation Abstract
within the topic Physics in Medical Imaging
with the presentation:

Risk-minimising tube current modulation (riskTCM) for CT – potential dose reduction across different tube voltages (16765)

L. Klein1, C. Liu2, J. Steidel1, L. Enzmann1, S. Sawall1, J. Maier1, A. Maier2, M. Lell3, M. Kachelrieß1; 1Heidelberg/DE, 2Erlangen/DE, 3Nuremberg/DE

AMERICAN ASSOCIATION of PHYSICISTS IN MEDICINE

Congratulations

This paper received the Sylvia&Moses Greenfield Award for the best scientific paper on imaging in Medical Physics in 2022.

[1]L. Klein, C. Liu, J. Steidel, L. Enzmann, M. Knaup, S. Sawall, A. Maier, M. Lell, J. Maier, and M. Kachelrieß.
Patient-specific radiation risk-based tube current modulation for diagnostic CT. Med. Phys. 49(7):4391-4403, July 2022.
This paper received the Sylvia&Moses Greenfield Award for the best scientific paper on imaging in Medical Physics in 2022.

riskTCM vs. Breast-Specific TCM

- osTCM mimics X-Care (Siemens Healthineers)
- Reduces the tube current to 25% for the anterior 120°
- Higher tube current for the remaining 240°

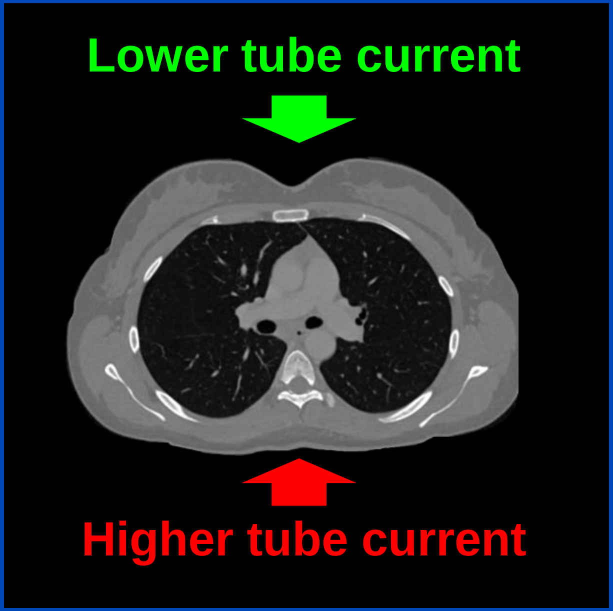

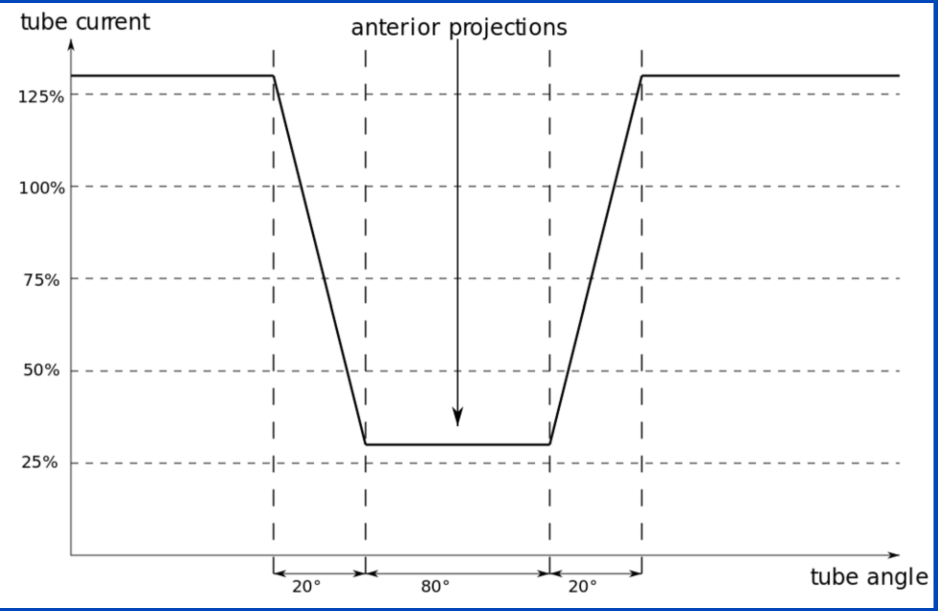

D. Ketelsen et al. Automated computed tomography dosesaving algorithm to protect radiosensitive tissues: estimation of radiation exposure and image quality considerations. Invest Radiol, 47(2):148–52, 2012

Results

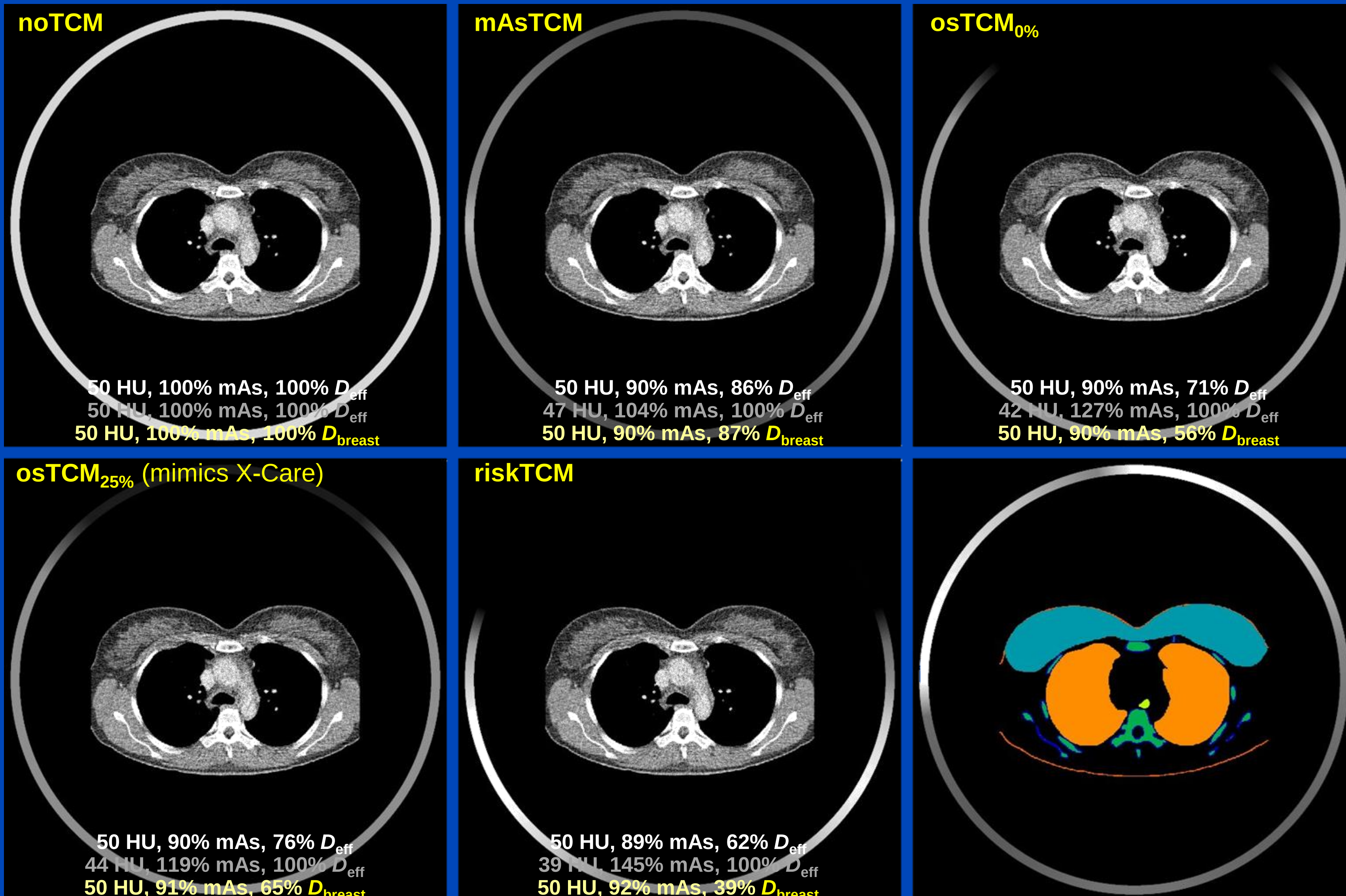

Data courtesy of Prof. Lell, Nürnberg. C = 25 HU, W = 400 HU

Dose Values for the Thorax at Same Image Noise for 70 kV

Average over all patients

TCM Method	Effective Dose D_{eff}	Dose to the Breast D_{Breast}
noTCM	**116%** from 111% to 132%	**108%** from 102% to 125%
mAsTCM	**100%**	**100%**
$\mathrm{osTCM}_{25\%}$	**95%** from 91% to 100%	**77%** from 74% to 90%
$\mathrm{osTCM}_{0\%}$	**91%** from 83% to 98%	**70%** from 65% to 87%
riskTCM	**77%** from 67% to 81%	**49%** from 40% to 66%

Conclusions on RiskTCM

- Risk-specific TCM minimizes the patient risk.
- With D_{eff} as a risk model riskTCM can reduce risk by up to 50% and more, compared with the gold standard mAsTCM.
- Other risk m… …eight- and sex-spec… …used with riskTCM as well.
- Note:
  - mAsTCM = good for the x-ray tube
  - riskTCM = good for the patient
  - detector flux equalizing TCM = good for the detector
- Compared with breast-specific TCM the riskTCM approach is 25% lower in dose.

It is up to the vendors to take action!

[1] L. Klein, C. Liu, J. Steidel, L. Enzmann, M. Knaup, S. Sawall, A. Maier, M. Lell, J. Maier, and M. Kachelrieß. Patient-specific radiation risk-based tube current modulation for diagnostic CT. Med. Phys. 49(7):4391-4403, July 2022.
This paper received the Sylvia&Moses Greenfield Award for the best scientific paper on imaging in Medical Physics in 2022.

Part 6: Registration and MoCo

4D CBCT MoCo with Deep Image Registration?

- 4D CBCT refers to respiratory-gated CBCT images
- Due to gating, streak artifacts typically occur
- A motion compensation (MoCo) helps to warp the respiratory phases into a target phase. MoCo requires to estimate the motion vector fields (MVFs).
- MVF estimation uses deformable registration.

Examples for CBCT MoCo

3D CBCT Standard	**4D gated CBCT** Conventional Phase-Correlated	**sMoCo** Standard Motion Compensation	**acMoCo** Artifact Model-Based Motion Compensation

sMoCo: Li, Koong, and Xing, "Enhanced 4D cone–beam CT with inter–phase motion model," Med. Phys. 51(9), 3688–3695, 2007.
cMoCo: Brehm, Paysan, Oelhafen, Kunz, and Kachelrieß, "Self-adapting cyclic registration for motion-compensated cone-beam CT in image-guided radiation therapy," Med. Phys. 39(12):7603-7618, 2012.
acMoCo: Brehm, Paysan, Oelhafen, and Kachelrieß, "Artifact-resistant motion estimation with a patient-specific artifact model for motion-compensated cone-beam CT" Med. Phys. 40(10):101913, 2013.

Demons Deformable Registration

- **Static target image s**
- **Model to be deformed m**
- **Find transformation vector field T, i.e. $s = m \circ \mathrm{T}$**
- **Demons algorithm**
  - **Displacement update u by intensity matching on linear approximation**

$$\boldsymbol{u} = \frac{m - s}{\|\boldsymbol{\nabla} s\|^2 + (m - s)^2} \boldsymbol{\nabla} s$$

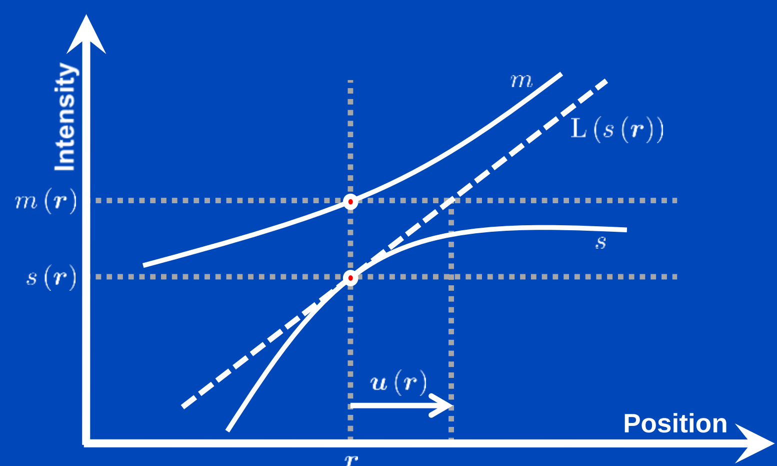

- **Regularization**
  - **Two Gaussian convolution kernels $G_{\text{fluid}}, G_{\text{diffusion}}$**

$$\mathrm{T} \leftarrow G_{\text{diffusion}} * (\mathrm{T} \circ \exp(G_{\text{fluid}} * \boldsymbol{u}))$$

Deformed model matching target

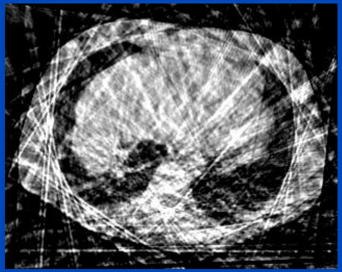

Thirion, "Image matching as a diffusion process: An analogy with Maxwell's demons," Medical Image Analysis 2(3), 243–260, 1998.

VoxelMorph Deformable Registration

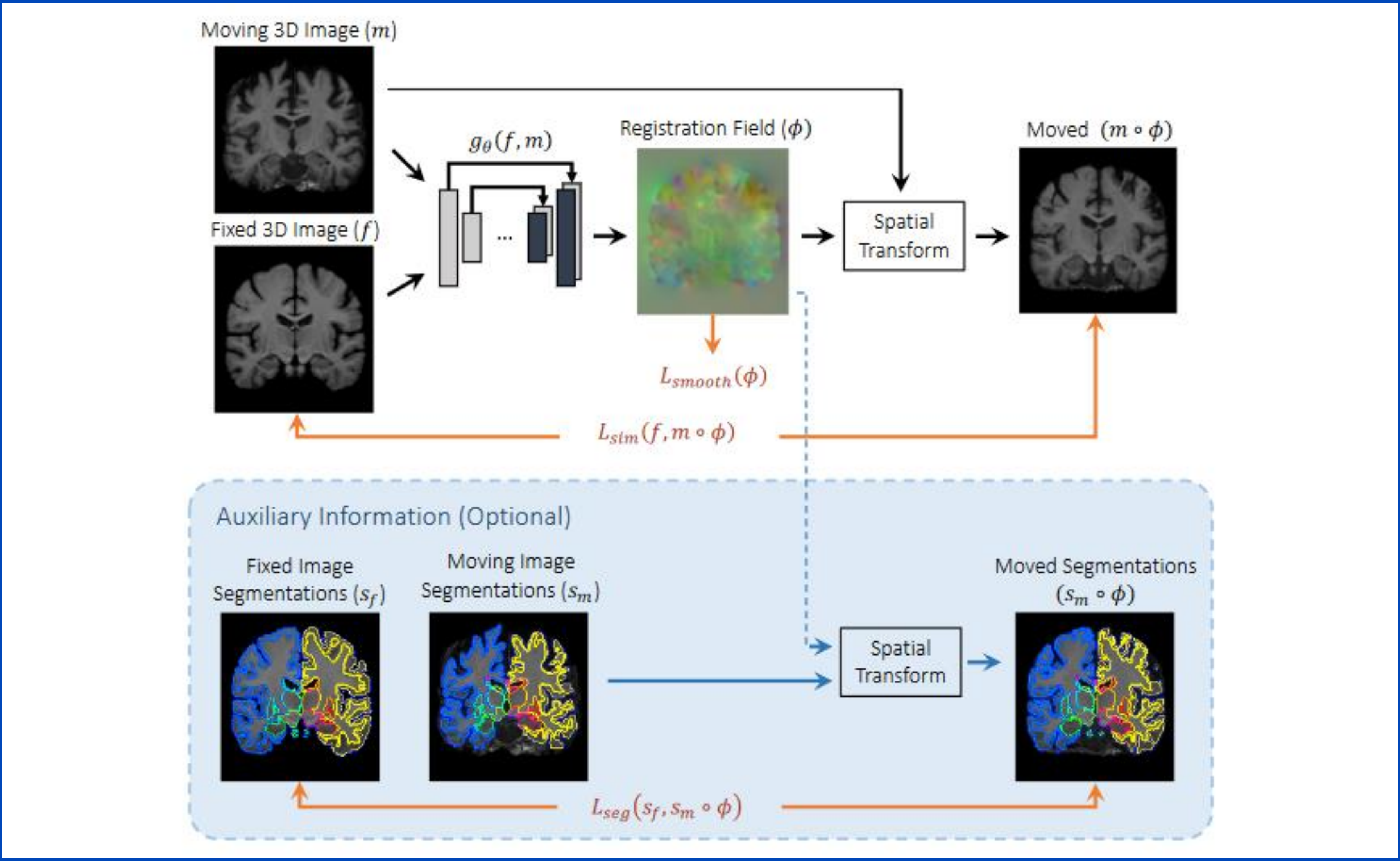

Balakrishnan, G., Zhao, A., Sabuncu, M. R., Guttag, J. and Dalca, A. V., "VoxelMorph: A Learning Framework for Deformable Medical Image Registration," IEEE Trans. Med. Imaging 38(8), 1788–1800, 2019.

Demons vs. VoxelMorph

- Cost/loss functions of Demons and VoxelMorph are identical if we use the L_2-norm for the vector field regularization and the MSE for the image similarity

$$C = \arg\min_{\phi} \left\| m(\phi) - f \right\|_2^2 + \lambda \left\| \nabla \phi \right\|_2^2$$

- Demon's hierarchical registration cascade corresponds to VoxelMorph's hierarchical encoder/decoder stages.
- Both methods can be extended to estimate a diffeomorphic vector field, i.e. a differentiable and invertible vector field.
- Demons minimizes the cost function for every patient, while VoxelMorph learned to minimize it for the training parients and then applies its knowledge to other patients.
- Demons may be slower than VoxelMorph (a thorough comparison is missing), but is potentially more reliable and predictable.
- Voxel morph may learn motion patterns from training patients that are not visible in the test patient and then apply such patterns during inference (e.g. contrasted vs. non-contrasted liver).
- A combination of VoxelMorph followed by one Demons iteration may be ideal.

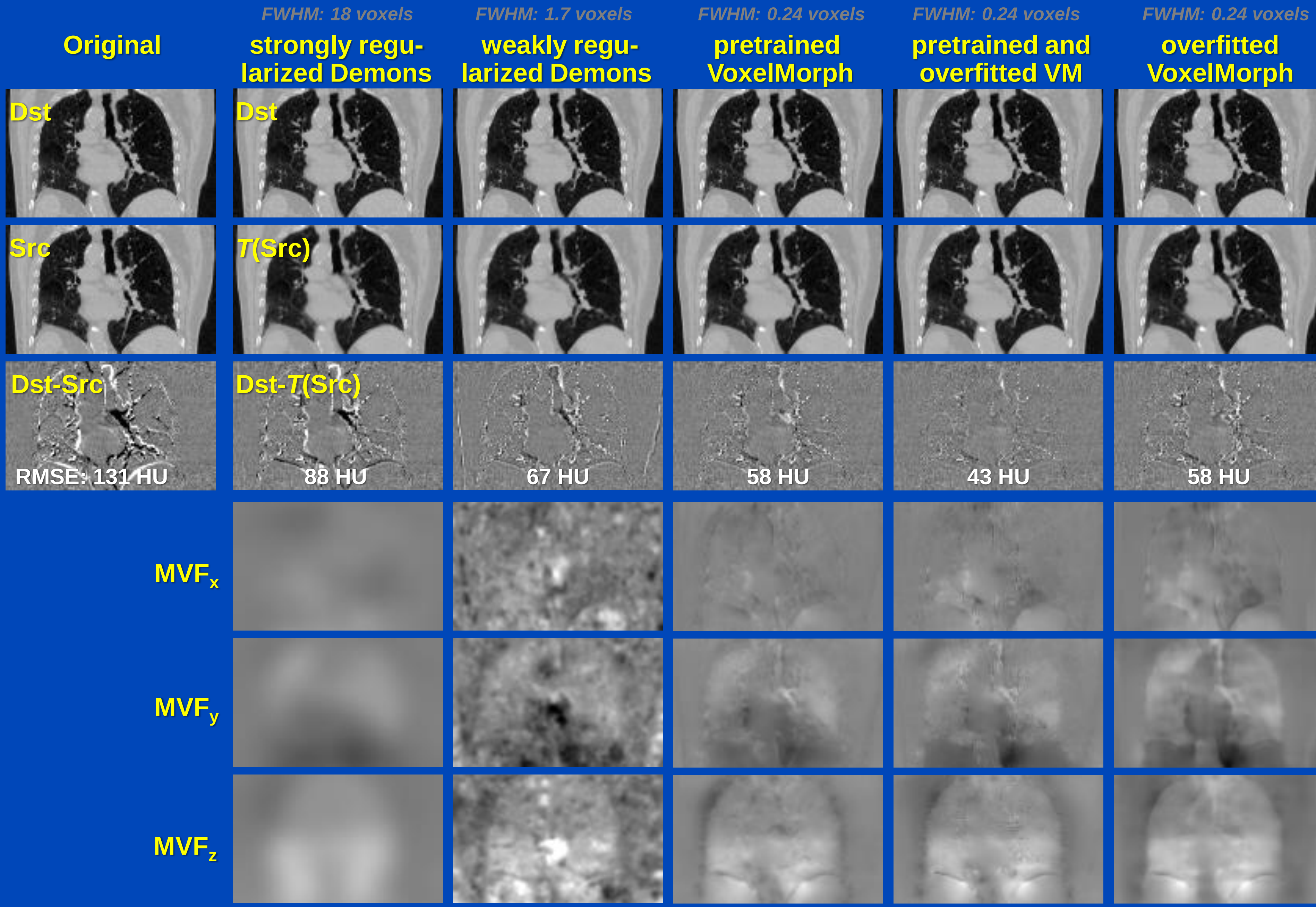

CBCT images: C = 0 HU, W = 2000 HU. Difference images: C = 0 HU, W = 400 HU.
MVFs: C = 0 mm, W = 12 mm.

Deep Cardiac Motion Compensation

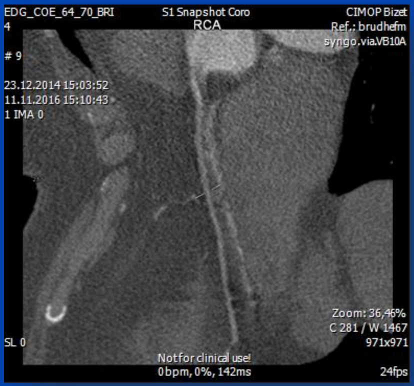

???

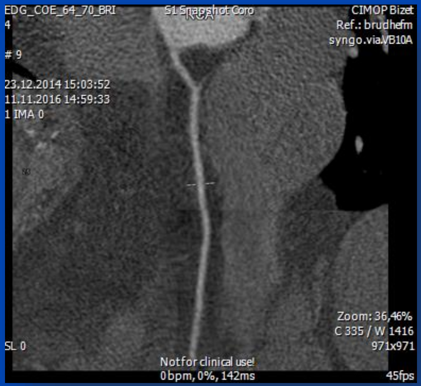

Motivation

- Cardiac CT imaging is routinely used for the diagnosis of cardiovascular diseases, especially those related to coronary arteries.
- Imaging of coronary arteries places high demands on the spatial and temporal resolution of the CT reconstruction.
- Motion artifacts and image noise may impair the diagnostic value of the CT examination.

CTCA image of the right coronary artery[1]

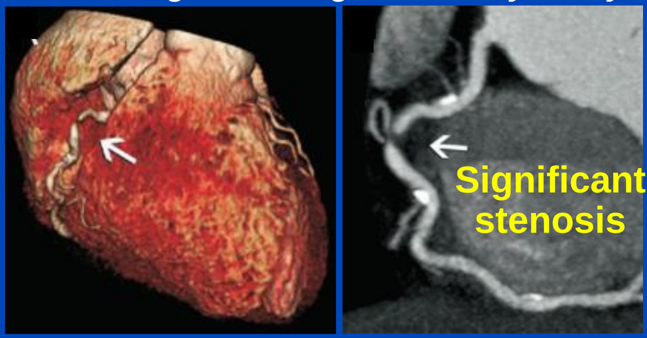

CTCA image of the left coronary artery[2]

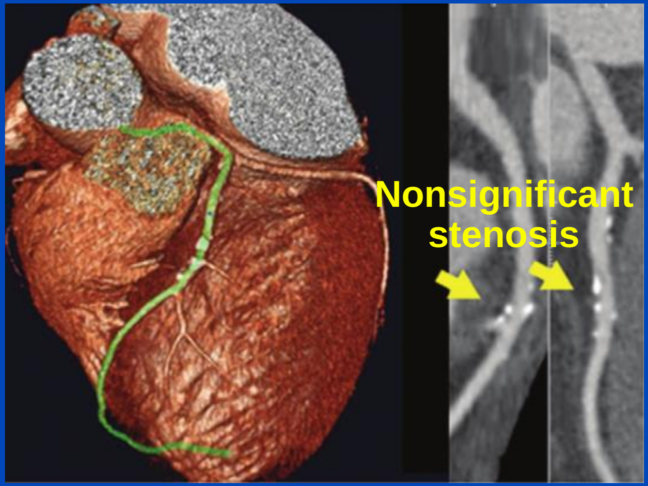

[1] W. B. Meijboom et al., "64-Slice Computed Tomography Coronary Angiography in Patients With High, Intermediate, or Low Pretest Probability of Significant Coronary Artery Disease", J. Am. Coll. Cardiol. 50 (15): 1469–1475 (2007).
[2] R. Leta et al., "Ruling Out Coronary Artery Disease with Noninvasive Coronary Multidetector CT Angiography before Noncoronary Cardiovascular Surgery", Heart 258 (2) (2011).

Motivation

C = 0 HU, *W* = 1200 HU

Motion artifacts

High noise levels

Table 3: Reason for FFR_{CT} Rejection in the ADVANCE Registry and Clinical Cohort *

Reason for Rejection	FFR_{CT} Rejected* ADVANCE Registry (n = 80)	Clinical Cohort (n = 892)
Inadequate image quality†		
Blooming	4 (5.0)	29 (3.0)
Clipped structure	4 (5.0)	39 (4.3)
Motion artifacts	63 (78.0)	729 (81.4)
Image noise	2 (2.5)	198 (22.1)
Inappropriate submission		
Stent or previous coronary artery bypass graft present	5 (6.2)	116 (13.0)
Cardiac hardware present	2 (2.5)	29 (3.2)

The rejection rate was 892 of 10416 cases submitted

* G. Pontone et al., "Determinants of Rejection Rate for Coronary CT Angiography Fractional Flow Reserve Analysis", *Radiology*, *292*(3), 597–605 (2019)

Motivation

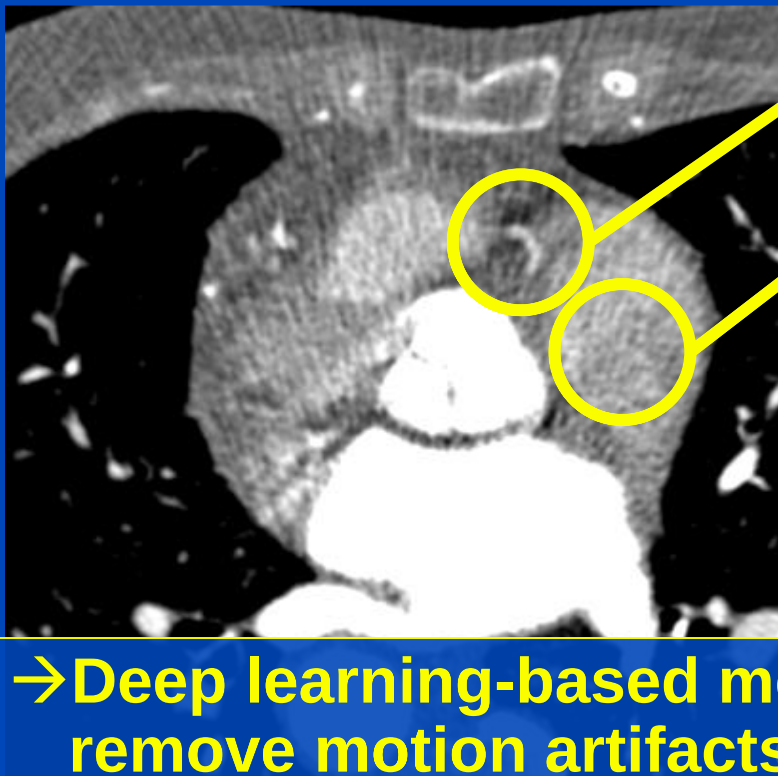

Motion artifacts

High noise levels

Table 3: Reason for FFR_{CT} Rejection in the ADVANCE Registry and Clinical Cohort		
	FFR_{CT} Rejected*	
Reason for Rejection	ADVANCE Registry (n = 80)	Clinical Cohort (n = 892)
Inadequate image quality†		
Blooming	4 (5.0)	29 (3.0)
[illegible]	[illegible]	[illegible]
[illegible]	[illegible]	[illegible]
Image noise	2 (2.5)	198 (22.1)
Inappropriate submission		
[illegible] artery bypass graft present	[illegible]	[illegible]
Cardiac hardware present	2 (2.5)	29 (3.2)

The rejection rate was 892 of 10416 cases submitted

*

→Deep learning-based motion compensation to remove motion artifacts.

→Iterative reconstruction (Siemens ADMIRE) to reduce noise.

* G. Pontone et al., “Determinants of Rejection Rate for Coronary CT Angiography Fractional Flow Reserve Analysis”, *Radiology*, *292*(3), 597–605 (2019)

dkfz.

Partial Angle-Based Motion Compensation (PAMoCo)

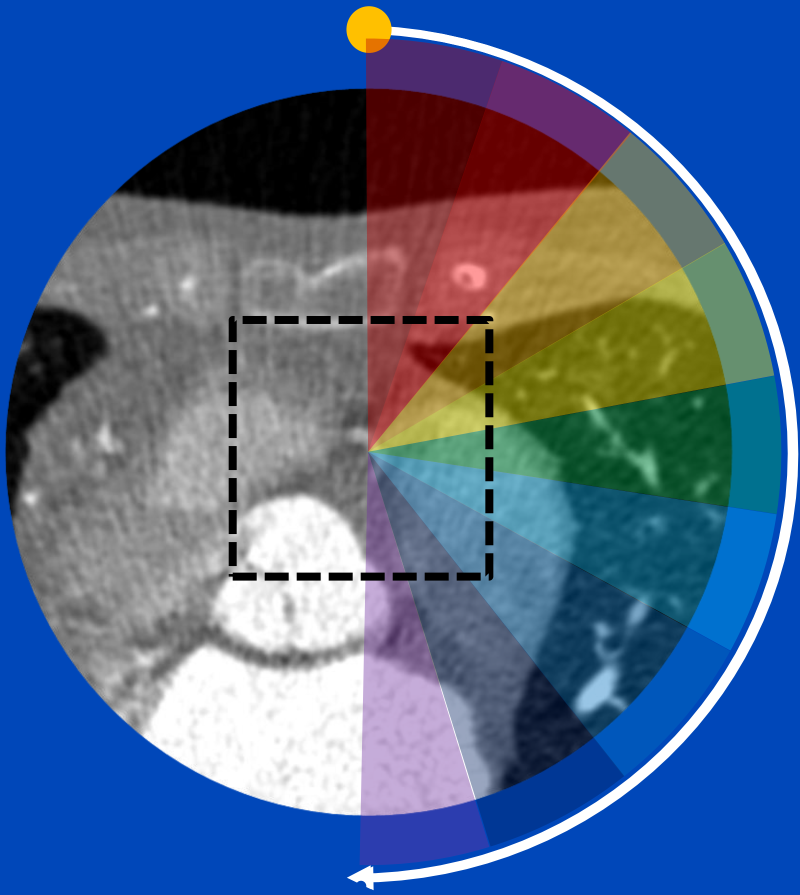

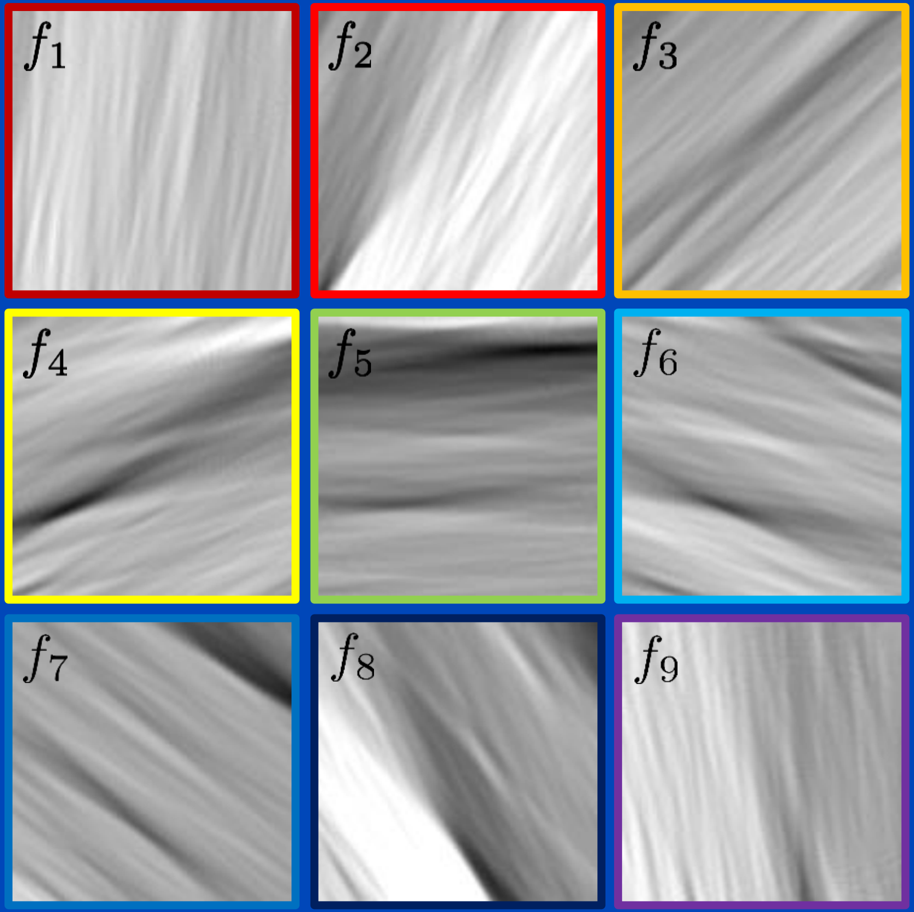

Animated rotation time = 100 × real rotation time

dkfz.

Partial Angle-Based Motion Compensation (PAMoCo)

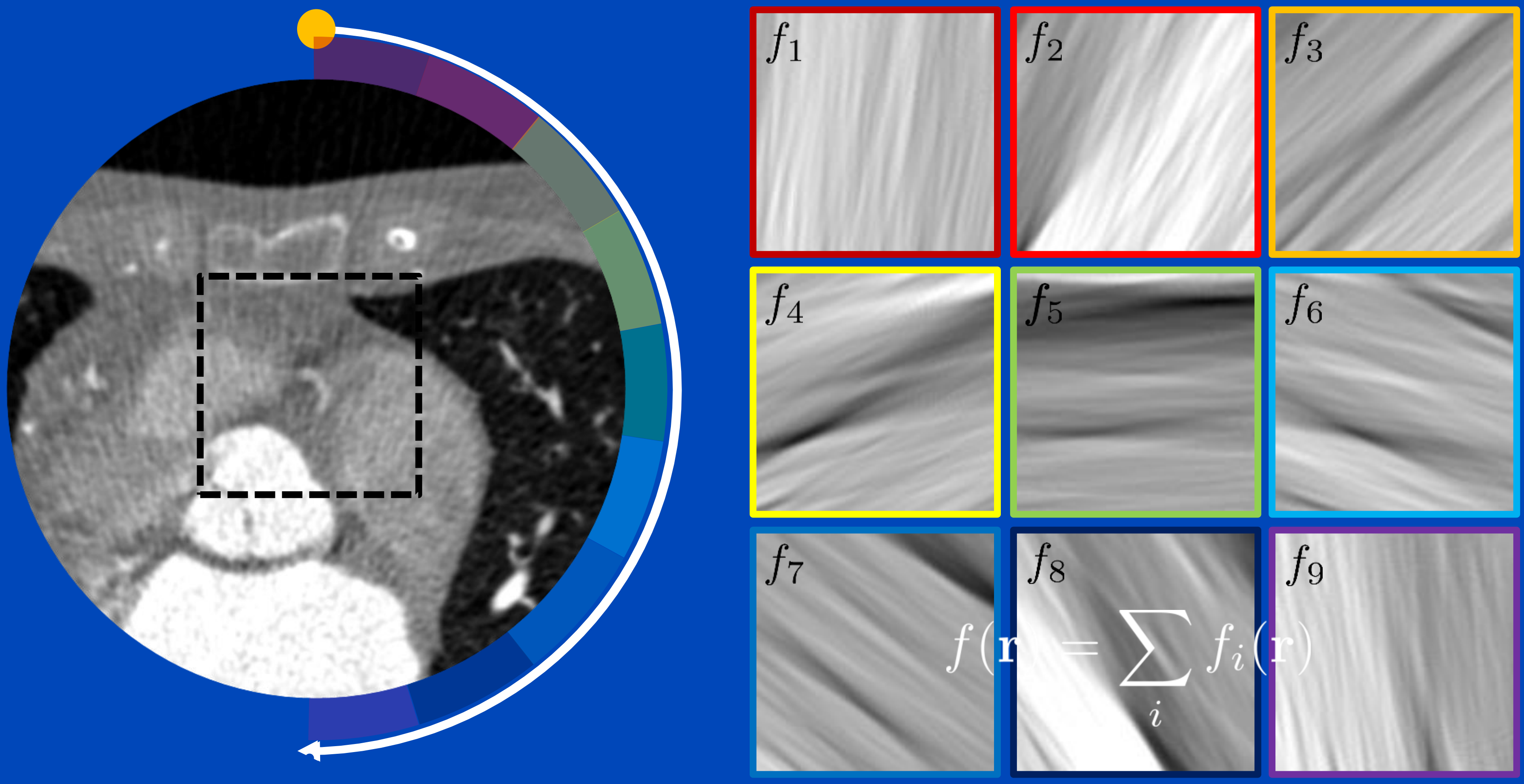

Partial Angle-Based Motion Compensation (PAMoCo)

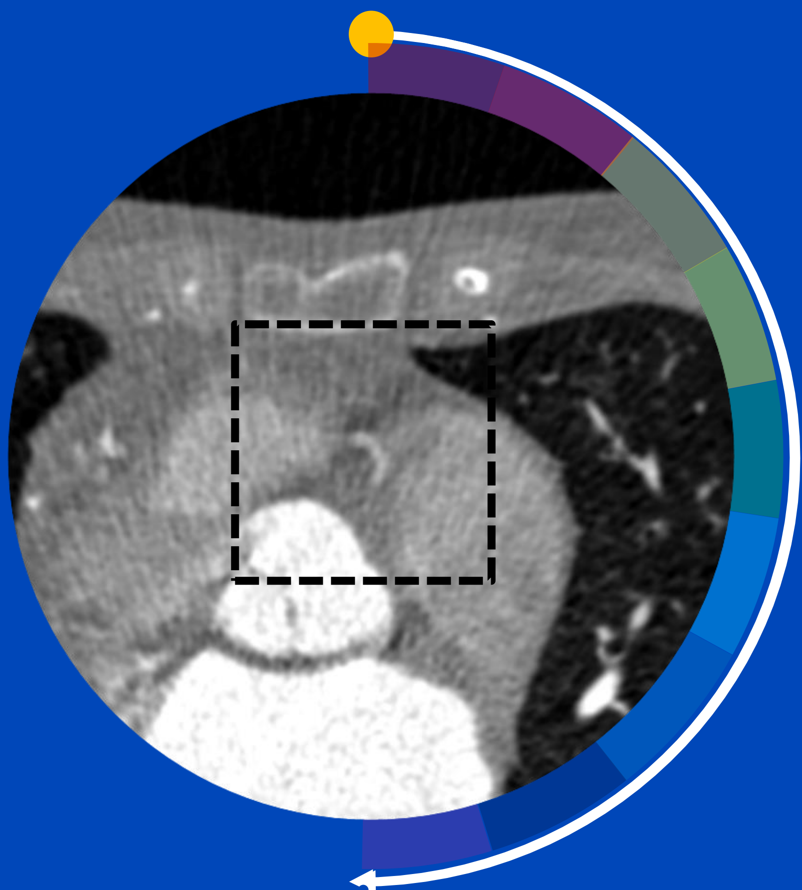

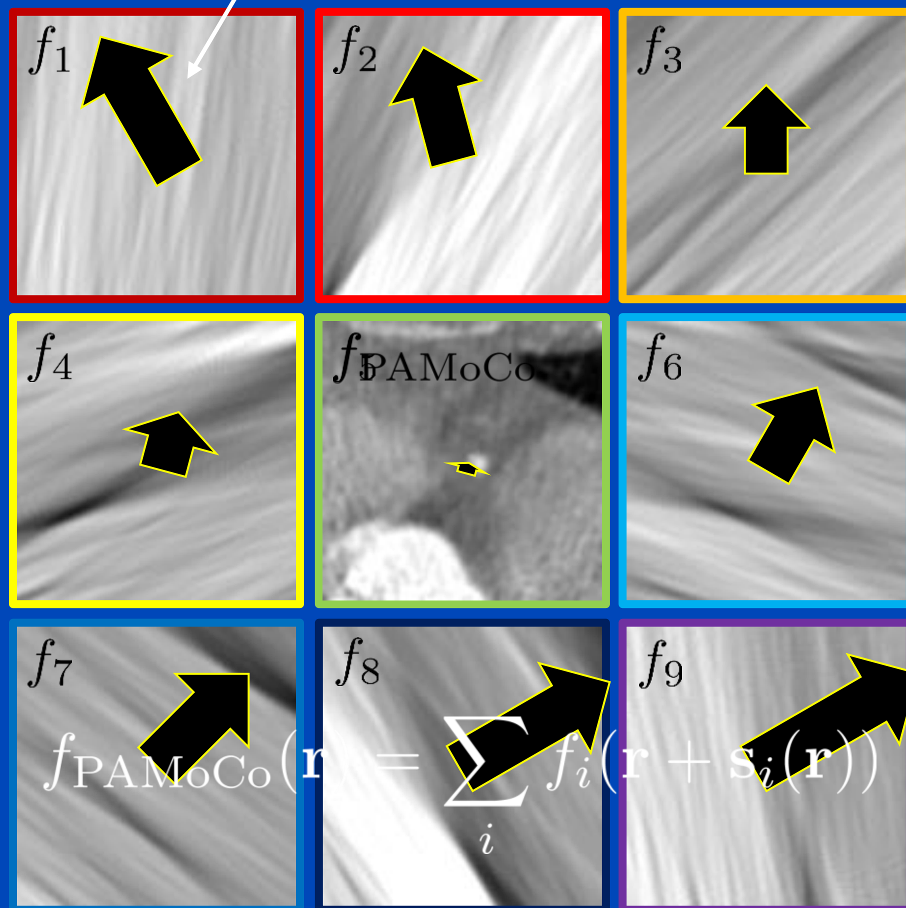

$$f_{\mathrm{PAMoCo}}(\mathbf{r}) = \sum_i f_i(\mathbf{r} + \mathbf{s}_i(\mathbf{r}))$$

Apply motion vector fields (MVFs) to partial angle reconstructions

Partial Angle-Based Motion Compensation (PAMoCo)

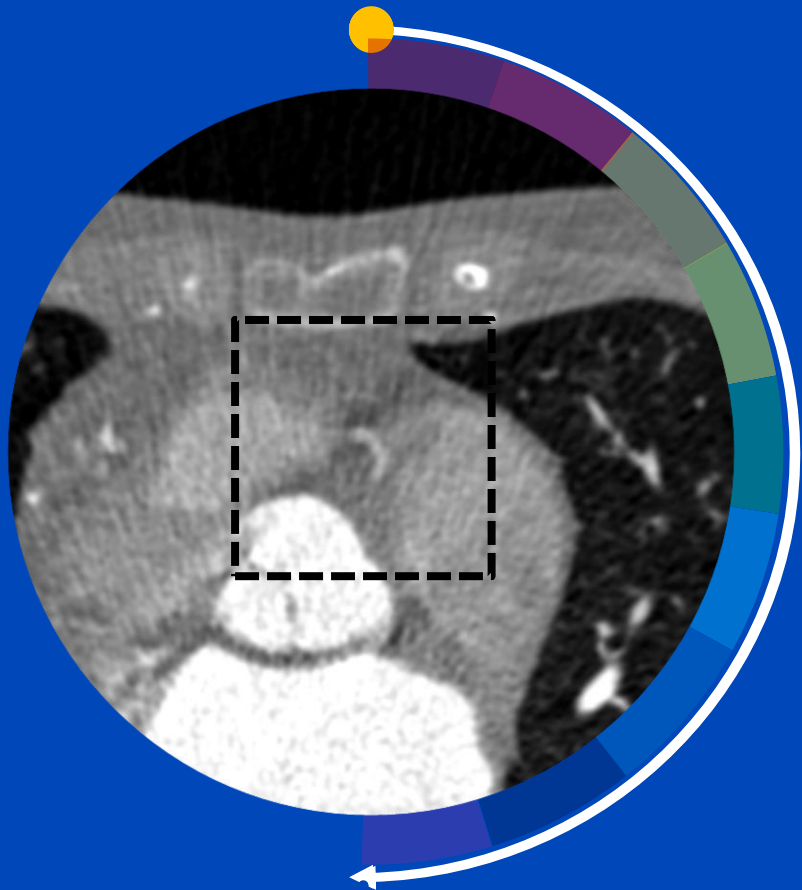

Prior work:

[1] S. Kim et al., "Cardiac motion correction based on partial angle reconstructed images in x-ray CT", Med. Phys. 42 (5): 2560–2571 (2015).

[2] J. Hahn et al., "Motion compensation in the region of the coronary arteries based on partial angle reconstructions from short-scan CT data", Med. Phys. 44 (11): 5795–5813 (2017).

[3] S. Kim et al., "Cardiac motion correction for helical CT scan with an ordinary pitch", IEEE TMI 37 (7): 1587–1596 (2018).

→ Limitation: Challenging / time-consuming optimization

Deep Partial Angle-Based Motion Compensation (Deep PAMoCo)

PARs centered around coronary artery

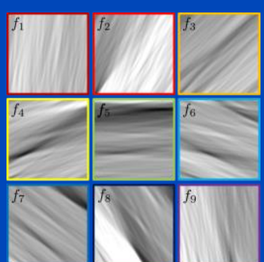

Neural network to predict parameters of a motion model

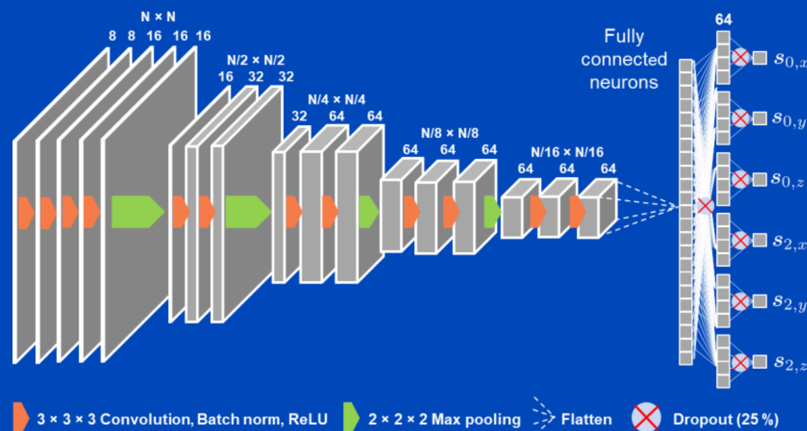

Reinsertion of patch into initial reconstruction

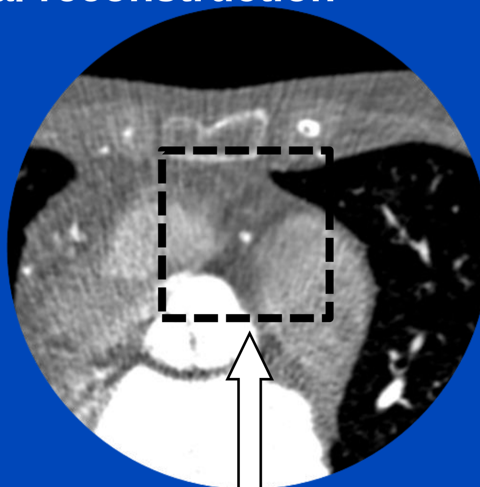

Spatial transformer

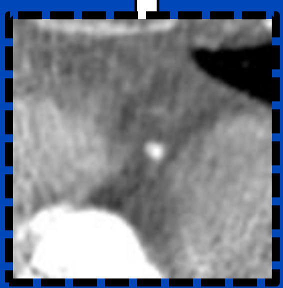

Application of the motion model to the PARs via a spatial transformer[1]

[1] M. Jaderberg et al., "Spatial transformer networks", NIPS 2015: 2017–2025 (2015).

Deep Partial Angle-Based Motion Compensation (Deep PAMoCo)

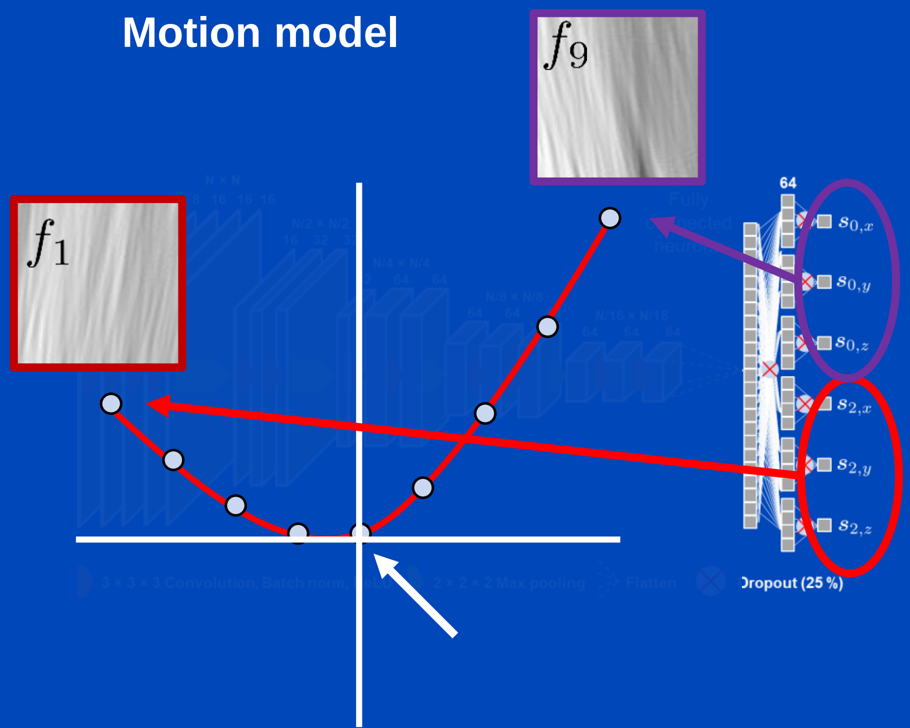

[1] M. Jaderberg et al., "Spatial transformer networks", NIPS 2015: 2017–2025 (2015).

Deep Partial Angle-Based Motion Compensation (Deep PAMoCo)

PARs centered around coronary artery

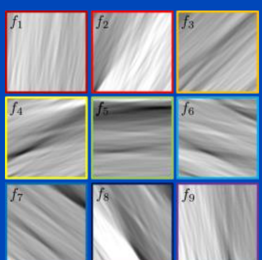

Neural network to predict parameters of a motion model

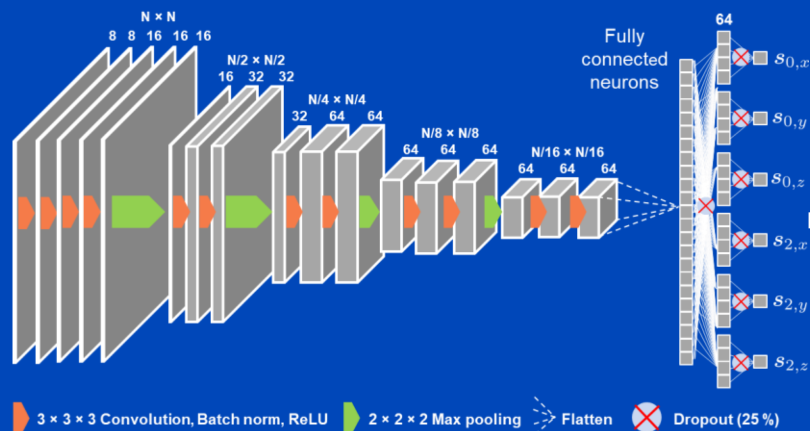

Reinsertion of patch into initial reconstruction

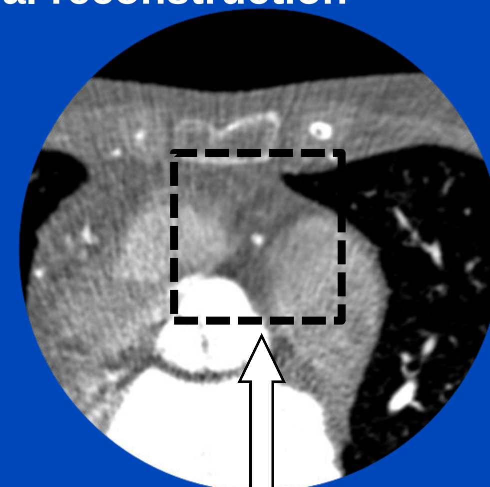

Spatial transformer

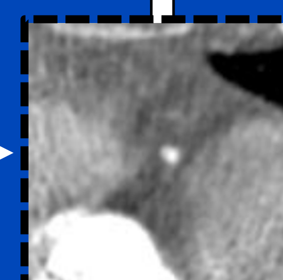

Application of the motion model to the PARs via a spatial transformer[1]

[1] M. Jaderberg et al., “Spatial transformer networks”, NIPS 2015: 2017–2025 (2015).

dkfz.

Training Data Generation

- Removal of coronary arteries from real CT reconstructions.
- Insertion of artificial coronary arteries with different shape, size, and contrast.
- Simulation of CT scans with coronary artery motion.

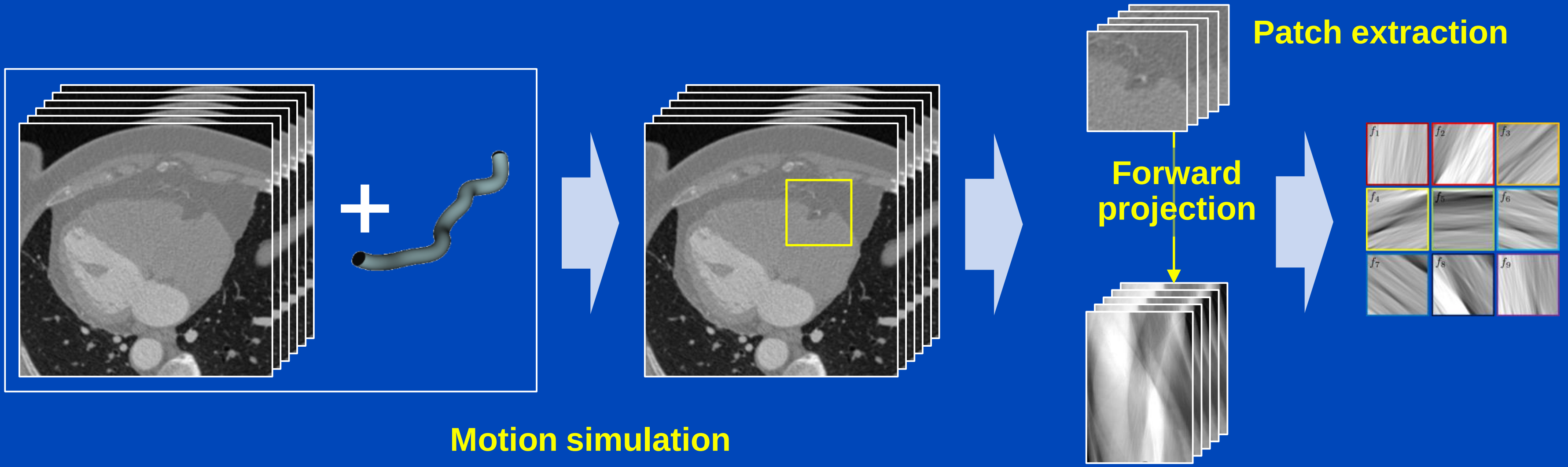

Results

Measurements, patient 1

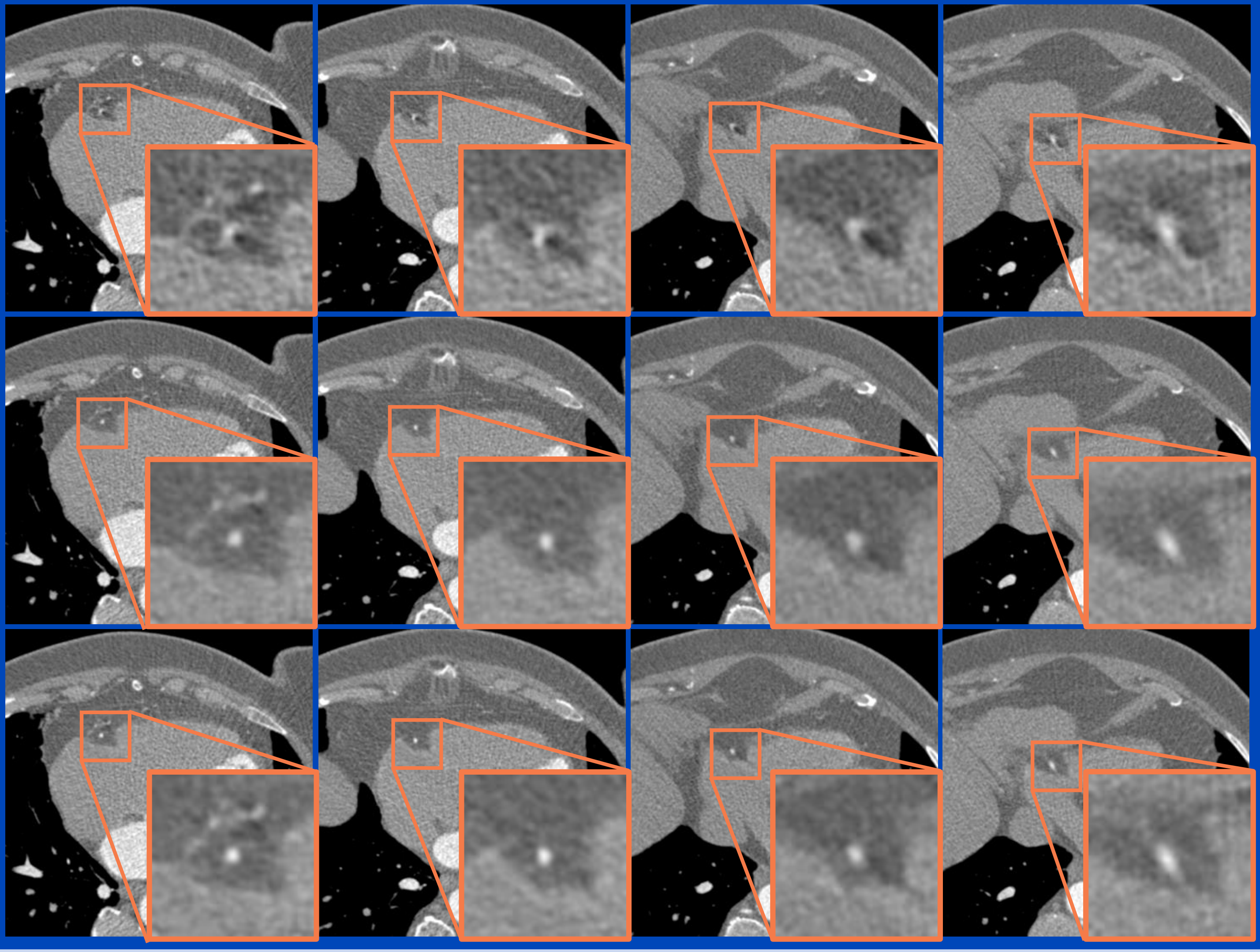

C = 1000 HU
W = 1000 HU

J. Maier, S. Lebedev, J. Erath, E. Eulig, S. Sawall, E. Fournié, K. Stierstorfer, M. Lell, and M. Kachelrieß. Deep learning-based coronary artery motion estimation and compensation for short-scan cardiac CT. Med. Phys. 48(7):3559-3571, July 2021.

Results

Measurements, patient 2

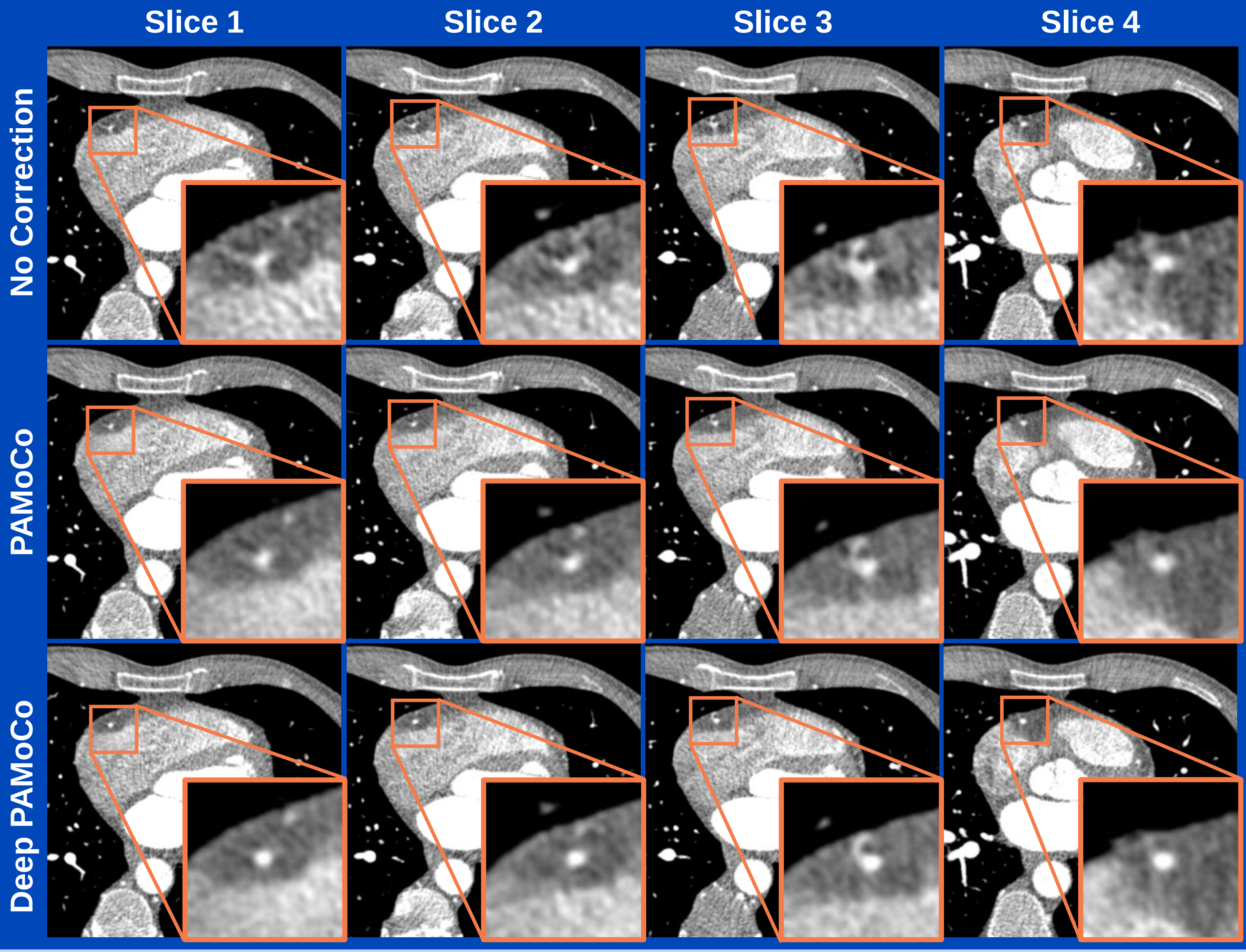

C = 1000 HU
W = 1000 HU

J. Maier, S. Lebedev, J. Erath, E. Eulig, S. Sawall, E. Fournié, K. Stierstorfer, M. Lell, and M. Kachelrieß. Deep learning-based coronary artery motion estimation and compensation for short-scan cardiac CT. Med. Phys. 48(7):3559-3571, July 2021.

Results

Measurements, patient 3

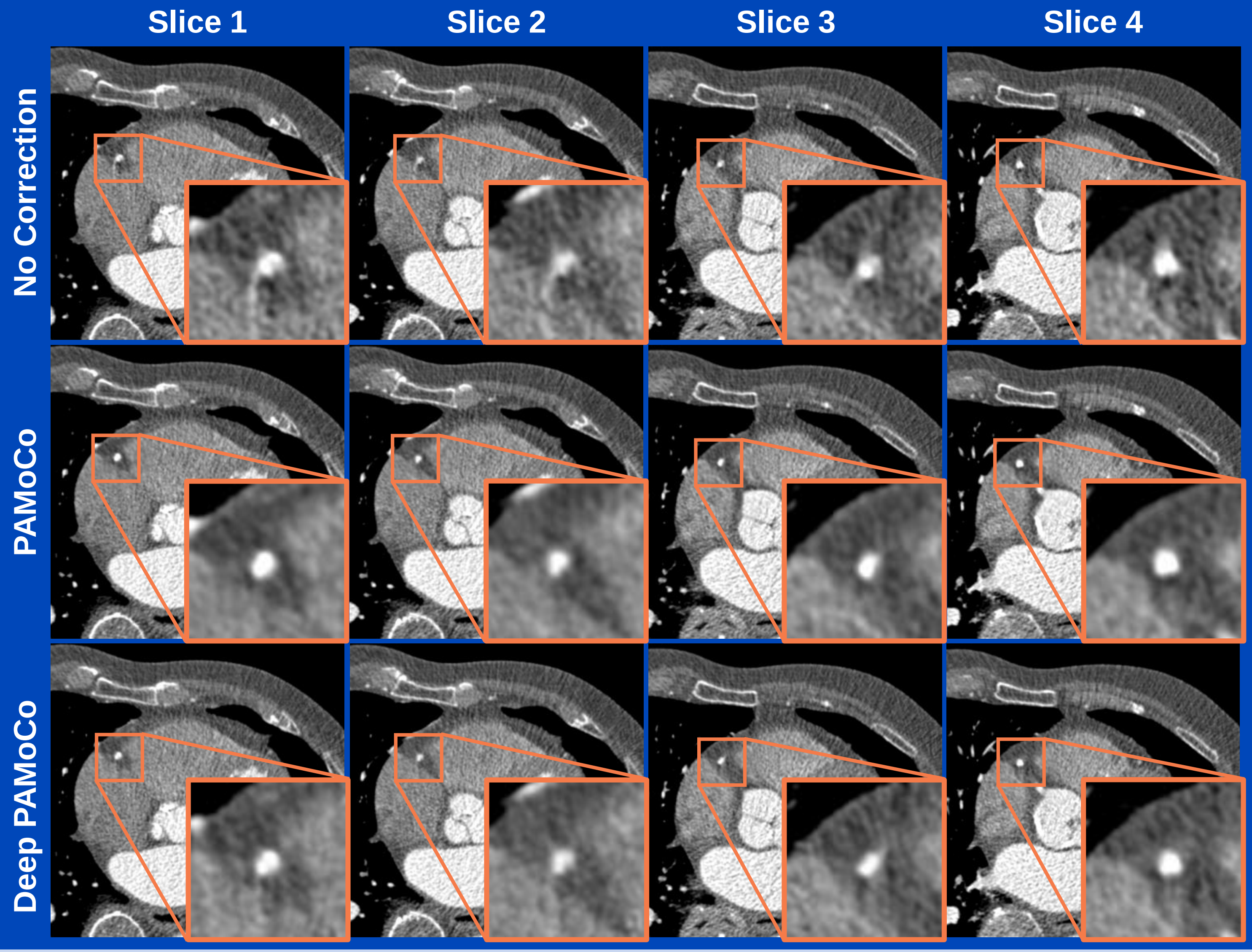

C = 1100 HU
W = 1000 HU

J. Maier, S. Lebedev, J. Erath, E. Eulig, S. Sawall, E. Fournié, K. Stierstorfer, M. Lell, and M. Kachelrieß. Deep learning-based coronary artery motion estimation and compensation for short-scan cardiac CT. Med. Phys. 48(7):3559-3571, July 2021.

Patient 5

Original

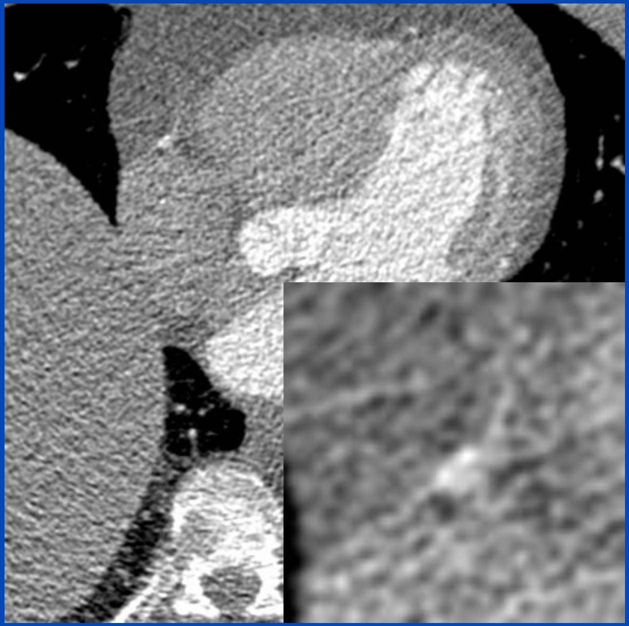

Deep PAMoCo

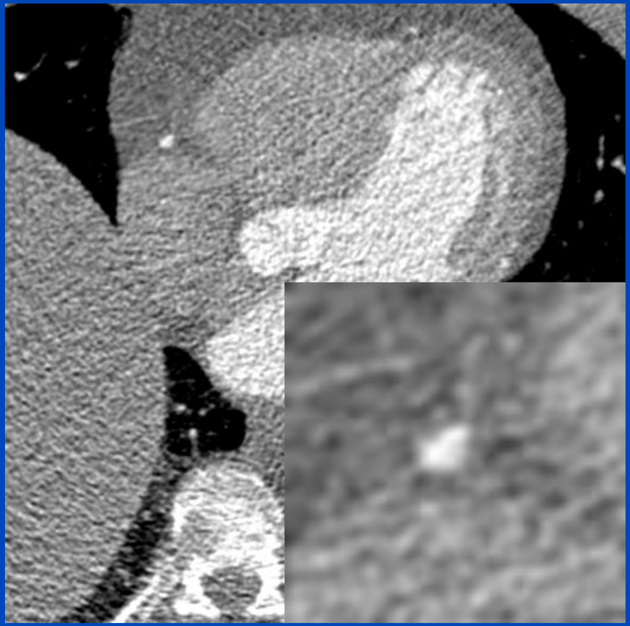

C = 0 HU, W = 1200 HU

Patient 6

Original

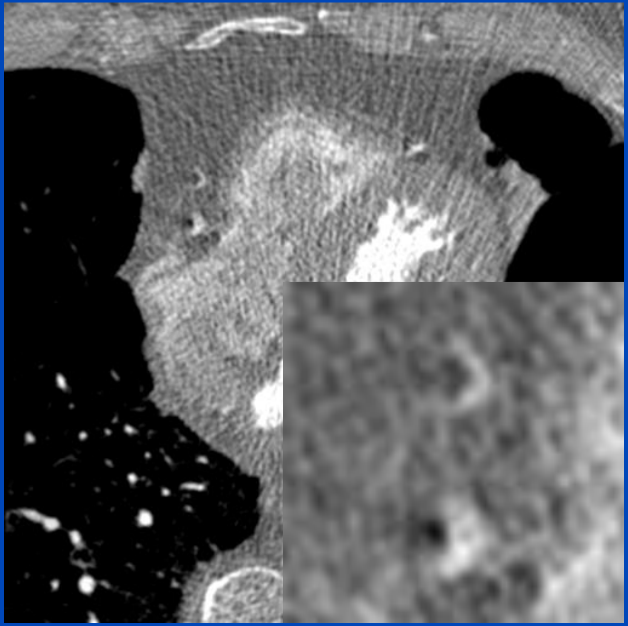

Deep PAMoCo

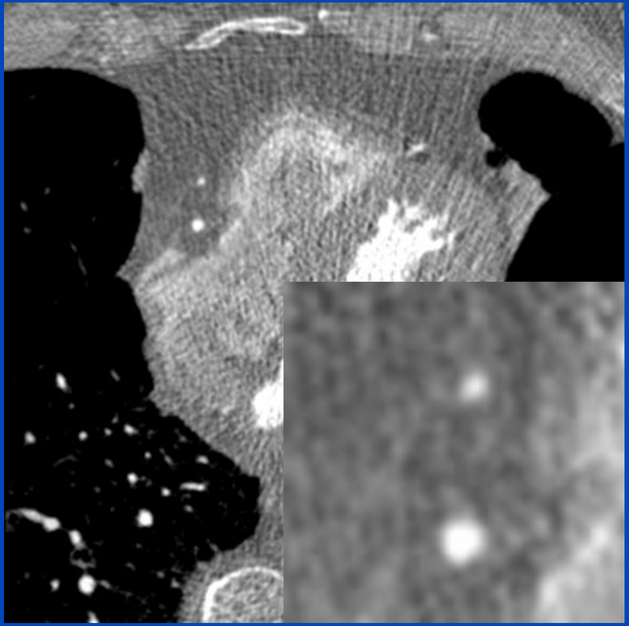

C = 0 HU, W = 1400 HU

J. Maier, S. Lebedev, J. Erath, E. Eulig, S. Sawall, E. Fournié, K. Stierstorfer, M. Lell, and M. Kachelrieß. Deep learning-based coronary artery motion estimation and compensation for short-scan cardiac CT. Med. Phys. 48(7):3559-3571, July 2021.

Patient 7

Original

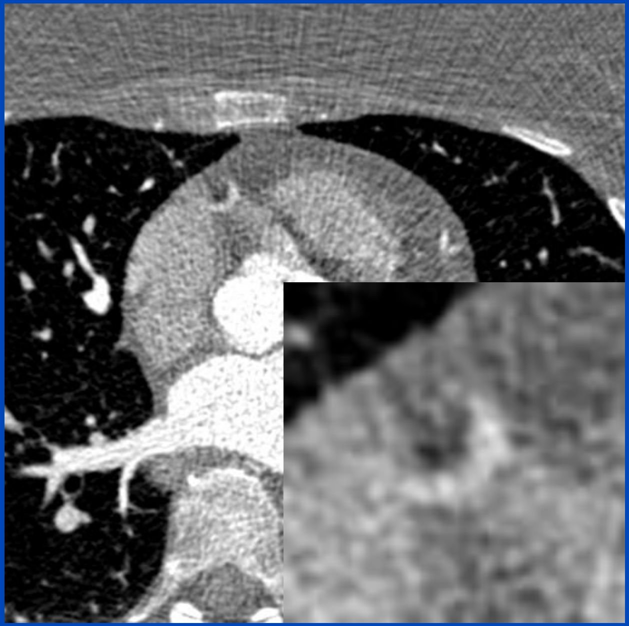

Deep PAMoCo

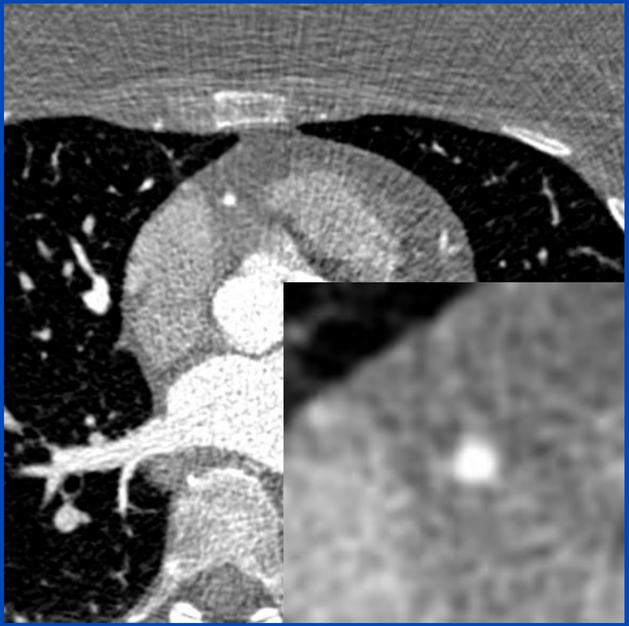

***C* = 0 HU, *W* = 1600 HU**

J. Maier, S. Lebedev, J. Erath, E. Eulig, S. Sawall, E. Fournié, K. Stierstorfer, M. Lell, and M. Kachelrieß. Deep learning-based coronary artery motion estimation and compensation for short-scan cardiac CT. Med. Phys. 48(7):3559-3571, July 2021.

Patient 8

Original

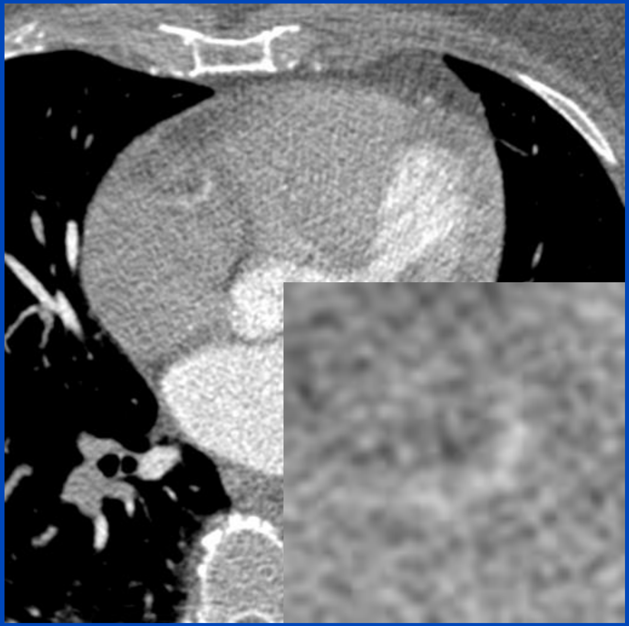

Deep PAMoCo

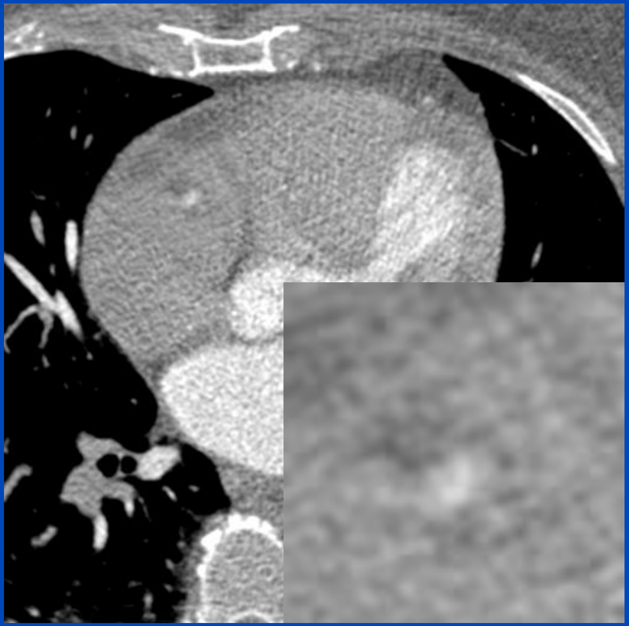

C = 0 HU, W = 1000 HU

J. Maier, S. Lebedev, J. Erath, E. Eulig, S. Sawall, E. Fournié, K. Stierstorfer, M. Lell, and M. Kachelrieß. Deep learning-based coronary artery motion estimation and compensation for short-scan cardiac CT. Med. Phys. 48(7):3559-3571, July 2021.

Adaptions for CBCT

- Consideration of the entire FOM
  - Estimation of a dense vector field for every voxel within the FOM.
- Slow rotation speed
  - Projections can only be grouped into tiny groups (here, no grouping is performed at all)
  - Partial angle reconstruction (PAR)
- 4D output
  - Estimation of MVF from two arbitrary PARs
  - Similar to Voxelmorph but with PARs
- Modification of PARs to add morphological context.

Workflow

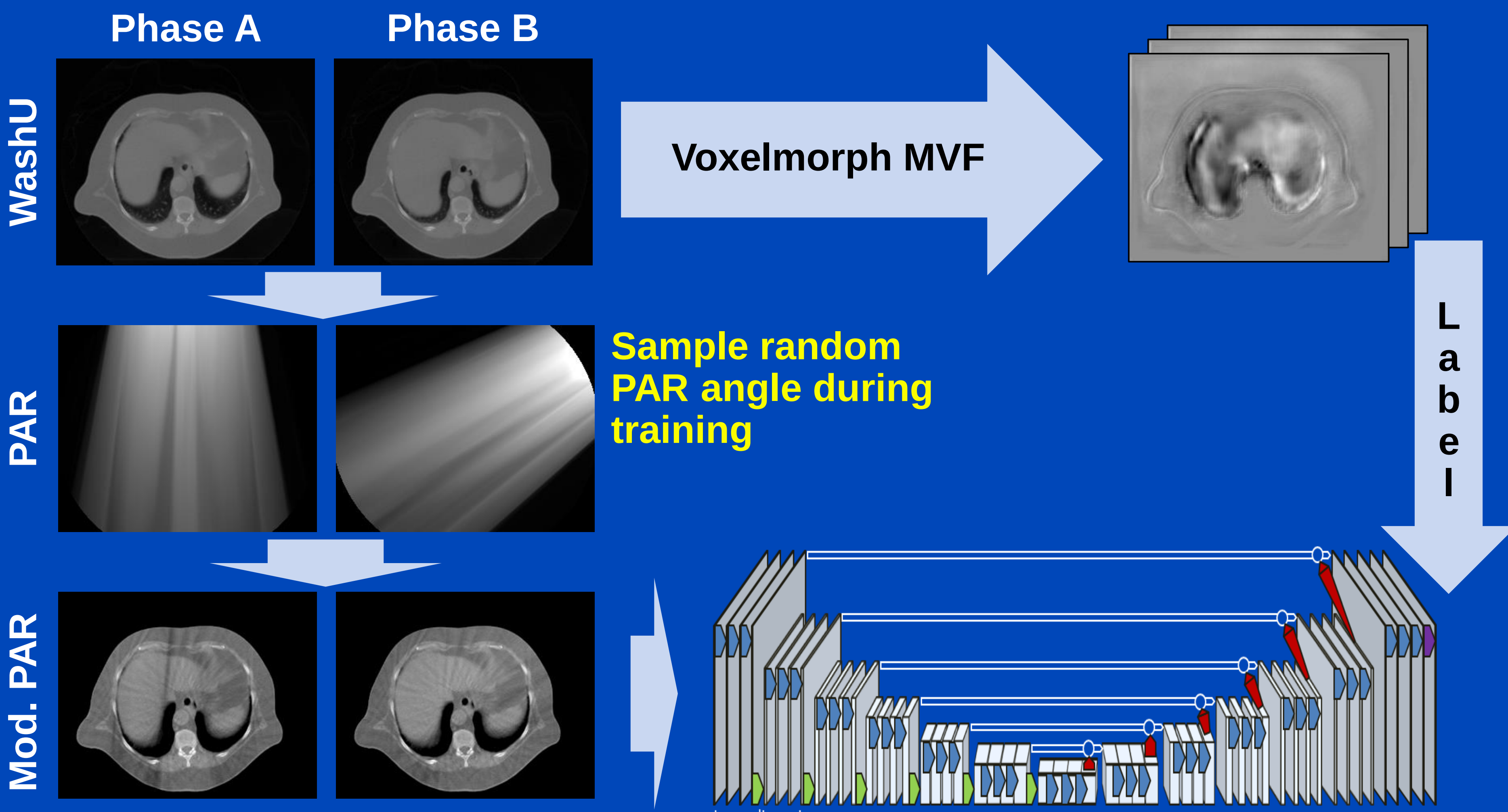

Phase A
Phase B
WashU
PAR
Mod. PAR
Voxelmorph MVF
Sample random PAR angle during training
Label

Modified SARs

- Modified PARs are calculated as

$$f_{\mathrm{PAR},\vartheta} = C(f_{\mathrm{3D}}) + \frac{1}{\mathsf{X}_\vartheta^{\mathrm{T}} 1} \mathsf{X}_\vartheta^{\mathrm{T}} \frac{p_\vartheta - \mathsf{X}_\vartheta C(f_{\mathrm{3D}})}{\mathsf{X}_\vartheta 1}$$

  wich is a kind of SART update.
- Here *X* is the x-ray tranform operator, f_{3D} is the 3D reconstruction of the moving projections, and *C* is a cast operator that converts its argument to the nearest integer multiple of 50 HU.

Modified SARs

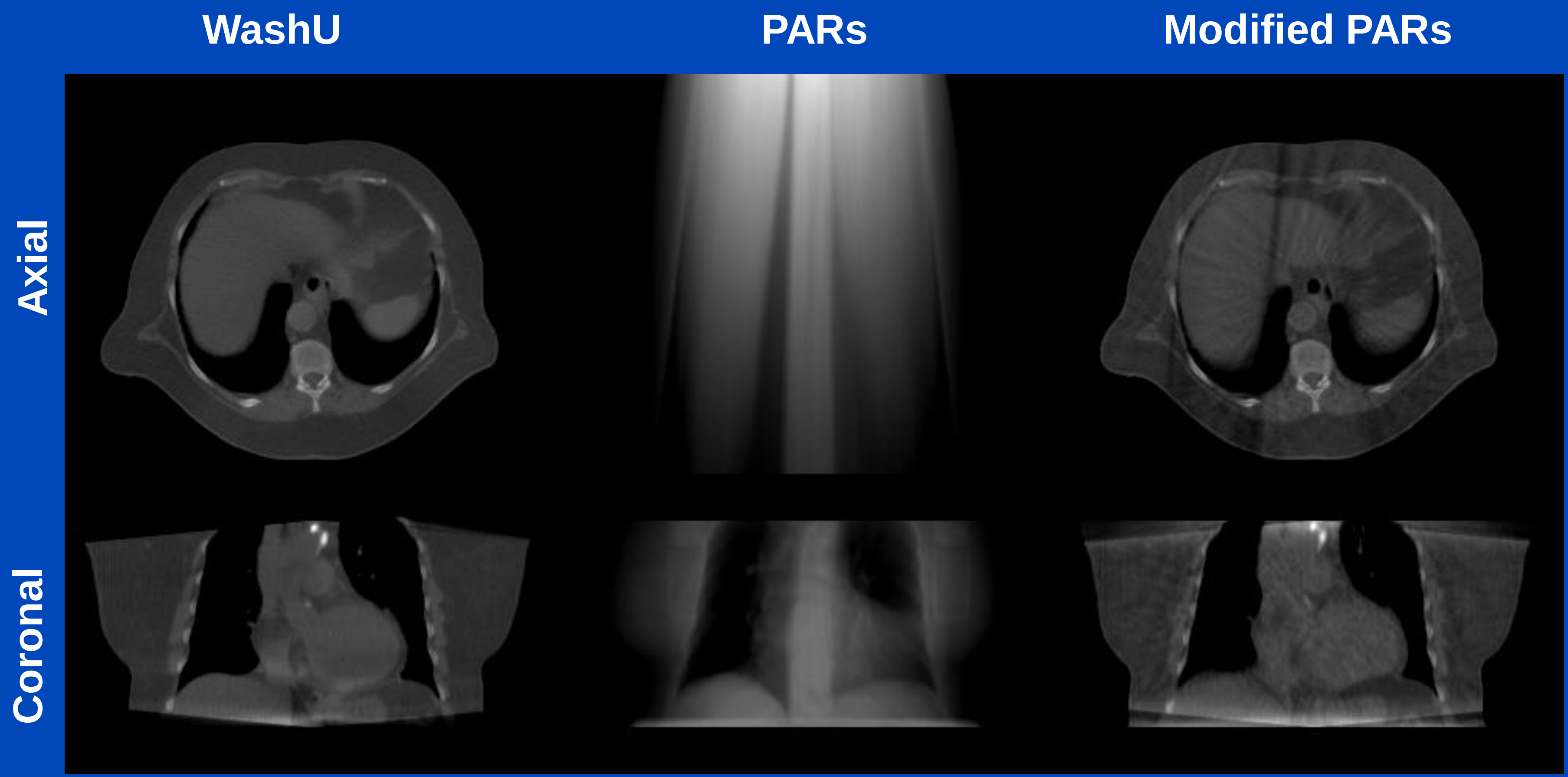

Data Generation & Training

- 49 4D CT scans (10 respiratory phases each) of the WashU dataset were used as prior images.
- For each of the 10 phases of every patient, modified PARs were calculated.
- For any of the 100 combination of the 10 phases a ground truth vector field was calculated using a Voxelmorph-like approach.
- Subsequently a U-net-like architecture was used to predict these ground truth vector fields from two arbitrary input PARs of the same patient.

Measurement MSK 1

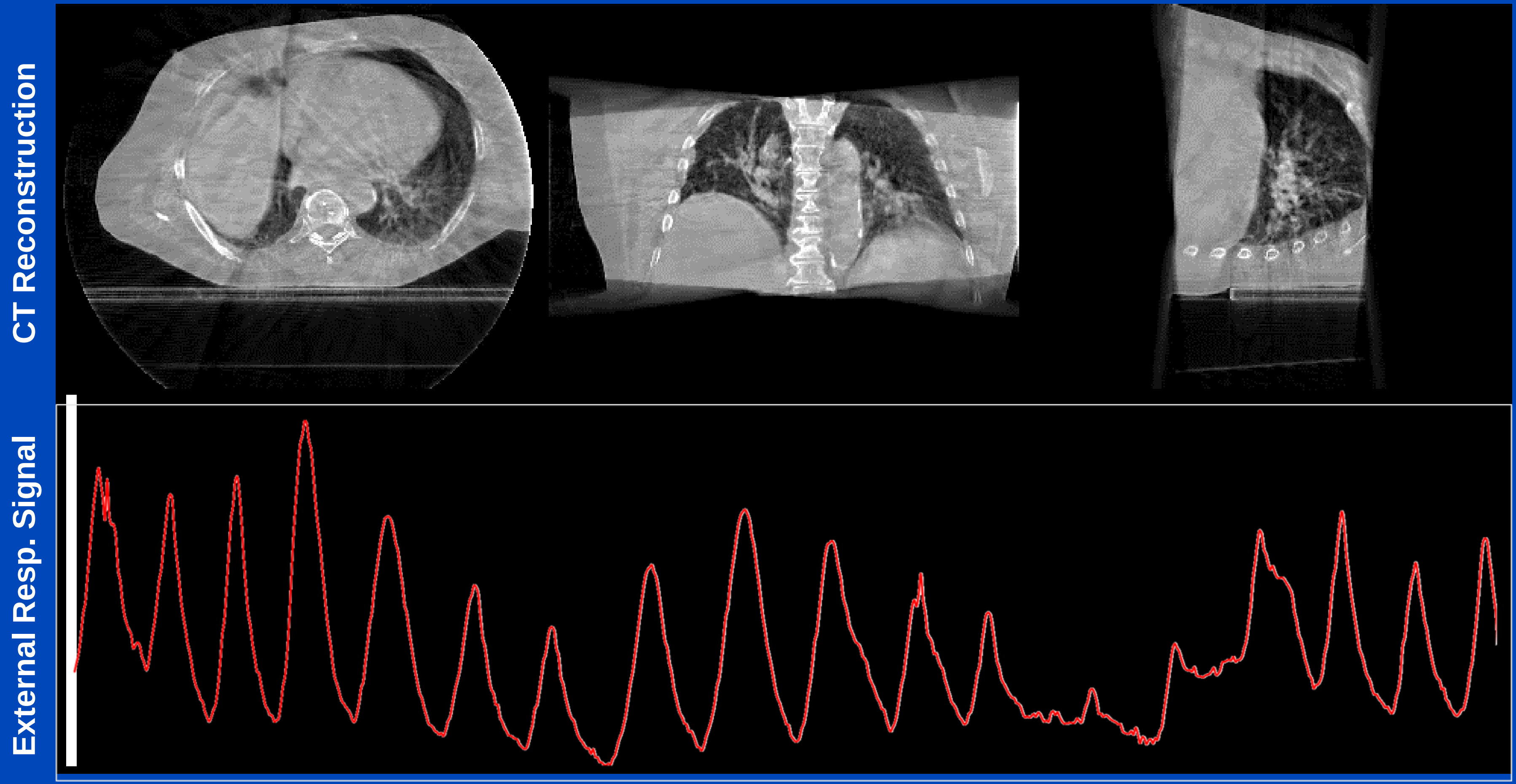

Measurement MSK 1
External Respiration Signal vs. Intrinsic Signal

- **Intrinsic signal:**
  - Threshold: All voxels < -100 HU = 1, other voxels = 0
  - Signal = mean inside ROI containing lung and diaphragm.
- **Normalization of both signals to [0,1].**

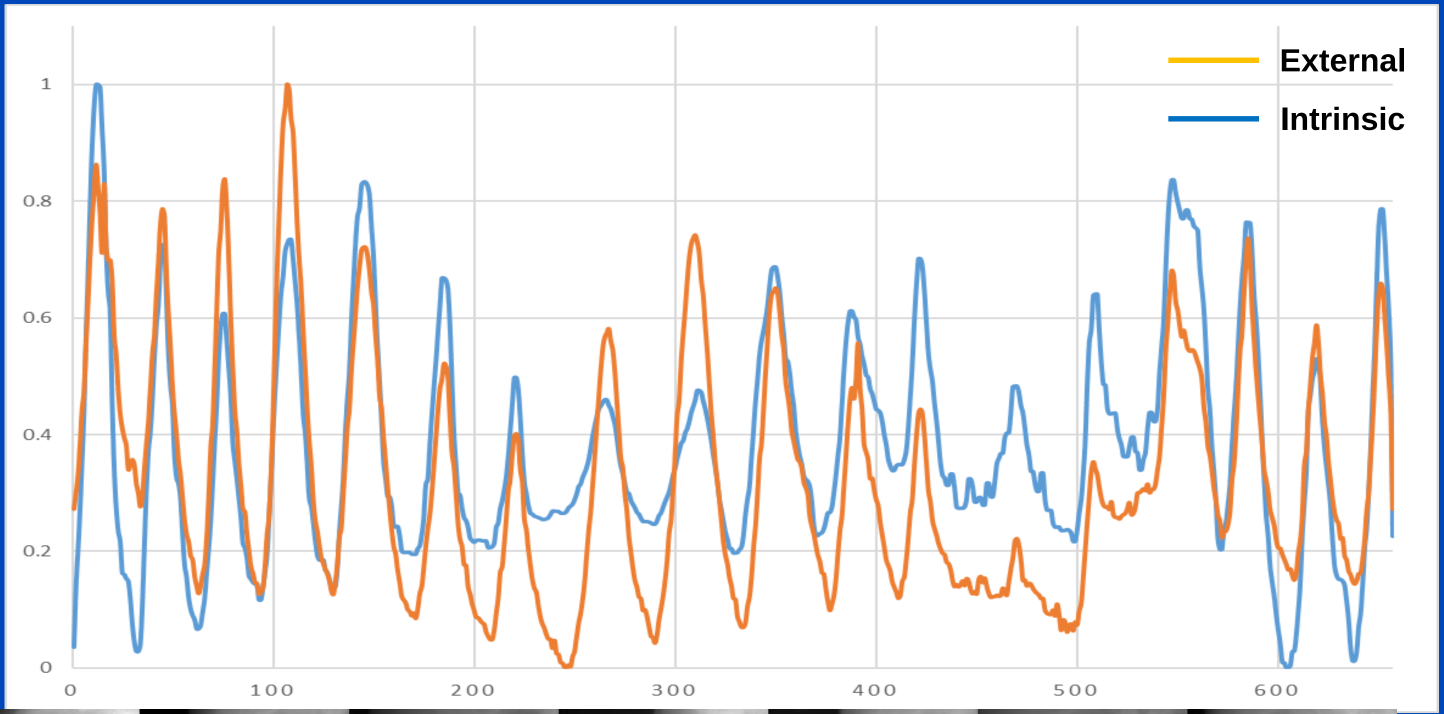

dkfz.

Measurement 20120629_VUMC_4DThorax

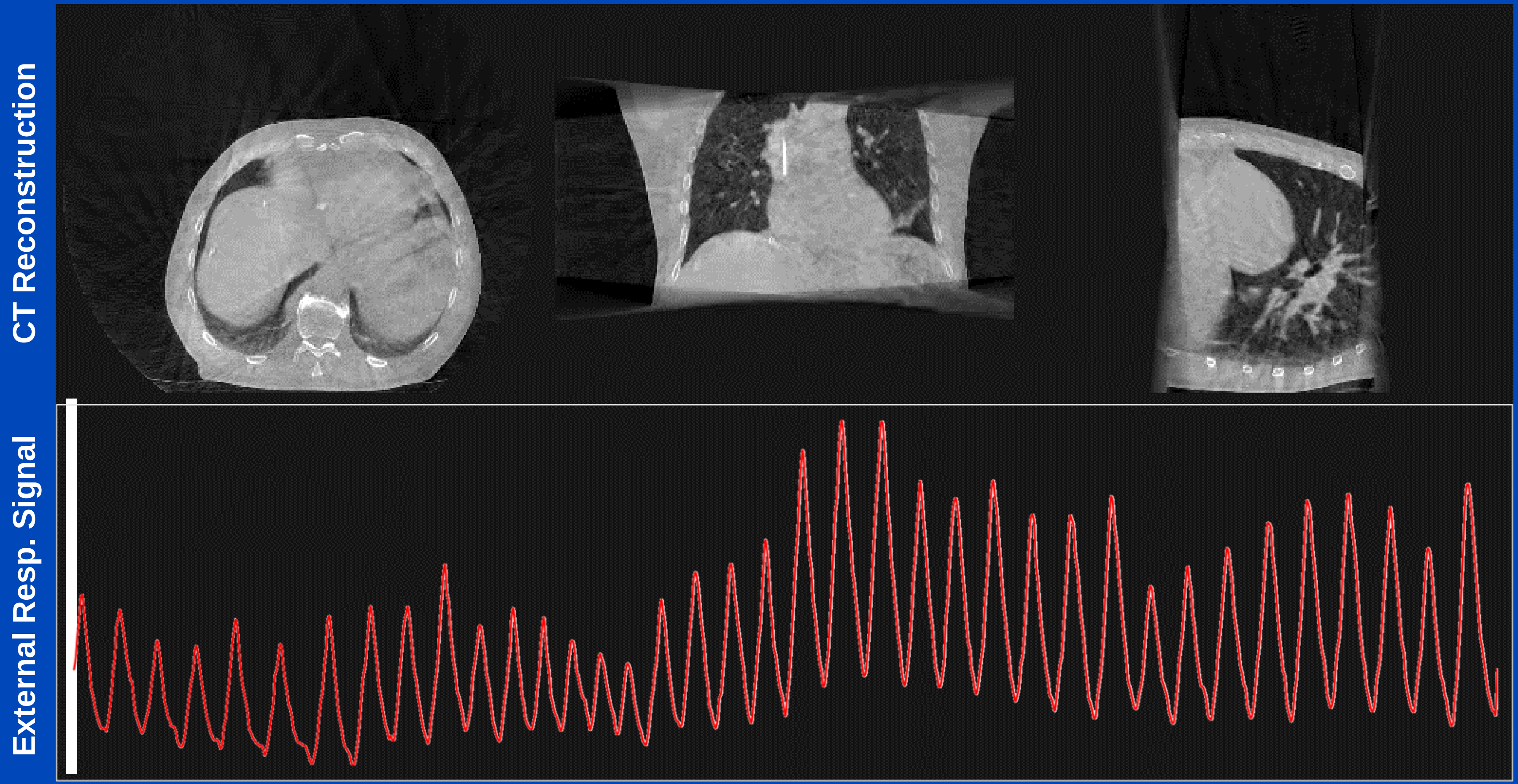

Measurement 20120629_VUMC_4DThorax External Respiration Signal vs. Intrinsic Signal

- **Intrinsic signal:**
  - Threshold: All voxels < -100 HU = 1, other voxels = 0
  - Signal = mean inside ROI containing lung and diaphragm.
- **Normalization of both signals to [0,1].**

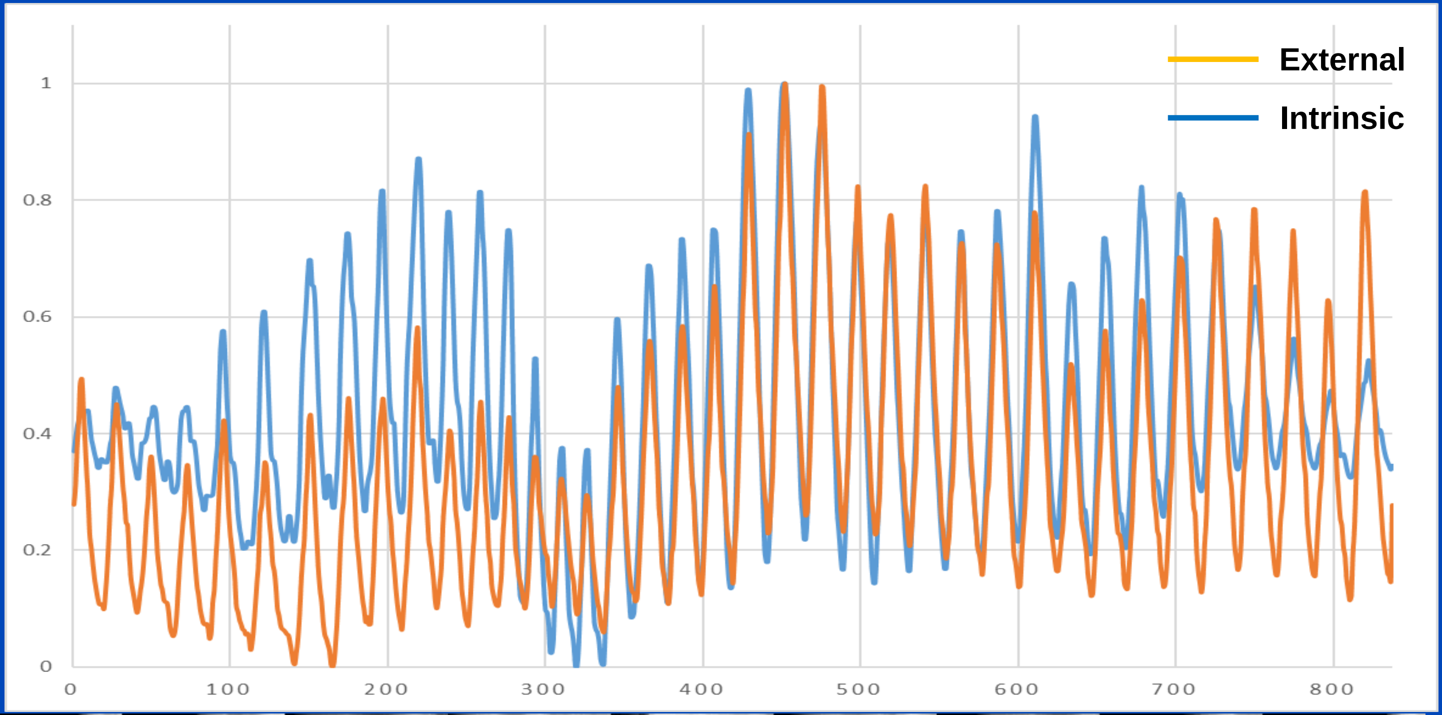

Part 7: Interventional Imaging

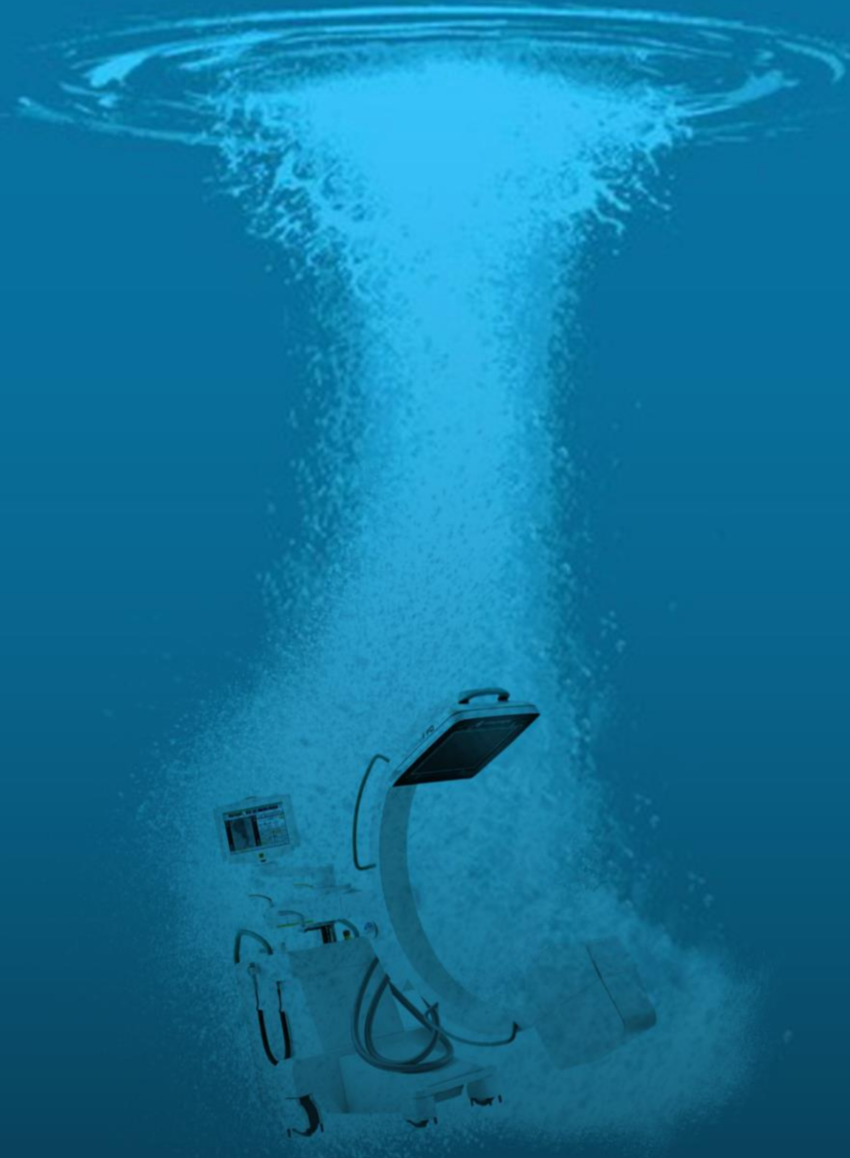

Intervention goes Deep!

Deep DSA

???

Without mask?

Methods

General principle

Conventional DSA

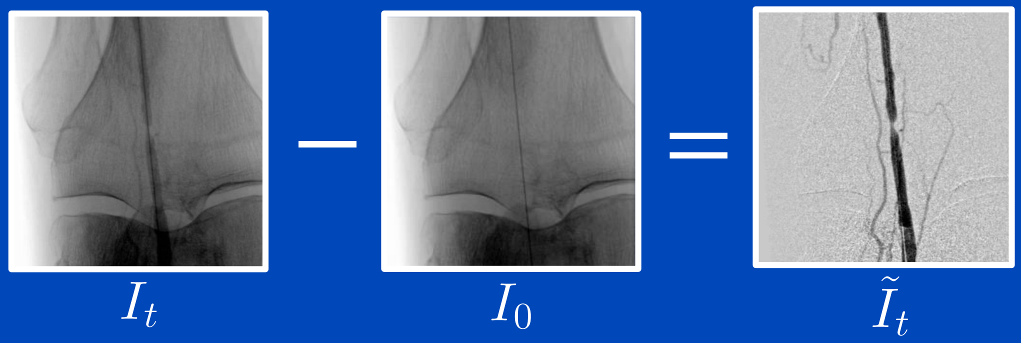

Deep DSA

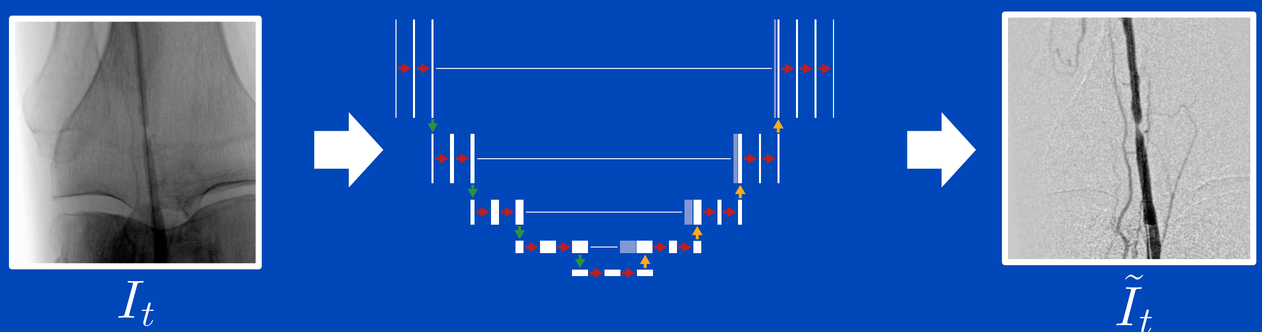

- **Train on static cases where ground truth is conventional DSA**

E. Eulig, M. Kachelrieß, et al. "Learned digital subtraction angiography (Deep DSA): method and application to lower extremities". Proc. SPIE 11072, 15th International Meeting on Fully Three-Dimensional Image Reconstruction, 1107223:1-4, May 2019.

Methods
General principle

Conventional DSA

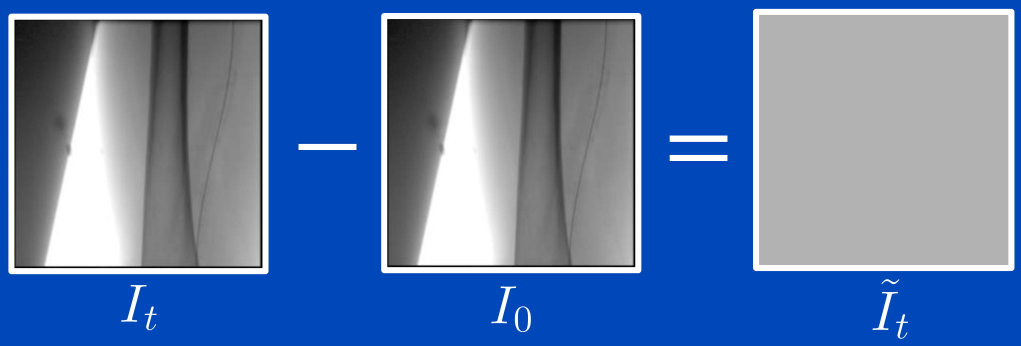

Deep DSA

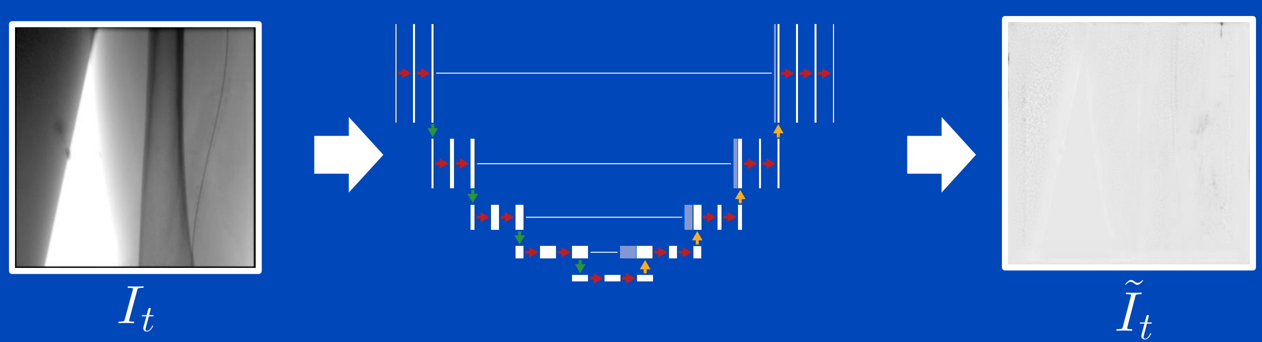

- **Train on static cases where ground truth is conventional DSA**
- **During inference CNN can be applied to both static and dynamic cases**

E. Eulig, M. Kachelrieß, et al. "Learned digital subtraction angiography (Deep DSA): method and application to lower extremities". Proc. SPIE 11072, 15th International Meeting on Fully Three-Dimensional Image Reconstruction, 1107223:1-4, May 2019.

Results

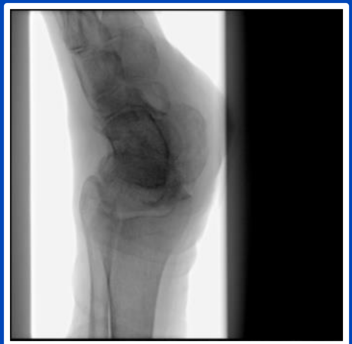

Original x-ray sequence

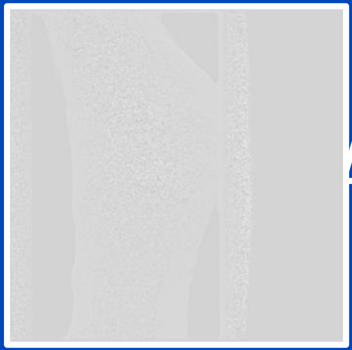

Ground truth DSA

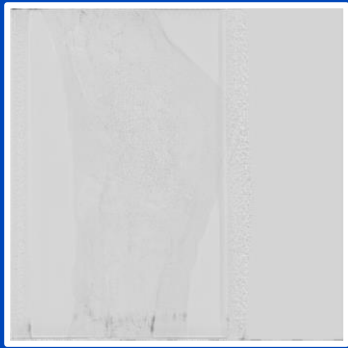

CNN output

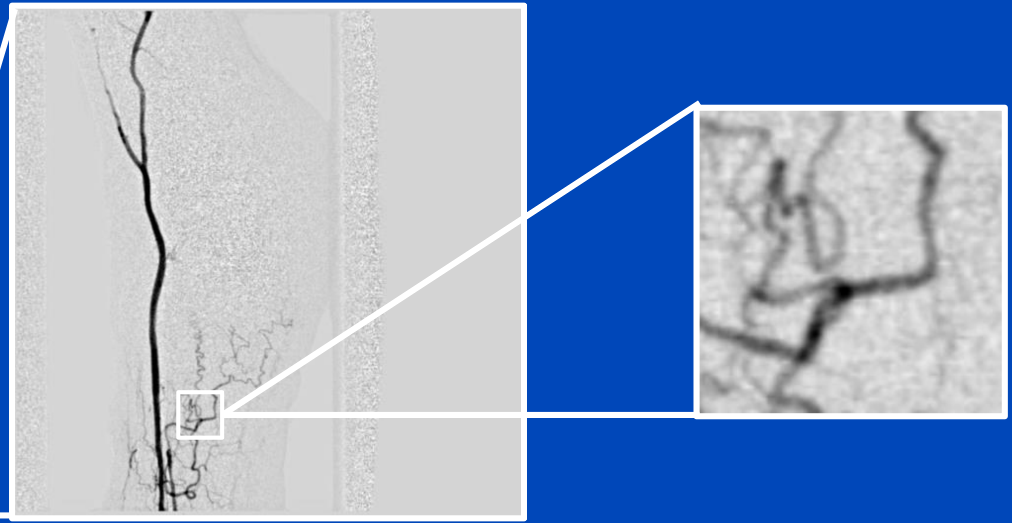

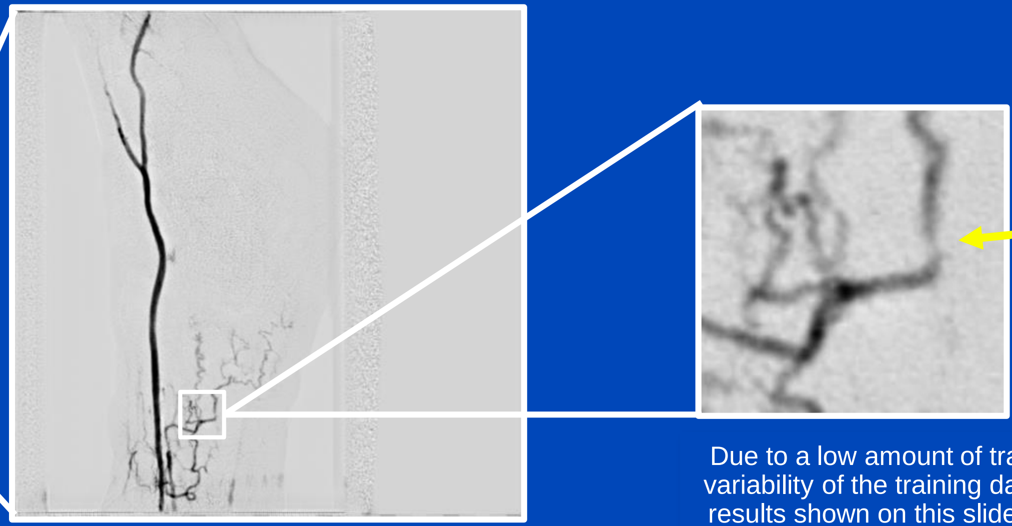

Artificially introduced stenosis?

Due to a low amount of training data and a low variability of the training data available to us the results shown on this slide are not optimal, yet.

Deep DSA

Fluoroscopy	DSA (fluoro minus mask)	Deep DSA (from fluoro only)

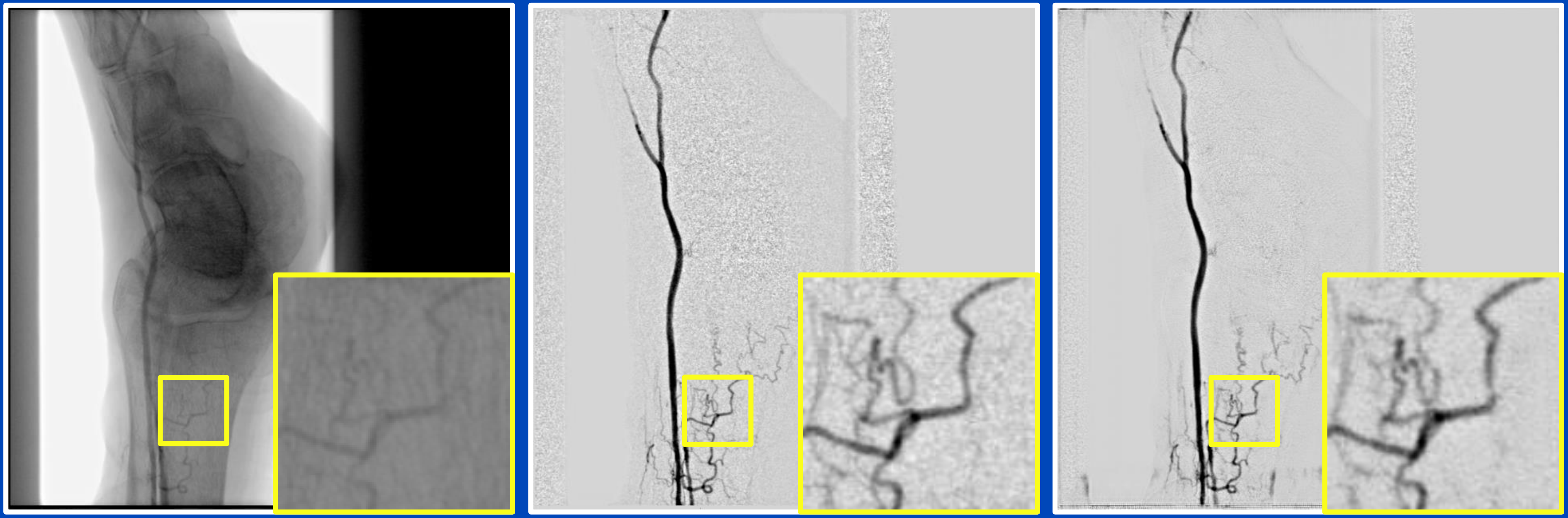

Due to a low amount of training data and a low variability of the training data available to us the results shown on this slide are not optimal, yet.

E. Eulig, M. Kachelrieß, et al. "Learned digital subtraction angiography (Deep DSA): method and application to lower extremities". Proc. SPIE 11072, 15th International Meeting on Fully Three-Dimensional Image Reconstruction, 1107223:1-4, May 2019.

Results

Bolus chase study

Dynamic fluoroscopy

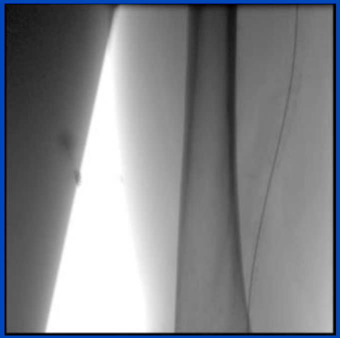

Conventional DSA

Conventional DSA infeasible due to C-arm motion

Deep DSA

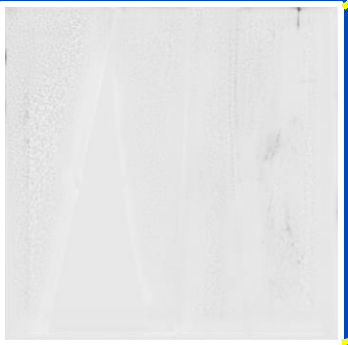

Deep DSA at $\mathrm{t} = t_a$

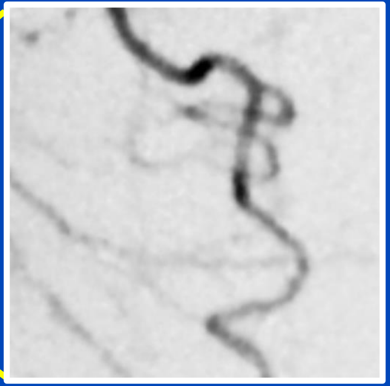

Deep DSA at $\mathrm{t} = t_a$

E. Eulig, M. Kachelrieß, et al. "Learned digital subtraction angiography (Deep DSA): method and application to lower extremities". Proc. SPIE 11072, 15th International Meeting on Fully Three-Dimensional Image Reconstruction, 1107223:1-4, May 2019.

Deep 3D+T Fluoroscopy

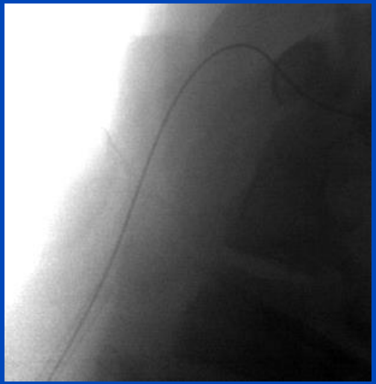

???

At 2D+T dose?

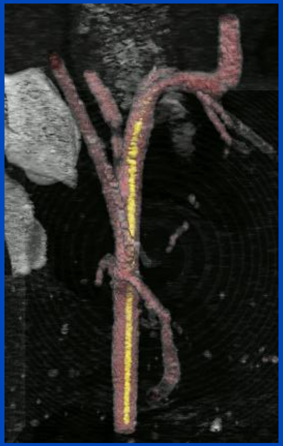

Deep 3D+T Tomographic Fluoroscopy

either 2D+T fluoroscopy

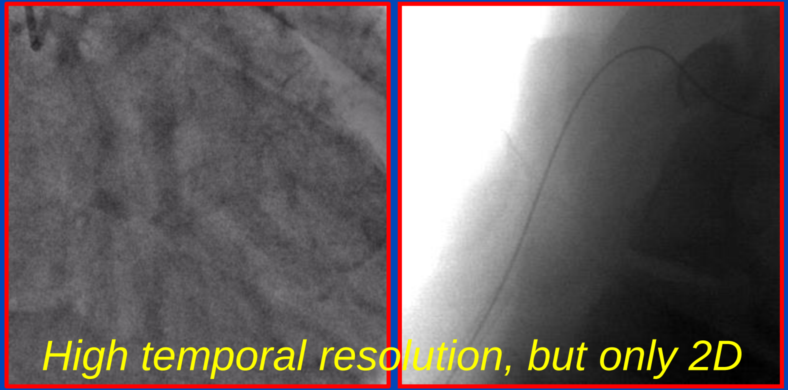

High temporal resolution, but only 2D

or 3D tomography

Low temporal resolution, but 3D

3D+T tomographic fluoroscopy? At low dose? How???

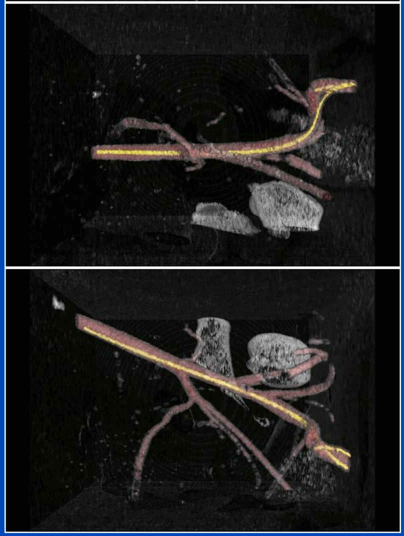

How to Realize 3D+T Fluoroscopy

- Low dose by:
  - Low tube current
  - Very few projections (pulsed mode)
- Advantages of intervention guidance:
  - Repetitive scanning of the same body region: changes are sparse.
  - Interventional materials are fine structures (few voxels) of high contrast (metal).

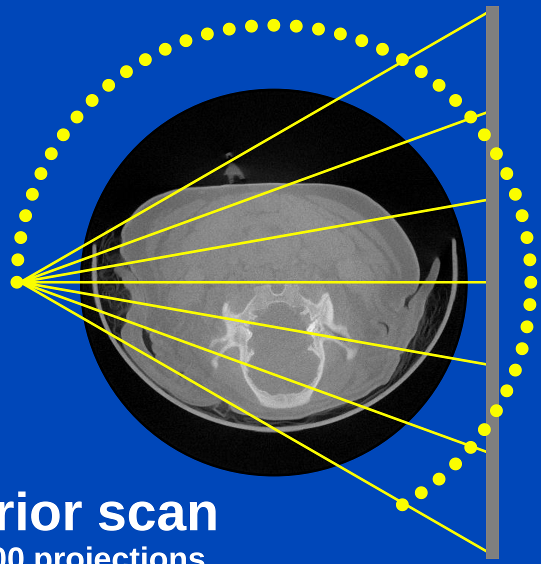

Prior scan
400 projections

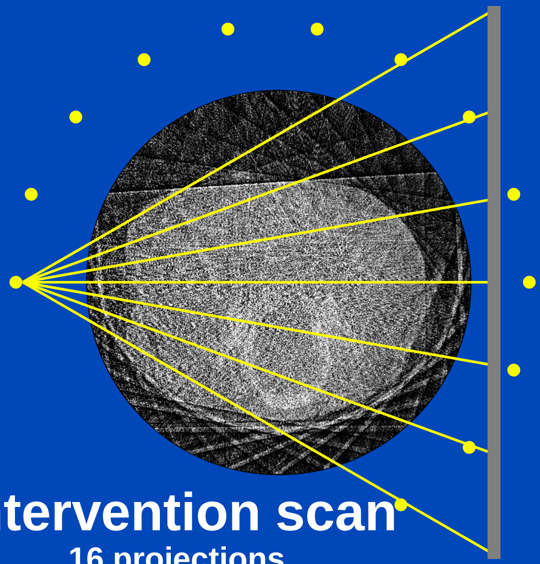

Intervention scan
16 projections

Experimental setup

B. Flach, J. Kuntz, M. Brehm, R. Kueres, S. Bartling, and M. Kachelrieß. "Low dose tomographic fluoroscopy: 4D intervention guidance with running prior.", Med. Phys. 40:101909, 11 pages, October 2013.

3D+T Image Guidance at 2D+T Dose

Stent Expansion in the Carotis of a Pig with Angio Roadmap Overlay

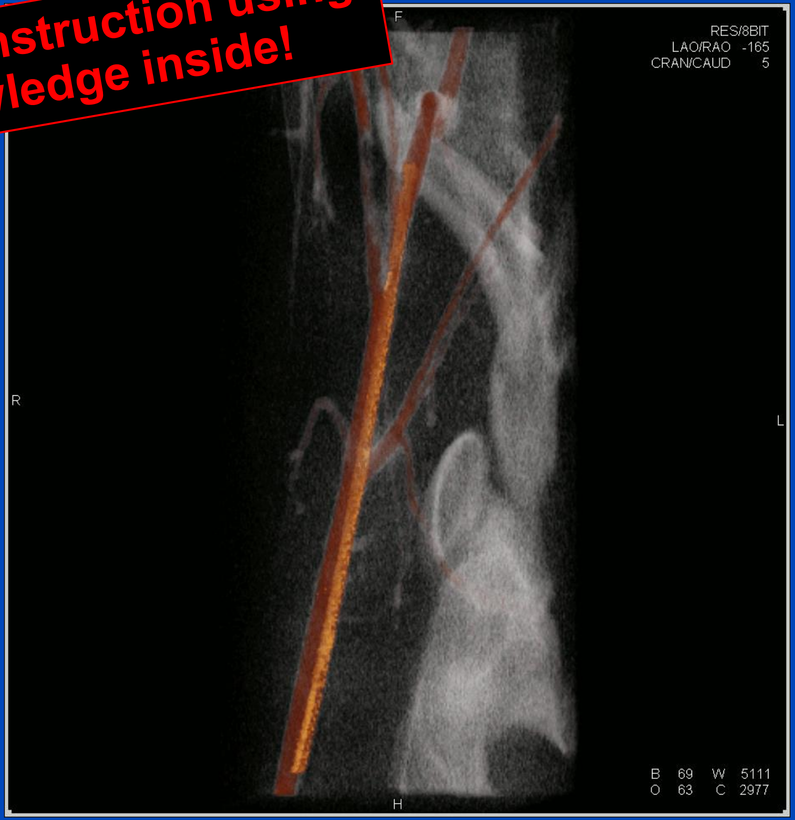

Iterative reconstruction using prior knowledge inside!

Dose of the yet unoptimized approach: 20 to 50 µGy/s.

This work was awarded the intervention award 2013 of the German Society of Neuroradiology (DGNR).
This work was further selected as the Editor's Pick for the Medical Physics Scitation site.

3D+T Fluoroscopy at 2D+T Dose

Guide Wire in the Carotis of a Pig with Angio Roadmap Overlay

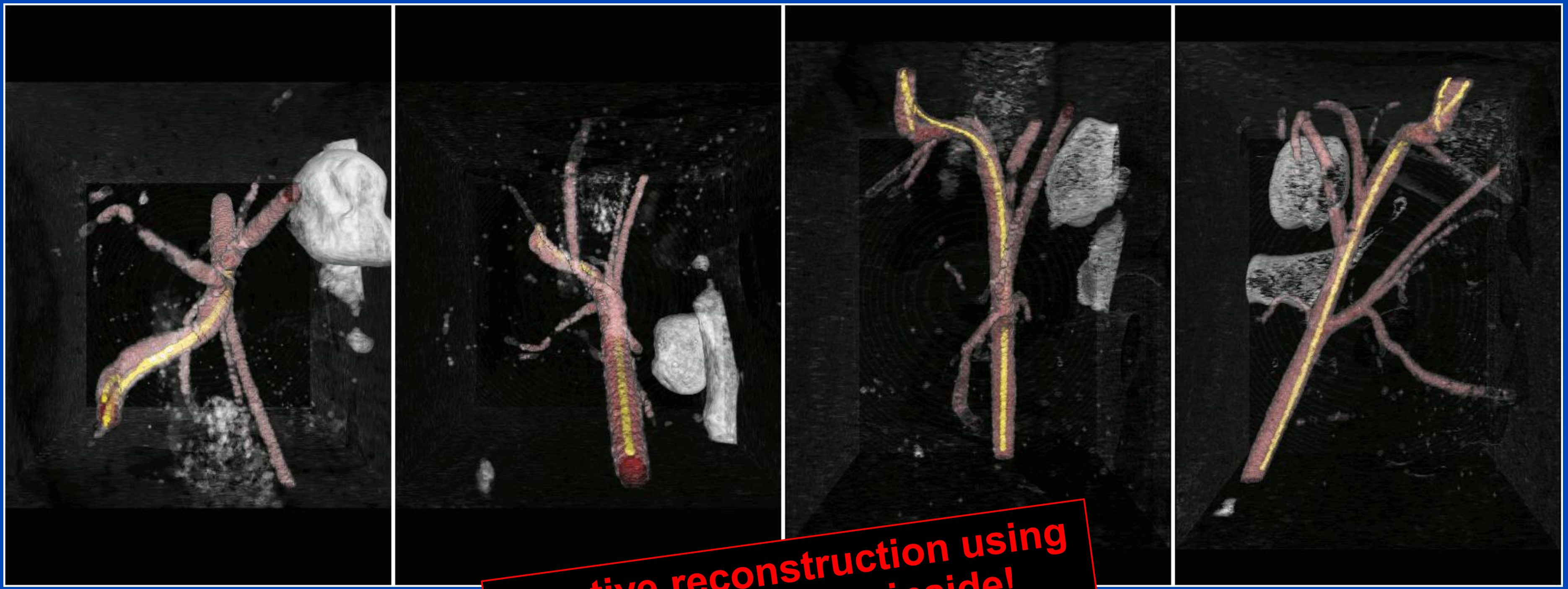

Iterative reconstruction using prior knowledge inside!

Dose of the yet unoptimized approach: 20 to 50 µGy/s.
Obviously, 16 projections are still too much.
Deep learning will help (5 years later)!

Deep Learning-Based 3D+T Fluoroscopy

Deep Tool Extraction (DTE) + Feldkamp Recon (FDK) + Deep Tool Reconstruction (DTR)

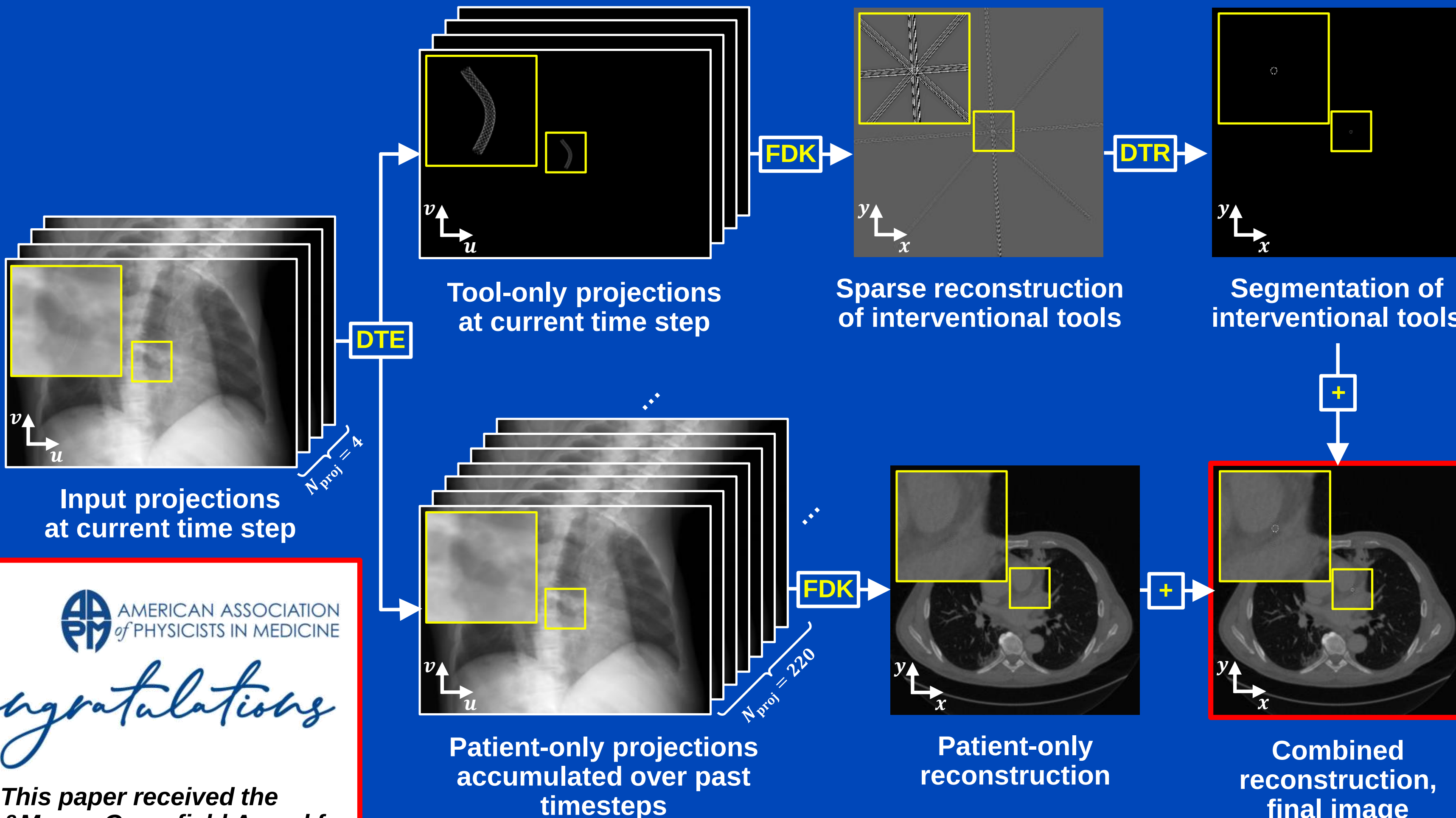

AMERICAN ASSOCIATION of PHYSICISTS IN MEDICINE

Congratulations

This paper received the Sylvia&Moses Greenfield Award for the best scientific paper on imaging in Medical Physics in 2021.

E. Eulig, J. Maier, M. Knaup, R. Bennett, K. Hörndler, A. Wang, and M. Kachelrieß. Deep learning-based reconstruction of interventional tools and devices from four x-ray projections for tomographic interventional guidance. Med. Phys. 48(10):5837-5850, October, 2021.

This paper received the Sylvia&Moses Greenfield Award for the best scientific paper on imaging in Medical Physics in 2021.

dkfz.

DTE Example 1

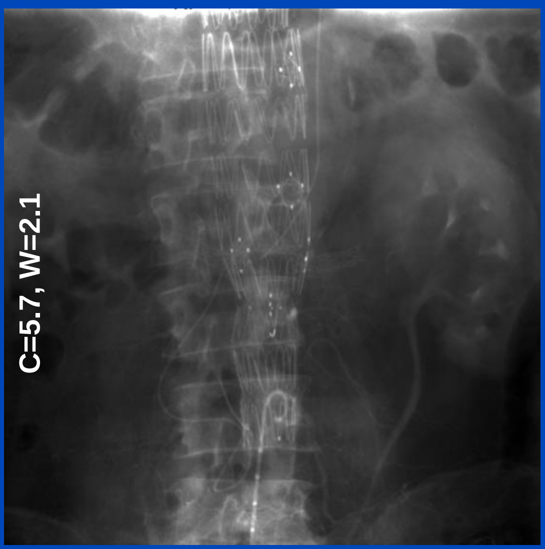

Input

Attention U-net

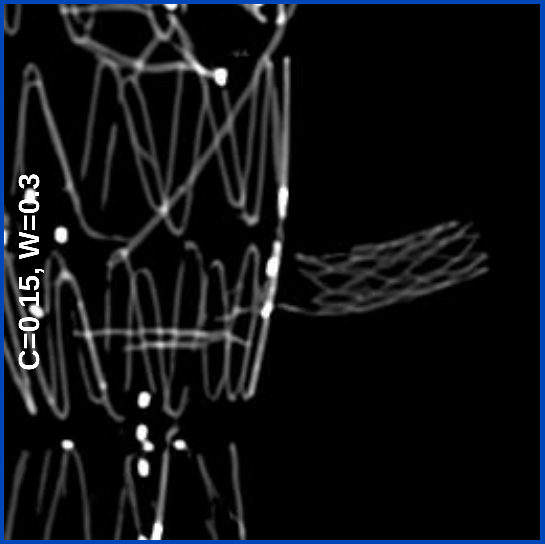

U-net

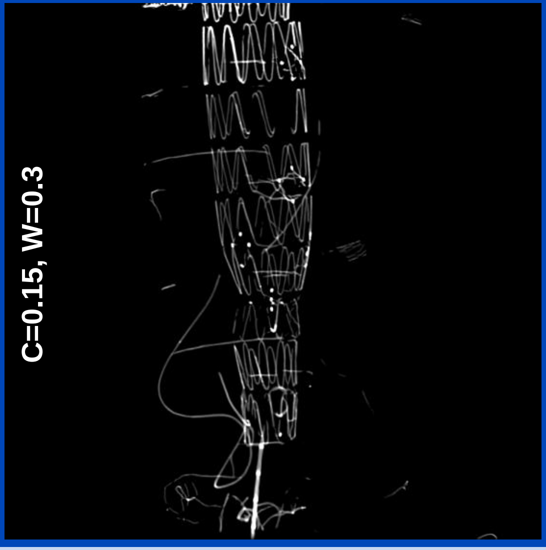

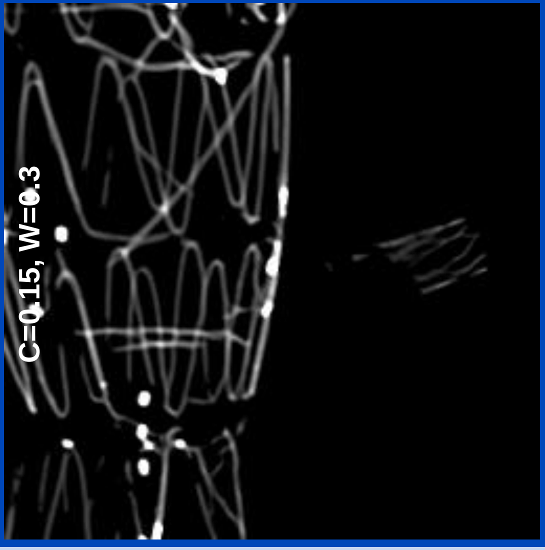

E. Eulig, J. Maier, M. Knaup, R. Bennett, K. Hörndler, A. Wang, and M. Kachelrieß. Deep learning-based reconstruction of interventional tools and devices from four x-ray projections for tomographic interventional guidance. Med. Phys. 48(10):5837-5850, October, 2021.
This paper received the Sylvia&Moses Greenfield Award for the best scientific paper in Medical Physics in 2021.

DTE Example 2

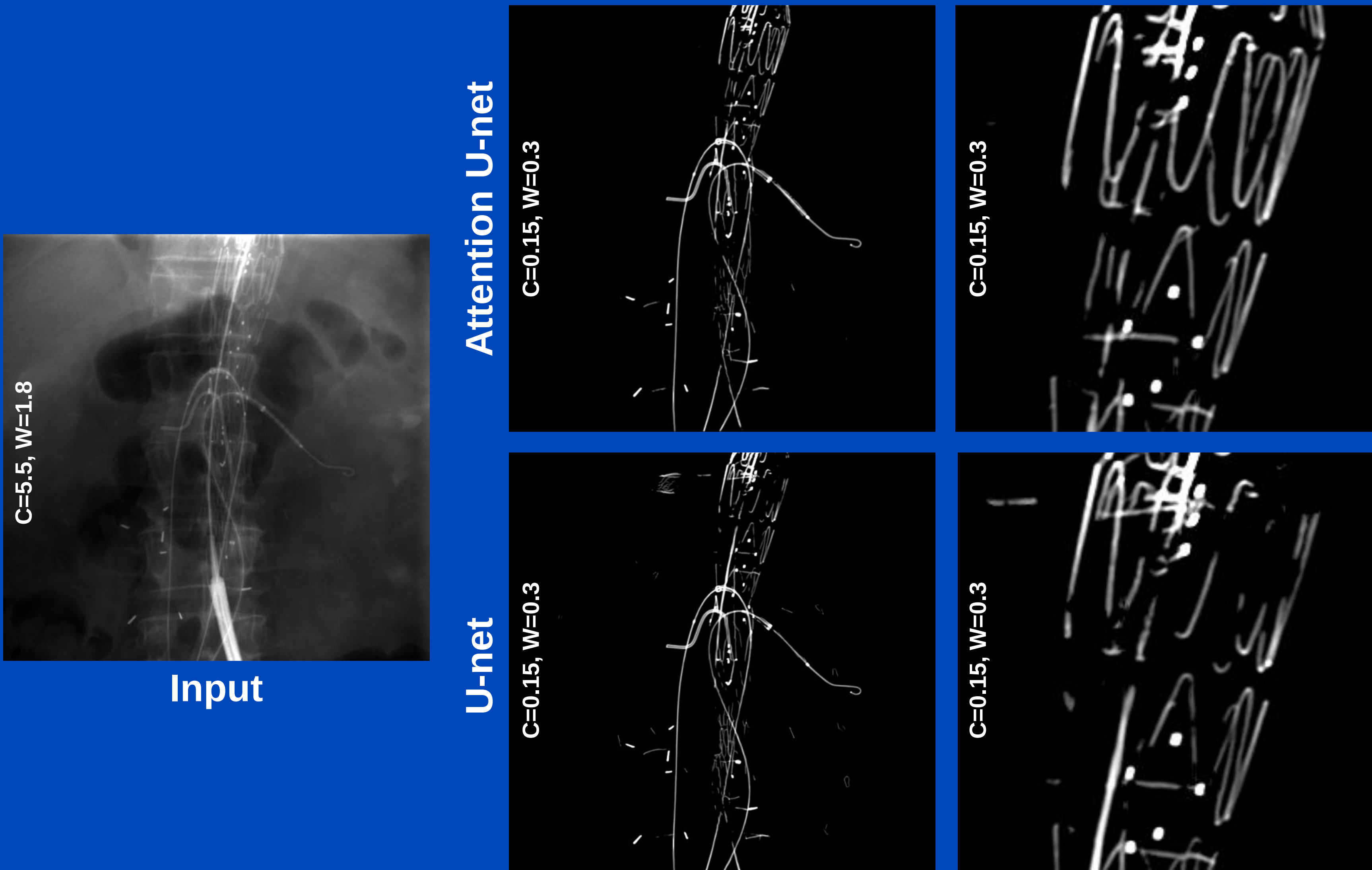

E. Eulig, J. Maier, M. Knaup, R. Bennett, K. Hörndler, A. Wang, and M. Kachelrieß. Deep learning-based reconstruction of interventional tools and devices from four x-ray projections for tomographic interventional guidance. Med. Phys. 48(10):5837-5850, October, 2021.

This paper received the Sylvia&Moses Greenfield Award for the best scientific paper in Medical Physics in 2021.

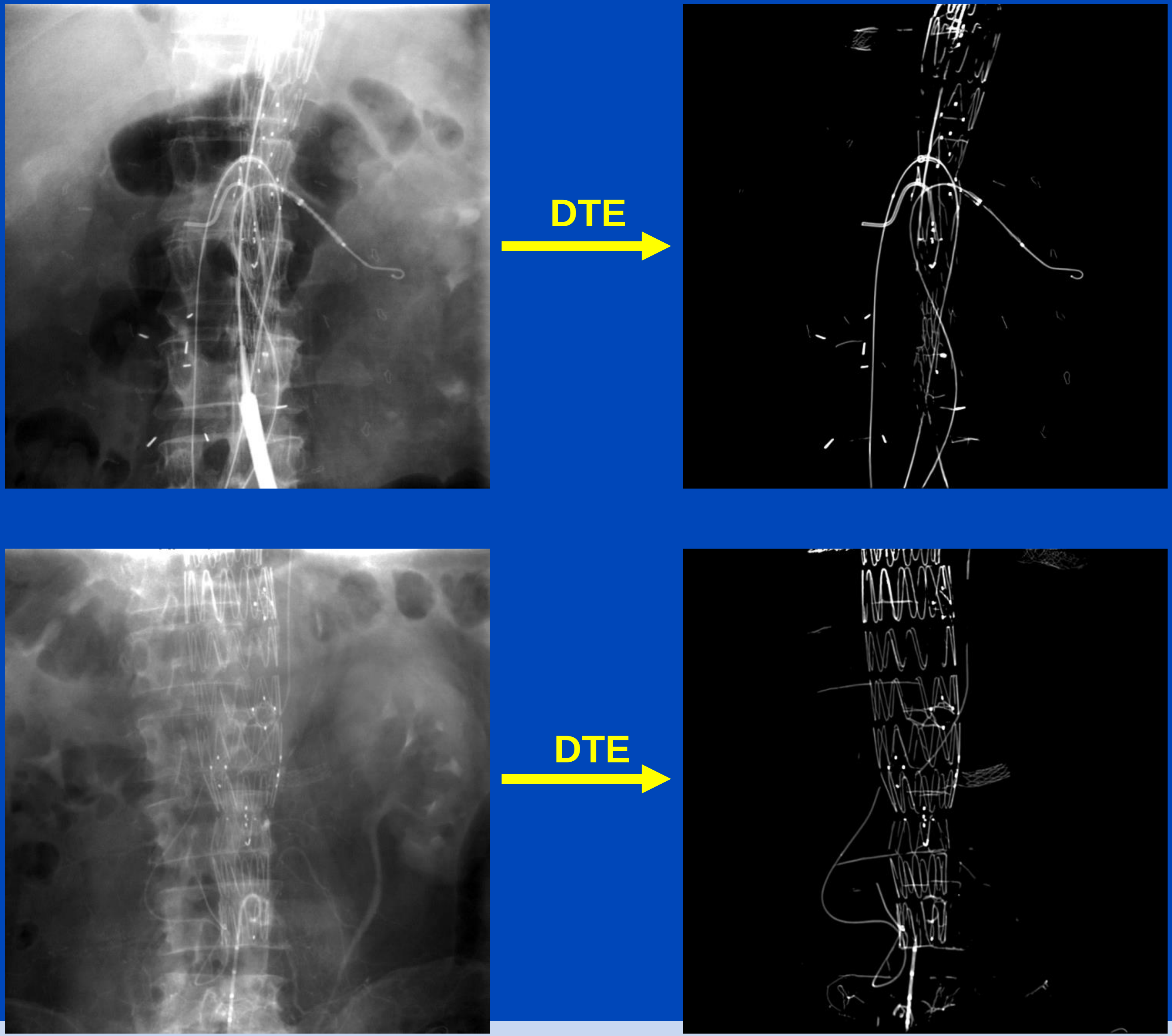
DTE
DTE

More DTE Results

Evaluate DTE on

- **Fluoroscopy scans (top)**
- **Measurements of interventional tools and devices superimposed with patient CBCT (bottom)**
- **Good qualitative results on fluoroscopy data even though it differs from training data**
- **Good qualitative & quantitative results on superimposed data**

Tool	MAPE [%]
Guide wires	6.0 ± 0.1
Stents	13.4 ± 2.1
Coils	13.2 ± 1.6

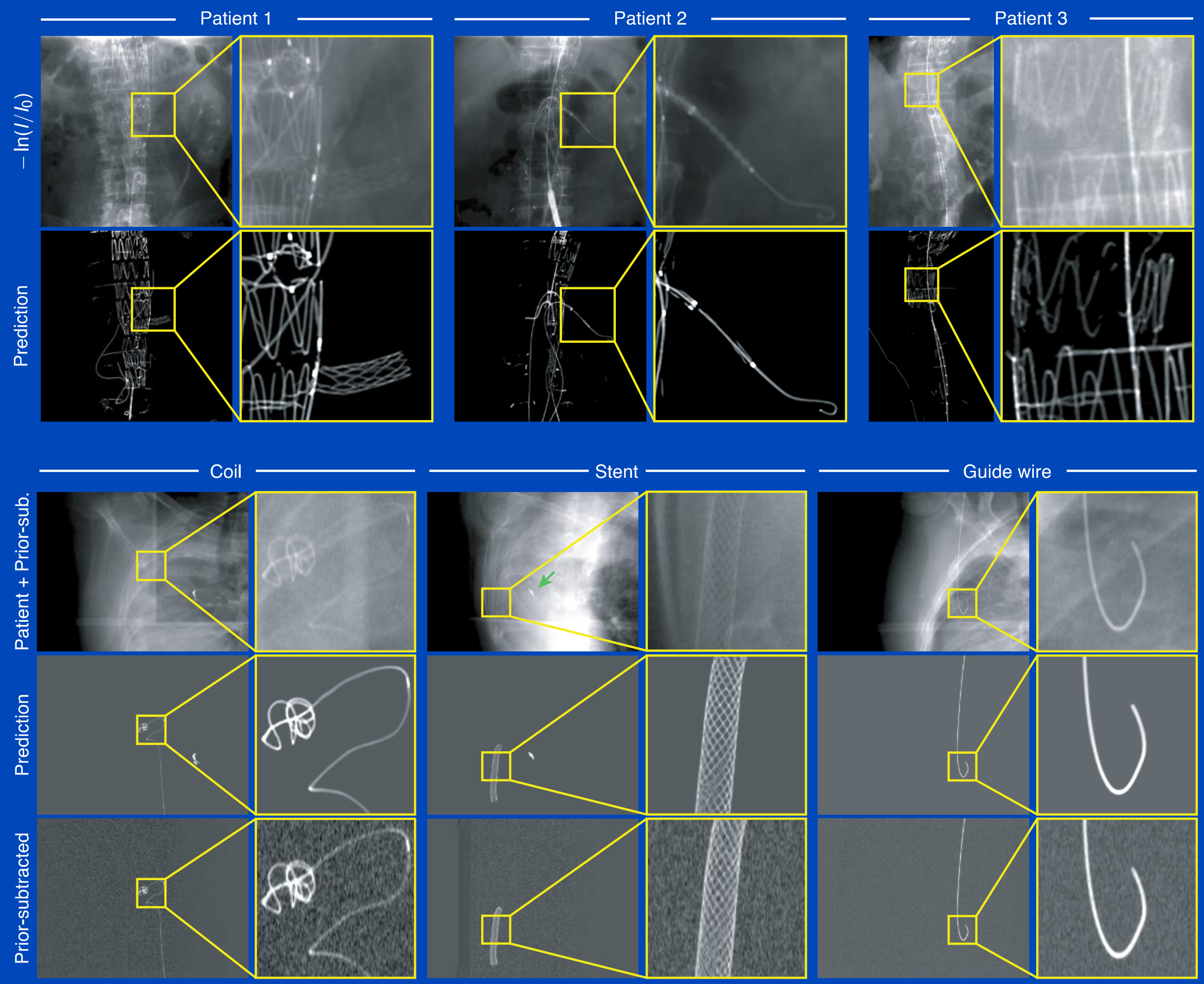

E. Eulig, J. Maier, M. Knaup, R. Bennett, K. Hörndler, A. Wang, and M. Kachelrieß. Deep learning-based reconstruction of interventional tools and devices from four x-ray projections for tomographic interventional guidance. Med. Phys. 48(10):5837-5850, October, 2021.
This paper received the Sylvia&Moses Greenfield Award for the best scientific paper in Medical Physics in 2021.

Zeego @ Stanford University

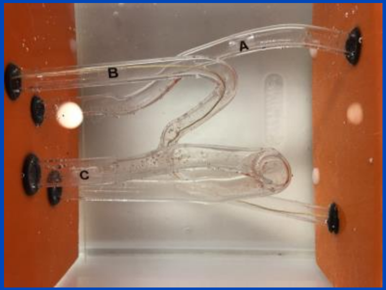

E. Eulig, J. Maier, M. Knaup, R. Bennett, K. Hörndler, A. Wang, and M. Kachelrieß. Deep learning-based reconstruction of interventional tools and devices from four x-ray projections for tomographic interventional guidance. Med. Phys. 48(10):5837-5850, October, 2021.
This paper received the Sylvia&Moses Greenfield Award for the best scientific paper in Medical Physics in 2021.

Zeego Measurements with Just 4 Projections

Ground truth (measurements from 400 projections)

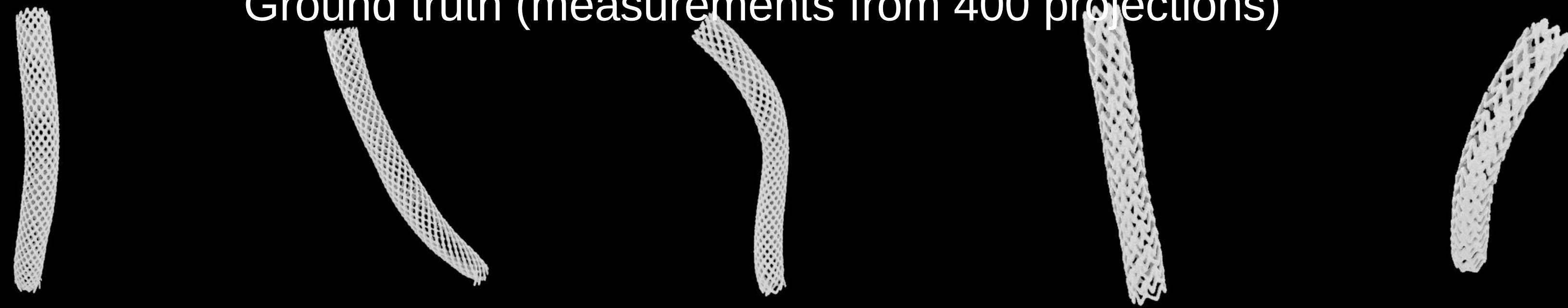

Neural network output (from just 4 projections)

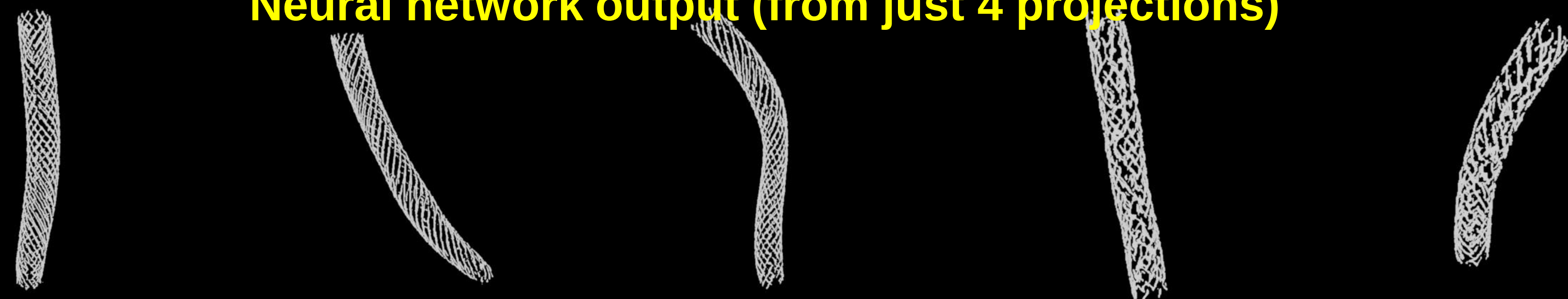

Loop through slices reconstructed from just 4 projections without AI:

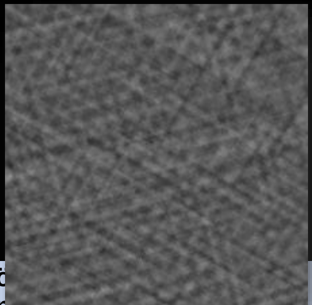

Stent examples:

E. Eulig, J. Maier, M. Knaup, R. Bennett, K. Hö… Kachelrieß. Deep lea… al tools and devices from four x-ray projection… ventional guidance. Me… 2021.
This paper received the Sylvia&Moses Greenfield Award for the best scientific paper in Medical Physics in 2021.

Conclusions on Deep CT

- Machine learning will play a significant role in CT image formation.
- High potential for
  - Artifact correction
  - Noise and dose reduction
  - Real-time dose assessment (also for RT)
  - …
- Care has to be taken
  - Underdetermined acquisition, e.g. sparse view or limited angle CT, require the net to make up information!
  - Nice looking images do not necessarily represent the ground truth.
  - Data consistency layers and variational networks with rawdata access may ensure that the information that is made up is consistent with the measured data.
  - …

Thank You!

The 8th International Conference on

Image Formation in X-Ray Computed Tomography

Conference Chair

Marc Kachelrieß, German Cancer Research Center (DKFZ), Heidelberg, Germany

This presentation will soon be available at www.dkfz.de/ct.

Job opportunities through DKFZ's international PhD programs or through marc.kachelriess@dkfz.de.

Parts of the reconstruction software were provided by RayConStruct® GmbH, Nürnberg, Germany.